

https://dspace.org/

Graphical techniques for analysing and synthesising separation processes

Beneke, Daniel Andries

2012-02-01
http://hdl.handle.net/10539/11231

Downloaded from a DSpace repository. https://dspace.org/

Graphical Techniques for Analysing and Synthesising Separation Processes

By

Daniel Andries Beneke

A thesis submitted to
Faculty of Engineering and the Built Environment
University of the Witwatersrand, Johannesburg
In fulfillment of the requirements for the degree of
Doctor of Philosophy.
Johannesburg, 2010

DECLARATION

I declare that, except where acknowledged, this thesis is my own, unaided work. It is being submitted for the degree of Doctor of Philosophy to the University of the Witwatersrand, Johannesburg. It has not been submitted before for any degree or examination at any other University.

_____

Daniel Andries Beneke

_____ day of _____, year _____

ABSTRACT

Recently, Column Profile Maps were developed as a generalized, graphically based distillation synthesis method. Unlike several other synthesis methods, it is not specific to any configuration and therefore allows the designer to devise almost any separation before being constrained by equipment. This thesis attempts to expand the theory of Column Profile Maps.

Specifically, it is shown how new, and somewhat counter intuitive, column sections may be designed by merely imposing a sharp split constraint on a particular system. This special mathematical constraint makes it possible to maneuver topological characteristics of the system in almost any imaginable direction. This could lead to new designs being sought to exploit these profile behaviors, specifically in columns that require internal column sections (complex columns).

Thermally coupled columns have received considerable attention for their ability to drastically reduce operating expenditures. Here, we have extended the Column Profile Map technique to encompass a systematic procedure for the design of single and multiple side rectifying and stripping units. It is shown how one may go about designing such columns rigorously without making simplifying assumptions with regard to the phase equilibrium behaviour and/or product specifications (as classical methods such as Underwood do), with the use of a Temperature Collocation method, as well as through a shortcut technique for rapid synthesis assuming ideal phase equilibrium behavior based on Column Profile Map eigenvectors. The efficacy of the shortcut technique is demonstrated with finding the best thermally coupled column comprising of a large main column and appending side-units. Naturally, the best structure is dependent on the objective function, and simple calculations presented here allow one to choose the best structure with regard to both heat quantity and

quality. Furthermore, the eigenvector method allows one to construct an Attainable Region consisting of all potential designs for even the most complex column.

The Column Profile Map technique is also extended to Reactive Distillation, which allows one to graphically assess the complex interaction of phenomena. Valuable conclusions can be gleaned from this method, specifically that improving a single piece of equipment's performance may prove detrimental to the overall system's operation. The methods developed here allow one to understand exactly why a complex process such as reactive distillation has some of the strange characteristics often reported in literature. Furthermore, it is shown how non-ideal phase equilibrium behavior may improve the column's operability and in fact improve the overall feasibility of the unit. Using this method, one may quickly assess desirable process chemistry, feed compositions, desirable phase equilibrium and equipment sizes. Again, an Attainable Region is presented which shows *all* possible modes of operation that would give rise to a predefined product specification.

Finally, computational techniques are presented which allows for swift calculation of stationary points in systems ranging from constant volatility to highly non-ideal, multi azeotropic systems. The importance of quickly and accurately knowing where pinch points are located, even in negative composition space, is demonstrated by critically looking at several design methods. Notably, it is shown that the Rectification Body Method is neither a necessary nor sufficient condition for design and cannot be safely extrapolated to complex column design. With knowledge of *all* pinch points and using the Column Profile Map technique it is shown how one may synthesise new and counter-intuitive column sections, so much so that azeotropes can be shifted outside the physically realizable space.

ACKNOWLEDGEMENTS

"*Want by U is die fontein van die lewe; in U lig sien ons die lig*." - Psalm 36:10

Firstly, I would like to thank my advisors, Professor Diane Hildebrandt and Professor David Glasser. Apart from their guidance in the field of distillation, and science in general, they have always indulged and encouraged me to pursue my ideas, no matter how farfetched they were or how wrong they turned out to be. Their impact on my life stretches much further than that which is contained in this thesis. It has been a massive privilege working with both of them.

Most importantly, to Enette, I cannot thank you enough for your love and the constant source of inspiration you have been to me. Throughout the course of this thesis, you remained (mostly) patient with me and showed more confidence in my abilities than I myself had. Thank you.

To my mother. Not one day has gone by where she became impatient or unsupportive of my academic pursuits. I will always be grateful for your love and support.

I would like to thank my family, as without their support and love, this thesis would never have come to fruition. I'm grateful towards Bryan for always taking interest in my work and to Adele for reminding me that there are more important things in life. I am also indebted to my father, for his constant enquiries about "when are you going to get a *real* job?" has played a large part in completing this work. Granny, Ouma, Oom Koos and Marie, your love and support has meant the world. Also, to Oom Mark, thanks for being a perfect role model.

To the friends I have made in the field of separations for countless hours of discussion, debate and argument, thank you! Specifically I would like to mention

Ronald Abbas, by far the most passionate person I have encountered in distillation. His enthusiasm for his work has been truly inspirational. Also, a special thanks to Dr. Gerardo Ruiz, Seon Kim and Alex Ivanchenko for their patience, guidance and warm-heartedness during my stay in Chicago. There are of course numerous friends and colleagues that I have made during my graduate studies at Wits and UIC that have made the whole experience enjoyable and insightful; to all of them, thanks! These acknowledgements would also not be complete without thanking my best non-Chemical Engineering friends, Hammy and Fran, for offering a (mostly) healthy distraction when I needed it most.

I would also like to express my gratitude towards Professor Andreas Linninger for hosting my stay at the University of Illinois at Chicago.

Financial support from all taxpayers in South Africa via the National Research Foundation; the Centre of Material and Process Synthesis (COMPS), The University of the Witwatersrand and Professor Andreas Linninger is greatly appreciated.

TABLE OF CONTENTS

DECLARATION I

ABSTRACT II

ACKNOWLEDGEMENTS IV

TABLE OF CONTENTS VI

LIST OF FIGURES X

LIST OF TABLES XX

NOMENCLATURE XXI

CHAPTER 1 : INTRODUCTORY OVERVIEW 1

1.1 Background and Motivation 1

1.2 Contribution of thesis 7

1.3 Thesis outline 8

CHAPTER 2 : COLUMN PROFILE MAPS: APPLICATION TO SHARP SPLITS IN CONSTANT VOLATILITY SYSTEMS 10

2.1 Introduction 11

2.2 Background 13

2.2.1 Derivation of Column Profile Maps 13

2.2.2 The effect of R_Δ 17

2.2.3 The effect of X_Δ 19

2.3 Sharp splits 20

2.3.1 Pinch Point Curves 21

2.3.2 Triangle shifting 22

2.3.3 Classification and behaviour of nodes 23

2.3.4 Node Bumping 24

2.3.5 The critical R_Δ 27

2.3.6 Ternary sharp splits 31

2.4 Validation and potential application 35

2.5 Conclusions 40

CHAPTER 3 : THERMALLY COUPLED SIDESTREAM COLUMN DESIGN USING COLUMN PROFILE MAPS AND TEMPERATURE COLLOCATION 42

3.1 Introduction 43

3.2 Methodology 46

3.2.1 Column Profile Maps 46

3.2.2 Temperature Collocation 50

3.3 Design Aspects 52

3.3.1 Structural aspects 52

3.3.2 Degree of Freedom analysis 53

3.3.3 Mass Balances aspects 54

3.3.4 Feasibility criteria 57

3.3.5 Choice of design variables 59

3.3.6 Side Stripper Column Section interaction 60

3.3.7 Side Rectifier Column Section interaction 62

3.3.8 Additional design constraints 63

3.3.9 Automatic design procedure 65

3.4 Design trade-offs 67

3.4.1 Reboiler Duty 69

3.4.2 Capital Cost 71

3.4.3 Energy Efficiency 73

3.5 Finalising the design 75

3.5.1 Extension to higher order systems 79

3.6 Discussion and Conclusions 81

CHAPTER 4 : DESIGN AND ANALYSIS OF MULTIPLE THERMALLY COUPLED CONFIGURATIONS USING COLUMN PROFILE MAPS 83

4.1 Introduction 84

4.2 Background: Column Profile Maps 87

4.3 Design procedure 91

4.3.1 Initialisation 91

4.3.2 Net flow patterns 93

4.3.3 Difference Point placement 95

4.3.4 Variable selection 97
4.3.5 Feasibility criteria 98
4.3.6 Thermally coupled column sections 105
4.3.7 Stepwise design algorithm 107

4.4 Finalising the design 108
4.4.1 Iso-reflux analysis 108
4.4.2 Identifying optimal designs 118

4.5 Discussion and conclusions 123

CHAPTER 5 : A PHENOMENA BASED COLUMN PROFILE MAP APPROACH TO UNDERSTANDING COUPLED REACTOR-COLUMN SECTIONS 125

5.1 Introduction 126

5.2 Derivation of model 128
5.2.1 Reactive distillation 128
5.2.2 Column Profile Maps 132

5.3 Process integration 135
5.3.1 Low boiling product 135
5.3.2 High Boiling Product 143
5.3.3 Intermediate Boiling Product 147
5.3.4 The MTBE process 151

5.4 Conclusions 158

CHAPTER 6 : PINCH POINT CALCULATIONS AND ITS APPLICATION TO ROBUST DISTILLATION DESIGN 160

6.1 Introduction 161

6.2 Theoretical Background 163
6.2.1 The Difference Point Equation 163
6.2.2 Rectification Body Method 166
6.2.3 Vapour – Liquid Equilibrium models 167
6.2.4 Thermodynamic consistency of negative compositions 169

6.3 Robust and efficient Pinch Point location 171
6.3.1 Pinch Point location for constant relative volatilities 172
6.3.2 Pinch Point location for Ideal solutions 175

6.3.3 One dimensional deflation method 177
6.3.4 Pinch Point location for Non-Ideal solutions 179
6.3.5 Multi-dimensional deflation method 180
6.3.6 Hybrid sequential niche algorithm 182

6.4 Design Observations 186
6.4.1 Limitations of the Rectification Body Method 186
6.4.2 Column Section design through Column Profile Maps 189
6.4.3 Rigorous separation design using Temperature Collocation 190

6.5 Conclusions 193

CHAPTER 7 : DISCUSSION 195

7.1 Overall Thesis Conclusions 195

7.2 Future Work 199

REFERENCES 201

PUBLICATIONS AND PRESENTATIONS 212

APPENDIX A: NODE DERIVATION AND CLASSIFICATION 214

APPENDIX B: THE BUMPING POINTS 216

APPENDIX C: MULTICOMPONENT EXAMPLE 219

APPENDIX D: THERMODYNAMIC EFFICIENCIES 220

APPENDIX E: REFLUX RATIO EQUATIONS 223

APPENDIX F: FOCAPD 2009 SUMMARY PAPER 225

APPENDIX G: DERIVATION OF DPE 229

APPENDIX H: TEMPERATURE COLLOCATION 231

LIST OF FIGURES

Figure 2.1: A generalised column section 14
Figure 2.2 : A Residue curve map with curves shown inside the MBT, i.e. $\Sigma x_i=1$ and $x_i \geq 0$; as well as outside the MBT where $x_i<0$. 16
Figure 2.3 : A CPM with $R_\Delta = 9$ and $X_\Delta = [0.2, 0.2]$ (marked with a dot) with a "shifted triangle" in blue indicating the movement of stationary points. 16
Figure 2.4: Movement of Transformed Triangles with varying reflux ratio for $X_\Delta = [0.3, 0.2]$ 18
Figure 2.5 a-g: Pinch point locus behaviour for different placements of X_Δ 19
Figure 2.6: Pinch point curve for $X_\Delta = [0.5, 0]$ 21
Figure 2.7: Pinch point curve behaviour for a sharp split 22
Figure 2.8: Triangle movement for $X_\Delta = [0.5, 0]$ 23
Figure 2.9: Eigenvalue map for $x_i = [-0.5....1.5]$ at $R_\Delta = \pm \infty$ 24
Figure 2.10: CPM with shifted triangle and node classification at $R_\Delta = 2$ and $X_\Delta = [0.5, 0]$ 25
Figure 2.11: CPM with shifted triangle and node classification at $R_\Delta = 1$ and $X_\Delta = [0.5, 0]$ 26
Figure 2.12 Zone-graph for $X_S = [0.2, 0]$ 28
Figure 2.13: Eigenvalue map for $x_i = [-0.5...1.5]$ at $R_\Delta = 1.25$ 29
Figure 2.14: CPM for $X_\Delta = [0.5, 0]$ and at the critical $R_\Delta = 1.25$ 30
Figure 2.15: Triangle movement for $X_\Delta = [0, 0]$ 31
Figure 2.16: Zone-graph for $X_\Delta = [0, 0]$ with the critical R_Δ values 32
Figure 2.17: CPM for $X_\Delta = [0, 0]$ and $R_\Delta = 1.5$ 33
Figure 2.18: Zone-graph for $X_\Delta = [1, 0]$ with the critical R_Δ values 34
Figure 2.19: Zone-graph for $X_\Delta = [0, 1]$ with the critical R_Δ values 34
Figure 2.20: Column Profiles for $X_\Delta = [0, 0]$, with $R_\Delta = 4$ and $R_\Delta = 0.5$ respectively 35

Figure 2.21: Liquid composition profiles using Aspen Plus for X_Δ = [0, 0] with (a) R_Δ = 4 and (b) R_Δ = 0.5. 37
Figure 2.22: Column section breakdown of (a) a Petlyuk column with multiple internal column sections and (b) a Reactive distillation column with an internal reactive column section (R). 38
Figure 2.23: A feasible multiple feed column where the internal column section (2), operates with a difference point of X_Δ = [0, 0] and a reflux ratio of -1.90, forcing the intermediate boiling vertex to be an unstable node. 39
Figure 3.1: A generalised Column Section (CS), with liquid composition x and X^T, and vapour compositions y and Y^T. The superscript T indicates the compositions at the top of the CS, while *n* indicates a respective tray number 47
Figure 3.2: A Column Profile Map with a generalized reflux ratio of R_Δ=9 and a Difference Point of X_Δ = [0.2, 0.6] (black dot). The dashed blue lines represent principal profiles emanating from the Difference Point which corresponds to a CS with a product cut. Secondary column profiles, drawn in solid blue lines, represent CSs with the same Difference Point as the principal profile but with different entering liquid and vapour compositions. All profiles may be extended beyond the boundaries of the mass balance triangle (in black) for gaining a better understanding of both the topology and pinch points. Each profile approaches the stationary points indicated by the red triangle. 48
Figure 3.3: Distinguishing feasible and infeasible designs using the Bubble Point Distance Function. Red lines indicate isotherms while green and blue lines are compositional profiles for the rectifying and stripping sections in a simple column, respectively. 51
Figure 3.4: Basic thermally coupled sidestream columns with the associated Column Section breakdown for (a) a side stripper and (b) a side

rectifier, showing the vapour and liquid distribution at the side draw stage. 53
Figure 3.5: Mass Balance over feed stage. 55
Figure 3.6: Mass Balance over Side-draw stage. 55
Figure 3.7: A geometric interpretation of the Difference Points for (a) a side stripper configuration and (b) a side rectifier configuration, accompanied by the CS breakdown and numbering of each configuration. On both diagrams $X_{\Delta i}$ is the Difference Point of the i'th CS. 56
Figure 3.8: Feasibility of a side stripper arrangement for the Benzene / Toluene / p-Xylene system. The Bubble Point Distance between CS_2 and CS_3, and the triple Bubble Point Distance between CS_1, CS2 and CS_4, needs to be zero for the side stripper column to be feasible. This criterion is indicated by the highlighted areas 57
Figure 3.9: Comparison of column profiles generated via the Column Profile Map / Temperature Collocation method (solid lines) and AspenPlus (dashed cyan lines) 59
Figure 3.10: Parameter correlation maps for a Side Stripper showing the influence of $R_{\Delta 1}$ with varying liquid split ratios (Φ_L) on the reflux ratios of (a) CS_2, (b) CS_3 and (c) CS_4. 61
Figure 3.11: Parameter correlation maps for a Side Rectifier showing the influence of $R_{\Delta 3}$ with varying vapour split ratios (Φ_V) on the Reflux ratios of (a) CS_1, (b) CS_2 and (c) CS_4. 62
Figure 3.12: Feasible operating regions in R_Δ-Φ space for an equimolar feed and sharp split product specifications from external mass balance constraints for (a) the side stripper and (b) the side rectifier. 64
Figure 3.13: An information flow diagram for the systematic design of thermally coupled sidestream columns. Feasible designs require all Bubble Points Distances to be zero. 66

Figure 3.14: A Residue Curve Map for the non-ideal, zeotropic Methanol / Ethanol / p-Xylene system. The black circles indicate the points at which integration is initialized using an ideal model (dashed trajectories) and the NRTL model (solid trajectories). 67
Figure 3.15: Spectrum of feasible designs for (a) the Side Stripper in Φ_L-$R_{\Delta 1}$ space and (b) the Side Rectifier in Φ_V-$R_{\Delta 3}$ space, showing the effect on the total reboiler duty required in the columns. 70
Figure 3.16: Spectrum of feasible designs for (a) the Side Stripper in Φ_L-$R_{\Delta 1}$ space and (b) the Side Rectifier in Φ_V-$R_{\Delta 3}$ space, showing the effect on the total number of stages required in the columns. 73
Figure 3.17: Spectrum of feasible designs for (a) the Side Stripper in Φ_L-$R_{\Delta 1}$ space and (b) the Side Rectifier in Φ_V-$R_{\Delta 3}$ space, showing the effect on the Lost Work produced in the columns. 75
Figure 3.18: Change in liquid composition along the length of the side stripper unit using (a) the Temperature Collocation method and (b) using AspenPlus with precise initialization from the Temperature Collocation method. The main column and side stripper are represented by the solid and dashed lines, respectively. 77
Figure 3.19: Molar liquid and vapour flowrates in the main column. 78
Figure 3.20: A feasible side rectifier design for the Benzene / Toluene / p-Xylene / Phenol system, showing areas of profile intersection and the location of all respective Difference Points. 79
Figure 4.1: An example of a generalised column section 87
Figure 4.2: A quaternary CPM with R_Δ=9 and X_Δ = [0.2, -0.3, -0.2] and relative volatilities of 6, 4, 2 and 1. The "shifted tetrahedron" in red indicates the movement of stationary points at finite reflux from the pure component vertices at infinite reflux. 89
Figure 4.3: A liquid eigenvector map for relative volatilities of [3, 1, 1.5]. 90
Figure 4.4: A column section breakdown of the four possible structures to separate a quaternary mixture with a main column and thermally

coupled side stream units: (a) the DSS, (b) the DSR, (c) the HSSR, and (d) the Kaibel column. 92
Figure 4.5: A summary of the only possible net flow directions in the (a) DSR (b) DSS (c) HSSR and (d) Kaibel column. 94
Figure 4.6: Difference Point placement for (a) the DSS, (b) the DSR, (c) the HSSR, showing the relationship between the respective Difference Points and adjacent column sections. 96
Figure 4.7: A simple, one feed two product column with the associated column section breakdown. 98
Figure 4.8: A design for an equimolar quaternary mixture in a simple column for the AB-CD split at (a) minimum reflux, (b) above minimum reflux, (c) below minimum reflux and (d) planar intersection through eigenvectors evaluated at the feed condition. 100
Figure 4.9: Minimum reflux Transformed Triangle interaction depicting the co-linear common eigenvector. 101
Figure 4.10: Pinch point locations for various feed qualities 103
Figure 4.11: A generic thermally coupled (a) side rectifying and (b) side stripping with the corresponding net flow directions of each column section. 106
Figure 4.12: An iso-reflux plot for the DSS at minimum reflux. 109
Figure 4.13: Transformed tetrahedrons at minimum reflux for the DSS. (a) Column sections 1 and 3. (b) Column sections 4 and 6. (c) Column sections 2 and 5. (d) Column sections 1 and 2. (e) Column sections 2 and 4. 113
Figure 4.14: An iso-reflux plot for the DSR at minimum reflux. 113
Figure 4.15: Transformed tetrahedrons at minimum reflux for the DSR. (a) Column sections 5 and 6. (b) Column sections 3 and 4. (c) Column sections 1 and 2. (d) Column sections 2 and 4. (e) Column sections 4 and 6. 115

Figure 4.16: An iso-reflux plot for the HSSR and Kaibel column at minimum reflux. 116
Figure 4.17: Transformed tetrahedrons at minimum reflux for the HSSR and Kaibel columns. (a) Column sections 1 and 3. (b) Column sections 2 and 4. (c) Column sections 5 and 6. (d) Column sections 1 and 2. (e) Column sections 4 and 6. 117
Figure 5.1: A CSTR with a continuous feed and simultaneous vapour liquid equilibrium separation 129
Figure 5.2: Phenomena vector fields for (a) Mixing with x_F= [0.2, 0.3]; (b) Separation for a constant relative volatility system with α= [5, 1, 2]; and (c) Reaction for 1I+1H↔2L with elementary reaction rate and K_{eq}=25 130
Figure 5.3: Overall reactive distillation process vector field with a feed composition of x_F= [0.2, 0.3] indicated by a black dot. 131
Figure 5.4 A generalised column section. 132
Figure 5.5 : A CPM for X_{Δ}= *[0.2, 0.3]* (black dot) and R_{Δ}=*8.* The blue lines represent the Column Profiles inside and outside the black Mass Balance Triangle (MBT). 134
Figure 5.6: A CSTR coupled with a rectifying column section, a reactive reboiler. 136
Figure 5.7: The effect of reflux and amount of stages on bottom liquid composition profiles for X_{Δ} = [0.950, 0.025] 137
Figure 5.8: A CSTR coupled with a rectifying column section for R_{Δ} =3, n=5 and X_{Δ} = [0.950, 0.025]. The red and blue line represent the Column Profile and the Feed locus line, respectively, while the red, black and blue dots represent the bottom liquid composition of the column section, the reactor composition and the feed composition that contains no product, respectively. The black curve represents the reaction equilibrium curve. 139

Figure 5.9: The effect of the number of stages and reflux ratio on reactor size for X_{Δ} = [0.950, 0.025] and x_{FL} = 0 for a CSTR coupled to a rectifying, non-reactive column section. 141
Figure 5.10: A CSTR coupled with a stripping column section, a reactive condenser. 143
Figure 5.11: A CSTR coupled with a stripping column section for R_{Δ}=-7, n=5 and X_{Δ}=[0.025, 0.950]. The red and blue line represent the column profile and the feed locus line, respectively, while the red, black and blue dots represent the bottom liquid composition of the column section, the reactor composition and the feed composition that contains no product, respectively. The black curve represents the reaction equilibrium curve. 145
Figure 5.12: The effect of the number of stages and reflux ratio on reactor size for X_{Δ}=[0.025, 0.950] and x_{FH} = 0 for a CSTR coupled to a stripping, non-reactive column section. 146
Figure 5.13: A CSTR coupled with a rectifying column section for R_{Δ}=10, n=12 and X_{Δ} = [0.025, 0.025]. The red and blue line represent the column profile and the feed locus line, respectively, while the red, black and blue dots represent the bottom liquid composition of the column section, the reactor composition and the feed composition that contains no product, respectively. The black curve represents the reaction equilibrium curve. 148
Figure 5.14: The effect of the number of stages and reflux ratio on reactor size for X_{Δ} = [0.025, 0.025] and x_{FI} = 0 for a CSTR coupled to a rectifying, non-reactive column section. 149
Figure 5.15: The effect of the number of stages and reflux ratio on reactor size for X_{Δ} = [0.025, 0.025] and x_{FI} = 0 for a CSTR coupled to a stripping, non-reactive column section. 150
Figure 5.16: The IBUT-MEOH-MTBE system at 1atm: (a) a Residue Curve Map and (b), reaction equilibrium curves. 153

Figure 5.17: CSTR coupled with a stripping column section for the MTBE system at 1 atm, with R_Δ= -8, n=5 and X_Δ=[0.950, 0.025]. The red and blue line represent the column profile and the feed locus line, respectively, while the red, black and blue dots represent the bottom liquid composition of the column section, the reactor composition and the feed composition that contains no product, respectively. The purple line is the reaction equilibrium curve at 65.49^{o}C..... 154

Figure 5.18: The effect of the number of stages and reflux ratio on molar holdup for the MTBE process at 1 atm, with X_Δ=[0.950, 0.025] and x_{MTBE}=0 for a CSTR coupled to a stripping, non-reactive column section. 155

Figure 5.19 The effect of the number of stages and reflux ratio on reactor temperature for the MTBE process at 1 atm, with X_Δ=[0.950, 0.025] and x_{MTBE}=0 for a CSTR coupled to a stripping, non-reactive column section.. 156

Figure 5.20: The effect of the number of stages and reflux ratio on reactor size for the MTBE process at 8 atm, X_Δ=[0.950, 0.025] and x_{MTBE}=0 for a CSTR coupled to a stripping, non-reactive column section. 157

Figure 5.21: The effect of the number of stages and reflux ratio on reactor temperature for the MTBE process at 8 atm, X_Δ=[0.950, 0.025] and x_{MTBE}=0 for a CSTR coupled to a stripping, non-reactive column section. 157

Figure 6.1: (a) A single liquid composition profile with R_Δ=9 and X_Δ= [0.2, 0.2], with the definition of a generalized Column Section, and (b) a Column Profile Map with R_Δ=9 and X_Δ=[0.2, 0.2]where the blue lines represent the column profiles, inside and outside the positive composition space, and the red triangle indicates the shifted Pinch Points..... 165

Figure 6.2: Intersecting Rectification Bodies for the Benzene / Xylene / Toluene system 167
Figure 6.3: Residue curve map for the Acetone/Benzene/Chloroform using the NRTL activity coefficient model in positive and negative composition space showing multiple stationary points. 170
Figure 6.4: A Column Profile Map for a mixture with constant relative volatilities of (α_1=5, α_2=2) showing with only one real solution at a reflux of 0.6 and X_Δ= [1.2, -0.1]. The thick black trajectory indicates a realizable liquid composition profile of a typical Column Section..... 174
Figure 6.5: A one dimensional Pinch Point temperature search showing all pinch temperatures where f(T)=0 for $X_\measuredangle$=[0.9, 0.05, 0.03] and $R_\measuredangle$=5, accompanied by a table showing all pinch temperatures and compositions. The Pinch temperatures indicated on the graph (T1-T4) are the bubble point temperatures of the four pinch points..... 177
Figure 6.6: (a) Surrogate function $g_1(T)$ vs. Bubble Point temperature where the highest Pinch Point has been eliminated, (b) surrogate function $g_2(T)$ vs. Bubble Point temperature where the two highest Pinch Points have been eliminated, and (c) surrogate function $g_2(T)$ vs. Bubble Point temperature where the three highest Pinch Points have been eliminated..... 178
Figure 6.7: Comparison of stationary points using the NRTL model for the Acetone / Ethanol / Acetic Acid system (green circle) with the multivariable deflation method, the ideal solution model (black square), and the constant relative volatility model (red cross), for choices of X_Δ= [0.8, 0.1] and R_Δ=-3..... 181
Figure 6.8: Column Profile Maps showing all stationary points for the Acetone/ Methanol/ Chloroform system at (a) infinite reflux and (b) at a finite reflux of $R_\measuredangle$=8 and $X_\measuredangle$=[0.8, 0.1]. Composition profiles are indicated by blue lines, while pinched compositions

are given by black dots. Discontinuous regions are represented by a dashed black line. 184
Figure 6.9: Column Profile Maps showing all stationary points for the Isobutene / MTBE / Methanol system at (a) infinite reflux and (b) at a finite reflux of $R_{\measuredangle}$=-5 and $X_{\measuredangle}$=[0.8, 0.1]. Composition profiles are indicated by blue lines, while pinched compositions are given by black dots. Discontinuous regions are represented by a dashed black line. 184
Figure 6.10: An example of a feasible distributed feed column where the internal Column Section has complex Pinch Points. Constant relative volatilities of 5 and 2 have been assumed. All composition profiles intersect one another, indicating a feasible design. 187
Figure 6.11: A comparison of the design with complex Pinch Points shown in Figure 6.10 and an AspenPlus design 188
Figure 6.12: Failure of the Rectification Body Method as a rigorous feasibility test: (a) Composition profiles intersect indicating a feasible design, but Rectification Bodies do not touch, (b) Rectification Bodies intersect but composition profiles do not intersect. The design is infeasible despite the positive Rectification Body method indication. 189
Figure 6.13: The Acetone / Methanol / Chloroform showing (a) a Residue Curve Map with seven Pinch Points inside mass balance triangle, and (b) no Pinch Points inside the mass balance triangle at X_{Δ}= [1.0, 0.25] and R_{Δ}=-3 190
Figure 6.14: Intersecting liquid profiles by fitting a polynomial and finding all Pinch Points. Pinch points are marked for both rectifying (blue triangle), and stripping (red square) column sections. Profiles of rectifying (blue) and stripping (red) intersect, indicating a feasible design. 192

LIST OF TABLES

Table 2.1: Summary of stream table data for the two reflux ratio scenarios generated with a Radfrac column in AspenPlus, as annotated in the far right column. 36

Table 3.1: Stream table for a Benzene / Toluene / p-Xylene system. Text in boldface indicates that these parameters have been specified, while the rest have been calculated. 58

Table 3.2: Summary of feed and product specifications for the Methanol / Ethanol / p-Xylene system with coefficients for the Antoine equation calculated by $\log(P^{SAT})$ (mmHg)=A-B/(T(^{o}C)+C) 68

Table 3.3: Stream table for a Benzene / Toluene / p-Xylene / Phenol system 80

Table 4.1 A summary of X_{Δ} placement for various structures with sharp splits and an equimolar feed. Shaded cells indicate rectifying sections. 96

Table 4.2: Summary of pseudo feed streams to the generic side rectifying and stripping sections 107

Table 4.3: Reflux ratios at minimum reflux for all respective minimum structures 118

Table 4.4: Minimum vapour flows and thermodynamic efficiencies for all respective thermally coupled structures for volatilities of 6, 4, 2 and 1. 119

Table 5.1: Antoine constants for Isobutene, Methanol and MTBE 153

Table 6.1: All Pinch compositions and temperatures for both the Acetone / Methanol / Chloroform and the Isobutene / MTBE / Methanol systems. 183

Table 6.2: A comparison of various algorithms tested for Pinch Point location 185

NOMENCLATURE

Symbol	Unit	Description
x_1	[mol/mol].....	*Light component composition*
x_2	[mol/mol].....	*Heavy component composition*
x_3	[mol/mol].....	*Intermediate component composition*
i	[-].....	*Component index*
x	[mol/mol]	*Liquid composition vector*
y(x)	[mol/mol].....	*Vapour composition vector*
i,j,k,f,g,h	[-].....	*Column Section Index*
V	[mol/s]	*Vapour flow rate in a column section*
L	[mol/s].....	*Liquid flow rate in a in column section*
Δ	[mol/s].....	*(V – L) Net Flow in a column section*
R_Δ	[-].....	*Reflux ratio = L/(V-L)*
n	[-].....	*Stage number*
Y^T	[-].....	*Top vapour composition vector*
X^T	[-].....	*Top liquid composition vector*
Y^B	[-].....	*Bottom vapour composition vector*
X^B	[-].....	*Bottom liquid composition vector*
X_S	[-].....	*Stationary point coordinate*
X_Δ	[-].....	*Difference point* $= (VY^T – LX^T)/(V-L)$
Ptot	[bar].....	*Total system pressure*
P^{SAT}	[bar].....	*Vapour pressure of component i*
α_i	[-].....	*Volatility of component i relative to heavy component*
T	[^oK or ^oC].....	*Temperature*
λ	[-].....	*Eigenvalue*
r	[-].....	*Reaction rate*
v	[-].....	*Stoichiometric vector*
k_f	[s^{-1}].....	*Reaction rate constant*

F	[mol/s].....	*Feed flowrate*
D	[mol/s].....	*Distillate flowrate*
B	[mol/s].....	*Bottoms flowrate*
x_F	[mol/mol].....	*Feed flowrate*
x_D	[mol/mol].....	*Distillate flowrate*
x_B	[mol/mol].....	*Bottoms flowrate*
CS	[-].....	*Column Section*
H	[mol].....	*Reactor Holdup*
K_{eq}	[mol].....	*Equilibrium constant*
x_n	[mol/mol].....	*Composition on stage n*
φ	[mol/s].....	*Reactor size variable*
γ_i	[mol/s].....	*Activity coefficient*
$\Phi_{V,L}$	*[-]*.....	*Vapour/liquid split ratio*
η	*[-]*.....	*Thermodynamic efficiency*

Chapter 1 : INTRODUCTORY OVERVIEW

This thesis consists of five topics that are broadly related in that they all deal with the theoretical analysis of distillation systems, but they have been deemed unique enough to warrant their partition into separate chapters. As such, five working chapters are presented, all of which have been prepared in the form of papers for publication. However, the nomenclature, and references have been included as part of the main thesis body, and are not shown separately in the respective chapters. Below is an overall introduction and background to the thesis, covering the work in all five chapters.

1.1 BACKGROUND AND MOTIVATION

In almost all industrial chemical processes, one or more chemical reactions take place to manufacture a wide range of products. Unfortunately, these reactions invariably produce by-products which severely affect the quality and therefore the market value of the final product. Thus, in almost all chemical processes a separation scheme of some sorts is required. There are numerous technologies available for this task, such as distillation, membrane separation, crystallization, etc., but of these available technologies, distillation remains by far the most common in the chemical industry. Distillation is a commercial method of purifying binary and multi component mixtures on the basis of boiling point differences into final compositions which have greater use or a higher market value. Decades of work by researchers have made it possible for distillation to become one of the most widely used and effective methods of separation used in the chemical industry today.

However, even though distillation is by far the most widely used technique for separation, it is also an expensive process due to the high energy demands of the process. In fact, Soave and Feliu have reported that in 1995, distillation columns in

the United States consumed around 2.87×10^{18} J (2.87 million TJ), which is equivalent to a continuous power consumption of 91 GW or to 54 million tons of crude oil (Soave and Feliu, 2002) . In another study, it has been estimated that energy inputs into distillation columns in the United States accounts for approximately 3% of the entire country's energy consumption (Ognisty, 1995). It is evident that by saving or recovering only 1% of the heat used by distillation columns, the impact would be significant.

Many schemes have been proposed over the past several years to improve distillation energy requirements. Traditionally, when purifying a multicomponent mixture, a number of distillation columns are used in series, and the way in which these columns are sequenced may make a tremendous difference in the overall energy requirements. However, due to the large energy requirements of even the most optimal sequence, more complex column arrangements have been proposed and subsequently utilized. These arrangements include thermally coupled columns such as side rectifiers and strippers the Petlyuk and Kaibel columns, prefractionating columns, and multi-effect arrangements (Engelien and Skogestad, 2005a). Up to 50% savings in energy expenditures have been reported with these thermally coupled arrangements (Wolff and Skogestad, 1995, Agrawal and Fidkowski, 1998, Fidkowski and Agrawal, 2001, Brüggemann and Marquardt, 2004, Engelien and Skogestad, 2005b).

Side stripping columns have found widespread use in the petrochemical industry to produce various cuts of petroleum products (Watkins, 1979). On the other hand, side rectifying columns have found application in air separation (Petlyuk, 2004) as well as replacing entrainer regeneration columns in extractive distillation operations (Emmrich et al., 2001). Even more complex columns like the Petlyuk column for separating a given feed into three products in a single unit requires only one set of heating or cooling devices, thereby reducing the energy costs of the separation. Despite the significant advantages that complex configurations offer, simple (one-feed-two-product) distillation columns are overwhelmingly more utilised. One factor

contributing to the under-utilisation of the complex arrangements is, possibly, a lack of understanding of these columns. Simple columns, by comparison, are extremely well understood. Therefore, in an attempt to reduce energy and capital costs of separation systems, a considerable amount of effort has gone into the synthesis and design thereof.

Graphical methods for designing distillation schemes have been especially popular for design. In 1925, McCabe and Thiele published a landmark paper on a graphical design method for binary distillation (McCabe and Thiele, 1925b), still used today as a quick means of understanding the relationship between energy and capital costs for simple distillation. Multicomponent distillation systems have been traditionally designed through the Underwood set of equations (Underwood, 1946a). These equations are limited by the following assumptions: constant relative volatility between all components, constant molar overflow and a sharp separation between product streams, i.e. one or more of the components has a near-zero composition in at least one of the product streams (the same definition for a sharp splits used by used by Huss and Westerberg (Huss and Westerberg, 1996)). If there is a significant distribution of components, Underwood's method is no longer exact. This fact has been stated in several works (Levy et al., 1985, Poellmann et al., 1994, Lucia and McCallum, 2009). Shiras et al. also systematically demonstrate that for Class 2 separations (sharp split problems in terms of this thesis' terminology) that the Underwood equations are exact (Shiras et al., 1950). For cases where all components distribute (Class 1 problems), Underwood's method only serves as an approximation because the pinch points are not related to the feed compositions in a simple way. Moreover, Levy and Doherty proved convincingly that Underwood's geometry cannot be relied upon to give accurate values for minimum reflux when the mixture is non-ideal (Levy et al., 1985). These assumptions are however still very good approximations for a large number of industrial applications, and these equations have been applied by numerous authors to a plethora of distillation structures (Halvorsen and Skogestad, 2003a, Halvorsen and Skogestad, 2003b, Engelien and

Skogestad, 2005a, Engelien and Skogestad, 2005b, Wolff and Skogestad, 1995, Fidkowski and Krolikowski, 1987, Alstad et al., 2004, Carlberg and Westerberg, 1989, Glinos and Malone, 1985a, Glinos and Malone, 1985b).

Residue curve maps and distillation line maps (Schreinemakers, 1902, Doherty and Perkins, 1979, Stichlmair and Herguijuela, 1992) have also been a useful graphical technique for screening ternary separation feasibility, especially for simple separations. These maps are basically a range of trajectories that track the liquid compositions of the chemical species over time in a simple batch distillation operation, and conveniently present the relationship between liquid and vapour phases allowing one to quickly analyse potential splits, even for highly non-ideal systems. However, although these maps can tell one much about the feasibility of separation, they both have limitations in that they only give information at infinite reflux, i.e. an infinite energy requirement, quite an impractical condition for the design engineer.

Numerous other design techniques have evolved over the years with varying degrees of complexity. One of these are the shortest stripping line method proposed by Lucia and co-workers (Lucia et al., 2006) which states that the shortest stripping line will generally lead to the structure with lowest heat duty. Other, so-called non-equilibrium models (Taylor and Krishna, 1993) have also received considerable attention, and although these non-equilibrium methods are more rigorous than their equilibrium counterparts, they often permit limited insight into the design due to the large number of variables required to accurately converge the equations.

Even advanced simulation packages such as AspenPlus or Hysys, although their undoubted modelling capabilities, have not provided much insight into the design of complex distillation systems. This is largely due to the fact that these packages require precise initialization values to ensure convergence to the specified product purities. Without the necessary experience or advanced knowledge, rigorously

determining a complex column's feasibility is a time-consuming, if not impossible, task. Furthermore, because of the "black box" nature of the program, the user often does not have any insight into the final solution and how one might go about improving it.

Recently, in a series of papers by Holland, Tapp and co-workers a new distillation design technique was proposed, Column Profile Maps (CPMs) (Holland et al., 2004a, Tapp et al., 2004). CPMs were derived from an adaptation of ordinary differential equations for a simple single-feed-two product column (Van Dongen and Doherty, 1985a). CPMs were shown to display the same topological behaviour as residue curve maps, as well as being an extremely useful design tool for complex distillation systems by allowing the designer to set reflux ratios and net molar flows in a generalised column section. This generalisation has been shown to be extremely useful for designing and analysing complex distillation systems (Holland et al., 2010, Holland et al., 2004b). The method does not require simplifying assumptions regarding the phase equilibrium behaviour nor sharp splits. Furthermore, unlike the aforementioned rigorous simulation packages, highly insightful design parameters such as the total number of stages, feed stage, and reflux ratio are a product of the method, and do not require them to be set *a priori*. Furthermore, the Column Profile Map method is perhaps most useful in devising these new, previously unthought-of structures, since it is completely generalised and not limited to any particular piece of equipment, and thus allows the designer freedom for designing new, more efficient separation schemes.

In a further attempt to reduce capital and operating costs of a processing plant, researchers and engineers have proposed combining a chemical reactor and a distillation column into a single vessel. This process, reactive distillation, has been mentioned as early as 1948 (Berman et al., 1948). Reactive distillation may be implemented to replace conventional reaction-separation networks, and has the potential to greatly reduce expenditures. Taylor and Krishna compiled a

comprehensive review on reactive distillation and have identified several advantages, including significant savings on capital cost due to the simplification or elimination of the separation network; improved heat integration, especially if the reaction is exothermic, and an improvement in both selectivity and reactant conversion (Taylor and Krishna, 2000).

Although the case for reactive distillation is strong, it is much more complex than conventional distillation and therefore much more difficult to model, primarily due to the fact that a chemical reaction, phase separation and mixing occur in a single vessel. According to Taylor and Krishna, the major problem facing the large scale implementation of reactive distillation schemes is operability. As with the aforementioned complex column arrangements, this arises due to the complexity brought forward in the design of the process.

Strategies that have been proposed to solve this problem are divided into two main classes: equilibrium or non-equilibrium stage based, almost all of which are computer orientated (Taylor and Krishna, 2000). An example of such a computer aided model is determining the optimum number of equilibrium stages, feed tray location and reflux ratio by combining a tray-by-tray balances, kinetic rate based expressions and cost estimates using mixed integer non linear programming (Ciric and Gu, 1994). Although models such as these are extremely effective and rigorous, due to the large amount of simultaneous molar, energy and equilibrium equations to be solved they do not always allow the user to obtain insights into the final solution. In contrast to this, Hauan and co-workers have developed a phenomena-based approach for analyzing and synthesizing reactive separation processes, by considering the effects of the three phenomena present: chemical reaction, equilibrium separation and mixing (Hauan and Lien, 1996, Hauan and Lien, 1998, Hauan et al., 2000). Using this relatively simple technique, they showed how different phenomena influence the reactive distillation process, without using rigorous simulations. The advantages of this technique is that only physical and chemical data are required to estimate the

phenomena, both of which are independent of the structural design of the unit; and furthermore, only considering the key phenomena allows the designer to assess the process independently of equipment structure (Almeida-Rivera et al., 2004).

Currently, almost without exception, research in distillation is directed towards energy savings. More synthesis methods are constantly being sought to aid the design engineer in his task to devise the most efficient separation process. However, most synthesis methods require that a structure be determined before the actual mathematical design is performed, and thus the designer may have missed a significant opportunity in reducing energy costs by being constrained by existing equipment. What is really needed is a generalised method that allows at least preliminary insight into a design before resorting to rigorous and accurate modelling routines. This thesis thus centres on the Column Profile Map design methodology to design a great variety of distillation configurations, ranging from simple columns to thermally coupled columns to reactive distillation columns.

1.2 CONTRIBUTION OF THESIS

The main contribution of this work is to present new insights into distillation processes from a graphical point of view. The goal of the thesis is to expand the theory of Column Profile Maps and ultimately to provide steps to eventually design cheaper, energy efficient distillation structures, *before* resorting to time-consuming process simulation packages. This includes applying the methods to the design of new systems (Chapters 3, 4 and 5), highlighting interesting, potentially useful topology (Chapter 2) and proposing methods for rigorous computation for the purpose of design (Chapter 6).

1.3 THESIS OUTLINE

Each chapter in this thesis is constructed in the form of a journal article. Some of these have already been published, while others are due to be published in the future. Due to the fact that Column Profile Maps are a relatively new distillation synthesis tool there is a small degree of repetition in the introductions to each chapter, which covers the derivation and topological aspects of CPMs, but this should serve to strengthen the readers' understanding. Each chapter may thus be read independently of one another. A list of notable presentations and peer-reviewed publications, both in review and published, is given in on page 212 under Publications and Presentations. A brief outline of the thesis is given below:

Chapter 2 deals with Column Profile Maps, specifically for the special case when imposing a sharp split constraint on a column section. This constraint brings unique , interesting and previously unthought-of profile behaviour to the fore, and although it may not hold advantages in conventional column sections, it may find application in more complex structures with internal column sections.

Chapter 3 was completed at the University of Illinois at Chicago. The central idea behind this work is to apply the Column Profile Map technique to systematically and algorithmically find feasible designs for thermally coupled columns, traditionally very difficult columns to design, using a Temperature Collocation technique. The techniques shown in this chapter do not need to make simplifying assumptions regarding the product specifications or phase equilibrium as several current design techniques do, and rigorously ensures column feasibility by validation with state of the art process simulation software.

Chapter 4 builds on Chapter 3 to design multiple side rectifying and stripping units. The design tools presented here allows one to quickly assess feasibility for constant

volatility and sharp split systems. The unique manner in which results are presented allows one to find the minimum operating point as well as identify an Attainable Region and presents methods for quickly finding optimal structures, which severely depend on one's objective function of course. This work was done together with Ronald Abbas.

Chapter 5 covers the application of Column Profile Maps to the field of reactive distillation. The graphical nature of Column Profile Maps is shown to be very useful in understanding the simultaneous effect of chemical reaction, phase separation and mixing. An Attainable Region can be identified for a certain product specification which allows the designer to find the optimal combination of reactor size, column height and energy demand, and assess the counter-intuitive interaction between each.

Chapter 6 was also completed during my stay in Chicago. It presents several techniques for quickly and efficiently solving *all* pinch points in a given system, regardless of the number of components. Furthermore, it shows some interesting aspects of pinch point location and the influence it may have on certain, current design techniques.

Chapter 7 summarises the major results from this thesis and discusses the way forward.

Chapter 2: COLUMN PROFILE MAPS: APPLICATION TO SHARP SPLITS IN CONSTANT VOLATILITY SYSTEMS

This work has been prepared in the form of a paper for future publication. It has been presented at the AICHE annual meeting in Philadelphia, USA in 2008, and parts of it have been included in an overview of Column Profile Maps for the peer reviewed Foundations of Computer Aided Design (FOCAPD) conference journal in 2009 in Colorado, USA (see Appendix F: FOCAPD 2009 Summary Paper) It has also been published in Industrial and Engineering Chemistry under the title On Column Profile Maps: An analysis of sharp splits, 2011, 50 (10), pp 6331–6342. This work is entirely my own.

ABSTRACT

Column Profile Maps (CPMs) have recently been shown to be a useful tool in the design of distillation operations, especially complex configurations. CPMs are basically a family of composition trajectories for a single column section in a distillation column. They are essentially topological transforms of Residue Curve Maps, and are dependent on two main parameters: R_{Δ} (reflux ratio) and X_{Δ} (a pseudo composition vector), which effectively fixes the net flow in a column section. This paper focuses on the interaction between these parameters for the special case of sharp splits. With the CPM technique it has been shown that sharp splits behave differently to non-sharp splits, due to a phenomenon termed as "node bumping". In particular it has been shown that it is possible to sample an intermediate boiling component as a bottoms or distillate product when operating in certain ranges of R_{Δ}.

2.1 INTRODUCTION

In almost all industrial chemical processes, one or more chemical reactions take place to manufacture a wide range of products. Unfortunately, these reactions invariably produce by-products which severely affect the quality and therefore the market value of the final product. Thus, in almost all chemical processes a separation scheme of some sorts is required. There are numerous technologies available for this task, such as distillation, membrane separation, crystallization, etc., but of these available technologies, distillation remains by far the most common in the chemical industry.

Distillation is a commercial method of separating binary and multi component mixtures into individual pure components. Decades of work by researchers have made it possible for distillation to become one of the most widely used and effective methods of separation used in the chemical industry today. Unfortunately, distillation is a very energy intensive technique for separation. Ognisty conducted a study in the mid 1990's regarding the global effect of distillation, and estimated that energy inputs into distillation columns in the United States accounts for approximately 3% of the entire country's energy consumption(Ognisty, 1995). Approximately two thirds of the distillation energy is consumed by the petroleum refining industry, where it is widely used to separate crude oil into petroleum fractions, light hydrocarbons, and aromatic chemicals(Aristovich, 2004). Furthermore, it has been estimated that more than 55% of the total energy requirement for unit operations in today's petroleum refinery is expended to operate distillation processes(Mix, 1981).

Distillation exploits the fact the equilibrium composition of two or more chemical species are not equal across coexisting phases. The first attempts to describe distillation with a mathematical model was by Schreinemakers (Schreinemakers, 1902) and Sorel (Sorel, 1893). Much later, Van Dongen and Doherty proposed the use of Ordinary Differential Equations (ODE) to simplify the design procedure(Van

Dongen and Doherty, 1985a). While these ODEs model conventional rectifying and the stripping sections of a distillation column, they do not describe the transition from the rectifying to the stripping sections and are therefore no longer valid at the feed stage.

Graphical methods for designing distillation schemes have also been very popular. In 1925, McCabe and Thiele published a landmark paper on a graphical design method for binary distillation (McCabe and Thiele, 1925a). Residue Curve Maps have also been developed as a graphical method for designing multicomponent distillation systems. Residue Curve Maps are basically a range of trajectories that track the liquid compositions of the chemical species over time in a simple distillation operation. Residue Curve Maps can tell one much about the feasibility of separation and the nature of singular points, such as azeotropes and pure component vertices. Compositional changes for continuous rather than batch distillation can be represented by Distillation Curve Maps, which are from a mathematical point of view very closely related to Residue Curve Maps.

However, Residue Curve Maps and Distillation Curve Maps, have limitations in that they only give information at infinite reflux ratio, quite an impractical condition for the design engineer. Recently, in a series of papers by Tapp et al. and Holland et al. a new theory was explored in distillation: Column Profile Maps (CPMs) (Holland et al., 2004b, Tapp et al., 2004). CPMs were derived from an adaption of ODEs proposed by Van Dongen and Doherty (Van Dongen and Doherty, 1985a), which take into account the net molar flows and reflux ratios in a column section. CPMs were shown to display the same topological behaviour as RCMs, as well as being an extremely useful tool in distillation design by allowing the designer to set reflux ratios and net molar flows to suit the specifications of the separation. This contribution investigates interesting topological effects associated with CPMs for the special case where a sharp split constraint is placed on the process. These effects may have potential use

when designing unconventional column configurations which require multiple feeds or thermal coupling.

The paper is structured as follows: Section two gives a mathematical background of CPMs, briefly explaining what effects of operational parameters R_{Δ} and X_{Δ} are on the topological space. Section three introduces the special case where a sharp split constraint is imposed on a column section. Mathematical, as well as topological effects are covered in this section, concluding with validation and potential uses for these unique effects. Finally, section four presents several conclusions that may be drawn from this work.

2.2 BACKGROUND

2.2.1 DERIVATION OF COLUMN PROFILE MAPS

A CPM describes the behavior of a 3-component system by setting appropriate parameters such as the net molar flow and the reflux ratio. The first step in constructing a CPM is to define a column section, which is defined as "a length of column between points of addition or removal of material and/or energy"(Tapp et al., 2004).A generalized column section can be seen in Figure 2.1.

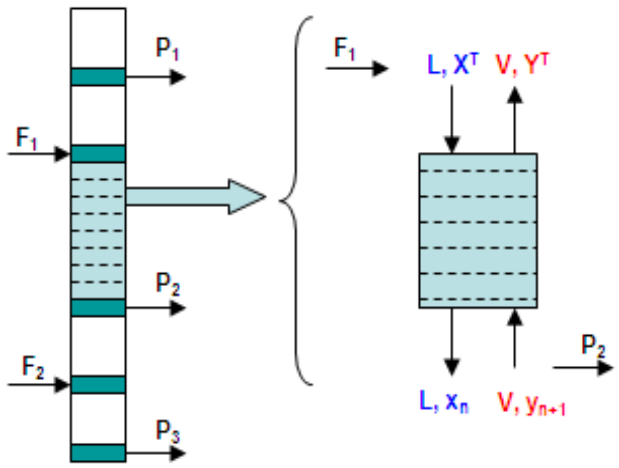


Figure 2.1: A generalised column section

A steady state material balance accompanied by a Taylor expansion over the highlighted section above yields:

$$\frac{dx}{dn} = \left(\frac{1}{R_\Delta} + 1\right)(x - y(x)) + \left(\frac{1}{R_\Delta}\right)(X_\Delta - x) \tag{2.1}$$

using the definition of R_Δ, a generalised reflux ratio:

$$R_\Delta = \frac{L}{V - L}, \tag{2.2}$$

and X_Δ, a compositional flux variable:

$$X_\Delta = \left(\frac{VY^T - LX^T}{V - L}\right) \tag{2.3}$$

Equation 2.1 is known as the Difference Point Equation (DPE). Its full derivation can be seen in Appendix G. By defining and fixing parameters R_Δ and X_Δ for a column section, one is effectively fixing the net flow in a column section (Δ=V-L), as well net flows of specific components ($X_{\Delta i}$). Once the aforementioned parameters are set, a CPM can be produced by integrating the DPE in positive and negative directions of n, where n is equivalent to the number of stages in a column. Negative integration can

be thought of as determining the composition profile from the bottom to the top, and vice versa.

Notice that in deriving the DPE that the vapour (V) and liquid (L) flowrates have been assumed to remain constant. This assumption is known as the constant molar overflow assumption and occurs quite frequently in distillation design methods because it reduces the complexity of the design equations significantly. The assumption essentially implies an energy balance for the column section and is generally a very good assumption for a wide variety of mixtures, but may be relaxed if needs be. The assumptions are exact when:

- The heat of mixing of components is zero
- All components have equal latent heats
- Zero heat loss through the column walls
- Negligible heat effects due to temperature

When taking a closer look at equation 2.4, it can be seen that at infinite reflux ratio ($R_\Delta = \infty$), the equation collapses to the residue curve equation:

$$\frac{dx_i}{d\zeta} = x_i - y_i \qquad (2.4)$$

The only difference between equations 2.4 and 2.5 is that the residue curve equation differentiation variable is time dependent, while in the DPE it is a variable representing stages. They are however identical in the x_1-x_2 composition space. Due to the fact that the residue curve equation and the DPE are not bound by physically relevant initial conditions, maps can be generated in the space outside of the Mass Balance Triangle (MBT). Using the assumption of ideal thermodynamics, a Residue Curve Map and a Column Profile Map can now be constructed (Figure 2.2 and Figure 2.3 respectively). In this paper and throughout this thesis, when the term ideal thermodynamics is used, it refers to assumption of constant relative volatilities. Thus

for our purposes $y_i(x) = \dfrac{\alpha_i x_i}{\alpha_1 x_1 + \alpha_2 x_2 + \alpha_3 x_3}$. Furthermore, unless it is otherwise stated the values used in this chapter are α_1 =3, α_2 =1, and α_3 = 1.5.

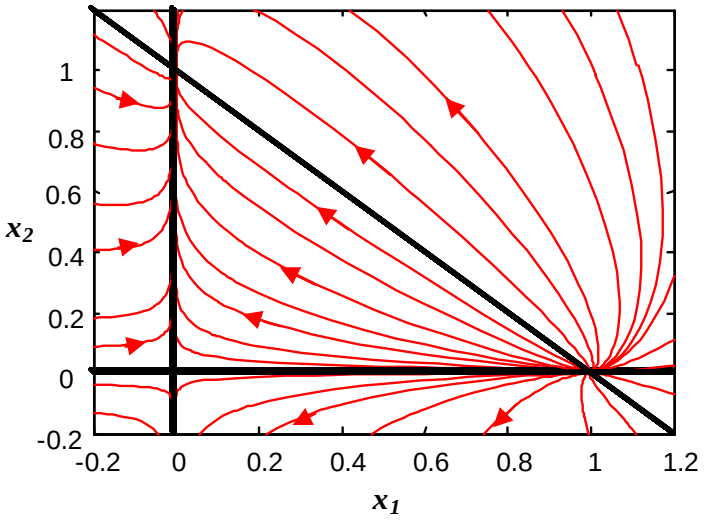


Figure 2.2 : A Residue curve map with curves shown inside the MBT, i.e. Σx_i=1 and $x_i \geq 0$; as well as outside the MBT where x_i<0.

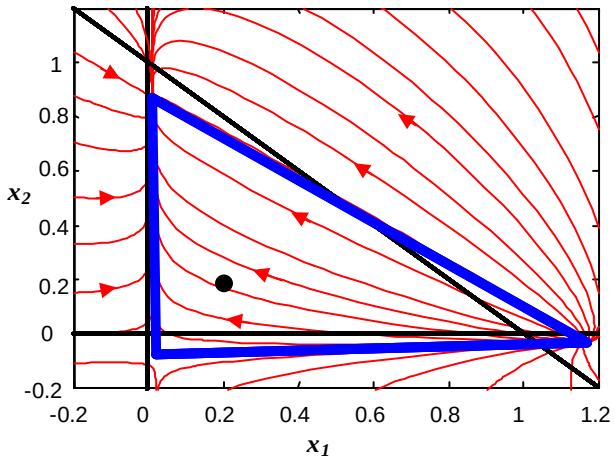


Figure 2.3 : A CPM with R_Δ= 9 and X_Δ = [0.2, 0.2] (marked with a dot) with a "shifted triangle" in blue indicating the movement of stationary points.

The two figures shown above illustrate that the CPM is topologically similar to the RCM. The stable node, i.e. the point **into** which all profiles run, that had been fixed

on the pure x_2 vertex in Figure 2.2, has been shifted within the MBT. The unstable node, i.e. the point **from** which profiles run, as well as the saddle point have also been shifted, which in effect means that a much wider range of separations are feasible than previously thought. The shifting of the nodes is dependent on fixing parameters R_Δ and X_Δ in a specific way.

The shifting of nodes in the composition space can hold various advantages for the design engineer. For example, if there was an azeotrope present in the system (this is impossible for ideal systems, but it's just used here to illustrate the use of CPMs), the profiles could in theory be shifted in such a way as to move the azeotrope outside the MBT by combining R_Δ and X_Δ in a specific manner, thus allowing one to achieve a separation past the azeotrope (Holland et al., 2004a, Tapp et al., 2004).

The coordinates of the nodes can be determined by algebraically solving the DPE=0. For an ideal system, nodes will always be connected by straight lines. By connecting these nodes, one can see that the shifting of nodes has lead to the phenomenon coined by Holland et al. as "moving triangles". They have shown that CPMs can be used with great effectiveness to understand complex column configurations (such as the Petlyuk column) and that new and exciting designs can be thought of through creative parameter selection (Holland et al., 2004b).

2.2.2 THE EFFECT OF R_Δ

The parameter R_Δ is defined as $\frac{L}{V-L}$. From the DPE it can be observed that when $R_\Delta = \pm\infty$, the DPE reduces to the Residue Curve equation. Thus, at infinite reflux ratio the nodes are not shifted in space and all of the nodes lie on the pure component vertices of the MBT. It therefore follows that in general, the further one moves from infinite reflux, the further the nodes are typically shifted from the MBT's pure component vertices. $R_\Delta \rightarrow 0$ will thus be the case where the nodes are shifted the

furthest away from the MBT's pure component vertices. An illustration of the general trend and the effect of R_Δ can be seen in the figure below, for an arbitrarily chosen X_Δ. Notice that the path (the pinch point curves) the triangles move on always pass through the pure component vertices of the MBT. Furthermore, notice that the pinch point curve passes through X_Δ. The pinch point curve always passes through X_Δ since there always exists a solution where the node or singular point corresponds to X_Δ.

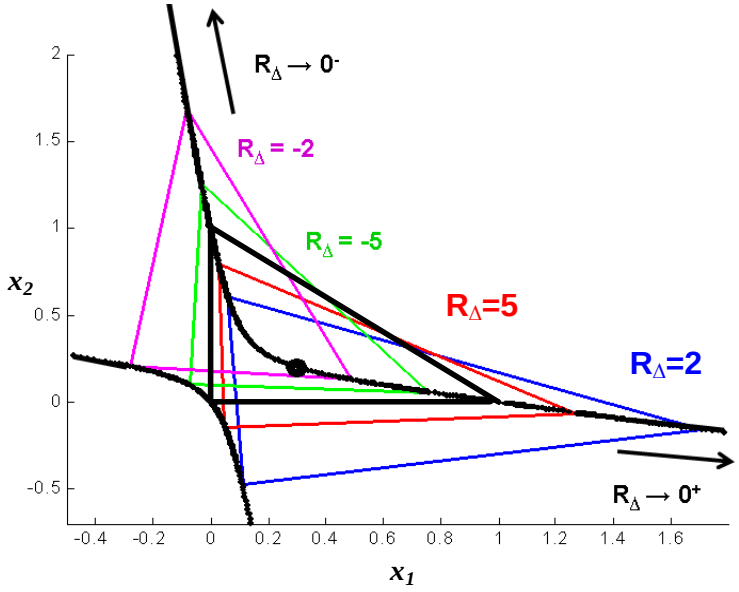


Figure 2.4: Movement of Transformed Triangles with varying reflux ratio for X_Δ = [0.3, 0.2]

It is important to point out that the reflux ratio can be both positive and negative. When a column section is said to be in rectifying mode, the vapour flow is larger than the liquid stream, resulting in positive refluxes. Conversely, when the column section is in stripping mode, the reflux ratio is less than zero as the bulk of the material is flowing downwards with the liquid stream.

2.2.3 THE EFFECT OF X_Δ

The X_Δ parameter can be thought of as fixing the compositional net molar flow in a column section. It may be placed anywhere in the composition space, even outside the MBT. A negative value for $X_{\Delta i}$ simply indicates a component flowing downwards in a column section. The only situation where X_Δ need be a physical composition is when a column section is terminated by a total reboiler or condenser.

As the pinch point curve always passes X_Δ, one can expect very different pinch point behaviour for a specific placement of X_Δ. In fact, Holland et al. identified 7 different regions of X_Δ placement in the composition space which each display unique pinch point curvature for an ideal system. The boundaries of the 7 distinct regions correspond to the extended axes of the MBT, which also corresponds to a change in the direction of the net flow of a component in a column section. Figure 2.5 a-g shows these regions along with the general trend of pinch point curves for each region.

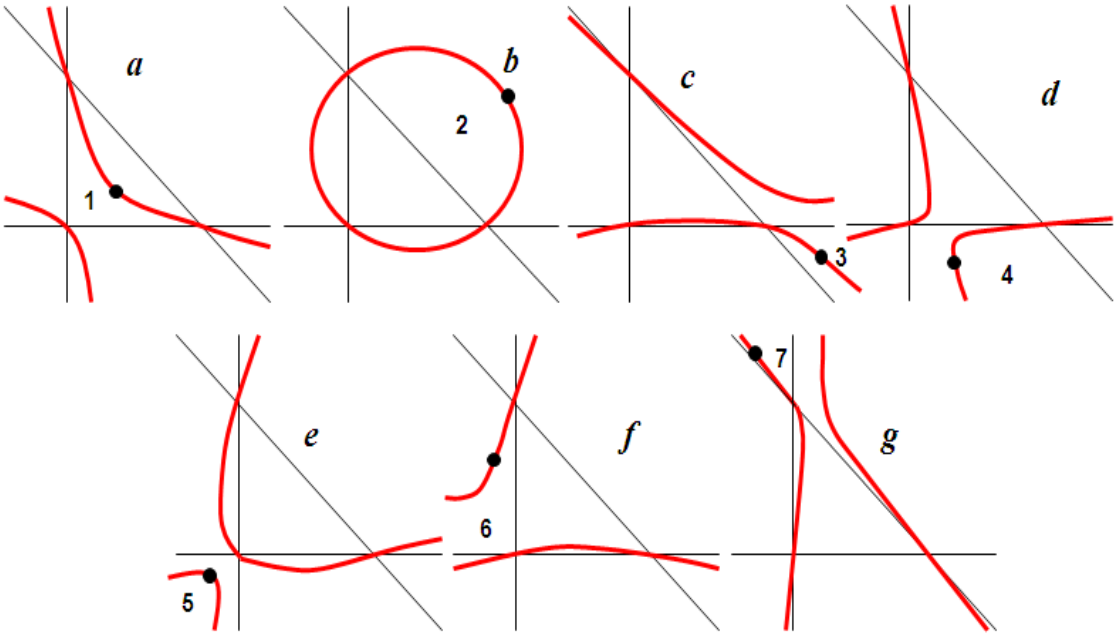


Figure 2.5 a-g: Pinch point locus behaviour for different placements of X_Δ

It is important to note that conventional one-feed-two-product columns only make use of the flow pattern in Figure 2.5 a. There are thus potentially six other flow patterns which the designer is missing out on which could influence topology in a desirable way. Importantly, flow patterns 2 and 5 in Figure 2.5 b and e do not contain any pinch points within the MBT, meaning that, theoretically, composition profiles can be constructed which do not pinch anywhere in the MBT and can therefore run from one side of the MBT to the other. Understanding the way in which the parameters X_Δ and R_Δ influence the topology of a CPM can be very useful for a design engineer. With knowledge of the effects and interaction of the aforementioned parameters, one is able to place nodes anywhere in the composition space to suit the requirements of the separation. However, it should be made clear that this is not necessarily a simple task. This is mainly due to the fact that distillation structures, as they are currently thought, are made up of a network of columns sections. These column sections are all related by mass balances, thus choosing particular flow behaviour in a certain column section will have, perhaps undesirable, effects on other column sections in the structure. Nevertheless, Holland et al. showed that some of these unconventional operating column sections may indeed be found in structures like the Petlyuk column (Holland et al., 2010) and distributed feed columns (Holland, 2005). A simplified Petlyuk problem where topology was placed at will to affect a certain separations was also demonstrated by Holland and co-workers (Holland et al., 2004b).

2.3 SHARP SPLITS

In the previous section, it was shown how CPMs are derived and how they differ from RCMs. Furthermore, it was shown what effects parameters X_Δ and R_Δ have on profiles and how they might influence design. However, during the study of CPMs thus far, very little attention has been given to sharp splits. Sharp splits are useful cases to look at as invariably when designing a distillation column, the objective is to

achieve bottoms, distillate and sidestream products that are either entirely pure or entirely depleted of a component. The results achieved for sharp splits are quite unique and differ somewhat from conventional "sloppy splits". This section focuses solely on sharp splits.

2.3.1 PINCH POINT CURVES

The previous chapter showed that different placements of X_Δ result in different pinch point curve behaviour. Sharp splits are special cases in CPM theory, as X_Δ no longer lies in one of the 7 distinct regions as shown in Figure 2.5, but on the boundary of these regions. Thus a sharp split product specification presents an interesting case not only from a practical point of view, but also from a mathematical point of view.

Figure 2.6 shows the pinch point curve for X_Δ = [0.5, 0] for an ideal system. It shows that the pinch point curves no longer have any curvature, but they are in fact linear. It is also important to point out that pinch point curves can never cross. Although at first glance it seems as if they're crossing, they are only "meeting" at a point and then going in a different direction.

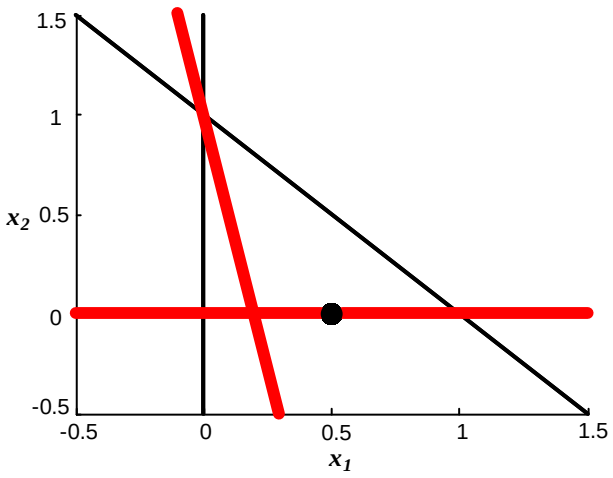


Figure 2.6: Pinch point curve for X_Δ = [0.5, 0]

The pinch point curve for a choice X_Δ that lies on the boundary of two regions can be thought of as a hybrid of the pinch point curve properties of two regions. For instance, if X_Δ is chosen to lie on the boundary of region one and five (see Figure 2.5), the pinch point curve displays properties of both regions. This effect can be seen in Figure 2.7. The closer X_Δ moves to the boundary of a region, the more linear the pinch point curves become. The color-coded arrows in Figure 2.7 illustrate the way and the direction in which pinch point curves move when approaching the boundary, i.e. a sharp split. It can also be seen that the pinch point curves do not intersect, but merely meet at a point.

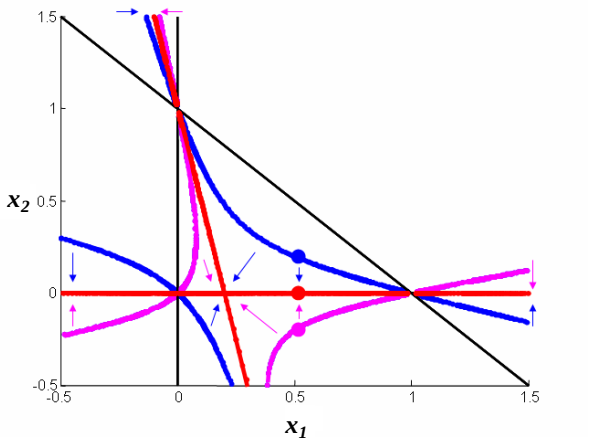


Figure 2.7: Pinch point curve behaviour for a sharp split

2.3.2 TRIANGLE SHIFTING

In previous sections we have seen that the "moving triangles" are shifted along the pinch point curve for a specific choice of X_Δ. Furthermore, the pinch point curves for a sharp split were shown to be linear. Since the pinch point curves for sharp splits differs somewhat from non-sharp splits, one expects that that the movement of the "moving triangles" also to be different. Consider then the case where X_Δ = [0.3, 0.2] (Figure 2.4), i.e. a "sloppy" split, and compare its triangle movement with a case where X_Δ = [0.5, 0], i.e. a sharp split (Figure 2.8).

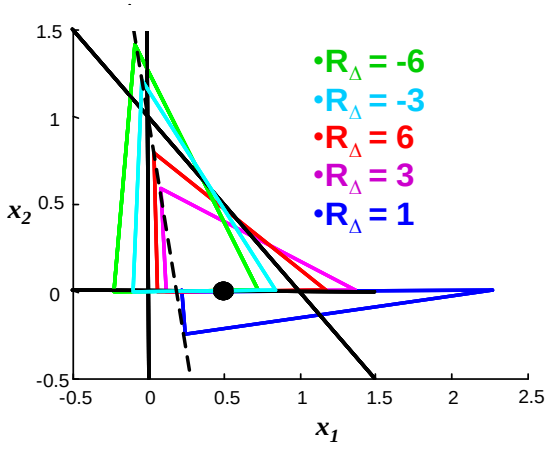


Figure 2.8: Triangle movement for X_Δ = [0.5, 0]

Notice how the triangles move along the pinch point curve in Figure 2.8. Observe that one side of the transformed triangle is always fixed to the MBT, the same side to which X_Δ is fixed. Moving from the purple triangle (R_Δ=3) to the blue triangle (R_Δ=1) in Figure 2.8 is of particular interest. Notice how the blue triangle (R_Δ=1) has suddenly flipped over, but still remains on the pinch point curve. As R_Δ becomes smaller from a large positive number, the triangles become smaller, until a point is reached where the triangle collapses completely. This collapsing of the Shifted Triangle takes place at a specific value of R_Δ, at the point where the 2 pinch point curves meet. We shall name this point the "bumping point"; the reason behind this will become apparent in the subsequent sections. From the bumping point, by making R_Δ smaller yet the triangles flip over and grow infinitely large as $R_\Delta \rightarrow 0$. Similar behaviour can be seen with regard to the movement of triangles when X_Δ is chosen on the other boundaries of the extended MBT.

2.3.3 CLASSIFICATION AND BEHAVIOUR OF NODES

In order to achieve a better understanding of what happens to the nodes when a collapsing of the Shifted Triangles occurs, it is necessary to firstly understand how nodes are defined in the composition space. The nature of nodes are discussed at

R_Δ=±∞ with the aid of an eigenvalue map, which is a useful illustration of singularity regions. It shows discrete node regions in the composition space, and is independent of the placement of X_Δ.

The nature of a singular point can be determined by solving the Jacobian matrix (***J***) when the DPE=0 such that $J(X_S) = [a_{ij}]$, where a_{ij} are entries of the n×n matrix A (the DPE matrix), and then calculating the eigenvalues λ_1 and λ_2 of matrix A. Nodes can then be classified according to the signs of λ_1 and λ_2. See Appendix A: Node Derivation and Classification. From this information one can generate an eigenvalue map as in Figure 2.9.

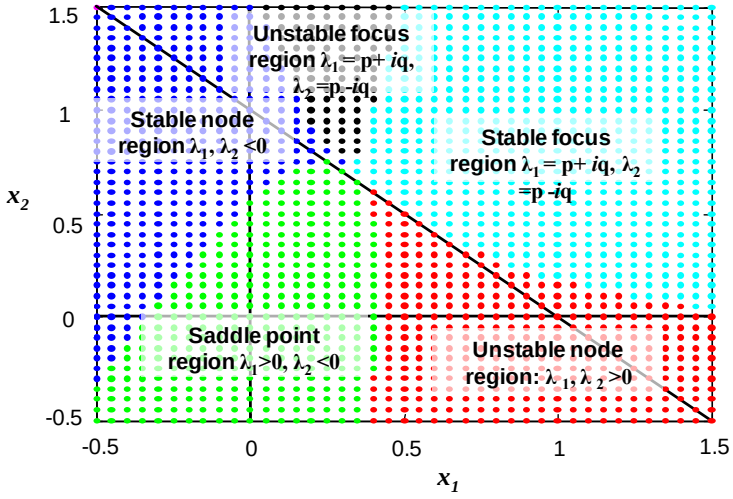


Figure 2.9: Eigenvalue map for x_i = [-0.5....1.5] at R_Δ=± ∞

The eigenvalue map above shows distinct regions of similar nodes in a RCM. By manipulating R_Δ these regions are also shifted in composition space. The 3 major nodes in CPMs are the stable and unstable nodes, and the saddle point. A region of complex eigenvalues is present outside the MBT, which is always the case.

2.3.4 NODE BUMPING

Once the nature of the nodes has been understood, a greater insight into the collapsing of triangles, i.e. the node bumping effect may be seen. To study the node

bumping effect for sharp splits, we shall study the case where X_Δ= [0.5, 0] (Figure 2.8), which can be seen as a binary sharp split. Figure 2.10 shows the CPM, with the accompanying shifted triangle and the classification of the nodes at R_Δ = 2. For this CPM, and for every CPM that follows, a red X will denote a stable node, a red circle will denote an unstable node and a red square will denote a saddle point. Furthermore, the blue triangle will always denote the shifted triangle and the black triangle will denote the MBT.

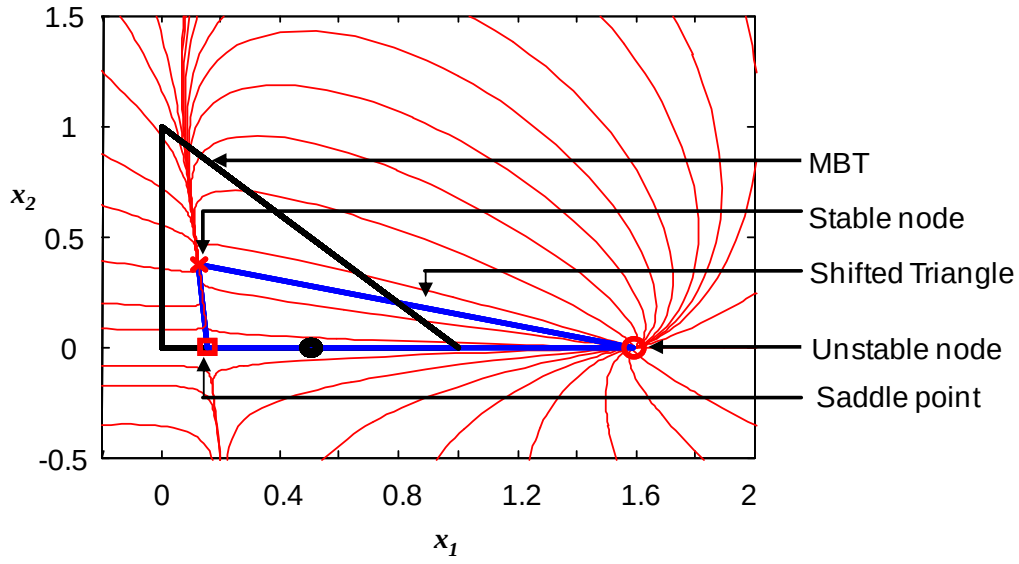


Figure 2.10: CPM with shifted triangle and node classification at R_Δ= 2 and X_Δ = [0.5, 0]

The shifted triangle shown above is in accordance with the trend shown in Figure 2.8. Notice the position of the saddle point as well as the stable node. Consider now a system where the triangle has been flipped over. Taking the same X_Δ as in the previous figure, but letting R_Δ=1, the following CPM can be seen.

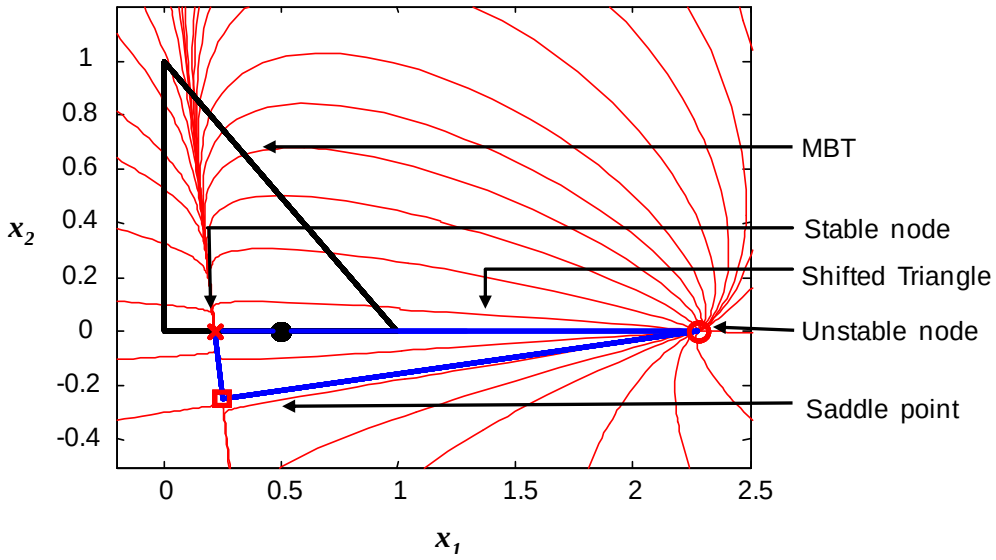


Figure 2.11: CPM with shifted triangle and node classification at R_Δ=1 and X_Δ = [0.5, 0]

Figure 2.11 makes for interesting viewing as it shows that the profiles, and nodes, have been altered by simply changing R_Δ by a relatively small amount. Notice the position of the saddle point and the stable node and how they have changed from Figure 2.10. The stable node has now replaced the position of the saddle point and as a consequence the profiles within the MBT have been changed dramatically. This is what is referred to as "node bumping", as the stable node has "bumped" the saddle point from its position.

The node bumping phenomenon could open the door to a much wider range of separations. Due to the fact that a stable node has been fixed on the x_1 axis, all the profiles in the MBT are in fact running into that point and one could separate close to that point with a finite number of stages. This was not the case when a saddle point was present on the axis where profiles were bending away from it. A stable or unstable node is generally a desirable property in distillation design as these points can be removed as bottoms or distillate products, respectively. Conversely, saddle points imply that these points cannot be sampled in a simple column section as there are no profiles running into or away from it.

Although the node bumping could make many more separations viable, it raises new questions such as: What happens to the nodes at the bumping point? At what R_Δ will the bumping occur? These questions will be addressed in the following sections. It is useful to note here that this analysis of bumping points is a strong function of the thermodynamics of the system. Thus, the exact answers obtained from the following calculations are only as accurate as the thermodynamic models used to predict phase equilibrium. Although the techniques can be applied to any phase equilibrium model, only constant volatility systems are used here.

2.3.5 THE CRITICAL R_Δ

As the profiles in the MBT are dramatically changed by the node bumping effect, the next logical steps to take are to determine where and why the bumping is taking place, as well as determining exactly what is happening to the nodes at this point. This would give us a better understanding of sharp split behaviour and could later assist the design engineer when designing the final column, as designing a column where a stable node is present (all profiles move into the stable node) is vastly different to the design of a column where a saddle point is present (all profiles swerve away from the saddle).

The eigenvalues in CPMs are independent on the placement of X_Δ, and are only dependent on R_Δ, the coordinates of the node being considered and the thermodynamics of the system. Thus by choosing an x_1-x_2 coordinate and specifying a value for R_Δ, the nature of the node can be determined. Thus to analyze the eigenvalues at the bumping point we have to calculate where exactly this point lies. With the knowledge that the pinch point curves for a sharp split are linear, and that the node bump takes place at the meeting point (i.e. the intersection) of the 2 curves, the bumping point can be easily calculated with simple geometrical maths. (see Appendix B: The bumping points). For the case study where X_Δ = [0.5, 0], the bumping point occurs at [0.2, 0]. It now becomes clear that one of the two

requirements for calculating eigenvalues at the bumping point is given, namely the x_1-x_2 coordinate, but a value for R_Δ is still required.

.

This hurdle can be overcome by taking a range of values of R_Δ for the specified x_1-x_2 coordinate, and tracing the two accompanying eigenvalues. This can be illustrated in a graph, called the *Zone-graph*. A Zone-graph for the example above can be seen in Figure 2.12. The Zone-graph shows when fixing a node in the composition space ([0.2, 0] in this case) how the nature of the nodes change when changing R_Δ.

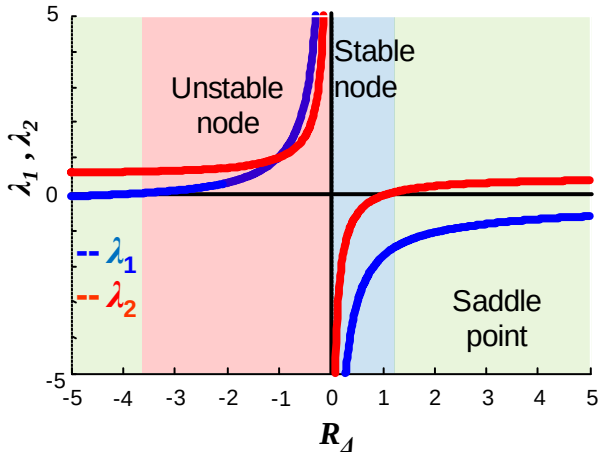


Figure 2.12 Zone-graph for X_S = [0.2, 0]

Recall that a stable node is characterized by both eigenvalues being negative, an unstable node by two positive eigenvalues, and a saddle point when the eigenvalues have opposite signs. By looking at the graph one can see at a large positive value for R_Δ (e.g. at R_Δ = 2) one can see that the both eigenvalues, i.e. the red **and** the blue line, have opposite signs and thus can be classified as a saddle. As one moves to smaller positive values of R_Δ there is a specific point, *the critical* R_Δ, where both the red and the blue lines become negative, which corresponds to a stable node.

In the example above we have seen that the stable node has "bumped" the saddle point from its position. By analyzing the Zone-graph above it can be seen that the transition between saddle point and stable node occurs when one of the eigenvalues are equal to zero. It can thus be said that a node bump will take place where either

one of the eigenvalues are equal to zero, as this is the point where nodes change their nature. By using this knowledge, the critical R_Δ can be calculated by finding the solution where the eigenvalues are 0. Generally, solving for R_Δ when the eigenvalues are 0, results in 2 critical values for R_Δ. For the particular scenario mentioned above, these critical values are found to be: R_Δ=-3.5714 and R_Δ=1.25. For this case, R_Δ=1.25 is the important solution as this corresponds to a saddle point-stable node bump. (R_Δ =-3.5714 represents a saddle point-unstable node bumping at X_S= [0.2, 0], but this is for a different selection of X_Δ). An eigenvalue map can be seen in Figure 2.13.

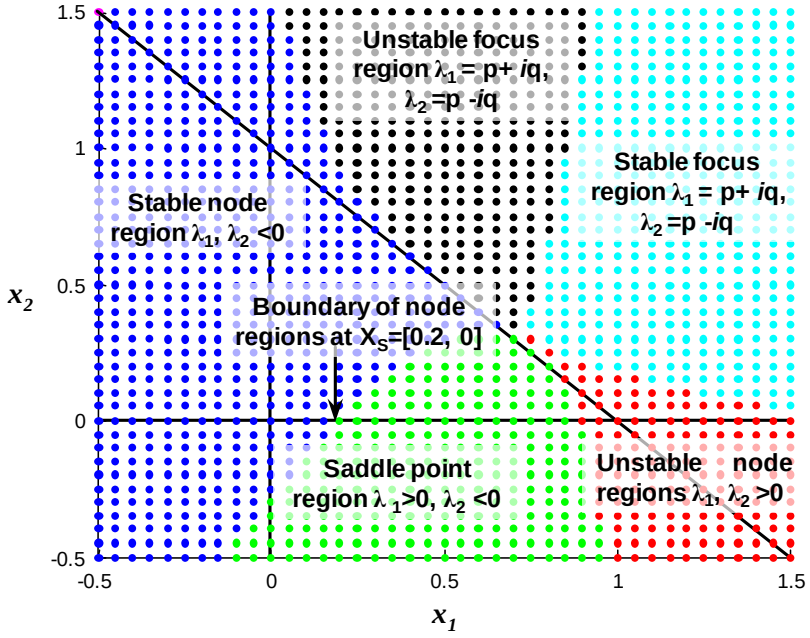


Figure 2.13: Eigenvalue map for x_i = [-0.5...1.5] at R_Δ=1.25

A CPM at the critical R_Δ for this specific case study can be seen below. An eigenvalue equal to zero corresponds to a hybrid node, and one can see that that at the bumping point [0.2, 0], the triangle has collapsed and a hybrid node has formed. In this case the node is classified as an asymptotically stable half-node/saddle. Notice how this node behaves as a saddle **and** a stable node. The existence of this type of node brings another type of node to the fore, an asymptotically unstable node. This

type of node occurs when both the eigenvalues are equal and positive. However, as can be seen from Figure 2.14 it behaves like an unstable node.

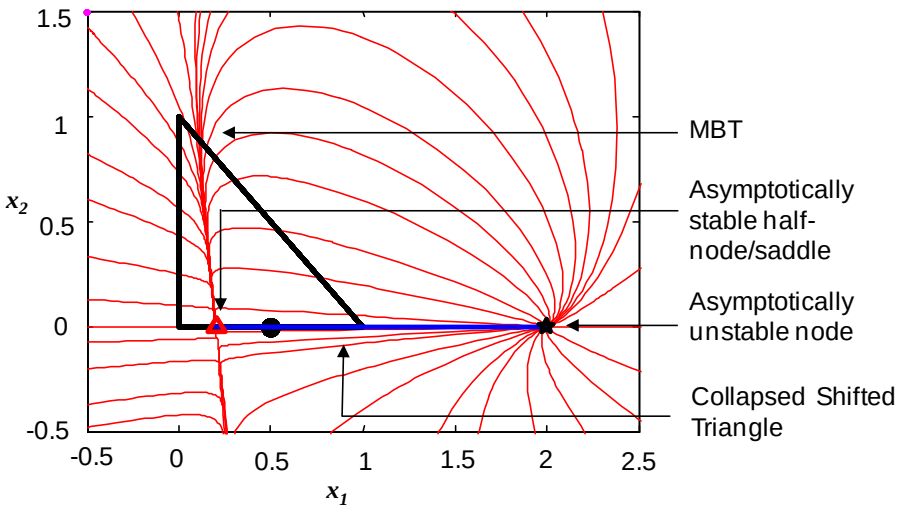


Figure 2.14: CPM for X_Δ = [0.5, 0] and at the critical R_Δ =1.25

From a design point of view, Holland et al. showed that if the transformed triangle in CPMs can be found algebraically by simply specifying R_Δ and X_Δ, then the reverse must also be true: By knowing the fixed points of a CPM transformed triangle, R_Δ and X_Δ can be determined. In fact, by only specifying R_Δ, only the value of one fixed point is required to determine the difference point, X_Δ. This is a very important result, because it implies that the designer can now set the position of the transformed triangle to meet the needs of the separation. However, with the use of Zone-graphs, one is now able to not only select the position of the transformed triangle, but the nature of a node too. A Zone-graph is not limited to sharp splits either. Thus, one could manipulate profiles with the help of Zone-graphs to achieve the separation required in a column section.

It has been shown that the node bumping phenomenon has potential to transform profiles such that a much wider range of separations are possible. However, only binary sharp splits have been considered, i.e. splits that occur on the sides of the

MBT. The next section will focus on ternary sharp splits, which present a whole new set of possibilities.

2.3.6 TERNARY SHARP SPLITS

Ternary sharp splits are very special cases in CPM theory, since this represents the case where X_Δ lays on either one of the three the vertices of the MBT. Ternary sharp splits do not only display pinch point behaviour of 2 regions, but of 4 regions. Since a separation process where a 100% pure component is produced is invariably the ultimate separation process, ternary sharp splits are of particular interest. Following the same route as for binary sharp splits, consider the movement of triangles with the accompanying pinch point curves for a ternary sharp split. Figure 2.15 shows this for X_Δ fixed at [0, 0] (the intermediate-boiler vertex).

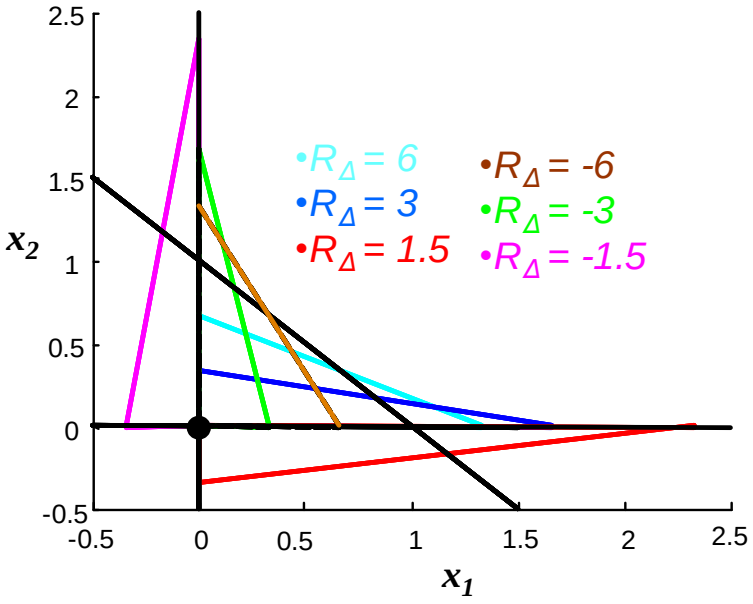


Figure 2.15: Triangle movement for X_Δ= [0, 0]

It can be seen from Figure 2.15 that when placing X_Δ at the vertex of the MBT, two sides of the Shifted Triangle are fixed to the MBT, or in other words, a corner of the

Shifted Triangle is fixed to a vertex of the MBT. This effectively means that a node is always fixed on a vertex of the MBT when X_Δ is fixed onto a vertex. The figure also shows the node bumping phenomenon (flipping over of triangles), both for positive and negative values of R_Δ. Notice that the pinch point curves for this scenario cascade to the sides of the MBT. For ternary sharp splits it is thus unnecessary to determine the bumping point (i.e. the meeting of pinch point curves), since this point occurs at X_Δ itself. The bumping point is thus at [0, 0] in this example.

Zone-graphs are particularly useful when looking at ternary sharp splits, since a node is always fixed to X_Δ. This means that one can track the nature of the node, and thus the direction of the profiles running into X_Δ. The Zone-graph for this system can be seen in the Figure 2.16. This figure also shows the different R_Δ values where node bumping occurs (i.e. the R_Δ value when one of the eigenvalues is equal to zero).

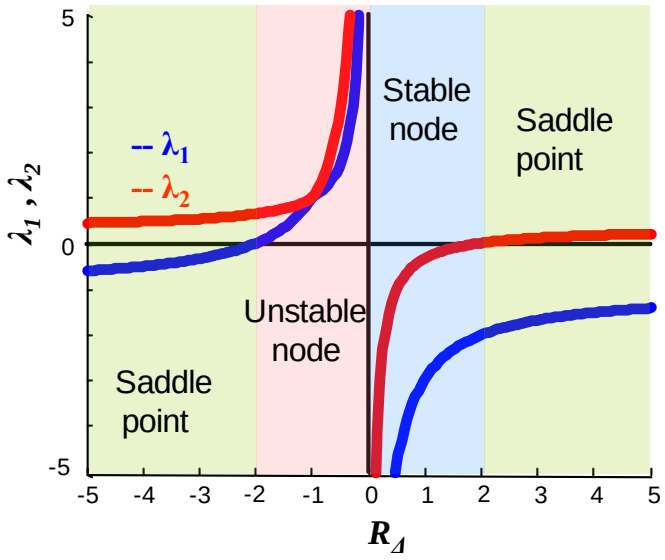


Figure 2.16: Zone-graph for X_Δ = [0, 0] with the critical R_Δ values

This Zone-graph tells a fascinating story, as it shows that when R_Δ<-2, the node fixed at the intermediate-boiler axis ([0, 0]), will always be a saddle point (eigenvalues have opposite signs). A node bump occurs at R_Δ=-2 after which the node turns to an

unstable node. For values of R_Δ such that $0<R_\Delta<2$, the node fixed at the [0, 0] vertex is stable, and returns to a saddle point for $R_\Delta>2$.

This means that when operating a column section in the $0<R_\Delta<2$ range one would have profiles running straight into the [0, 0] vertex. This interesting result could thus allow one to sample the intermediate boiler in a single column section as a bottoms product. A CPM that illustrates this can be seen in Figure 2.17.

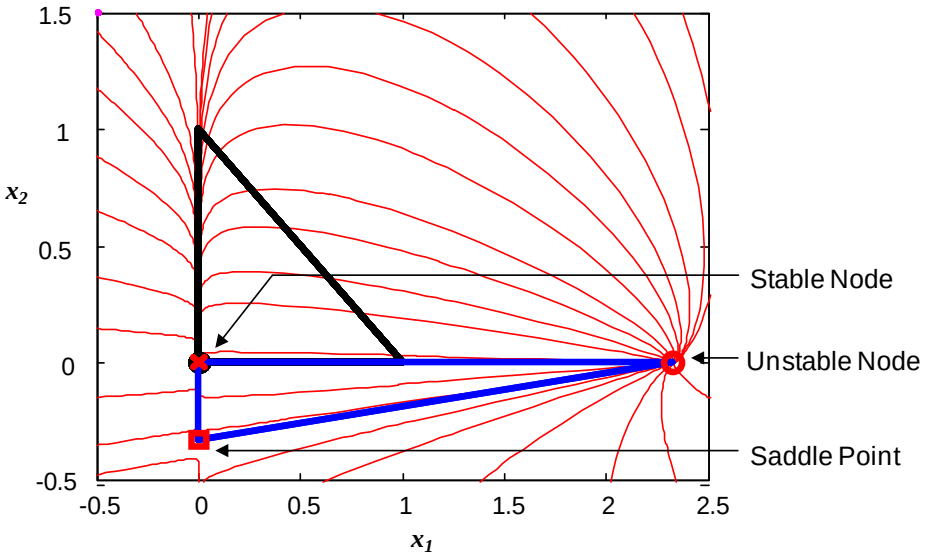


Figure 2.17: CPM for X_Δ = [0, 0] and R_Δ = 1.5

One can in a similar manner generate Zone-graphs for the other 2 pure-component vertices. Once again these graphs are extremely useful. Looking at the case where X_Δ = [1, 0] (Figure 2.18), the graph shows the regions where certain separations are or are not possible. The $0<R_\Delta<0.5$ region will result in a stable node and profiles will run straight into the high-boiler vertex. Conversely, operating in the $0.5<R_\Delta<1$ range results in saddle point region, making this separation much more difficult.

Looking at Figure 2.19 in the same way for X_Δ= [0, 1], one can see that $-1.5<R_\Delta<-3$ range represents a saddle region. Thus, if one wishes to remove a pure low-boiling

component from a ternary mixture, it would be advisable not to operate in this range. The Zone-graphs are a novel way of representing operating zones for ternary sharp splits. They show new and interesting possibilities for new separation schemes, most notably to potentially remove purely the intermediate-boiler from a multicomponent feed as a distillate or bottoms product.

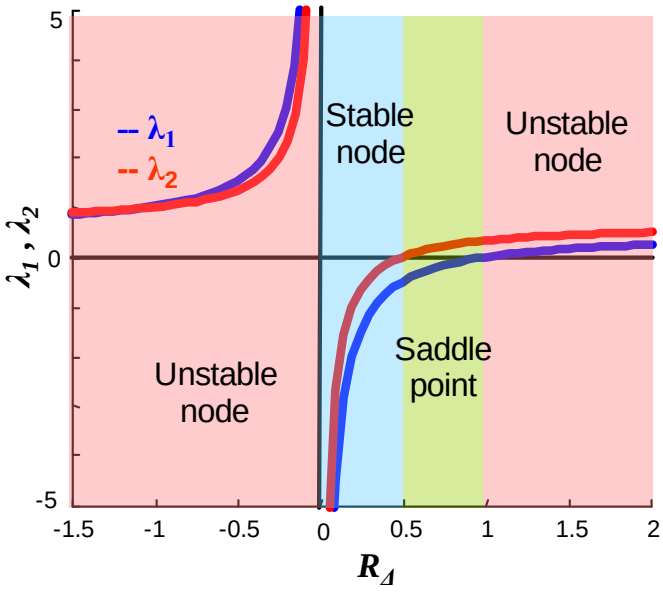


Figure 2.18: Zone-graph for X_Δ = [1, 0] with the critical R_Δ values

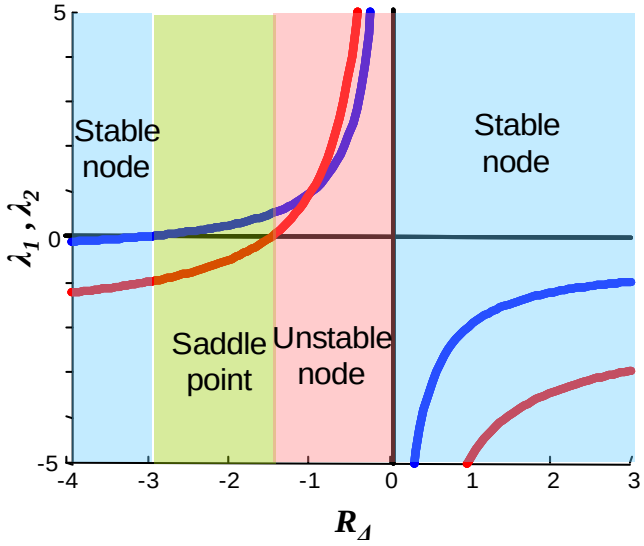


Figure 2.19: Zone-graph for X_Δ = [0, 1] with the critical R_Δ values

2.4 VALIDATION AND POTENTIAL APPLICATION

The CPMs presented in the preceding discussions may at first glance appear to be counter intuitive, as the nature of separations may almost be altered at will by the designer. To validate our findings, we have simulated a single column section in AspenPlus at two different refluxes whereby a sharp split condition is imposed on the column section. The n-nonane (heavy), n-octane (intermediate), n-heptane (light) system can be modelled extremely well with constant relative volatilities of 4 and 2 for n-heptane and n-octane relative to n-nonane, respectively. We shall demonstrate the case where X_Δ=[0, 0], i.e. where X_Δ is fixed to the intermediate n-octane vertex, at two refluxes of R_Δ, 4 and 0.5 respectively. With this known, Column Profiles may be constructed for both scenarios, as shown in Figure 2.20, with an entering liquid composition of [0.4, 0.4], illustrated with the red dot.

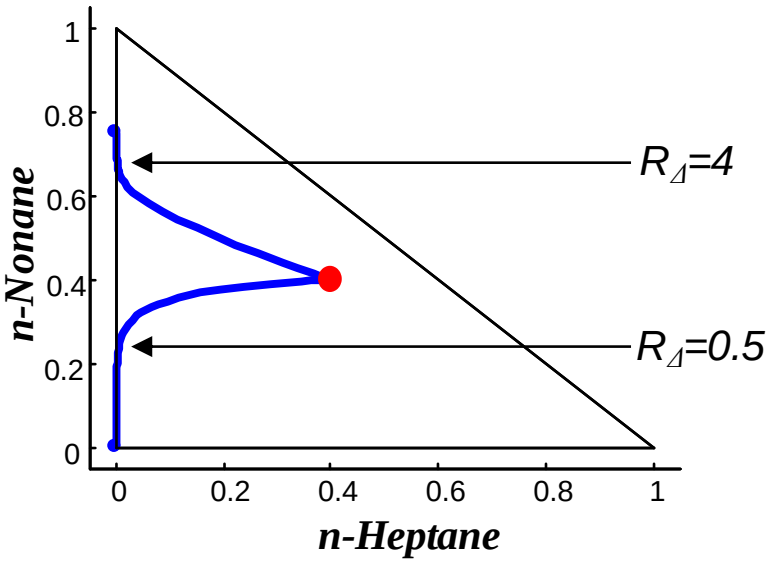


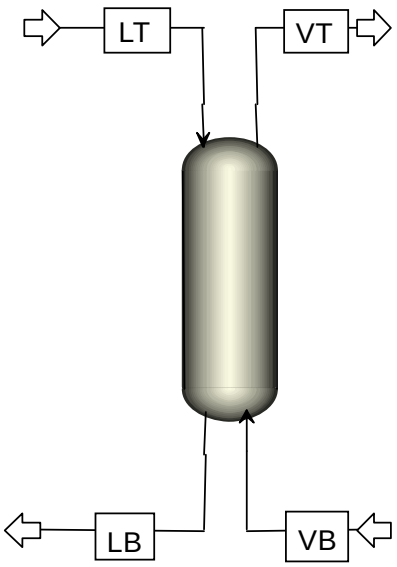
Figure 2.20: Column Profiles for X_Δ = [0, 0], with R_Δ = 4 and R_Δ = 0.5 respectively

Figure 2.20 shows that the profiles for R_Δ=4 and R_Δ=0.5 run in two distinct directions. When R_Δ=0.5, a stable node is fixed to the n-octane vertex, and hence the profiles runs directly towards this point. The stable node has effectively bumped the saddle from this vertex. For the case where R_Δ=4 the stable node is located higher up on the

axis, causing profiles to run towards this point. Using the AspenPlus simulation package, a generalized column section may be modelled using the RADFRAC modelling block, and the effects described above can be validated. The AspenPlus results are summarized for both refluxes in Table 2.1. The R_Δ=4 scenario may be seen in Figure 2.21 a, where the liquid is enriched to an n-nonane composition of approximately 0.85. Similarly, the R_Δ=0.5 scenario is shown in Figure 2.21 b.

Table 2.1: Summary of stream table data for the two reflux ratio scenarios generated with a Radfrac column in AspenPlus, as annotated in the far right column.

R_Δ=0.5, X_Δ=[0,0]					***AspenPlus Radfrac column***
	Mole flows	*x*-Heptane	*x*-Octane	*x*-Nonane	
LB	1.117	0.000	1.000	0.000	
LT	1.000	0.400	0.200	0.400	
VB	3.000	0.000	1.000	0.000	
VT	2.883	0.139	0.723	0.138	
X_Δ	-	0.000	1.000	-0.000	
R_Δ=4, X_Δ=[0,0]					
	Mole flows	*x*-Heptane	*x*-Octane	x-Nonane	
LB	1.025	0.000	0.150	0.850	
LT	1.000	0.400	0.200	0.400	
VB	1.200	0.000	0.250	0.750	
VT	1.125	0.356	0.295	0.349	
X_Δ	-	0.004	1.055	-0.059	



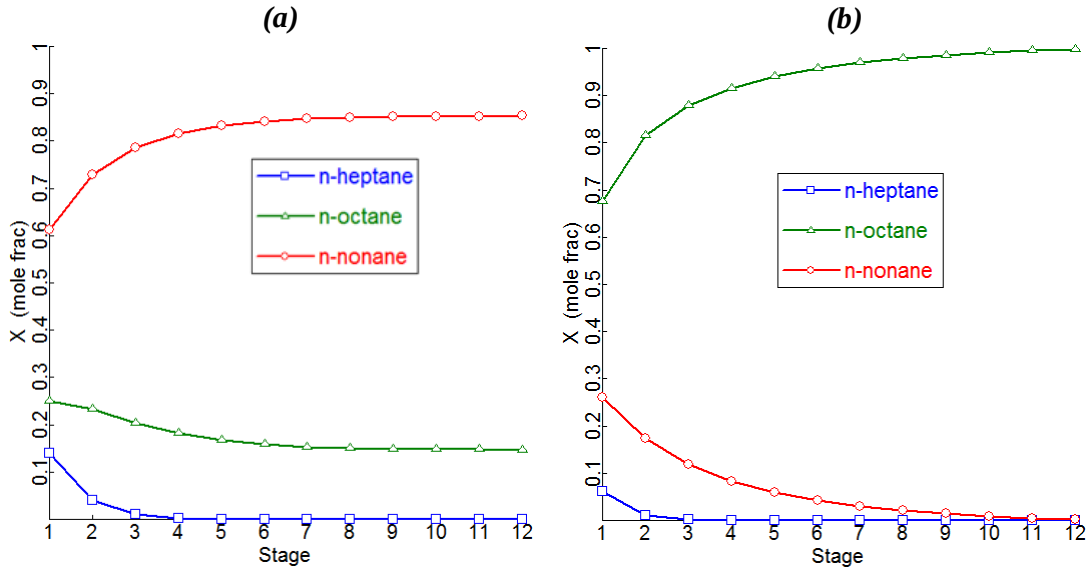


Figure 2.21: Liquid composition profiles using Aspen Plus for X_Δ = [0, 0] with (a) R_Δ = 4 and (b) R_Δ = 0.5.

The compositional trends generated through AspenPlus in Figure 2.21 a and b generally agree with those predicted through the CPM technique shown in Figure 2.20. Minor discrepancies in the exact value of X_Δ in Table 2.1 can be attributed to the assumption of constant molar overflow in the Difference Point Equation (notice that VT≠VB and LT≠LB in the Aspen simulations). The exact initial composition does not appear in Figure 2.21 a and b because the stage calculation starts from one, and not zero, in AspenPlus. Although the nature of stationary points on the intermediate boiling axis have changed from a saddle in the R_Δ = 4 case to a stable node in the R_Δ = 0.5 case, it appears as though this phenomenon does not necessarily affect a potential separation desirably. For instance, at R_Δ = 0.5 the column requires three times more vapour than liquid, thus producing a pure n-octane liquid stream requires three times more pure n-octane in the vapour stream to maintain the sharp split constraint. A similar result for a multicomponent hydrocarbon mixture may be seen in Appendix C: Multicomponent Example. Although such a column section may not be of practical use in conventional columns, it is important however to point out that there are unique regions of reflux ratio ranges which result in very different

profile behaviour. Thus, feeding pure octane vapour does not necessarily mean that a pure octane liquid can be produced, depending on the specific reflux ratio chosen and the node that is placed on the pure octane vertex.

Single column sections typically aren't considered meaningful pieces of separation equipment on their own, as distillation columns consist of a network of column sections. It is thought that the node bumping phenomena with a sharp split restriction imposed on it has a more practical use in non-simple column configurations that require internal column sections. That is, column sections that don't have final product cuts, but are merely situated between points of material addition or removal in a column. Examples of columns requiring such column sections include multiple feed-or-product columns, prefractionating columns, thermally coupled columns such as the Petlyuk column and even reactive distillation columns. A column section breakdown of a Petlyuk column and a reactive distillation column are shown in Figure 2.22 a and b respectively.

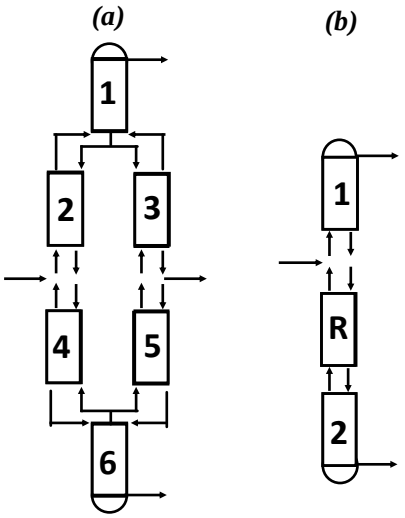


Figure 2.22: Column section breakdown of (a) a Petlyuk column with multiple internal column sections and (b) a Reactive distillation column with an internal reactive column section (R).

To illustrate the potential use of such column sections, consider the following multiple feed column shown in Figure 2.23 , where all liquid composition profiles intersect one another, rendering a feasible design. Constant relative volatilities of 3 and 1.5 with respect to the high boiling component, as well as saturated liquid feeds have been assumed.

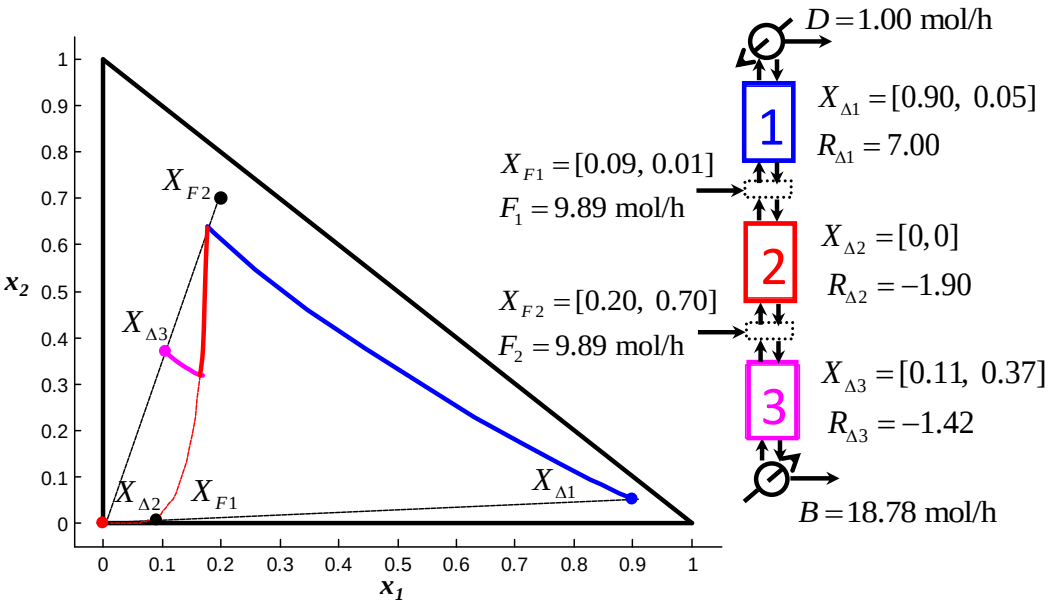


Figure 2.23: A feasible multiple feed column where the internal column section (2), operates with a difference point of X_Δ = [0, 0] and a reflux ratio of -1.90, forcing the intermediate boiling vertex to be an unstable node.

The parameters of the internal column section in Figure 2.23 have been chosen such that its difference point, $X_{\Delta 2}$, is fixed at the intermediate boiling axis, indicated by the red dot. The straight, dashed black lines indicate that all mass balances have been satisfied between column sections. Notice that the composition profiles of each column section are all connected, rendering a feasible design. At the specific reflux ratio chosen for the internal column section, the node at the intermediate boiling axis behaves as an unstable node (see Figure 2.16). This may be seen by the red, dashed profile extension of column section 2 that runs directly toward the intermediate boiling vertex. Notice that, due to the fact a sharp split constraint has been placed on

this column section and that the reflux ratio has been chosen such that the node is unstable, this profile runs in a qualitatively opposite direction to "conventional" profiles (as those illustrated by column section one and two). In this specific case study, this unique sharp split constraint in fact makes the separation feasible. If the reflux ratio in this column section was chosen such that the node on the intermediate boiling axis is a saddle, the profiles of this column section would run in a qualitatively similar direction to those depicted in column section one and two, and a feasible design will not be found.

2.5 CONCLUSIONS

It has been shown that sharp split column section design differs somewhat from conventional column section design. Sharp splits display special behaviour as such a specification displays behaviour of adjacent regions. The merger of adjacent regions presents an interesting situation as nodes can change nature due to a node bumping phenomenon. From this work it has also been shown that when fixing a sharp product specification in a column section (X_Δ), one can predict which range of values of R_Δ would result in certain behaviour, i.e. where a stable node might be placed instead of saddle. Zone-graphs are presented as a novel graphical tool that could assist one in determining such ranges of R_Δ for achieving a desired separation. An interesting application of the aforementioned is that by fixing R_Δ and X_Δ one could effectively remove an intermediate boiling component as a bottoms or distillate product in a single column section, by placing a stable node on the intermediate boiling vertex. However, these specific operating conditions seem to be impractical in a single column section. It is thought that these unique sharp split operating conditions are of more practical use when designing networks of columns where internal column sections are used, such as the Petlyuk column. A case study is given of a multiple feed column that uses this unique profile behaviour in a desirable way to affect a separation. Furthermore, it has been shown that there are certain ranges of R_Δ where

the high and low boiling components would be difficult to remove as the respective pure component vertex could change to a saddle point.

Chapter 3 : THERMALLY COUPLED SIDESTREAM COLUMN DESIGN USING COLUMN PROFILE MAPS AND TEMPERATURE COLLOCATION

This work has been recently published in the AIChE Journal under the same title, and is a product of my time spent at the University of Illinois at Chicago. As such, its style (specifically the ordering of axes) may differ slightly from other chapters. Both Gerardo Ruiz and Prof. Andreas Linninger assisted with implementation of the temperature collocation algorithm, but the work is almost exclusively my own.

ABSTRACT

Thermal coupling of individual distillation column units has in recent years attracted considerable attention, with reports that up to 50% average savings on the energy demand may be achieved when compared to the traditional approach for separating a multicomponent mixture. In this work a systematic procedure is presented to design thermally coupled sidestream units like side rectifiers and side strippers. The method combines the Column Profile Map technique to assess topological characteristics of the specific configuration with Temperature Collocation to rigorously ensure a realizable column design, without making assumptions with regard to the phase equilibrium or product specifications. Techniques are presented for highlighting superior designs or eliminating inferior ones, based on vapour flowrate, number of stages and thermodynamic efficiency. Design parameters such as the feed and side-draw trays that may require insight or experience are products of the procedure. Design solutions obtained using this methodology can be used to initialize the state of the art process flowsheeting tool, AspenPlus™, which typically leads to fast convergence to the desired product purities without further adjustments.

3.1 INTRODUCTION

Distillation is the most widely used method in modern chemical industries to separate liquid mixtures into pure components. Despite its wide use and functionality it is a very energy intensive method of separation, accounting for about 40% of the total energy used in the chemical and petroleum refining industries (DOE, 2005). With the price of energy and environmental concerns expected to increase even further, researchers and process engineers have set out to find new and creative ways to operate and design separation units. To this end, the notion of coupling individual columns through transferring heat between them has received considerable attention, with reports that up to 50% average savings on the energy demand may be achieved, when compared to the traditional approach, where simple columns are employed in series to achieve the desired product purities (Wolff and Skogestad, 1995, Agrawal and Fidkowski, 1998, Fidkowski and Agrawal, 2001, Brüggemann and Marquardt, 2004, Engelien and Skogestad, 2005b). These savings arise partly due to the fact that the number of reboilers and condensers are reduced, but it should be noted that these savings are dependent on numerous factors including the compositions and volatilities of the feed stream(Agrawal and Fidkowski, 1998). Furthermore, since thermally coupled arrangements reduce the number of reboilers and/or condensers required to affect the separation, significant capital savings can also be achieved.

The simplest method of thermal coupling is a large main column that pre-separates the light and heavy components in the feed, linked to a side unit which removes one or more intermediate components. These units, called side rectifiers or strippers or more generally thermally coupled sidestream units, have found considerable use in practice. The side stripping column has been extensively employed in petroleum refineries (Watkins, 1979), while the side rectifier columns have found application in air separation (Petlyuk, 2004) as well as replacing entrainer regeneration columns in extractive distillation operations (Emmrich et al., 2001). Other, more complex

arrangements such as the fully thermally coupled Petlyuk or Kaibel column arrangements have also been proposed, with even greater potential for energy and capital investments. Although thermally coupled structures promise significant cost reductions, their widespread implementation has been hampered somewhat by control and operational problems. The energy integration increases the control loop coupling in the system, so that the operating strategy for the columns is no longer apparent. This could lead to irregular start-up and shut-down procedures and may therefore offset any potential savings due to non-continuous production (Frey et al., 1984). However, numerous advances have been made in the operability of coupled columns in recent years (Alstad et al., 2004, Wolff and Skogestad, 1995, Alberto Porras-Rodríguez et al., 2007, Halvorsen and Skogestad, 1997, Hernandez and Jimenez, 1999, Segovia-Hernández et al., 2005), so much so that large companies like BASF (and others) now have fully functioning Petlyuk and Kaibel columns (Kaibel and Schoenmakers, 2002).

Numerous techniques have been proposed to design thermally coupled side rectifiers and strippers. Several of these methods deploy the Underwood equations (Glinos and Malone, 1985b, Glinos and Malone, 1985a, Fidkowski and Krolikowski, 1987), but this method is reliable only for near ideal systems and also assumes sharp product specifications. The vapor rate and the minimum reflux ratio, both of which are imperative for the column design and cost, will therefore be idealized using the Underwood methods. Another, more recent approach using the shortest stripping line (Lucia et al., 2006) shows a robust energy targeting strategy that provides a continuously differentiable description of column sequences. This approach can account for any phase equilibrium behavior (including azeotropes) and has the ability to find column sequences that contain non-pinched, minimum energy columns within a sequence as well as accounting for heat integration and capital / operational cost trade-offs, using numerical optimization techniques(Lucia and McCallum, 2009). Rigorous models using tray-by-tray computations which account for non-idealities have also been suggested (Lucia and McCallum, 2010), but global optimization

methods of synthesis problems involving both structural and parametric degrees of freedom is still a challenge for existing math programming algorithms. Furthermore, black box solutions also permit limited insight the designer can derive from the final solution.

Recently, a Column Profile Map technique has been proposed and was shown to be an efficient tool to synthesise distillation columns, including simple and thermally coupled columns (Tapp et al., 2004, Holland et al., 2004b, Holland et al., 2010). The graphical, and general, nature of this technique means that the designer is able to achieve considerable insight and flexibility in the design. However, the graphical aspect of this approach has a drawback that it involves trial-and-error for determining parameters to construct and validate composition profiles repeatedly until a suitable design is found.

A Temperature Collocation approach proposed by Linninger and co-workers transformed the governing equations in the work of Tapp et al. (2004) thermodynamically to rigorously synthesize simple columns (Zhang and Linninger, 2004). More recently, an expansion of Temperature Collocation has been shown to entire networks of simple and complex column configurations (Ruiz et al., 2009). The advantages of combining the two design approaches are (i) non-ideal mixtures may be easily modelled, (ii) multicomponent (>4) problems can be designed semi-automatically, (iii) any network configuration may be designed and tested for feasibility, and (iv) design variables such as the feed tray, side-draw tray and total number of stages can be determined rationally without much computational effort. Furthermore, they showed that the column specifications obtained from this methodology for entire separation networks can be validated with AspenPlus.

This paper aims to combine the advantages of the Column Profile Map and Temperature Collocation techniques, for the rational design of thermally coupled side stripper and rectifier columns. This paper does not attempt to find globally optimal

solutions to the problem of thermally coupled sidestream column, but instead presents a systematical and rigorous design strategy that offers design engineers clear insight into the behavior of these configurations. This paper is structured in the following manner: Section two discusses the design methodology and general properties of the Column Profile Map and Temperature Collocation techniques. The following section highlights the procedure for side stripper/rectifier design including its structural properties, a degree of freedom analysis, mass balance properties, feasibility criteria, and informed choices of design variables. Section four presents the spectrum of feasible designs for a Methanol / Ethanol / p-Xylene case study and specifically methods are proposed to direct one to superior designs based on the reboiler duty, the number of stages and energy efficiency. The paper closes with conclusions summarizing significant results from this work and suggesting areas of future work and applicability of the methods.

3.2 METHODOLOGY

3.2.1 COLUMN PROFILE MAPS

Continuous column profile equations were originally proposed by Van Dongen and Doherty for conventional rectifying and stripping sections (Van Dongen and Doherty, 1985b). These continuous equations were expanded to the Difference Point Equation for a generalized Column Section (CS), from which a Column Profile Map may be constructed, by setting parameters such as the reflux ratio and net compositional flows (Tapp et al., 2004). The general nature of the Column Profile Map method has the advantage that it is not specific to any configuration which consequently lends itself to model any structure, irrespective of its complexity. The equations have been developed by defining a CS as a length of column between points of material addition or removal, as shown in Figure 3.1.

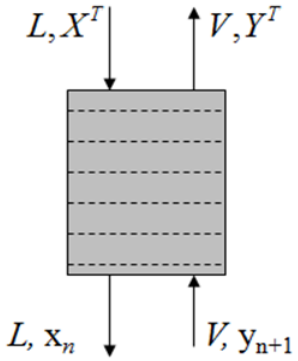


Figure 3.1: A generalised Column Section (CS), with liquid composition x and X^T, and vapour compositions y and Y^T. The superscript T indicates the compositions at the top of the CS, while *n* indicates a respective tray number

The equation describing the liquid compositional change along the CS may then be derived through a steady state mass balance over a CS, assuming constant molar overflow followed by a Taylor expansion, which yields:

$$\frac{dx}{dn} = \left(\frac{1}{R_\Delta} + 1\right)\left(x - y(x)\right) + \left(\frac{1}{R_\Delta}\right)\left(X_\Delta - x\right) \tag{3.1}$$

where $X_\Delta = \left(\frac{VY^T - LX^T}{V - L}\right)$ and $R_\Delta = \frac{L}{V - L} = L/\Delta$

Equation 3.1 is known as the *Difference Point Equation*, where R_Δ is a generalized reflux ratio in the CS, *n* the amount of stages. X_Δ is termed the Difference Point which can be thought of as a pseudo composition vector, valid anywhere in the composition space. Like regular compositions, the elements of the Difference Point sum to unity. Furthermore, X_Δ need only smaller and less than unity in CSs that are terminated by a condenser or reboiler. Negative element entries, corresponding to X_Δ located outside the mass balance triangle, merely implies that the respective component is flowing

downward in the CS. Accordingly, negative reflux ratios indicate that the section is in stripping mode, i.e. there is a net flow of material down the column ($L>V$) and conversely, positive reflux ratios indicate that a CS is in rectifying mode as there is a net flow of material upward. The vapour composition **y(x)** can be related to the liquid composition using an appropriate Vapour-Liquid Equilibrium model. Once the aforementioned parameters have been set a Column Profile Map may be constructed, as shown in Figure 3.2 for arbitrarily chosen process parameters. A complete derivation of the Difference Point Equation is given in Appendix G.

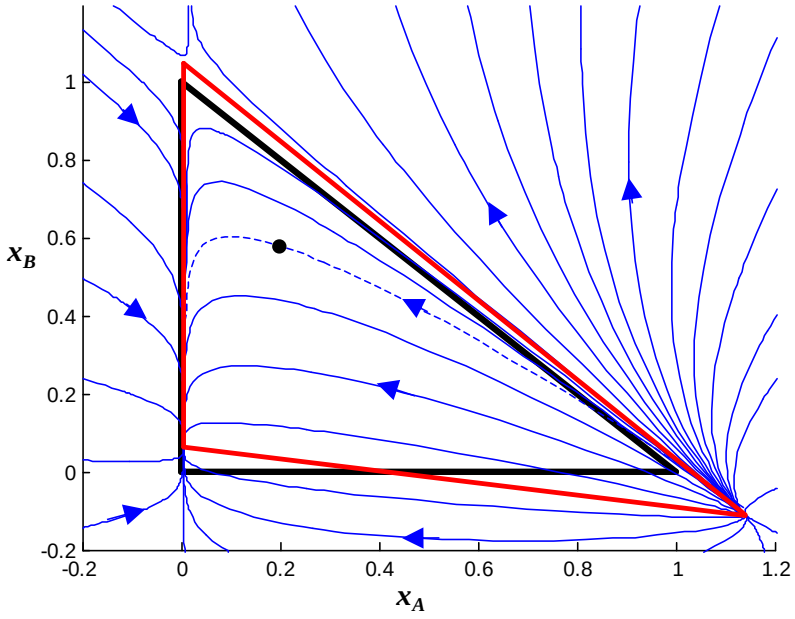


Figure 3.2: A Column Profile Map with a generalized reflux ratio of R_Δ=9 and a Difference Point of X_Δ = [0.2, 0.6] (black dot). The dashed blue lines represent principal profiles emanating from the Difference Point which corresponds to a CS with a product cut. Secondary column profiles, drawn in solid blue lines, represent CSs with the same Difference Point as the principal profile but with different entering liquid and vapour compositions. All profiles may be extended beyond the boundaries of the mass balance triangle (in black) for gaining a better understanding of both the topology and pinch points. Each profile approaches the stationary points indicated by the red triangle.

Figure 3.2 shows that stationary points have been shifted from the pure component vertices (black triangle), which corresponds to a Residue Curve Map (R_Δ=∞). The dashed trajectory in Figure 3.2 indicates a *principal profile* as the profile runs through

the Difference Point which corresponds to a CS producing an actual product cut of composition X_Δ. All other profiles are termed *secondary profiles*, which represents all possible trajectories of complex CSs which obey the same Difference Point, but originate from different compositions.

Notice that it is mathematically possible to track concentration profiles in regions outside the mass balance triangle. Even though these profiles are not physically realizable, the expansion of the scope of the topological space provides new insights into the feasibility of separation tasks inaccessible to the traditional view confined within the mass balance triangle. It has been shown that the analysis of negative compositions may add insight column synthesis, but this is beyond the scope of this paper and the reader is referred to Tapp et al. (2004) and Holland et al. (2004) for a more in depth analysis of the significance and topological effects of parameters, especially in negative composition space. It should be clearly noted however that the direction of composition profiles can be altered by a combination of reflux ratio and X_Δ, and they can even be attracted to points located outside the real composition space.

In order to gain a basic understanding into the relation of parameters and general design procedure for the Column Profile Map method, a simple case of a single-feed-two-product column is discussed. In this instance, there are two CSs (rectifying and stripping) and consequently two sets of Difference Point Equation parameters that need to be specified. As a product is being drawn off from both sections via a reboiler/condenser, X_Δ corresponds to the product specifications in both sections. As with conventional design methods, an internal column variable also has to be specified, either a reflux or reboil ratio. The generalized reflux ratio, R_Δ, is in this case equal to the traditional reflux ratio ($r=L/D$) in the rectifying section. By an energy balance over the entire column the generalized reflux ratio for the stripping section, which is analogous to the traditional reboil ratio, may also be determined. Once all Difference Points have been specified and/or calculated, the Difference Point

Equation for each CS may be integrated with the product compositions as the starting point. The design given by the purity specifications and reflux ratios is feasible if the concentration profiles of the rectifying and stripping CSs intersect.

3.2.2 TEMPERATURE COLLOCATION

The Temperature Collocation approach, originally proposed by Zhang and Linninger (2004) for conventional rectifying and stripping sections is based on a thermodynamic transformation whereby the independent integration variable in the Difference Point Equation is changed from the stage number (*n*) to the tray bubble point Temperature (*T*). This transformation has the advantage that designs may be rigorously and quickly assessed in an algorithm using a Bubble Point Distance (BPD) function, which eliminates the dimension of top and bottom trays to a single coordinate, the bubble point Temperature. The variable transformation yields a composition profile equation as a function of tray bubble point Temperature, given in vector form in Equation 3.2:

$$\frac{d\mathrm{x}}{dT} = \frac{-\left[\left(1+ 1/R_{\Delta}\right)(\mathrm{x}-\mathrm{y})+\left(1/R_{\Delta}\right)(X_{\Delta}-\mathrm{x})\right]\frac{d\mathrm{K}}{dT}\mathrm{x}}{\left[\left(1+ 1/R_{\Delta}\right)(\mathrm{x}-\mathrm{y})+\left(1/R_{\Delta}\right)(X_{\Delta}-\mathrm{x})\right]\mathrm{K}} \qquad (3.2)$$

where *K* is the vector of equilibrium constants relating vapour and liquid compositions with each other. The individual components are defined by $K_i = \frac{\gamma_i(\mathrm{x},T)P_{i,SAT}(T)}{P}$. Non-idealities can be incorporated into this equation by modelling the liquid activity coefficient with an appropriate phase equilibrium model. Numerical integration can be performed from a known bubble point Temperature (i.e. at a product composition) toward the profile termination point, calculated by solving

Equation 3.2 at steady state conditions. A complete derivation of Equation 3.2 is given in Appendix G.

In all column configurations, simple or complex, a design is feasible if and only if the liquid composition profiles of all adjacent CSs in a configuration intersect one another. In other words, all products are connected by one continuous profile. In terms of the Temperature Collocation methodology, this implies that the Euclidian distance, or Bubble Point Distance (BPD), between liquid composition profiles of adjacent Column Sections on a single Temperature isotherm is smaller than a certain predefined small tolerance, ϵ. This method is conveniently visualised in Figure 3.3, which shows how the BPD may be used to distinguish between feasible and infeasible designs.

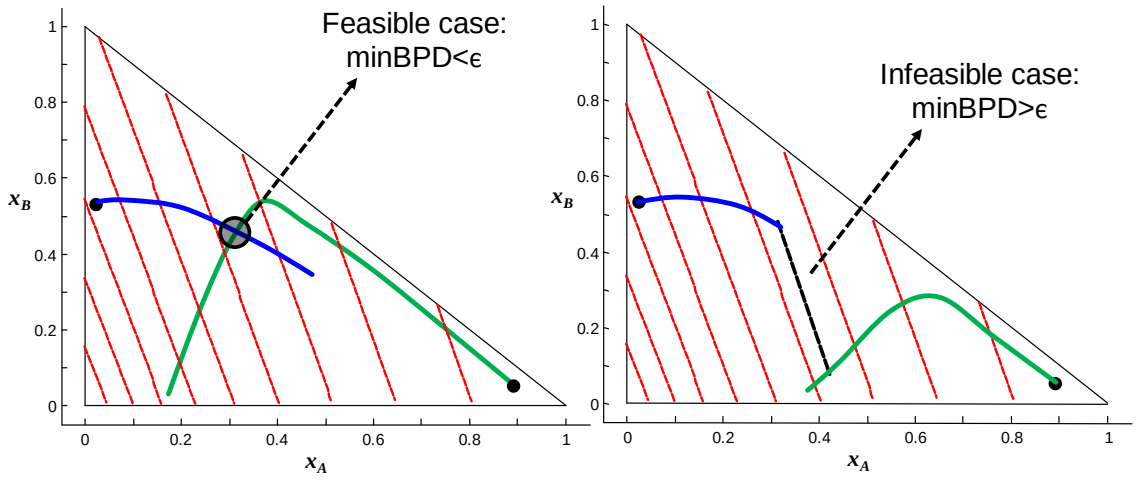


Figure 3.3: Distinguishing feasible and infeasible designs using the Bubble Point Distance Function. Red lines indicate isotherms while green and blue lines are compositional profiles for the rectifying and stripping sections in a simple column, respectively.

Each trajectory Figure 3.3 is essentially divided into a set of predefined finite elements; where each element is fitted with a polynomial containing a predetermined number of roots. This orthogonal collocation on finite elements (OCFE) method thus transforms the problem to a system of nonlinear algebraic equations (Zhang and

Linninger, 2006a). This method is an evolution of the first work on finite element analysis in distillation was put forward by Swartz and Stewart (Swartz and Stewart, 1987).

3.3 DESIGN ASPECTS

This section introduces procedures and properties of side stripper/rectifier design that aids in the understanding of the design of these configurations. Specific focus is given to structural properties and mass balances as well as a suitable choice of design variables which allows the designer to gauge the interaction between all CSs. Ultimately the graphical design and analysis allows one to gain insight into feasibility conditions and criteria for realizable designs from which a general design algorithm may be devised.

3.3.1 STRUCTURAL ASPECTS

Using the definition of a CS, any separation process may be represented by a network of CSs as shown in Figure 3.4 a and b for a side stripper and rectifier, respectively. Interestingly, from a structural point of view, even though these thermally coupled arrangements differ considerably from a conventional sequence of simple columns, the number of CSs in both configurations is equivalent in order to separate a multicomponent mixture into pure components. In fact, the number of CSs required to separate a multicomponent mixture into pure components, is equal in the thermally coupled sidestream arrangement to any other conventional column network (simple or complex), and is always $2(nc-1)$, where nc is the number of components in the system. The CSs in both configurations are labelled CS_1 through CS_4 as referred to in Figure 3.4 a and b and all subsequent discussions.

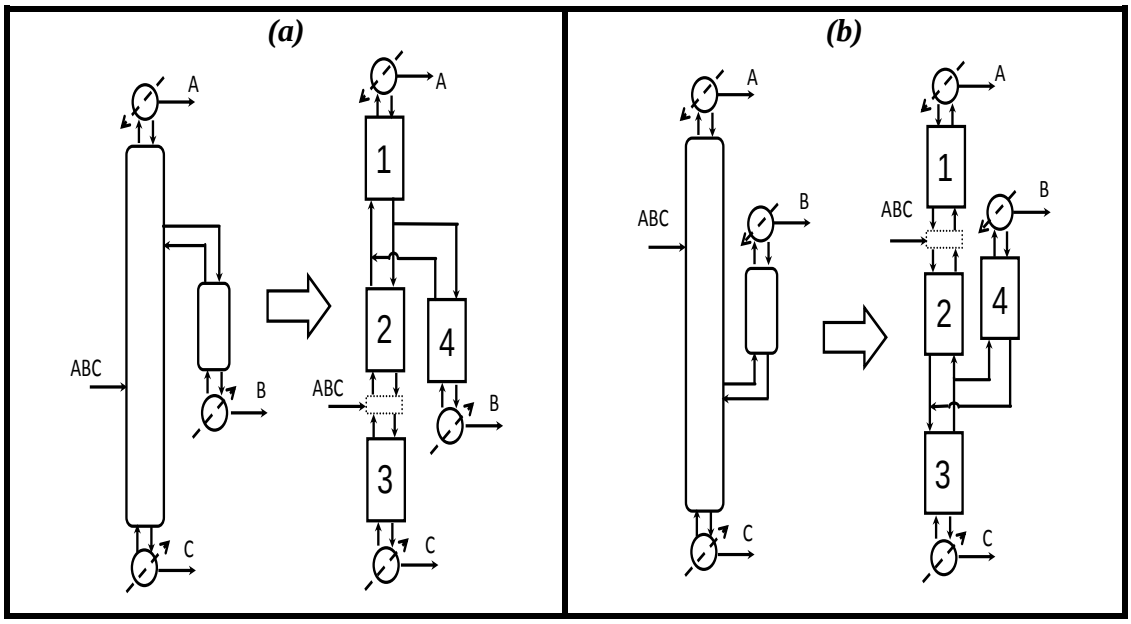


Figure 3.4: Basic thermally coupled sidestream columns with the associated Column Section breakdown for (a) a side stripper and (b) a side rectifier, showing the vapour and liquid distribution at the side draw stage.

Figure 3.4 a and b also indicate the manner in which the material flows in the thermally coupled CSs are linked to each other. For instance, in the side stripper configuration in Figure 3.4 a, the liquid flowing from CS_1 is divided between CS_2 and CS_4. The vapour flow in CS_1 is merely a mixture of the vapour flows of CS_2 and CS_4. The side rectifier operates in an analogous manner; the vapour stream in CS_3 is split between the two adjacent CSs and the liquid stream is a mixture. Furthermore, notice that the relative position of the feed and side-draw stage is reversed in the respective configurations.

3.3.2 DEGREE OF FREEDOM ANALYSIS

For both configurations depicted in Figure 3.4, the external degrees of freedom (or mass balance properties) for an *nc* component system with *P* product flows, may be summarized as follows, for a specified feed:

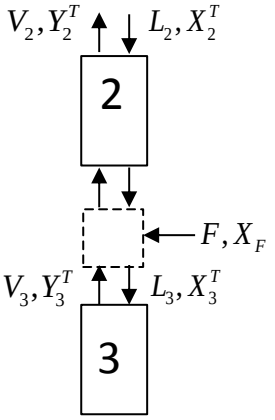
Total unknowns:	$P(1+nc)$	(3 Product Flows $+nc$ compositions in each product)
Mass Balance Equations:	$\boldsymbol{-nc}$	(number of components)
Summation Equations:	$\underline{\underline{\boldsymbol{-P}}}$	($\Sigma x_i=1$ in each product stream)
Total Degrees of Freedom	$nc(P-1)$	

In a traditional three component thermally coupled sidestream configuration as shown in Figure 3.4, there are consequently six free variables to be set by the designer before the design can be performed. Effectively, this means that setting the compositions in all product streams fixes the product flowrates, by mass balance. It is important to point out that setting the external degrees of freedom for the column by no means guarantees that the column will be feasible. Besides the $nc(P-1)$ external degrees of freedom, traditional thermally coupled sidestream arrangements also require two internal flow variables to be specified, i.e. the reflux ratio in two CSs. These internal degrees of freedom ultimately determine the feasibility of the design. Globally, a sequence of uncoupled columns that performs the same separation has an equivalent amount of degrees of freedom (internal and external). However, the major difference in the two designs is that the two internal degrees of freedom have a strong dependence on one another, whereas a sequence of simple columns is decoupled. Simply put, the reflux ratios in two simple columns may be chosen independently. Different selections of the internal degrees of freedom do however impact the capital investment as well as the total energy demand and efficiency of the process and therefore optimal choices have to be identified systematically. This point will be addressed in the subsequent discussion.

3.3.3 MASS BALANCES ASPECTS

Before designing the entire column configuration, it is important to understand the mass balance constraints on the unit. Figure 3.5 shows a material balance over the Column Sections above and below the feed tray for the side stripper configuration

shown in Figure 3.4 a, using the definition of X_Δ in the Difference Point Equation. Similar mass balance derivations and properties have been demonstrated for the Petlyuk column by Holland et al. (2010).



$$L_2 X_2^T + V_3 Y_3^T + F X_F = L_3 X_3^T + V_2 Y_2^T$$

Rearranging:

$$V_3 Y_3^T - L_3 X_3^T + F X_F = V_2 Y_2^T - L_2 X_2^T$$

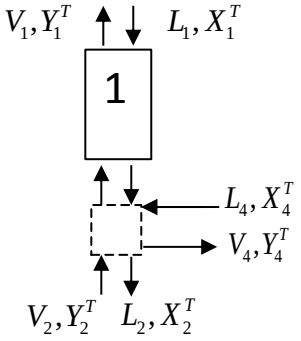
$$\Delta_3 \left(\frac{V_3 Y_3^T - L_3 X_3^T}{\Delta_3} \right) + F X_F = \Delta_2 \left(\frac{V_2 Y_2^T - L_2 X_2^T}{\Delta_2} \right)$$

Therefore:

$$\Delta_3 X_{\Delta 3} + F X_F = \Delta_2 X_{\Delta 2}$$

Figure 3.5: Mass Balance over feed stage.

Figure 3.5 yields a significant result, as it shows that the Difference Points (X_Δ) above and below the feed tray are linearly related to the feed composition. From a geometric point of view this relation implies that the feed composition, $X_{\Delta 2}$ and $X_{\Delta 3}$ lie on a straight line in composition space. A similar result may be obtained at the thermally coupled side-draw stage for both sidestream configurations, shown in Figure 3.6 the side stripper unit.



$$L_1 X_1^T + V_2 Y_2^T + L_4 X_4^T = L_2 X_2^T + V_1 Y_1^T + V_4 Y_4^T$$

Rearranging:

$$V_2 Y_2^T - L_2 X_2^T = V_1 Y_1^T - L_1 X_1^T + V_4 Y_4^T - L_4 X_4^T$$

$$\Delta_2 \left(\frac{V_2 Y_2^T - L_2 X_2^T}{\Delta_2} \right) = \Delta_1 \left(\frac{V_1 Y_1^T - L_1 X_1^T}{\Delta_1} \right) + \Delta_4 \left(\frac{V_4 Y_4^B - L_4 X_4^B}{\Delta_4} \right)$$

Therefore:

$$\Delta_2 X_{\Delta 2} = \Delta_1 X_{\Delta 1} + \Delta_4 X_{\Delta 4}$$

Figure 3.6: Mass Balance over Side-draw stage.

As CS_1, CS_3 and CS_4 in both configurations produce end products and are terminated by a condenser or reboiler, their composition profiles have to be principal profiles because the Difference Points of these sections are in fact identical to the product compositions in these sections. However, CS_2 does not yield a product cut; its Difference Point Placement is only constrained by mass balance through specifying the other CSs as well as the feed composition. Its column profile will therefore be a secondary profile.

Interestingly, it is entirely possible for Petlyuk arrangements, and other complex configurations, to have Difference Points that lie outside the mass balance triangle. This property is not even rare, and can occur quite naturally in CSs that do produce end products. This point is discussed more in depth in (Holland et al., 2010). However, this case is impossible in side rectifier and stripping arrangements as the Difference Points of all product producing CSs have to lie inside the mass balance triangle, in consequence the Difference Point of the internal CS also has to be inside the mass balance triangle. This result is depicted in Figure 3.7 for both arrangements.

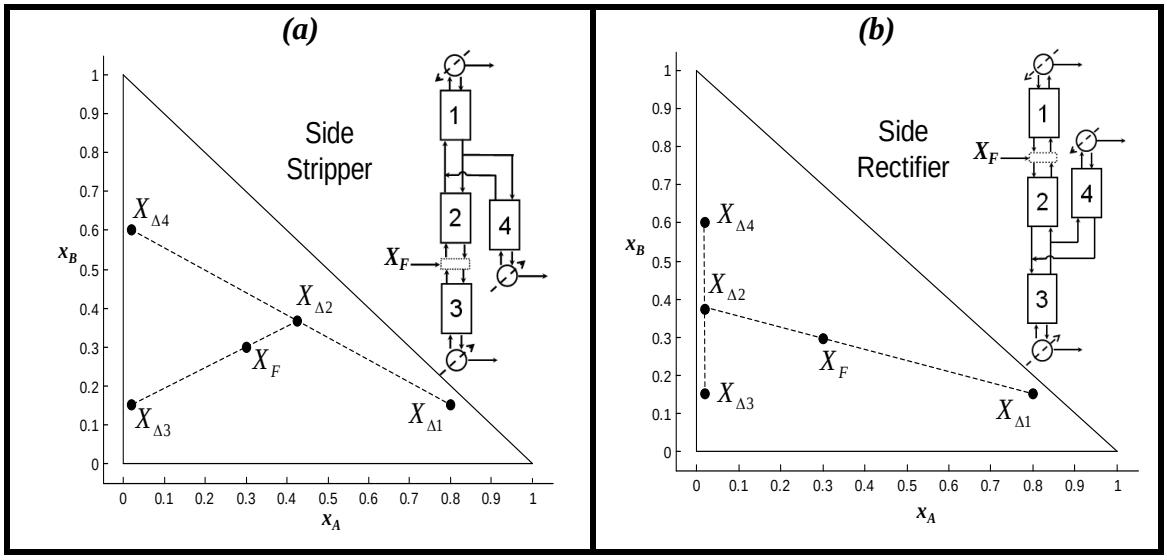


Figure 3.7: A geometric interpretation of the Difference Points for (a) a side stripper configuration and (b) a side rectifier configuration, accompanied by the CS breakdown and numbering of each configuration. On both diagrams $X_{\Delta i}$ is the Difference Point of the i'th CS.

3.3.4 FEASIBILITY CRITERIA

Similarly to conventional columns, a thermally coupled column design may be rendered feasible if and only if liquid composition profiles of adjacent CSs intersect. Liquid profile intersection was shown to be a suitable criterion for column feasibility by among others Doherty and co-workers (Doherty and Caldarola, 1985, Levy et al., 1985, Levy and Doherty, 1986), and using this condition, has also been validated by Linninger and co-workers on process simulation packages like AspenPlus, even for complex columns (Zhang and Linninger, 2004, Zhang and Linninger, 2006a, Kim et al., 2010a). This condition is the same as ensuring that there exists a continuous path of column profiles which connect all products with one another without a gap. Figure 3.8 shows a feasible side stripper configuration for the ideal Benzene / Toluene / p-Xylene system, where all liquid composition profiles intersect. In practice, this criterion means that the Bubble Point Distance is almost zero. The specifications for this separation are summarized in Table 3.1.

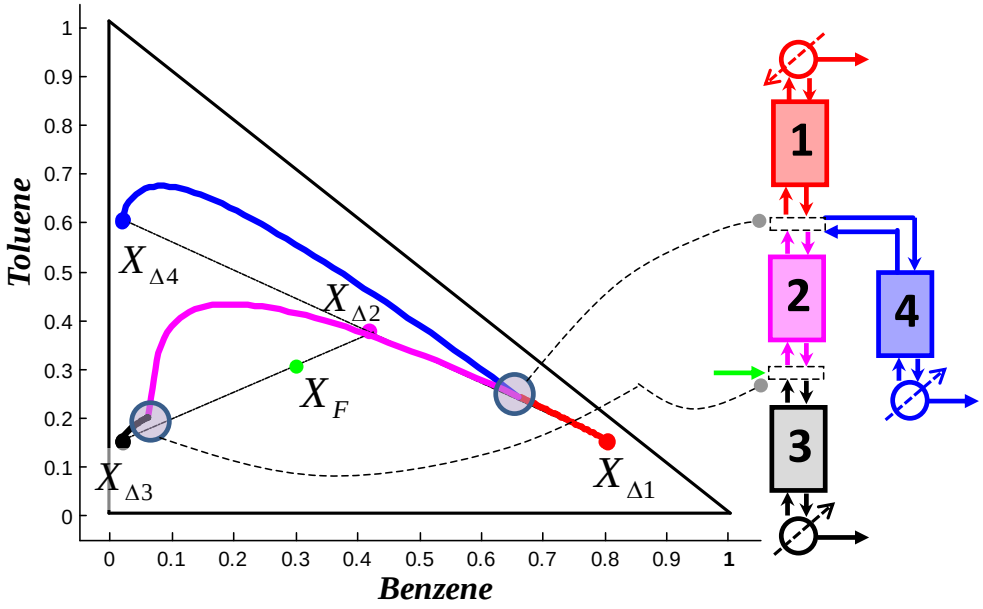


Figure 3.8: Feasibility of a side stripper arrangement for the Benzene / Toluene / p-Xylene system. The Bubble Point Distance between CS_2 and CS_3, and the triple Bubble Point Distance between CS_1, CS2 and CS_4, needs to be zero for the side stripper column to be feasible. This criterion is indicated by the highlighted areas

Table 3.1: Stream table for a Benzene / Toluene / p-Xylene system. Text in boldface indicates that these parameters have been specified, while the rest have been calculated.

Column Section	Difference Point	Reflux ratio	Net flow (Δ) (mol/s)
Feed	[0.300; 0.300; 0.400]	-	1 (pure liquid)
CS_1	[**0.80**; **0.150**; 0.050]	**7**	0.359
CS_2	[0.424; 0.367; 0.209]	1.452	0.692
CS_3	[**0.020; 0.150**; 0.830]	-6.524	-0.307
CS_4	[**0.020**; **0.600**; 0.380]	**-4.523**	-0.333

For this example, the reflux ratios in CS_1 and CS_4 were chosen as the two internal degrees of freedom, although this choice is completely arbitrary. As mentioned, negative reflux ratios as in CS_3 and CS_4 indicate that a CS is in stripping mode, while CS_1 and CS_2 are in rectifying mode. At this point, it is not immediately obvious how the two internal degrees of freedom are related to each other and how one might go about designing an optimal column. These questions will be addressed in chapter 3.3.5.

Notice specifically in Figure 3.8 that for side stripper configurations, there are three profile intersections in the highlighted area of the side product withdrawal. The liquid composition profiles of CS_1, CS_2 and CS_4 all have to share a common point, or in other words, a *triple Bubble Point Distance junction*. Furthermore, the profiles of CS_2 and CS_3 also have to intersect one another. Since CS_1, CS_2 and CS_4 all produce end-products, the composition profiles go through their respective Difference Points (principal profiles). The internal CS, CS_2, requires that a so-called secondary profile be constructed, since its starting composition vector is not a Difference Point.

The design below was performed using the Column Profile Map / Temperature Collocation approach described in the preceding section using the NRTL phase

equilibrium model. This has a pure liquid feed and operates at 1 atm pressure. The design above also has the following properties: Total stages in main column: 9; feed stage: 6 (from the top); thermally coupled stage: 2 (from the top); total stages in side stripping unit: 7. The aforementioned values may then be inserted into a commercial process simulator (like AspenPlus). This particular design is shown in Figure 3.10 and a reasonably good agreement between AspenPlus and the profiles predicted using the column profile based method can be seen.

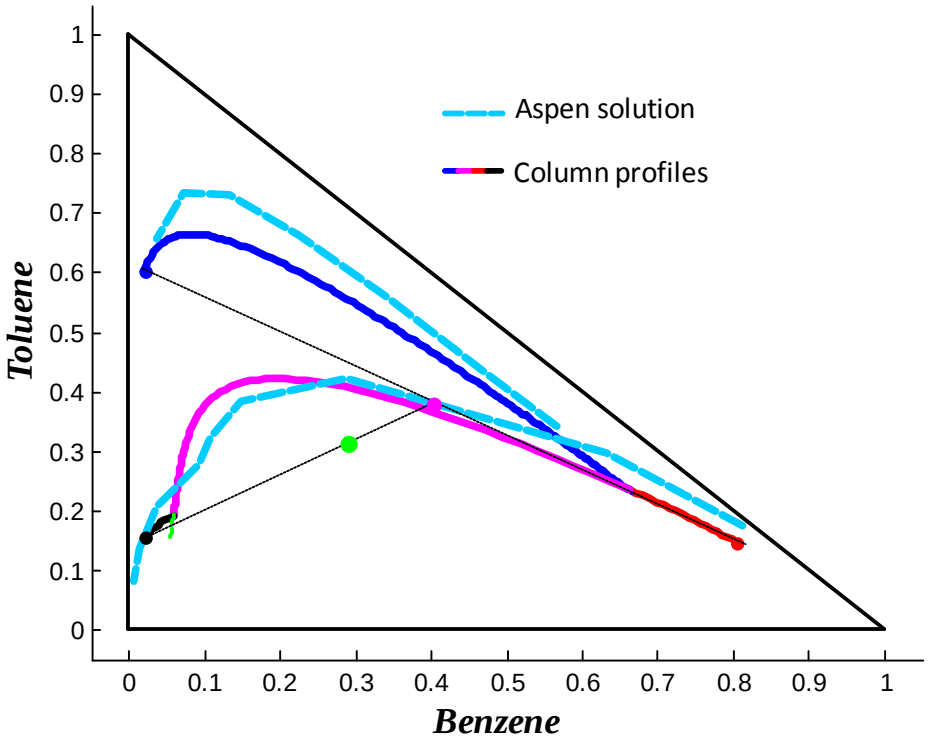


Figure 3.9: Comparison of column profiles generated via the Column Profile Map / Temperature Collocation method (solid lines) and AspenPlus (dashed cyan lines)

3.3.5 CHOICE OF DESIGN VARIABLES

Using the techniques described in the preceding section allows intuitive understanding into the design procedure and attributes of thermally coupled column design. However, it is often the case that the designer needs quick and reliable

answers to the question whether a given set of process specifications are feasible for distillation separation. This task is somewhat more complicated in the case of side rectifiers and strippers, as choosing certain design variables invariably have multiple coupled effects on the entire column. A major design decision in thermally coupled columns is deciding on the internal degrees of freedom. Generally, for the single sidestream arrangement, the reflux ratios of two sections have to be specified. This task is generally not simple one, because reflux ratios can be chosen to lie anywhere between zero and infinity for rectifying sections and zero to negative infinity for stripping sections.

Apart from the fact that reflux ratios are unbounded parameters, it is also difficult to anticipate the interaction between reflux ratios in different CSs. It is more convenient to define a split ratio, Φ, (Hernandez and Jimenez, 1999) which governs the fraction of material sent to the thermally coupled side sections and internal sections. For instance, in the side stripper configuration we will define a reflux ratio in CS_1 and a liquid split ratio, defined as $\Phi_L = L_{CS4}/L_{CS1}$, where L_{CSi} is the liquid flowrate in the *i*'th CS and where the subscript *L* denotes a liquid phase split. Analogously for the side rectifier arrangement, the generalized reflux ratio in CS_3 may be specified (effectively the reboil ratio) along with a vapour split ratio $\Phi_V = V_{CS4}/V_{CS3}$. This specific variable choice narrows the search for a feasible design because Φ is a bounded dimensionless parameter valid only between zero and one. Even though the defined split ratios narrow the search space somewhat, it is not immediately obvious which combination of split ratios and reflux ratios the designer should choose. The interaction between different choices will be demonstrated next.

3.3.6 SIDE STRIPPER COLUMN SECTION INTERACTION

It is helpful to visually comprehend the effects and interaction that our choices of internal design variables have on other CSs. To this end, *parameter correlation maps*

are a particularly useful tool, which are presented and discussed for both the side stripper and side rectifier. For simplicity, a liquid feed (*q=1)* with an equimolar composition has been chosen, with pure bottoms, intermediate and distillate products for both configurations. Although these parameter correlation maps may vary for different feed and product specifications, their qualitative interpretation is similar for all systems. It is important to point out that these regions do not indicate regions of feasibility, but merely show the correlation of CSs for certain combinations of design variables.

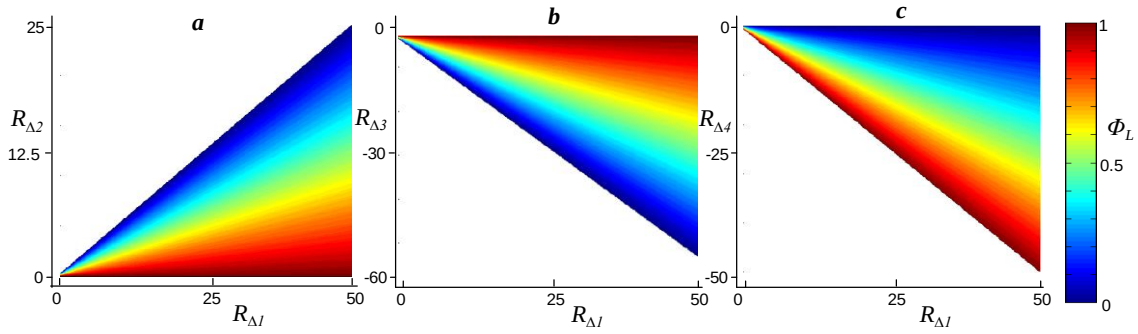


Figure 3.10: Parameter correlation maps for a Side Stripper showing the influence of $R_{\Delta 1}$ with varying liquid split ratios (Φ_L) on the reflux ratios of (a) CS_2, (b) CS_3 and (c) CS_4.

Figure 3.10 a, b and c show the effects on the reflux ratios in a side stripper of the two chosen internal degrees of freedom ($R_{\Delta 1}$ and Φ_L) on CS_2, CS_3 and CS_4 respectively. From Figure 3.10 it may be inferred that there are for any combination choice of the free design variables, there are always two pairs of equivalent rectifying (CS_1 and CS_2) and stripping (CS_3 and CS_4) sections. A specific example of the relationship between CSs can be seen, for instance, for a reflux ratio of 25 and a split ratio of 0.5 (the green region on the colour bar), which corresponds to generalized reflux ratios of 6.6,-15.2, and -13.8 in CS_2, CS_3 and CS_4, respectively.

An important factor to consider is the interaction of reflux ratios in CSs that have utilities attached to them (CS_3 and CS_4), as these are major contributors to the

operating cost of the column. CS_3 requires its reboiler to operate at a higher Temperature than CS_4 as it has to operate at the boiling point of the highest boiling component, while CS_4 only operate at the boiling point of the intermediate boiling component. In general it can be said that it is more expensive to operate a CS_3 reboiler than a CS_4 reboiler when both are operating at equivalent refluxes.

3.3.7 SIDE RECTIFIER COLUMN SECTION INTERACTION

Analogously to the side stripper, parameter correlation maps may be obtained for the side rectifier indicating the relationship of the two chosen design variables ($R_{\Delta 3}$ and Φ_V) on the reflux ratios of CS_1, CS_2 and CS_4 as shown in Figure 3.11 a, b and c respectively. Again there are two pairs of equivalent rectifying and stripping sections, but intuitively the role of specific CSs have changed when compared to the side stripper: The internal CS, CS_2, and CS_4 are in stripping mode, while both CS_1 and CS_3 are in rectifying mode. Specifically notice that for a choice of $R_{\Delta 3}$=-25 and Φ_V=0.5 (the green region on the colour bar), the respective corresponding refluxes in CS_1, CS_2 and CS_4 are 11.2, -7.5 and 12.5.

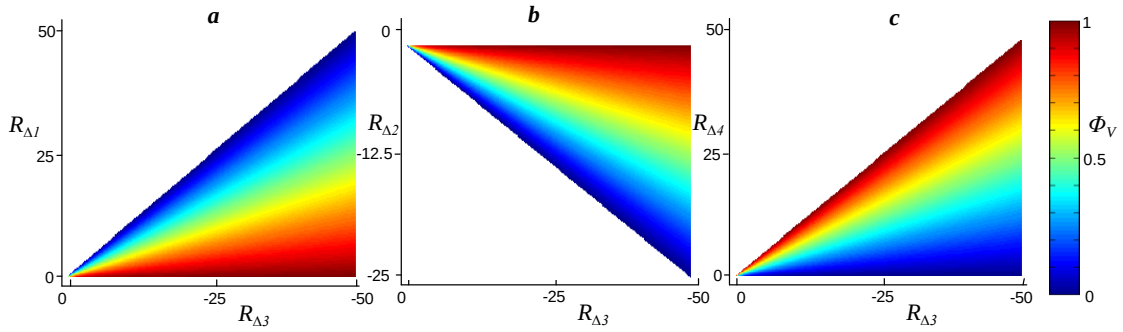


Figure 3.11: Parameter correlation maps for a Side Rectifier showing the influence of $R_{\Delta 3}$ with varying vapour split ratios (Φ_V) on the Reflux ratios of (a) CS_1, (b) CS_2 and (c) CS_4.

Noticeably, the side rectifier unit only contains one reboiler and consequently *all* the vaporisation takes place in CS_3. Thus, generally the reflux ratio required in this section is larger than the reflux ratio in the corresponding section (CS_3) of the side stripping unit where the reboil duty is divided between two CSs. Although the cost of operating reboilers are, in relative terms, much more expensive than condensers, it is still worthwhile considering what the qualitative effects of our process decisions are on the condensing load. The two condensing units in this configuration are CS_1 and CS_4. Here, CS_1 is the lowest Temperature at which condensing takes place and therefore requires a lower duty than an equivalent reflux ratio in CS_4.

3.3.8 ADDITIONAL DESIGN CONSTRAINTS

It is apparent from the previous discussion that some of the complexities that arise in thermally coupled sidestream columns are due to the fact that there are multiple reboilers/condensers operating at different Temperature levels, as well as multiple and simultaneous effects on all CSs for a certain selection of design variables. Apart from the interaction between CSs there is however a further constraint to be considered, when deciding on a reflux and/or split ratio, which is the constraint that the external mass balance places on the system. In short, a product producing CS has to have a minimum flow of material flowing into it, which is greater than the amount of product that has to be drawn off from that section. For example, the liquid material that is directed toward the side stripper from CS_1 has to be greater than the amount of intermediate product calculated by the overall mass balance. In general, there are two such constraints for each system. For the side stripper, in terms of our two chosen variables ($R_{\Delta 1}$ and Φ_L), these constraints are given in Equation system 3.3:

$$\Phi_L \geq \frac{\dot{I}}{R_{\Delta 1}\dot{D}} \text{ and } \Phi_L \leq 1 - \frac{\dot{B} - \dot{F} \times q}{R_{\Delta 1}\dot{D}} \qquad \text{(Equation system 3.3)}$$

And for the side rectifier, in terms of our two chosen variables ($R_{\Delta 3}$ and Φ_V), in Equation system 3.5:

$$\Phi_V \geq \frac{\dot{I}}{(-R_{\Delta 3}-1)\dot{B}} \text{ and } \Phi_V \leq 1-\frac{\dot{D}-\dot{F}\times(1-q)}{(-R_{\Delta 3}-1)\dot{B}} \qquad \text{(Equation system 3.4)}$$

where $\dot{D}, \dot{B}, \dot{I}$ and $\dot{F}$ are the flowrates of the Distillate, Bottoms, Side and Feed Streams respectively and q is the thermodynamic condition of the feed. Graphically, these constraints can be summarized in R_Δ-Φ space for both configurations, as shown in Figure 3.12 for the sharp split scenario described in section 3.3.6.

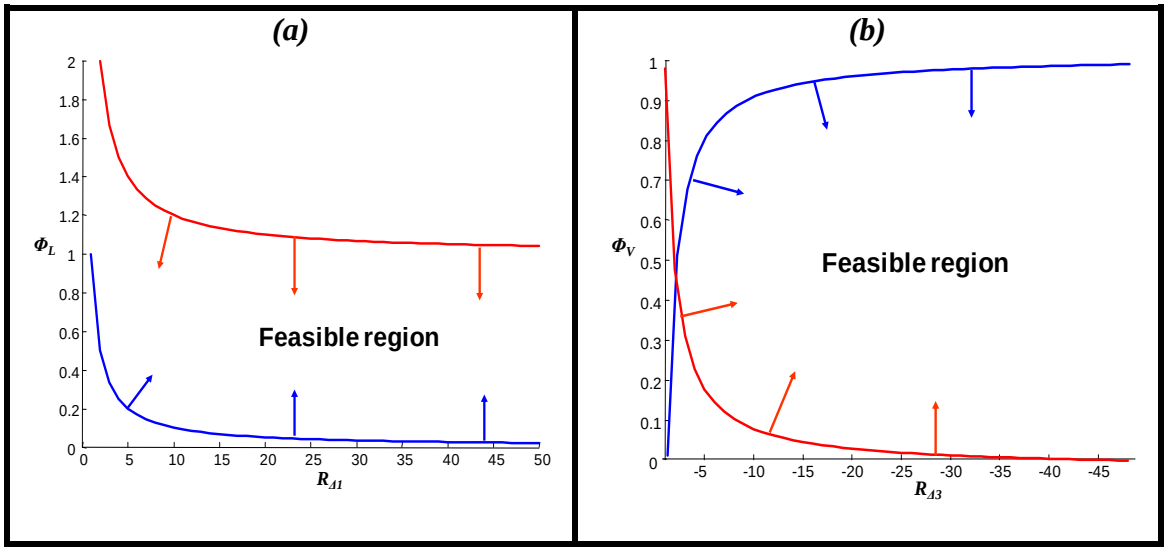


Figure 3.12: Feasible operating regions in R_Δ-Φ space for an equimolar feed and sharp split product specifications from external mass balance constraints for (a) the side stripper and (b) the side rectifier.

Figure 3.12 indicates that the search space has been considerably reduced for deciding on operation parameters. The side stripper has only one meaningful constraint for this particular system, as the other constraint is above the maximum

allowable value for Φ_L. This is due to the fact that the CS_3 (the distillate CS) always has enough material entering it as the feed has been assumed to be pure liquid and hence all the feed is solely directed to this CS and will never violate the mass balance. However, for different thermodynamic feed compositions there will be multiple constraints on the system, as for the side rectifier arrangement in Figure 3.12 b. As the product and feed specifications determine the product flows, a different specification will result in different feasible regions.

3.3.9 AUTOMATIC DESIGN PROCEDURE

With a greater understanding about the interaction of process variables and the degrees of freedom available for manipulation by the designer, it is possible to devise a general design algorithm. The set of steps shown in Figure 3.13, allows one to systematically find feasible solutions quickly and efficiently. Using the Temperature Collocation approach with the minimum BPD as feasibility criterion allows one to judge a certain structure's feasibility in an algorithmic, computational manner.

The algorithm requires in the first step for the designer to set all product specifications. In step two, the internal degrees of freedom are specified. Once steps one and two have been completed, all Difference Points and internal flows may be determined in step 3. Step 4 requires one to construct all principal profiles in CSs that produce final products. The subsequent step evaluates whether there is intersection between two adjacent sections, which means the BPD criterion has been satisfied. If this BPD condition is met, the secondary profiles may be generated in Step 6 starting from the intersection point. Step 7 evaluates the second profile intersection, and if the BPD is again within the specified tolerance, a feasible design has been found. However, if Step 5 or 7 violates the BPD requirement, the procedure requires that either the product specifications or the internal degrees of freedom (or both) have to be modified. With these new specifications, the procedure may be repeated until a feasible design has been found.

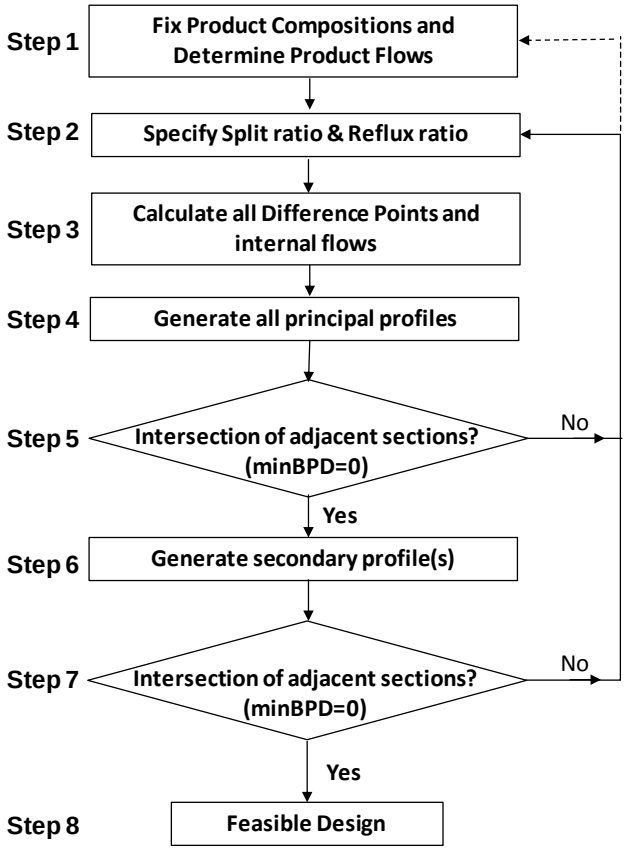


Figure 3.13: An information flow diagram for the systematic design of thermally coupled sidestream columns. Feasible designs require all Bubble Points Distances to be zero.

Once all feasible design specifications have been identified, we may then proceed to judge which of the feasible designs is optimal with respect to some predefined objective function. A frequently used objective function in distillation design is minimum vapour flow as this usually corresponds to minimum energy usage. However, as discussed in previous sections, it is not trivial in thermally coupled sidestream units because there are several utility inputs at multiple Temperature levels which have to be optimally balanced. This point is discussed more in depth in the following example.

3.4 DESIGN TRADE-OFFS

By setting the product and feed specifications and executing the design algorithm described in the preceding section with a continuous combination of the chosen internal design variables for each system, we are able to obtain a spectrum of feasible design solutions. Once all governing equations have been determined, a computer can, relatively quickly and efficiently, render feasible solutions and assess them with respect to suitable objective functions. In this section we shall evaluate a side rectifier/stripper design case study for the Methanol / Ethanol / p-Xylene system using the Non Random Two Liquid (NRTL) activity coefficient model to predict VLE behaviour. The NRTL model is used in all cases to demonstrate this method's ability to model any given system and does not need to make idealized assumptions regarding the VLE behaviour. The Methanol / Ethanol / p-Xylene system, although being zeotropic, displays significant non-ideal behaviour that cannot be sufficiently modelled with the assumption of ideal phase equilibrium, as seen in the comparative Residue Curve Map in Figure 3.14.

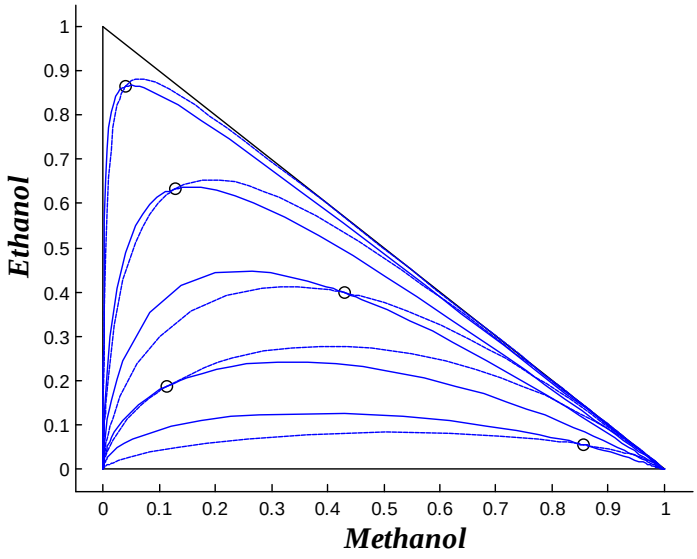


Figure 3.14: A Residue Curve Map for the non-ideal, zeotropic Methanol / Ethanol / p-Xylene system. The black circles indicate the points at which integration is initialized using an ideal model (dashed trajectories) and the NRTL model (solid trajectories).

Figure 3.14 shows large deviations from ideal behaviour for this particular system, implying that the final design solution is strongly dependent on idealized assumptions regarding the thermodynamic model. The feed and product specifications, along with the Antoine vapour pressure coefficients are summarized Table 3.2, followed by the NRTL equation used to incorporate non-ideal mixtures in Equations 3.5 and 3.6. The Antoine coefficients we obtained from the book *Elementary Principles of Chemical Processes* by Felder and Rousseau, while the NRTL coefficients were obtained from the AspenPlus VLE databank.

Table 3.2: Summary of feed and product specifications for the Methanol / Ethanol / p-Xylene system with coefficients for the Antoine equation calculated by log(P^{SAT}) (mmHg)=A-B/(T(^{o}C)+C)

Component	Feed	Distillate	Side	Bottoms	Antoine Coefficients
	Mol fraction				[A,B,C]
Methanol	0.3333	0.9000	0.0800	0.0001	[8.072, 1574.990, 238.870]
Ethanol	0.3333	0.0999	0.9100	0.0499	[8.112, 1592.864, 226.184]
p-Xylene	0.3334	0.0001	0.0100	0.9500	[6.991, 1453.430, 215.307]

The NRTL equation for Methanol (i=1), Ethanol (i=2) and p-Xylene (i=3) for parameters obtained from the ApenPlus Properties Database (AspenPlus):

$$\gamma_i = \exp\left[\frac{\sum_j x_j \tau_{ji} G_{ji}}{\sum_k x_k G_{ki}} + \sum_j \frac{x_j G_{ij}}{\sum_k x_k G_{kj}}\left(\tau_{ij} - \frac{\sum_m x_m \tau_{mj} G_{mj}}{\sum_k x_k G_{kj}}\right)\right] \qquad (3.5)$$

where $\tau_{ij} = a_{ij} + b_{ij}/T(K)$, $G_{ij} = \exp(-c_{ij}\tau_{ij})$, and: (3.6)

$$a=\begin{bmatrix} 0 & 4.7119 & 0.6776 \\ -2.3127 & 0 & 4.0754 \\ -3.2587 & -5.6391 & 0 \end{bmatrix}, b=\begin{bmatrix} 0 & -1162.29 & 295.535 \\ 483.8436 & 0 & -1202.43 \\ 1677.6212 & 504.2010 & 0 \end{bmatrix},$$
$$c=\begin{bmatrix} 0 & 0.3 & 0.47 \\ 0.3 & 0 & 0.3 \\ 0.47 & 0.3 & 0 \end{bmatrix}$$

3.4.1 REBOILER DUTY

Using an inverse design methodology, the product specification will be the primary concern when searching for feasible solutions. Hence, a solution is acceptable only if the exact product specification is met. The product specifications given here obtain a purity of at least 90% in each product stream. These rough targets have been chosen merely for the purpose of illustrating the method and to obtain a sufficiently large spectrum of feasible designs. Furthermore, notice that the product specifications are non-sharp, to exemplify that the proposed method is not bound by sharp split product restrictions. As mentioned in section 3.3.6, thermally coupled sidestream columns have two internal degrees of freedom to be specified. It is thus convenient to compare design trade-offs in terms of the split ratio and reflux ratio for each configuration. This is shown in Figure 3.15, which depicts the spectrum of feasible solutions and the effect on the total reboiler duty (kJ/s) for a feed of 1 mol/s. The overall reboiler duty is equal to the total reboiler duties in each configuration. It should be noted that the regions of feasibility depicted here are strictly system specific, and one may find entirely different regions depending on the phase equilibrium behaviour, product and feed specifications, etc.

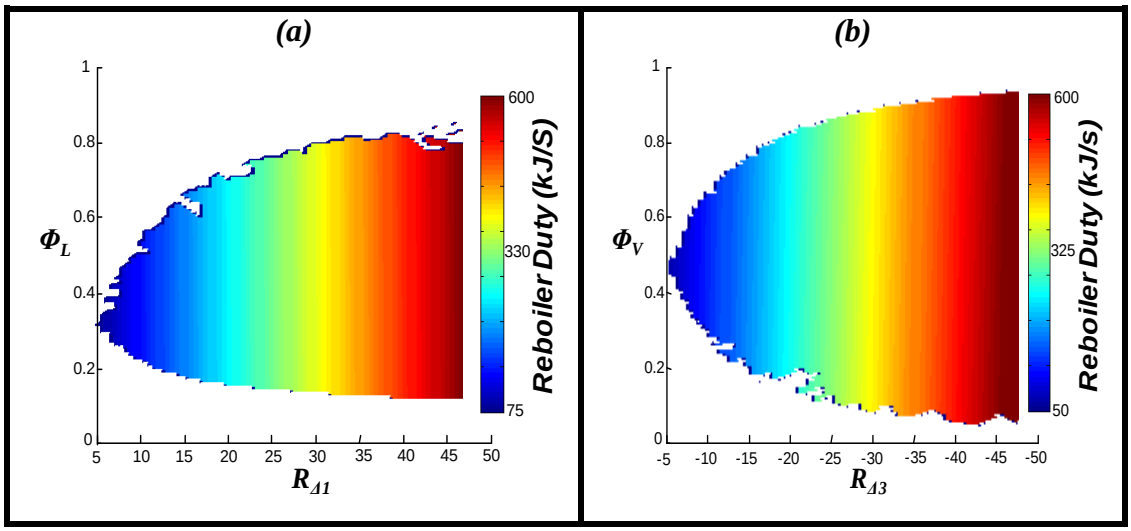


Figure 3.15: Spectrum of feasible designs for (a) the Side Stripper in Φ_L-$R_{\Delta 1}$ space and (b) the Side Rectifier in Φ_V-$R_{\Delta 3}$ space, showing the effect on the total reboiler duty required in the columns.

The design spectra in both Figure 3.15 a and b were constructed by automatically evaluating $10,000$ different combinations of free design variables for each configuration, and shows that there exists a unique region for each configuration where designs may be realized. Any combination of the two internal values that correspond to the coloured region in Figure 3.15 produces a feasible design. However, all feasible designs are not equivalent which gives an opportunity for the assessment of good designs, or at least eliminating bad design decisions. Intuitively, Figure 3.15 shows that the total reboiler duty is minimized when the specified reflux ratio in each configuration is minimized, and vice versa. Furthermore, the reboiler duty of the side stripper is a weak function of the split ratio, because the components in the system have very similar molar latent heats of vaporisation. Since there is only one reboiler in the side rectifier, it is entirely independent of the split ratio.

It is worthwhile to note that the feasible design space was constructed using an exhaustive search, i.e. all solutions were tested. This may of course be time consuming in large scale problems, and more intelligent scanning methods may be need. One may for instance elect to use a sparse search to roughly identify the

feasible region and then hone on a certain area of interest with a denser search. This will significantly reduce the computational time because irrelevant parameters are quickly discarded. However, in this paper we have aimed at producing an entire region of feasibility and therefore have used a dense search throughout.

There are several valuable conclusions that may be drawn from Figure 3.15. First, at the lower ends of the reflux ratio spectrum in this example the side stripper feasible design region is smaller than that of the side rectifier. The spectrum of the side rectifier is much closer to split ratios of zero and one while that of the side stripper is narrower. However, the feasible design region for both these configurations in this case study is infinitely large as feasible designs can still be found at infinite reflux. The larger feasible space open to the side rectifier permits its operation in a wider range compared to the side stripper unit. The additional flexibility may be of relevance in some process plants. Second, even though the relative sizes and shapes of feasible design spectra differ considerably, the range of reboiler duties that suffices the product splits in both configurations are relatively similar, but the side rectifier has a slightly lower minimum duty of approximately 50 kJ/s, while the side stripper requires around 75 kJ/s. Operating at minimum reflux is however an impractical condition. As the ranges for reboiler duty are relatively similar we can conservatively state both designs are equivalent with no significant advantage that may be gained in either one in terms of heat requirements. However, it will become apparent in subsequent sections there are several factors which distinguish these designs.

3.4.2 CAPITAL COST

The reboiler heat demand in a distillation unit constitutes the majority of the operating cost in a distillation unit. Hence we may conclude from a first law point of view that minimum reflux is the optimal operating condition. However, as with conventional columns, operating at minimum reflux requires an infinite number of stages and hence some compromise between these extremes have to be sought. By

combining the Temperature Collocation with the Column Profile Map approaches, it is possible to obtain an expression that allows for the calculation of number of stages too, as shown in Equation 3.7.

$$\frac{dn}{dT} = \frac{\partial n}{\partial \mathrm{x}} \frac{\partial \mathrm{x}}{\partial T} = \frac{\frac{d\mathrm{K}}{dT}\mathrm{x}}{\left[\left(1 + {}^{1}\!/\!_{R_{\Delta}}\right)(\mathrm{x} - \mathrm{y}) + \left({}^{1}\!/\!_{R_{\Delta}}\right)(X_{\Delta} - \mathrm{x})\right]\mathrm{K}} \tag{3.7}$$

It should be noted that the transformation from composition to temperature as the dependent integration variable shown in Equation 3.7 requires a one-to-one mapping between compositions and temperature and thus implies monotonicity of temperature profiles. Some authors point out that in highly non-ideal as well as in reactive distillations, which have additional temperature effects, that temperature monotonicity may not hold (Al-Arfaj and Luyben, 2000, Cheng and Yu, 2005, Bausa et al., 1998). However, the collocation method on generalized column profiles can also be employed without temperature transformation in terms of traditional tray numbers. Thus the proposed design method is not limited to temperature integration. Even though the practical significance of separation trains with non-monotonic temperature profiles has yet to be shown, the existence of special cases where temperature effects can occur should be duly noted.

Using the same approach as above, but applying it to show how the number of stages change in the respective feasible regions results in Figure 3.16. Our analysis accounts for the number of stages in the main column as well as the side unit.

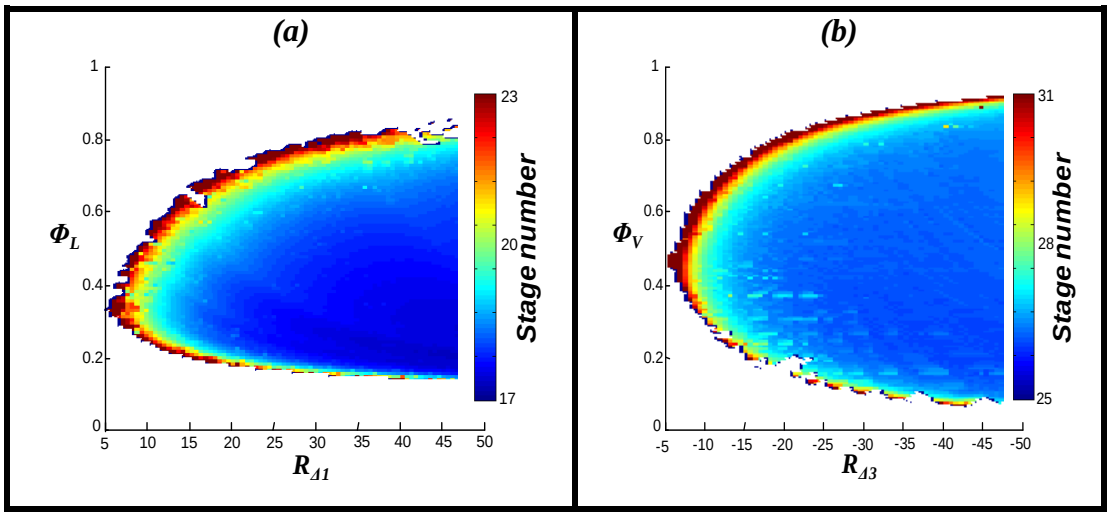


Figure 3.16: Spectrum of feasible designs for (a) the Side Stripper in Φ_L-$R_{\Delta 1}$ space and (b) the Side Rectifier in Φ_V-$R_{\Delta 3}$ space, showing the effect on the total number of stages required in the columns.

It may be seen that, as with distillation design for conventional columns, the designer is faced with a trade-off between two extreme operating choices. Operating at minimum reflux generally corresponds to infinitely many stages, but if one is willing to compromise on first law expenditures, a smaller column may be constructed resulting in reduced capital costs. In both configurations, there is a sharp rise in the number of stages required for a feasible separation as one approaches minimum reflux. The side stripper configuration seems to have a distinct advantage in this instance, as generally for any specific reboiler duty (see Figure 3.15) a saving of about 6-8 stages can be achieved. At the high end of the reflux ratio spectrum in both configurations, the stage numbers start to level off and no further capital cost saving can be achieved.

3.4.3 ENERGY EFFICIENCY

A unique property of side rectifier/stripper columns are the multiple Temperature levels to which heat is added to the reboiler(s) or rejected in the condenser(s). Although there are a multitude of factors that may influence the final choice on how

much heat should be generated at a certain Temperature (economics, heat integration with other process, heat availability, etc), a second law thermodynamic analysis is a valuable method of judging operating conditions in accordance with the modern drive toward energy efficient processes. Such an analysis will direct one toward the most thermal efficient process by searching for the minimum amount of Lost Work (LW) generated. The LW calculation is given in Equation 3.8 by:

$$LW = -T_0\left(\sum\frac{Q_R}{T_R} - \sum\frac{Q_C}{T_C} + F\Delta S_{MIX,F} - P\Delta S_{MIX,P}\right) \tag{3.8}$$

Where Q_R and Q_C are the heat duties in the reboiler and condenser calculated by the product of the respective vapour flowrates and the composition weighted latent heats of vaporization. T_R and T_C are the Temperatures at which the corresponding units require or reject heat at and ΔS_{MIX} is the entropy of mixing of Product (P) and Feed (F) streams, given by definition in Equation 3.9 as:

$$\Delta S_{MIX} = -R\sum_{i=1}^{nc} x_i \ln(x_i) + S^E \tag{3.9}$$

where S^E is the excess entropy for taking non-ideal mixtures into account calculated here by the NRTL activity coefficient model, and R is the universal gas constant. Note that we only use the LW quantity to denote energy efficiency, because the ideal work of separation is exactly the same for both the side stripper and side rectifier. Thus, the LW quantity is directly related to energy efficiency of both structures, i.e. low LW implies high efficiency, and vice versa. This entropy model allows one to assess process alternatives based on the thermal efficiency, as shown in Figure 3.17.

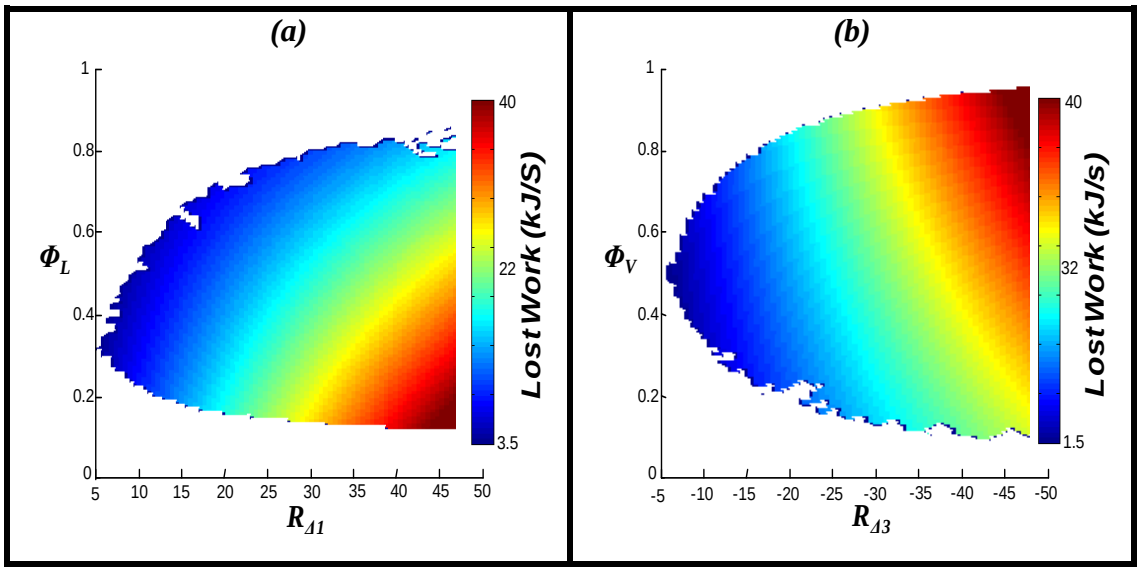


Figure 3.17: Spectrum of feasible designs for (a) the Side Stripper in Φ_L-$R_{\Delta 1}$ space and (b) the Side Rectifier in Φ_V-$R_{\Delta 3}$ space, showing the effect on the Lost Work produced in the columns.

The LW calculation provides additional insight into which split ratio to choose to achieve a thermodynamically efficient process. For the side rectifier, the LW is minimized at low split ratios for a specific reflux ratio, i.e. where less material flow is directed toward the side rectifying unit. The side stripper unit indicates that the minimum LW occurs at higher split ratios, i.e. where more material is directed toward the side stripper. As with the reboiler heat demand however, both units seem to generate similar quantities of LW at the lower end of the spectrum, and from a second law point of view no structure seem to be advantageous when operating near the lower feasibility bound.

3.5 FINALISING THE DESIGN

From the relatively simple calculations shown above it may inferred that, from an energy usage and efficiency point of view, both structures are qualitatively similar. However, the side stripper does offer a marked improvement in the number of stages required, hence for this design we shall choose the side stripper. Guidelines reported

in literature (Seader and Henley, 2006b, Kister, 1992) state that, depending on the system, it is desirable to operate at around 1.05 – 1.5 times minimum reflux ratio to ensure the amount of stages required do not rise too sharply. By comparing all the analyses for stage number and reboiler duty in the side stripper, we decide on operating at a reflux ratio of 13 as this is the point where the number of stages starts to plateau. Refluxes lower than 13 typically lead to a rapid rise in the number of stages. Finally, the second law analysis indicates that the most efficient columns are at a high split ratio, but one should still be aware of the rapid growth in the number of stages. Using these guidelines, conservative design parameters may then be chosen. In this case, a reflux ratio of 13 and a split ratio of 0.45 seems like a good choice, resulting in n=20 equilibrium stages. It should be noted however that this example is merely an illustration of the applicability of the Temperature Collocation with Column Profile Map approach to thermally coupled sidestream column design, and the optimal results may vary with a different objective function for design.

A valuable attribute of the methods described in this paper is a method to solve the *inverse design problem*. Product specifications are set and then internal degrees of freedom specified globally until a feasible design range is identified. If the feasible design space is empty, it can be guaranteed that the product specifications are thermodynamically impossible to realize. Process simulation packages such as AspenPlus have been shown to be an effective and robust tool for interactive process design. In general however, distillation design in such packages is performed by forward performance simulation which predicts product purities based on a given feed and column design specifications (e.g. total column tray, feed tray, reflux ratio ratio, and etc). Although these packages rigorously solve mass, equilibrium, summation and enthalpy (MESH) balances, this approach has the drawback that the designer has to have precise initialization knowledge about the design, and it can be a tedious task to search for design specifications that precisely meet the desired product quality. Furthermore, user effort and adjustment is often proportional to the complexity of the system. Due to this fact, for thermally coupled configurations it is

even harder to achieve convergence to the desired product purities. However, using the method advocated in this paper, the designer is able to set the product specifications, and from this determine what the structural and operating characteristics of the column are.

Once a general idea of the design has been obtained, the results may be used to initialize a process simulator such as AspenPlus for the chosen design specifications. Even parameters that require a large amount of insight or design experience to obtain, such as the location of the feed tray or side-draw trays, can be easily found by locating the stage number where composition profiles intersect. For this design, the side-draw stage and feed stage were found to be at stages 6 and 16, respectively. For this same scenario, the compositional change in the liquid is then verified with AspenPlus. The resulting profiles depicted in Figure 3.18 show an excellent agreement with one another.

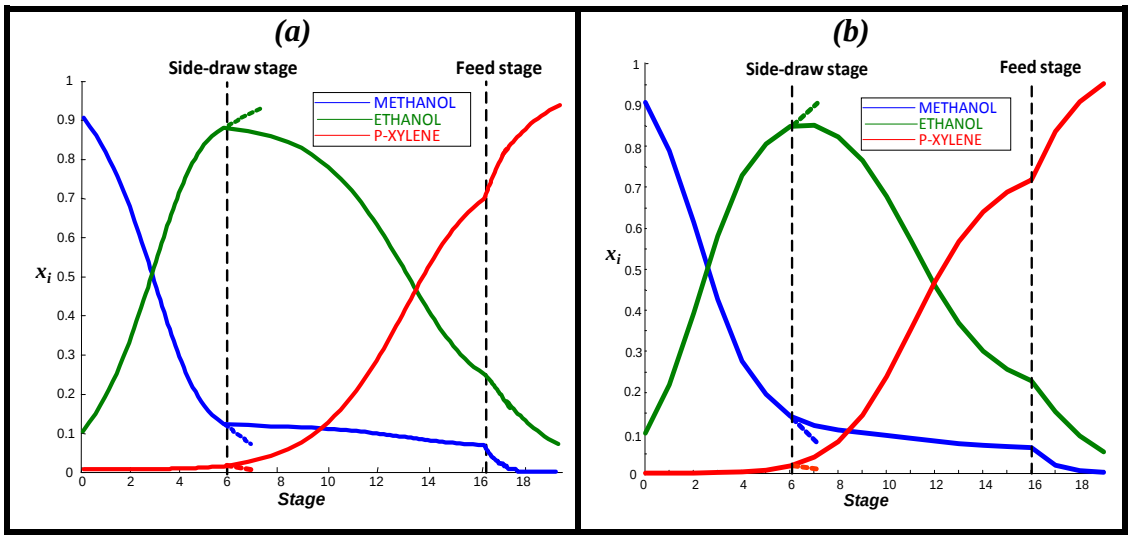


Figure 3.18: Change in liquid composition along the length of the side stripper unit using (a) the Temperature Collocation method and (b) using AspenPlus with precise initialization from the Temperature Collocation method. The main column and side stripper are represented by the solid and dashed lines, respectively.

Small discrepancies in the comparison of compositional change between the proposed method and AspenPlus may be attributed to the assumption of constant molar overflow that is made in the DPE. The predicted molar vapour and liquid flowrates from AspenPlus for the main column body are shown in Figure 3.20. Here one can see that the molar flowrates remain relatively constant, but that there is still some degree of change. Notice however that the product specifications in Figure 3.18 have been precisely met in both cases. Using the information obtained from the above design procedure as input to an AspenPlus simulation generally leads to convergence within a few seconds. Thus, using the techniques described in this work, one can save on valuable engineering design time as well as gain a unique graphical insight into the problem and interaction of all operating variables.

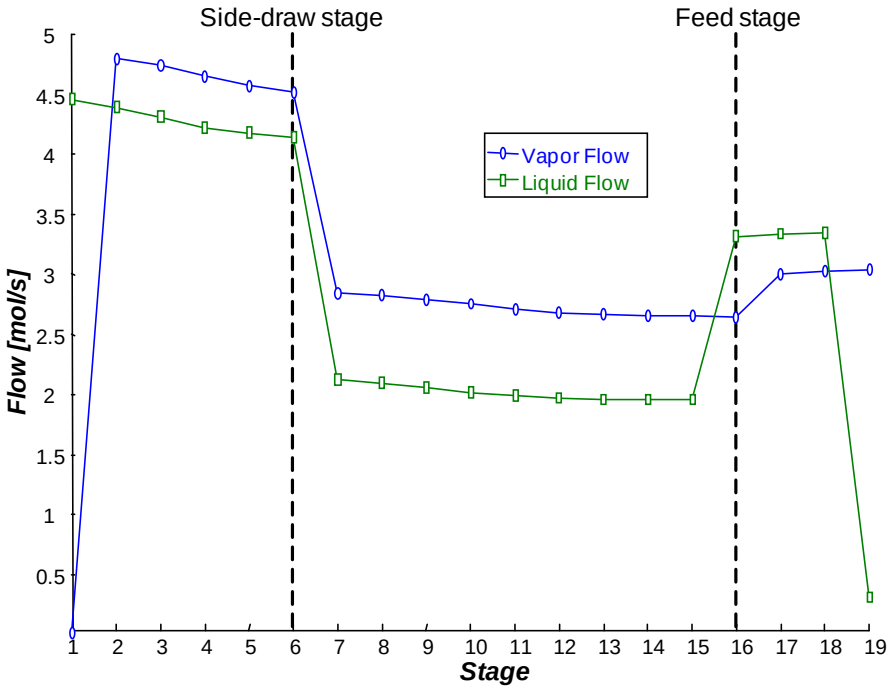


Figure 3.19: Molar liquid and vapour flowrates in the main column.

3.5.1 EXTENSION TO HIGHER ORDER SYSTEMS

The preceding discussions handled the generic case of a single side stripper and rectifier for a ternary system. For higher order systems, i.e. for systems containing more than three components, the design algorithm using the techniques described above can be naturally extended without any modification. However, it should be noted that in higher dimensions, exact intersection of trajectories is more difficult to attain than in the two dimensional case, since the profiles of two adjacent column section may miss each other in additional dimensions (Julka and Doherty, 1990). The advantage of using the minimum BPD approach is that a small BPD function value indicates closeness to a feasible design, and can aid in steering the designer toward a feasible design, rather than being merely a Boolean success or fail intersection criterion. A feasible side rectifier design for a non-ideal quaternary mixture of Benzene / Toluene / p-Xylene / Phenol is shown in Figure 3.20 along with all relevant parameters summarized in Table 3.3.

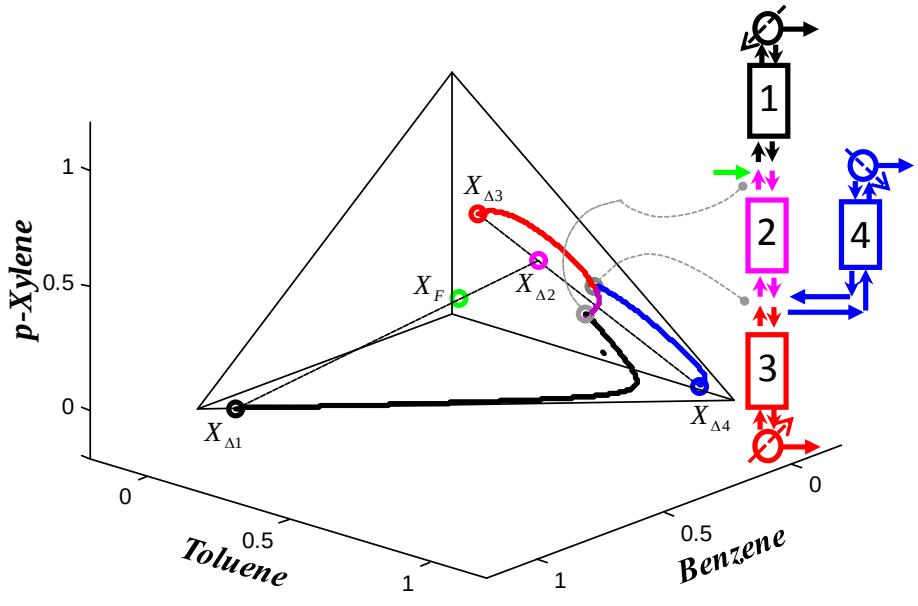


Figure 3.20: A feasible side rectifier design for the Benzene / Toluene / p-Xylene / Phenol system, showing areas of profile intersection and the location of all respective Difference Points.

Table 3.3: Stream table for a Benzene / Toluene / p-Xylene / Phenol system

Column Section	Difference Point	Reflux ratio	Net flow (Δ) (mol/s)
Feed	[0.250; 0.250; 0.250; 0.250]	-	1 (pure liquid)
CS_1	[**0.929; 0.071; 2.38E-4;** 2.20E-5]	4.743	0.260
CS_2	[0.011; 0.313; 0.338; 0.339]	**-3.015**	0.740
CS_3	[**2.61E-5; 0.092; 0.447;** 0.461]	**-4.830**	-0.540
CS_4	[**0.042; 0.910; 0.042**; 0.006]	1.900	0.200

Intuitively for a higher order single side rectifying or stripping unit, at least one product stream will not contain a high purity of a single component (Bottoms product in this case), but once these product specifications have been selected, the design procedure remains the same. Notice that the linear relationship between the relevant Difference Points still holds and that the profile intersection criterion is the same as for the ternary case.

Although the extension to higher order mixtures is, in principle, a mere extrapolation of the procedures presented here it does involve more careful selection of variables. An additional component in a single side stripper/rectifier arrangement requires that two external degrees of freedom be set and may thus requires some additional design experience. Since the composition profiles are extremely dependent on the X_Δ choices of the designer, more components introduce additional difficulties with respect to finding profile intersections. This has been shown in a recent paper where a ten component separation synthesis problem was successfully dealt with in a simple column using the BPD as a feasibility criterion (Kim et al., 2010b). This design was performed for a variety of feeds and product specifications and was subsequently validated with Aspen Plus. Although the graphical characteristics of the method are somewhat lost in higher order systems, the algebraic BPD criterion naturally extends

to these systems. It should be noted that for single side rectifying/stripping unit there are however only two internal degrees of freedom regardless of the number of components. Thus, the feasibility diagrams shown in Figure 3.12 will always be applicable. If, however, there are multiple thermal couplings with multiple stream splits this diagram also becomes multidimensional.

Furthermore, it has been well publicized that composition profiles that originate near pure component vertices are extremely sensitive to the presence of trace components (Levy et al., 1985) , and therefore the refluxes and stage numbers (and feasibility) may differ vastly for only small changes in composition. However, the advantage of using the minimum BPD approach in dealing with both these inherent difficulties (high order systems and trace compounds) is that a small BPD function value indicates closeness to a feasible design, and can aid in steering the designer toward a feasible design, rather than being merely a Boolean success or fail intersection criterion. Thus, by tracking the BPD function value the designer knows how far away a feasible design may be and may adjust parameters accordingly.

3.6 DISCUSSION AND CONCLUSIONS

In this work, a systematic procedure has been proposed to rigorously design and analyze thermally coupled sidestream units, without making use of simplifying assumptions such as constant relative volatilities, sharp splits, or pinched column profiles. The method combines the advantages of the Column Profile Map technique to assess parameter interaction of a specific configuration, with the Temperature Collocation technique to rigorously search for liquid composition profile intersections. This methodology allows a unique graphical insight into the challenging problem of thermally coupled columns. The interaction of internal process variables can easily be assessed with this method and furthermore methods are presented to identify superior design decisions and immediately eliminate poor

design choices, based on reboiler duty, column height and thermodynamic efficiency. Although the aim of the paper is not to search for optimal design solutions, it has been shown that using these novel design techniques, the designer can make informed design decisions to assess feasibility relatively quickly. Furthermore, the inverse design procedure is presented, which allows one to find key operating parameters such as the feed tray and side-draw tray, by setting product specifications and searching feasibility. Designs can be validated with an industrially accepted process simulator such as AspenPlus and in our examples typically lead to fast convergence without further adjustment. Future work in this area includes applying this technique to fully thermally coupled columns such as the Petlyuk and Kaibel columns as well as searching for improvements and a better understanding on other applications of thermally coupled sidestream columns, such as crude distillation. The methods proposed here are also ideal for the design of bio-refineries and azeotropic distillation problems.

Chapter 4 : DESIGN AND ANALYSIS OF MULTIPLE THERMALLY COUPLED CONFIGURATIONS USING COLUMN PROFILE MAPS

The work in this chapter was done together with Ronald Abbas, with equal contributions of from us both. This work is as of yet still unpublished but has been prepared in the form of a paper for future publication. It has also been presented at the AIChE spring meeting in 2011 in Chicago.

ABSTRACT

This paper presents a method for assessing the feasibility of multiple thermally coupled units. The Column Profile Map technique has been applied to the design of a variety of quaternary feeds for a column consisting of a main column with various combinations of side rectifiers and strippers, as well as a fully thermally coupled column in the form of a Kaibel column. Using the Column Profile Map technique one can easily assess feasible designs for systems using novel iso-reflux plots which allows one assess the minimum operating conditions of a specific column and also shows part of an Attainable Region, i.e. a region containing *all* potential designs. Although side stripping units generally require the lowest heat demand for the widest range of feeds (excluding fully thermally coupled arrangements), it is important to also consider the thermodynamic efficiencies as an additional design objective which will generally lead one to choosing an entirely different structure. The fully thermally coupled arrangement presented here was shown to require the least amount of heat addition for a variety of feeds, but also has by far the lowest second law efficiencies.

4.1 INTRODUCTION

The separation of a multi-component mixture via distillation is, although extremely effective, a very energy intensive means of separation. Probably the most widely used application of distillation technology is in petroleum refineries, where a crude oil mixture is separated into gasoline, diesel and kerosene cuts, among others. It has been estimated that the atmospheric distillation unit in a modern refinery consumes energy equivalent to 2% of the crude processed (Bagajewicz and Ji, 2000). The modern atmospheric distillation tower essentially consists of a large main column with several (usually three) thermally coupled side stripping units attached which allows for the removal of all intermediate product cuts.

There have been numerous advances in distillation design, most notably in the area of thermally coupled columns. Fully thermally coupled columns, known as Petlyuk type columns, promise large gains in energy as well as capital expenditures, although it has been suggested that these columns may not be as thermodynamically efficient (Agrawal and Fidkowski, 1998) as other columns. Other thermally coupled columns such as side rectifying columns have found application in air separation (Petlyuk, 2004) as well as replacing entrainer regeneration columns in extractive azeotropic distillation (Emmrich et al., 2001). Numerous other configurations have been proposed that are thermodynamically equivalent to thermally coupled columns and have the potential for similar degrees of cost saving (Engelien and Skogestad, 2005a, Agrawal, 2000c, Agrawal, 2000b, Agrawal and Fidkowski, 1999).

Strangely, with all these advances made in thermally coupled distillation, very little has transpired to crude refineries, with multiple side stripping columns still used in the vast majority of processing plants. Literature contains numerous, rigorous optimization techniques for current crude refinery practice (Bagajewicz, 1998, Bagajewicz and Ji, 2000, Bagajewicz and Soto, 2003, Bagajewicz and Soto, 2000),

but almost no investigation into whether the current structure is fundamentally superior to other options has been found. Even advanced process simulation packages such as AspenPlus only allows one to model and design traditional refinery columns, i.e. side stripping type columns. Only one study in 1995 by (Liebmann and Dhole, 1995) has attempted to address this issue and found that a main column with thermally coupled side rectifiers attached to it, instead of strippers, actually does offer advantages in terms of energy expenditures in certain cases. Thus, it would be useful to fundamentally understand when a certain thermally coupled structure is superior to another, as this could result in potential savings not only in crude refineries, but also in the applications listed above.

Recently, a novel graphical tool for distillation design and analysis, Column Profile Maps (CPMs), was proposed by Holland, Tapp and co-workers (Holland et al., 2004a, Tapp et al., 2004). This technique is a generalisation of a set of ordinary differential equations for conventional rectifying and stripping sections pioneered by Doherty and co-workers (Van Dongen and Doherty, 1985a). This generalisation has been shown to be applicable to the design of any configuration, not only conventional rectifying and stripping sections. The CPM technique has subsequently been applied to the design and analysis of complex thermally coupled configurations such as single side rectifying and stripping units as shown in the preceding chapter, Petlyuk columns (Holland et al., 2010), as well as fully thermally coupled structures for quaternary mixtures such as the Kaibel column (Abbas, 2010).

Due to its graphical nature, the CPM design method offers a unique insight into distillation design problems. The special problem of multiple thermally coupled columns presents an interesting design challenge since there is not only an interaction between the main column and the thermally coupled side units to consider, but also between the thermally coupled units themselves. This problem has been approached by other authors using the Underwood equations (Carlberg and Westerberg, 1989), but these methods have the drawback that they are purely algebraic and the designer

often lacks insight into the interaction of column sections and the internal flow and separation mechanisms. For instance, if a mistake was made in calculating the minimum vapour flows of a complex column using a purely algebraic method, it would be very difficult to pick this mistake up by only looking at the numbers produced through the algebraic equations. Through a graphical technique, this problem is partially eliminated because the designer can quickly see whether there is an error in a particular column section. Moreover, a design using graphical methods often provides more insight into variable interaction (for example, the Mccabe-Thiele method for binary systems allows one to easily gauge the interaction of stage numbers versus reflux). Thus, in this work we shall investigate whether there is a fundamental difference between several options of multi-component thermally coupled distillation configurations by utilising the graphical CPM technique, and therefore determine whether there is a superior structure under certain conditions in terms energy demand and efficiency. To utilise the graphical nature of the method we shall limit the study to quaternary mixtures, and this should lay the foundation for a more advanced study of higher order systems, which are mathematically extendable using this technique. Furthermore, only structures with a main column and thermally coupled side stream units (side rectifying and/or stripping) attached to it will be considered, as this is in line with common refinery practice and existing columns could therefore be retrofitted if possible. The aforementioned structures are compared to themselves as well as to the fully thermally coupled Kaibel column. It should however be noted that there are of course a multitude of other designs that may be considered. Formulating all these structures is not a simple task in itself and work by Agrawal and co-workers have shown that there are thousands of possible structures for a any given separation (Giridhar et al., 2005, Agrawal, 2000a, Agrawal, 2001, Agrawal and Fidkowski, 1999, Agrawal, 1996)of other (perhaps more optimal) columns may be considered utilising combinations of simple, complex and thermally coupled columns

4.2 BACKGROUND: COLUMN PROFILE MAPS

As mentioned in the introduction, CPMs were developed for a generalised column section, enabling it to be used for the design and analysis of almost any conceivable structure, irrespective of the complexity. Thus, this method allows the designer to analyse a specific design before being constrained by pre-conceived structures or other equipment limitations. The generalised column, by definition, is a length of column section between points of material or energy addition or withdrawal (Tapp et al., 2004), as shown in Figure 4.1.

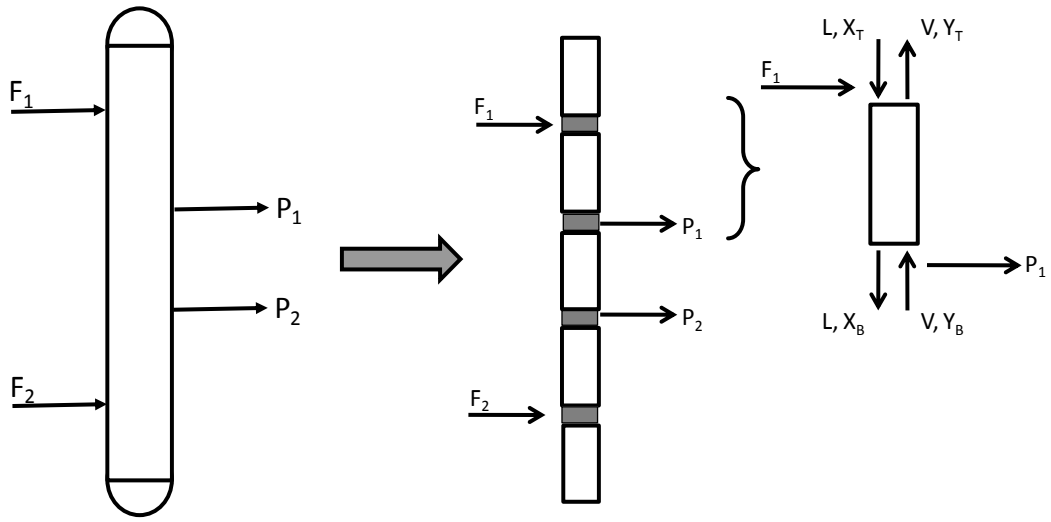


Figure 4.1: An example of a generalised column section

By performing a material balance over the column section followed by a Taylor expansion around stage *n+1*, assuming constant molar overflow, yields:

$$\frac{d\mathrm{x}}{dn} = \left(\frac{1}{R_{\Delta}} + 1\right)\left(\mathrm{x} - \mathrm{y(x)}\right) + \left(\frac{1}{R_{\Delta}}\right)\left(X_{\Delta} - \mathrm{x}\right) \qquad (4.1)$$

where $X_{\Delta} = \left(\frac{VY^{T} - LX^{T}}{V - L}\right)$ and $R_{\Delta} = \frac{L}{V - L} = L / \Delta$

Equation 4.1 is known as the *Difference Point Equation*, where R_{Δ} is a generalised reflux ratio in the column section and n the number of stages. A complete derivation of the Difference Point Equation is given in Appendix G. The parameter X_{Δ} is termed the Difference Point which is regarded as a pseudo composition vector, valid anywhere in the composition space. Like regular compositions, the individual elements of the X_{Δ} sum to unity. Furthermore, in column sections that are terminated by a reboiler or condenser, X_{Δ} is exactly equivalent the composition of the product stream. Negative elements of X_{Δ} are perfectly valid and merely imply that the respective component is flowing downward in the column section. This unique property of X_{Δ} is not even rare, and may be found in complex columns with multiple feeds or product streams (Holland et al., 2010). Accordingly, negative reflux ratios indicate that the section is in stripping mode, i.e. there is a net flow of material down the column ($L>V$) and conversely, positive reflux ratios indicate that a column section is in rectifying mode as there is a net flow of material upwards. The vapour composition, **y(x)**, can be related to the liquid composition using an appropriate phase equilibrium model. Once the aforementioned parameters have been set a CPM may be constructed from different initial compositions, as shown in Figure 4.2 for arbitrarily chosen process parameters.

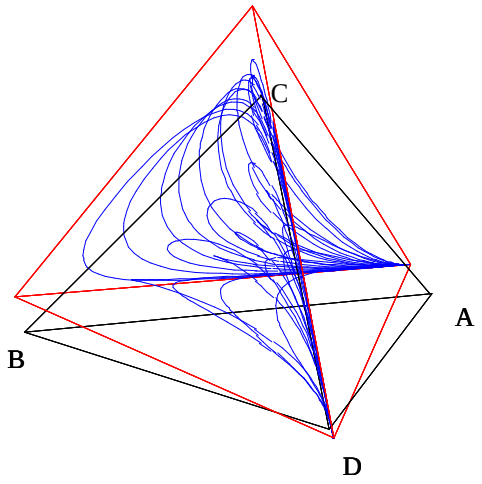


Figure 4.2: A quaternary CPM with R_{Δ}=9 and X_{Δ} = [0.2, -0.3, -0.2] and relative volatilities of 6, 4, 2 and 1. The "shifted tetrahedron" in red indicates the movement of stationary points at finite reflux from the pure component vertices at infinite reflux.

Figure 4.2 represents possible composition trajectories for a single column section. It should be noted that it is mathematically possible to populate the entire composition space with profiles, even in the negative composition space, but these profiles have not been presented in Figure 4.2 for simplicity. This has been shown to add considerable insight to the synthesis of distillation column sections. For a design to be classified as feasible i.e. a network of column sections constituting a column, composition profiles of adjacent column sections have to intersect one another. Figure 4.2 also shows that stationary points have been shifted in composition space, and for the special case of constant relative volatilities, these shifted points may be connected by a straight line, constituting a shifted tetrahedron. It is important to note that these shifted stationary points are obtained by algebraically solving the pinched Difference Point Equation (dx/dn=*0*), and no integration is required. From a synthesis point of view, these shifted tetrahedrons are especially useful for sharp split problems as one of the sides of these tetrahedrons runs precisely through the product compositions. This unique feature has recently been applied to the design of three component Petlyuk columns (Holland et al., 2010, Holland et al., 2004b) with the aid of shifted triangles.

In the sections that follow we shall apply this property to column synthesis by making use of eigenvector theory. It is thus convenient to introduce properties of the eigenvectors of CPMs in this section. The eigenvectors may be determined by finding the $n \times n$ Jacobian matrix of the Difference Point Equation and solving the corresponding eigenvalues and eigenvectors of this matrix. Because the fourth component of a quaternary system is implied through the unity summation property, a quaternary system will have three significant eigenvectors (and a ternary system two). For a range of stationary points we may then generate an eigenvector map for a ternary system, as shown in Figure 4.3. The ternary map in Figure 4.3 essentially represents a plane where the composition of a single component is zero for a quaternary system. Only a ternary map is presented as a quaternary eigenvector map will be too cumbersome to fully visualise as a single point produces a three dimensional eigenvector (three eigenvectors).

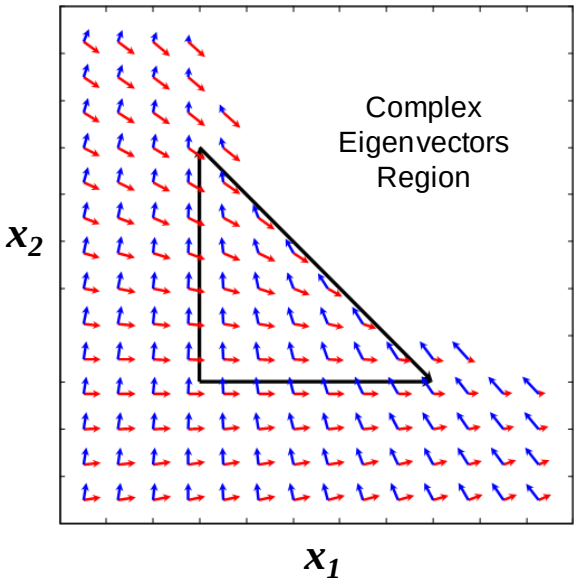


Figure 4.3: A liquid eigenvector map for relative volatilities of [3, 1, 1.5].

Interestingly, the eigenvectors of the Difference Points Equation are only a function of the thermodynamics of the system and not the reflux ratio nor X_{Δ} placement. Thus,

a unique eigenvector map exists for a particular vapour-liquid phase equilibrium model. The eigenvectors characterise the asymptotic direction of the trajectories in the neighbourhood of the singularity. For constant volatility systems, the direction of the eigenvectors at a singularity also indicates the direction where the remaining singularities may be found. Thus, when a stationary point is located at one of the eigenvector points shown in Figure 4.3, the eigenvectors evaluated at the remaining stationary node will point exactly towards one another.

It is worthwhile to mention that the graphical based techniques advocated in this chapter are limited by the number of components in the system. It is extremely difficult to visualise higher order systems (nc>4) on a two dimensional surface, as we have for four components. Nevertheless, the methods are based on sound algebra using concepts like eigenvectors and co-linearity conditions, among others, and may be extended to systems with any number of components, although the visual aspect of the method will be lost.

4.3 DESIGN PROCEDURE

4.3.1 INITIALISATION

The first step in synthesising a distillation column using the CPM technique is identifying a potential structure. We will only consider thermally coupled columns consisting of one main column with multiple side rectifiers and/or strippers attached to it. Thus, to separate a quaternary mixture, four possible structures may be conceived. These are the Double Side Stripper (DSS), the Double Side Rectifier (DSR), the Hybrid Side Stripper-Rectifier- (HSSR) and the fully thermally coupled Kaibel column. Although there are a plethora of thermally coupled arrangements that may be considered, only those that have one main column are presented here as this aligns closely to modern crude refinery practice and therefore represents a more

realistic case study, especially with regards to retrofitting existing columns. However, it should be stressed that *any* column structure can be considered using the techniques presented here. These four columns, along with their respective column section breakdowns are depicted in Figure 4.4. Components have been labelled A through D from the lowest to highest boiling components, and F denotes the system feed.

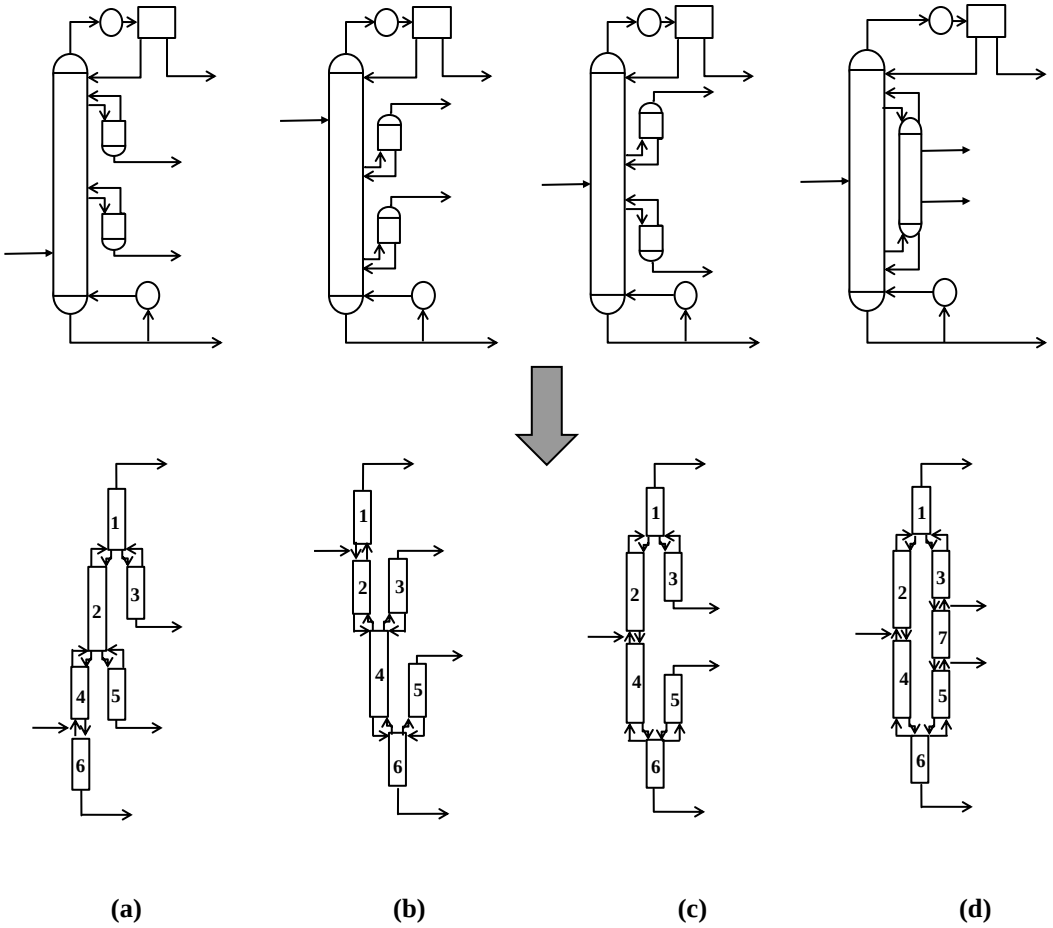


Figure 4.4: A column section breakdown of the four possible structures to separate a quaternary mixture with a main column and thermally coupled side stream units: (a) the DSS, (b) the DSR, (c) the HSSR, and (d) the Kaibel column.

For the purpose of consistency, the column sections of the main column in all structures have been numbered 1, 2, 4 and 6, and the thermally coupled side stream units are labelled column sections 3 and 5. Notice however that the Kaibel column consists of seven column sections, whereas the other structures only consist of six.

The HSSR and the Kaibel column are in fact very similar from a structural point of view, but the addition of a seventh column section to the Kaibel column allows one to remove another set of reboilers/condensers. In total, the DSS, DSR and HSSR each require four energy inputs or removals (condensers and reboilers) while the Kaibel column only requires two. Thus, when compared to a sequence of simple column for performing this separation, each thermal coupling allows one to eliminate one reboiler/condenser when compared to the conventional simple column sequences, and the fully thermally coupled Kaibel column allows one to eliminate four reboilers/condensers. In all structures, the vapour and liquid points of entry and exit at the thermally coupled junction are located at the same position.

Notice that the DSS configuration is closely related to crude refinery columns with multiple thermal coupling through side stripping units, although conventional crude refinery columns are slightly more complex containing even more thermally coupled units and liquid pump-arounds. Interestingly, the DSS, DSR and HSSR are analogous to the simple direct, indirect and pre-fractionating split column sequences between components B and C, respectively. This will become apparent in subsequent discussions. These structures are the only thermally coupled structures with a single main column that permit feasible flow patterns, as it is a necessary condition for the feed to lie below a side stripping section and above a side rectifying section. The reason for this necessary condition will be elaborated in the following section on net flow patterns.

4.3.2 NET FLOW PATTERNS

Any distillation configuration consists of a network of column sections that are either in rectifying or stripping mode. Rectifying sections are characterised by a net flow of material upwards in the column section, while column sections in stripping mode dictate that flow is directed downwards. Therefore, a column section terminated by a reboiler is *always* in stripping mode, and conversely a section terminated by a

condenser is *always* in rectifying mode. This can be proven by mass balance around the reboiler or condenser. However, it is not immediately obvious what the flow directions of internal column sections are. In fact, for fully thermally coupled columns such as the Kaibel column these internal column sections may even change direction depending on the operation of the column. Holland et al. (2010) have shown that there are five potential flow patterns for the Petlyuk column, but only one was shown to be optimal for ideal systems. Similarly, the Kaibel column with a non-sharp product specification has six potential flow patterns but only one is considered optimal. The special case of a sharp product specification, column section 7 in the Kaibel column (Figure 4.4 d) reduces to an infinite reflux section (*V=L),* and therefore has only one viable flow pattern(Abbas, 2010) . This implies that there is no directional flow of material in this column section.

Somewhat counter-intuitively, the DSR, DSS and HSSR depicted in Figure 4.4 have only one permissible flow pattern regardless of the product specification, since the internal column section flow directions are predetermined by the product producing column sections coupled to them. The net flow directions of each column section in the aforementioned structures are summarised in Figure 4.5.

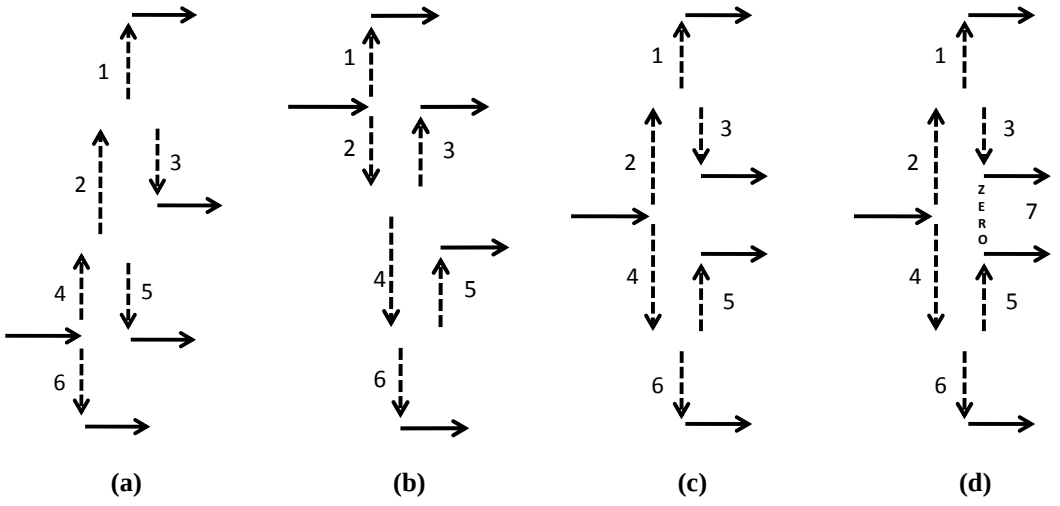


Figure 4.5: A summary of the only possible net flow directions in the (a) DSR (b) DSS (c) HSSR and (d) Kaibel column.

Notice that the column sections above and below the column feed stream always flow up and down, respectively. This is effectively a rectifying and stripping column section below and above the feed. Furthermore, notice that all these structures merely break down into a network of equivalent rectifying or stripping sections, or in other words, a network of simple columns. Consider for example Figure 4.5 a. Column sections 4 and 6 are considered equivalent rectifying and stripping sections for the feed stream. Similarly, column section 4 can be seen as the feed to the equivalent rectifying and stripping sections consisting of column sections 2 and 5, and so on. As mentioned previously, these four structures are the only ones that permit feasible flow patterns. This is due to the fact placing the stream below a rectifying unit or above a stripping unit would lead to a contradiction of flow patterns, since, somewhere in the column, there would be either two stripping or rectifying sections coupled to each other, essentially a simple column with two reboilers and no condensers, or vice versa, which is an impossible mode of operation for ideal systems.

4.3.3 DIFFERENCE POINT PLACEMENT

The Difference Point, X_{Δ}, can be seen as a pseudo composition that corresponds exactly to the product specification in column sections terminated by a reboiler or condenser. It has been shown in previous work that X_{Δ} in adjacent column sections are linearly related to one another, similarly to distillate, bottoms and feed compositions in simple columns (Holland et al., 2010). The Difference Points in internal column sections also have to abide by the same material balance constraints and are also linearly related to the adjacent column sections, and therefore portray similar behaviour as real bottoms or distillate products. For the DSS, DSR and HSSR structures introduced in the previous section, the relationships between the respective Difference Points are presented in Figure 4.6 for pure component product specifications and an equimolar feed.

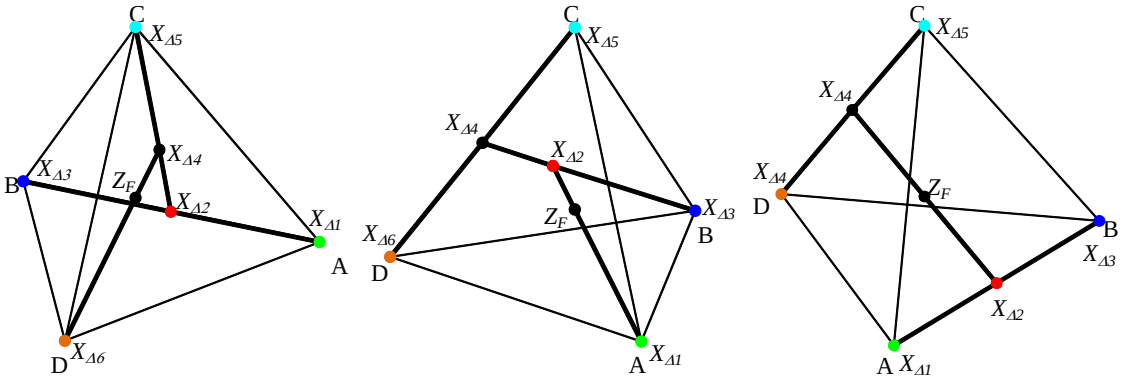


Figure 4.6: Difference Point placement for (a) the DSS, (b) the DSR, (c) the HSSR, showing the relationship between the respective Difference Points and adjacent column sections.

Due to the fact that column section 7 of the Kaibel column operates at infinite reflux, its component mass balance properties, i.e. its X_{Δ} placement, is equivalent to the HSSR. A summary of all Difference Points in the respective column sections are given in Table 4.1 for the same specifications for Figure 4.6.

Table 4.1 A summary of X_{Δ} placement for various structures with sharp splits and an equimolar feed. Shaded cells indicate rectifying sections.

Column Section	DSS	DSR	HSSR	Kaibel
1	[1,0,0]	[1,0,0]	[1,0,0]	[1,0,0]
2	[0.5, 0.5, 0]	[0, 0.33, 0.33]	[0.5, 0.5, 0]	[0.5, 0.5, 0]
3	[0, 1, 0]	[0, 1, 0]	[0, 1, 0]	[0, 1, 0]
4	[0.33, 0.33, 0.33]	[0, 0, 0.5]	[0, 0, 0.5]	[0, 0, 0.5]
5	[0, 0, 1]	[0, 0, 1]	[0, 0, 1]	[0, 0, 1]
6	[0, 0, 0]	[0, 0, 0]	[0, 0, 0]	[0, 0, 0]
z_F	[0.25, 0.25, 0.25]	[0.25, 0.25, 0.25]	[0.25, 0.25, 0.25]	[0.25, 0.25, 0.25]

The shaded cells in Table 4.1 indicates an equivalent rectifying column section, therefore the Difference Points in these column sections may be treated as distillate

compositions. In the same manner, the un-shaded cells indicate equivalent stripping sections which Difference Points are pseudo bottoms compositions.

4.3.4 VARIABLE SELECTION

Intuitively, each thermally coupled unit introduces an additional degree of freedom because the designer may specify the amount of liquid or vapour that is directed toward the side unit. This implies that a reflux ratio has to be specified in each thermally coupled side stream unit. However, reflux ratios are unbound parameters and may, theoretically, be specified from zero to negative or positive infinity. Thus, it is convenient to define a split ratio (Φ), which governs the amount of material sent to the side unit. For side stripping and rectifying units this ratio is given in Equations 4.2 and 4.3, respectively.

$$1-\Phi_L = \frac{L_{SS}}{L_{MC}} \tag{4.2}$$

$$1-\Phi_V = \frac{V_{SR}}{V_{MC}} \tag{4.3}$$

The subscripts *SS, SR* and *MC* indicate a Side Stripper, Side Rectifier and the Main Column, respectively. The parameters Φ_L (for liquid splits) and Φ_V (for vapour splits) specify the fraction of material being sent from the main column to the adjacent main column section at the split location. The fraction of material directed toward the side unit is thus given by subtracting the respective split ratio from unity. Conveniently, this parameter is bound between zero and one regardless of rectifying or stripping sections, and thus allows for representation in a constrained, positive space, regardless of rectifying or stripping section. Furthermore, it is more convenient to represent internal variables such as the reflux ratio in the Φ-space when searching for feasible designs. This will become apparent in subsequent discussions.

4.3.5 FEASIBILITY CRITERIA

Eigenvector criteria

A realizable column design has been shown to exist when liquid composition profiles intersect one another (Van Dongen and Doherty, 1985a). The constant relative volatility, sharp split design problem is very useful as feasible designs may be found algebraically by solving the pinched Difference Point Equation. In terms of a quaternary separation, the shifted stationary points thus result in a shifted tetrahedron, as depicted in Figure 4.2. A sharp split design may then be rendered feasible if their respective shifted tetrahedrons overlap one another on the same plane and the line of the product specifications. In order to illustrate this feasibility criterion, consider the one feed-two product simple column shown in Figure 4.7.

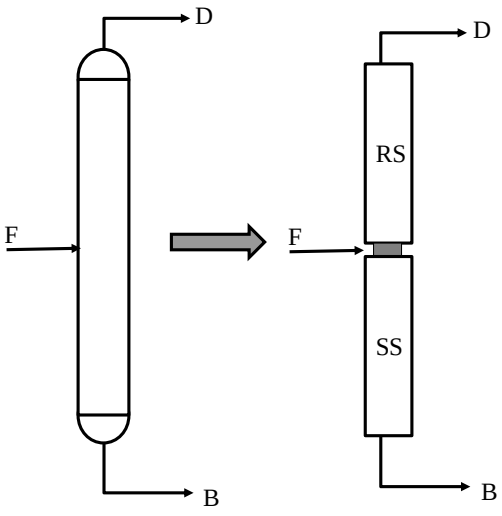


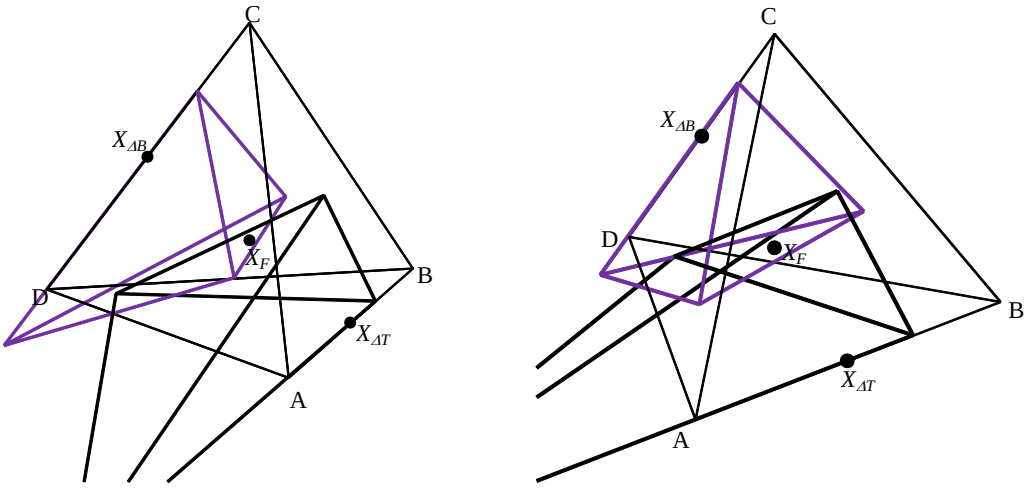
Figure 4.7: A simple, one feed two product column with the associated column section breakdown.

The simple column in Figure 4.7 consists of a rectifying (*RS*) and stripping (*SS*) section. The column is fully specified by choosing the product compositions and the reflux ratio, either in the rectifying or stripping section. Once either reflux ratio has

been specified, the other may be determined from an energy balance around the column, but the assumption of constant molar overflow (similar latent heat and heat effects of all components) allows one to determine the remaining reflux ratio by a material balance at the feed stage. The rectifying and stripping sections are thus related by Equation 4.4:

$$R_{\Delta S} = \frac{Fq + DR_{\Delta R}}{D - F} \qquad (4.4)$$

Where the subscripts *S* and *R* indicate rectifying and stripping column sections and *q* is the vapour quality of the feed. All parameters for both column sections are thus completely specified (as X_{Δ} is equivalent to the product specification in each column section) to construct their associated shifted tetrahedrons. These shifted tetrahedrons are presented in Figure 4.8 a-c, showing a feasible design at minimum reflux, an over-refluxed feasible design and an under-refluxed infeasible design for a quaternary feed. Note that for the design at minimum reflux (Figure 4.8 a) that the planes of the purple and black tetrahedrons are exactly co-planar. The over-refluxed design (b) is characterised by the purple and black tetrahedrons overlapping one another i.e. *past* the co-planar condition, while the under-refluxed design (c) shows that the purple and black tetrahedrons do not touch each other at all, i.e. *before* the minimum reflux condition.”



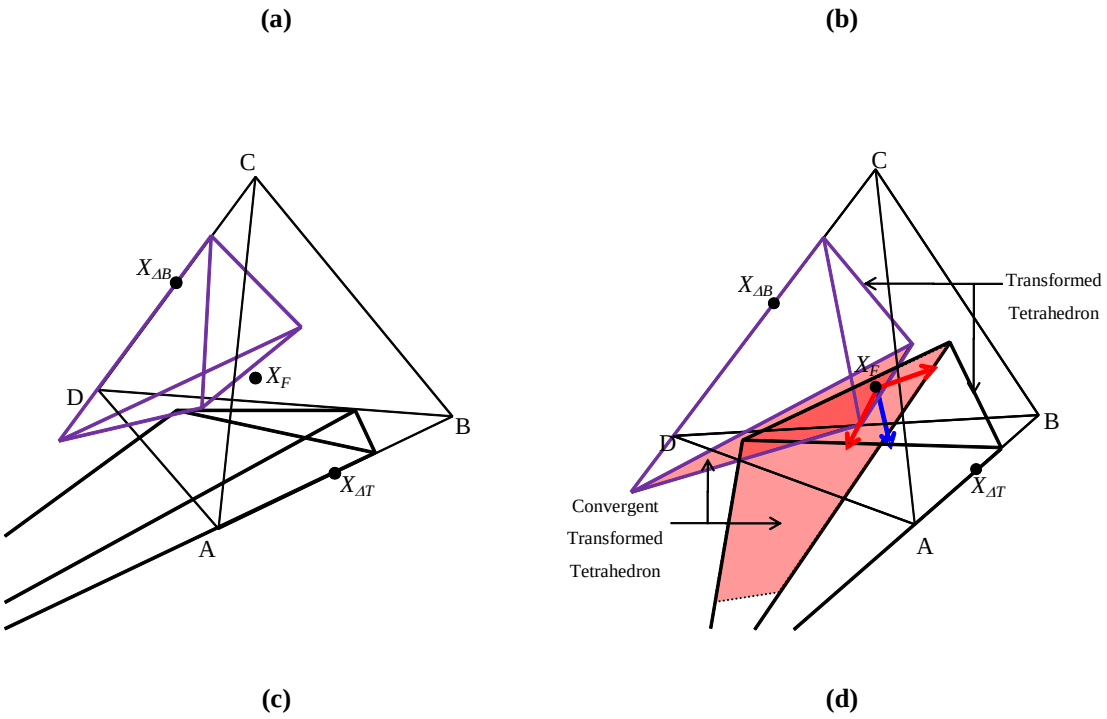


Figure 4.8: A design for an equimolar quaternary mixture in a simple column for the AB-CD split at (a) minimum reflux, (b) above minimum reflux, (c) below minimum reflux and (d) planar intersection through eigenvectors evaluated at the feed condition.

Figure 4.8 shows how feasible designs may be graphically discriminated using this simplifying case of the CPM technique. The interactions of the transformed tetrahedrons with one another under minimum reflux conditions provides a unique, geometric opportunity for evaluating the feasibility of a certain column (see Figure 4.8 a and d). Other authors have shown that the minimum reflux for ternary systems based on any sharp split would be established when the transformed triangles of the rectifying and stripping section meet along a boundary through the feed (See Figure 4.9) (Abbas et al., 2010, Holland et al., 2010). With specified feed, distillate and bottoms compositions, the exact condition for minimum reflux is thus that the tangent to the saddle pinch profile and the feed pinch point is a straight line through the feed composition. This creates a co-linearity criterion under minimum reflux conditions based on the feed where the saddle node of the rectifying section is collinear with the unstable node of the stripping section and the feed composition. The boundaries

between stationary points for constant relative volatility systems are straight lines since the eigenvectors evaluated at the stationary nodes point directly towards the other stationary points. For a ternary system this is easily visualised, and can be seen in Figure 4.9.

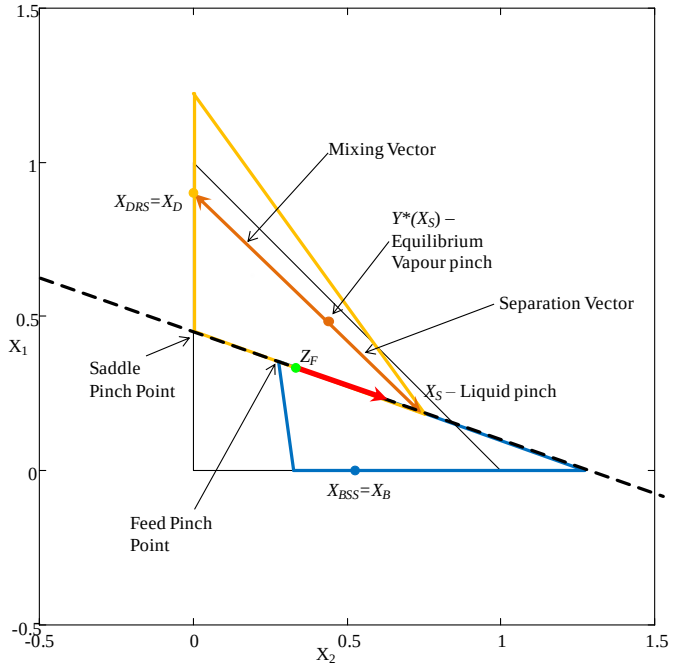


Figure 4.9: Minimum reflux Transformed Triangle interaction depicting the co-linear common eigenvector.

Figure 4.9 shows that one of the eigenvectors (in red) at the feed are exactly co-linear to the shifted triangle indicated in blue. Although there exists two eigenvectors at the feed, only one is pertinent to the system. This is regarded as the common (or dominant) eigenvector, analogous to the common roots of the Underwood Equation. The selection of the appropriate eigenvector based on product specifications of the column. A more in depth analysis is given on eigenvectors for distillation design is given by Abbas, Halvorsen and Holland (Abbas et al., 2010).

For the quaternary system, a minimum reflux solution is based on interactions of the *planes* of the transformed tetrahedrons. More specifically, the minimum reflux

solution is found when the planes of the rectifying and stripping sections are co-planar through the feed. Thus, the eigenvectors evaluated at the feed condition provides the co-planar surface where the transformed tetrahedrons interact under minimum reflux conditions. If the feed is a liquid the planes of the liquid transformed tetrahedrons will pass through the feed and vice versa for a vapour feed. Therefore by evaluating the eigenvectors at the feed condition produces the co-planar surface where the saddle pinch and feed pinch lie on the same plane through the feed at minimum reflux. The eigenvector evaluation at the feed composition thus produces an opportunity to determine the stationary points along the co-planar surface and therefore the reflux associated to the minimum transformed tetrahedrons.

Finding the stationary points, for any system irrespective of thermodynamic properties, would involve solving the right hand side of the Difference Point Equation when it is equivalent to zero. At a stationary point this implies from a geometrical point of view that the mixing vector, $\widetilde{m} = X_{\Delta} - x$, becomes co-linear with the separation vector, $\tilde{s} = x - y(x)$. In order to determine the pinch point of the transformed tetrahedron on the co-planar surface, simple analytic tools may be used as the roots for a constant relative volatility system can be relatively easily. In fact, Chapter 6 of this thesis shows that for constant relative volatility systems, it is possible to calculate the stationary points of the difference point equation (very swiftly) for a given column section by simply finding the roots of a polynomial, using a variable transformation technique. The commonality of the co-planar surface eigenvectors and the co-linear mixing and separation vectors allows for the determination of the stationary point associated to the minimum reflux transformed tetrahedrons. This feasibility criterion using the eigenvectors is depicted in Figure 4.8 d. Importantly, the solutions obtained using the techniques described above for finding minimum reflux is exactly equivalent to the minimum reflux solutions predicted by the Underwood method.

Special feed conditions

The solution discussed above is only applicable to feeds that are either pure liquid i.e. *q=1*, or pure vapour i.e. *q=0*. Since this paper utilises two-phase feeds with *0<q<1*, as well as super-heated vapour (*q<0*) and sub-cooled liquid (*q>1*) feeds, and not only pure liquid or vapour feeds, a slight modification to the aforementioned minimum reflux solution is required. The solution involves finding the minimum reflux transformed tetrahedrons for both pure liquid and pure vapour feeds first and then determining the transformed tetrahedrons for a different quality of feed. Due to the fact that shifting of the liquid and vapour transformed tetrahedrons are very similar when changing the reflux, it is remarkable to note that it is only necessary to focus on the liquid or the vapour transformed tetrahedrons to find the solution for a different quality of feed. This can be seen in Figure 4.10.

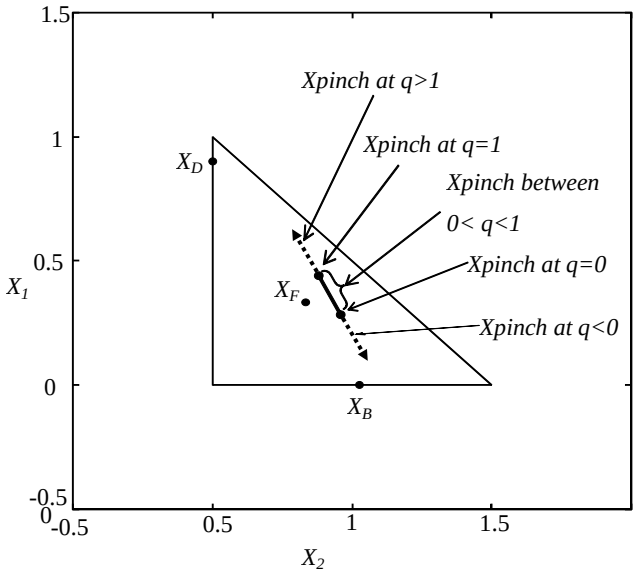


Figure 4.10: Pinch point locations for various feed qualities

The solid black line is the location of the rectifying pinch points where the feed has two phases. The dashed lines indicate the pinch location of superheated vapour and sub-cooled liquid on either side of two-phase region. The two phase feed solution will

thus involve using the two stationary points at the minimum reflux conditions; one point on the liquid feed solution and the same nature of node on the vapour feed solution will arise. A straight line through these nodes sets the relative bound of the two phase feed ($0<q<1$). The liquid stationary point solution with a feed quality of 0.5 for example will then lie on the middle point of the line between these nodes. As the difference points are already known, the only variable left to calculate is the relative minimum reflux solution which is now based on the set quality of the feed. If the solution for a super heated vapour feed is required, the same interpolation like procedure can be used. When a super heated vapour is required, then the stationary point is found in the direction of the vapour transformed tetrahedron on the same straight line and vice versa for a super cooled liquid feed.

The extension to the equivalent higher order systems minimum reflux solution is based on the same principles as the ternary and quaternary systems. As mentioned previously the minimum reflux solution for the ternary system is based on the linear interactions of the eigenvectors, mixing vectors and separation vectors. The quaternary solution is based on the planar interactions of the transformed tetrahedrons for the rectifying and stripping sections and the evaluated eigenvectors at the feed.

.

In the same way in which we evaluated the eigenvectors at the feed composition and produced the co-linear and co-planar lines and surfaces where the transformed triangles/tetrahedrons met, the eigenvector evaluation at the feed composition for higher order systems produces the co-hyper-planar boundaries where the transformed hyper planes touch. In order to determine higher order system minimum reflux solutions the stationary points must thus interact on hyper planes of the desired number of components as required. In order to determine the pinch point of the transformed hyper planes, the point where the co-linear mixing and separation vector intersects with the co-hyper-planar boundary is one of the minimum reflux stationary points. The exact same solution as mentioned above for different quality of feeds is directly applicable to any higher order systems, but cannot be graphically visualised.

The minimum reflux solution discussed above is called the Column Profile Map-Eigenvector technique (CPM-E). Figure 4.8 d shows the interaction of planes at minimum reflux conditions. The CPM-E technique and hence the eigenvector evaluation at the feed composition depending on the quality of the feed is thus an exact criterion for finding a feasible design and is not limited by the number of components to be considered. This criterion can be extended to non-ideal systems as an approximation, since the eigenvectors at stationary points do not exactly line up with one another along lines/planes. It is important to note that even though a wide variety of feed conditions are encountered in our design problems, the generic liquid *and* vapour transformed polygons both always intersect with one another when the design is feasible. It is therefore only necessary to evaluate the liquid transformed polygons and profiles (Holland et al., 2010) for discriminating between feasible and infeasible designs.

4.3.6 THERMALLY COUPLED COLUMN SECTIONS

Section 4.3.5 discusses how designs may be classified as feasible for a simple column. The design procedure outlined thus far allows for a unique graphical insight into the design of simple distillation columns at minimum reflux. In order to analyse more complex thermally coupled columns, it is therefore useful to retain the general design ideas for simple columns and extrapolate it to more complex systems. A similar approach to the one described in this section has been adopted by other authors using the Underwood equations (Carlberg and Westerberg, 1989), but it is somewhat laborious in that new parameters have to be defined for each thermal coupling. We present is here in terms of our generalised defined variables to show the applicability of the CPM-E technique to the analysis of thermally coupled columns. Fortunately, the definition of X_{Δ} allows one to easily extend this methodology to any structure since it is in fact a pseudo composition. Using the techniques described here, any column may be broken down into a network of simple columns with the

same general design procedure described for the simple column. To illustrate this fact, consider a generic thermally coupled side rectifying and stripping unit as shown in Figure 4.1 a and b.

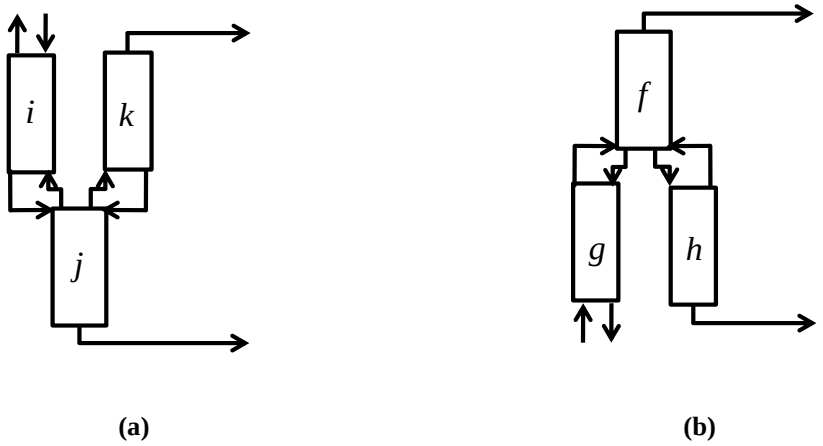


Figure 4.11: A generic thermally coupled (a) side rectifying and (b) side stripping with the corresponding net flow directions of each column section.

In the side rectifying arrangement Figure 4.11 a, the vapour from column section *j* feeds both column sections *i* and *k,* while column section *i* and *k*'s combined liquid streams feed column section *j*. The amount of vapour to be distributed between sections *i* and *k* are governed by the vapour split ratio. Since the vapour split and liquid feed point is assumed to take place at the same location in the column and column sections *j* and *k* are producing end products, the net material flow from column section *i* is effectively the feed to column sections *j* and *k*. Thus, by adding the directional vapour and liquid in the feed column section, *i*, the net feed flowrate may be obtained. In terms of our CPM parameters this results in: $F_i = |\Delta_i|$, since the feed always has to be positive. This is then essentially the pseudo feed to the simple column comprising of rectifying section *k* and stripping section *j*. Furthermore, the composition of this pseudo feed stream is equivalent to the Difference Point of column section *i* ($X_{\Delta i}$), which may be calculated *a priori* once the product compositions have been set (see section 4.3.2) as shown in Figure 4.6 and Table 4.1.

The quality of the pseudo feed is the fraction of liquid in the feed, and can thus be written as:

$$q_i = \frac{L_i}{F_i} = \frac{L_i}{|\Delta_i|} = \frac{L_i}{-\Delta_i} = -R_{\Delta i} \tag{4.5}$$

Since Column Section *i* is in stripping mode and Δ_i is negative. In a similar manner, the flowrate, composition and quality of the pseudo feed may be derived for the generic stripping section. The parameters for both configurations are summarised in Table 4.2.

Table 4.2: Summary of pseudo feed streams to the generic side rectifying and stripping sections

Structure	**Feed flowrate (*F*)**	**Feed composition (X_f)**	**Feed quality (*q*)**
Side Rectifier	$V_i - L_i = \Delta_i$	$X_{\Delta i}$	$-R_{\Delta i}$
Side Stripper	$-(V_g - L_g) = -\Delta_g$	$X_{\Delta g}$	$-R_{\Delta g}$

Interestingly, the pseudo feed quality is always the negative of the generalised reflux ratio in the feed column section, regardless of the structure. Thus, the feed to a column section with a side rectifier can be seen as pseudo superheated, since $R_{\Delta i}$ is always positive, and conversely the feed to a column section with a side stripper can be seen as pseudo sub-cooled since $R_{\Delta g}$ is always negative. The key parameters in the CPM technique thus extend naturally to incorporate thermally coupled columns. Essentially, these definitions aid in breaking down the complex structures to a set of pseudo binary columns which may easily be analysed and interpreted.

4.3.7 STEPWISE DESIGN ALGORITHM

The theory described in the preceding sections can now be put together in a stepwise design algorithm which allows one to evaluate virtually any given structure. This design procedure is summarised as follows:

- ***Step 1:*** Formulate a configuration to evaluate or design.
- ***Step 2:*** Set the product specifications for each product producing column section and determine the overall mass balance.
- ***Step 3:*** Define the appropriate split ratios, choose a reference reflux ratio for one column section (usually one located above/below the feed) and determine the generic internal mass balances, which specify all internal Difference Points and material flows.
- ***Step 4:*** Determine the minimum reflux for the "pseudo simple column" using the CPM-E technique with column sections located above and below the feed, using the Difference Points as bottoms and distillate compositions.
- ***Step 4b:*** If necessary, specify an over-refluxed factor, i.e. a factor that will account for a non-pinched design.
- ***Step 5:*** Determine all net material flows and reflux ratios in the respective "pseudo simple column" and use these as the new feed for the new adjacent "pseudo simple column" with the feed conditions outlined in section 4.3.6.
- ***Step 6:*** Repeat from Step 4 until the entire column has been specified.

4.4 FINALISING THE DESIGN

4.4.1 ISO-REFLUX ANALYSIS

Once a fundamental understanding of the design procedure has been gained, we may easily evaluate our given structures. In order to determine what the minimum operational conditions of a particular structure is, it is at first useful to specify that all column sections operate at minimum reflux. This constraint allows one to search for feasible design using the eigenvector theory discussed above and allows for a fair basis of comparison between various structures. However, this constraint can be easily relaxed and one can decide to operate a certain set of column sections above minimum reflux once it has been determined. Since our thermally coupled units

described above have three internal degrees of freedom (one reflux ratio and two split ratios), it is convenient to represent all column sections in one diagram to obtain an intuitive understanding of the interaction of column sections. This can be done in an iso-reflux plot, shown in Figure 4.12 for the DSS, where Φ_{L1} and Φ_{L2} indicate the top and bottom liquid split ratios in the DSS as shown in Figure 4.4. This plot is obtained by writing all the reflux ratios in the column sections in terms of the split ratios (see Appendix E). Once the minimum reflux for each column section has been obtained through the eigenvector techniques outlined above, these reflux values can be simply substituted into the equations given in Appendix E for each given structure. One can then obtain what range of split ratios that will satisfy the minimum reflux condition for each column section and conveniently represent this in a split ratio space.

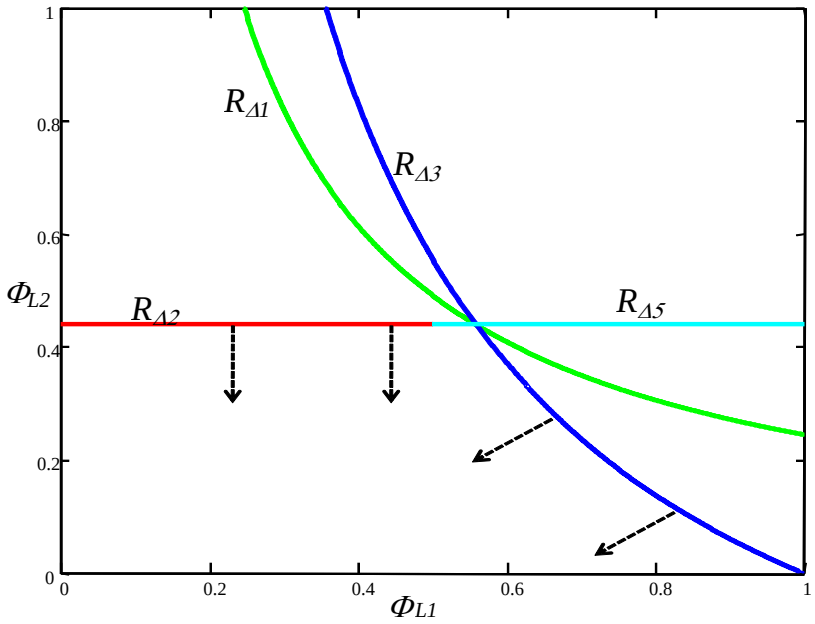


Figure 4.12: An iso-reflux plot for the DSS at minimum reflux.

Figure 4.12 shows the range of split ratios that result in specific column sections operating at minimum reflux. The specific reflux ratios at minimum reflux are given at the end of this section in Table 4.3. From this diagram one is able to quickly realise that there is a certain combination of Φ_{L1} and Φ_{L2} that results in a specific

combination of a column sections operating at minimum reflux to the one adjacent to it. However, there is only a single point where all sections are at minimum reflux with one another. This point occurs where all the iso-reflux lines intersect one another, as every simple pseudo simple column operates at minimum reflux, therefore the entire column operates at minimum reflux. Thus, we have now determined from this relatively simple plot what the reflux ratios in each column section is required to be, and therefore the split ratios too, for the entire column to operate at minimum reflux. Figure 4.12 shows that there is only one selection of Φ_{L1} and Φ_{L2} that satisfies the minimum reflux criterion, where all iso-reflux lines intersect one another.

Each curve in Figure 4.12 represents the reflux ratio that a particular column section is required to be at. It is important to note that the mass balance has been performed by starting across the feed stage and working upwards. From this mass balance perspective, the reflux of top column sections, i.e. 1 and 3, are dependent on both Φ_{L1} and Φ_{L2} (blue and green curves), while the refluxes of column sections 2 and 5 are only dependent on Φ_{L1} (red and cyan curves) .The iso-reflux curves of column sections 1 and 3 are thus curved, while those of column sections 2 and 5 are straight lines that fall exactly on one another. From this figure it may also be inferred that there not only is the interaction between the main column and the thermally coupled side units, but also between the side units themselves.

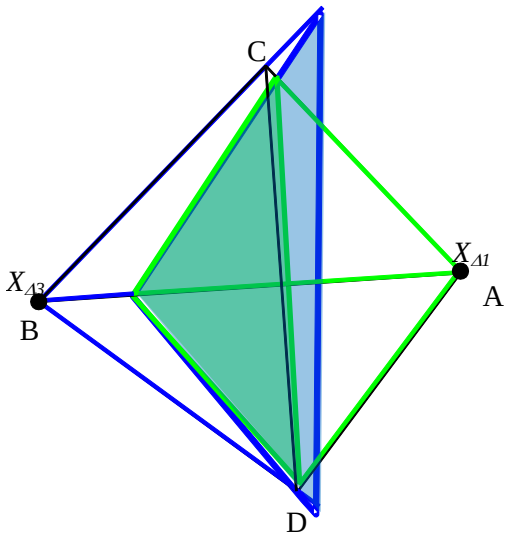
Apart from showing the absolute minimum reflux of all column sections, these iso-reflux lines also depict an Attainable Region. By Attainable Region we mean the region containing all possible operating modes of the process (Hildebrandt and Glasser, 1990). In other words, any selection of parameters within the Attainable Region will result in a feasible design for the given feed and product specifications. However, it should be noted that not all points within the Attainable Region are equal, i.e. some point may be more desirable than others. Although the Attainable Region idea was first used to identify optimal reactor structures, it has also been applied to distillation by other researchers for simple columns (Kauchali et al., 2000,

Jobson et al., 1995), although not using the same ideas expressed in this work. Specifically, this is the Attainable Region when the column sections adjacent to the feed stream are at minimum reflux. All possible combinations of Φ_{L1} and Φ_{L2} that would lead to a feasible design between minimum reflux and infinite reflux for the other column sections are depicted in the direction of the arrows. Any values of Φ_{L1} and Φ_{L2} that do not lie in inside this region will lead to design where at least one pair of adjacent column sections are below minimum reflux, and therefore are classified as infeasible designs. It is important to reiterate that the column sections across the feed are still at minimum reflux, and thus this iso-reflux does not depict the entire Attainable Region, but merely a part of it. If this minimum reflux condition were to be relaxed for these column sections, the Attainable region would expand, until an infinite reflux condition is specified whereby the entire Φ-space would be attainable.

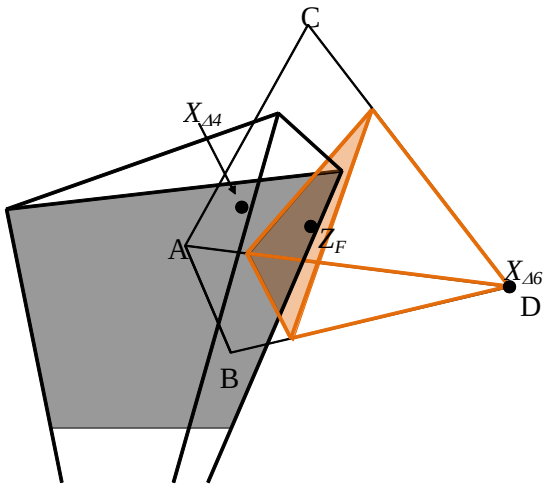
Notice that there are four iso-reflux lines in Figure 4.12, and not one for each column section, since the minimum reflux condition across the feed stage is completely independent of both split ratios. Interestingly, this Attainable Region shows that there are in fact infeasible designs when one pair of column sections, 1 and 3 in this case, operate at infinite reflux ($\Phi_{L1}\rightarrow 1$), but there are still feasible designs when the other pairs of adjacent column sections, 1 and 2, and 2 and 4 respectively, operate at infinite reflux ($\Phi_{L1},\ \Phi_{L2}\rightarrow 0$). The shifted tetrahedrons at minimum reflux are shown in Figure 4.13a-e for each pair of adjacent column sections. The colour of the shifted tetrahedrons corresponds to the colours of the iso-reflux lines in Figure 4.12.

Figure 4.13 a-e shows that, as with the simple columns design, that each pair transformed tetrahedrons of adjacent column sections just touch each other. The column is thus said to be operating at overall minimum reflux. The shaded regions in Figure 4.13 a-e show the planes that touch one another at minimum reflux. A "real" column is often said to operate at a factor between 1.05 and 1.50 times the minimum reflux (Seader and Henley, 2006a). Thus, using these guidelines, *each* simple column in the entire column has to operate at a factor above minimum for the entire column

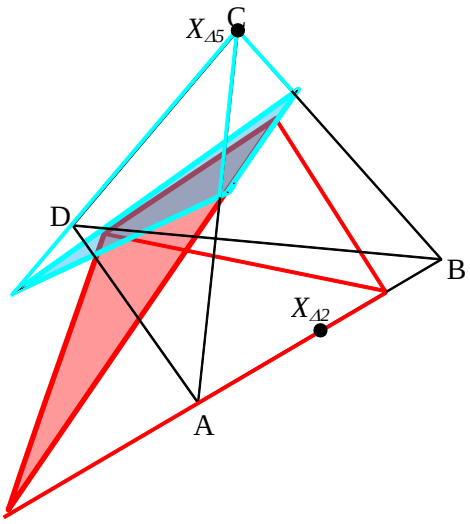
to operate above minimum reflux and a similar iso-reflux plot can be generated to depict the over-refluxed design. Using the same procedure outlined previously, similar iso-reflux figures for the DSR in its respective Φ-space may be constructed along with their shifted tetrahedrons.



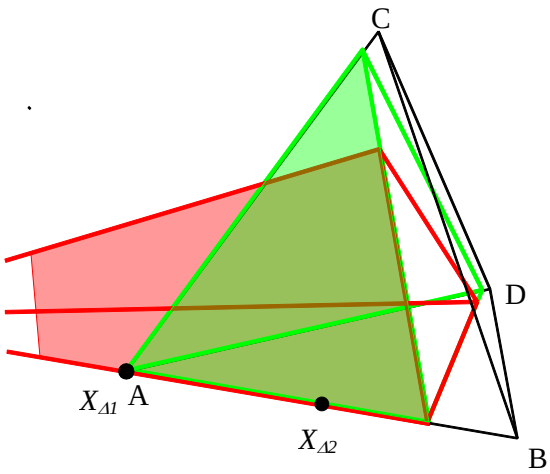
(a)



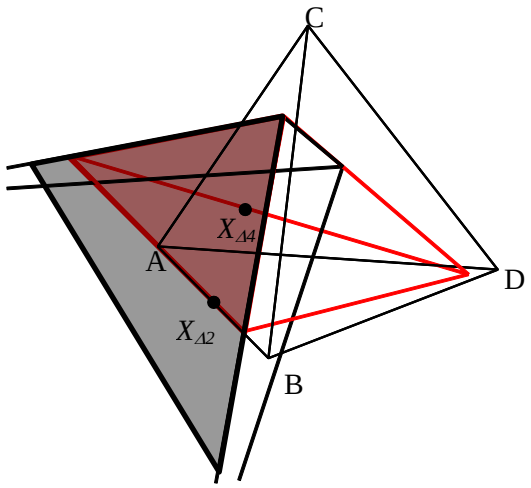
(b)



(c)



(d)



(e)

Figure 4.13: Transformed tetrahedrons at minimum reflux for the DSS. (a) Column sections 1 and 3. (b) Column sections 4 and 6. (c) Column sections 2 and 5. (d) Column sections 1 and 2. (e) Column sections 2 and 4.

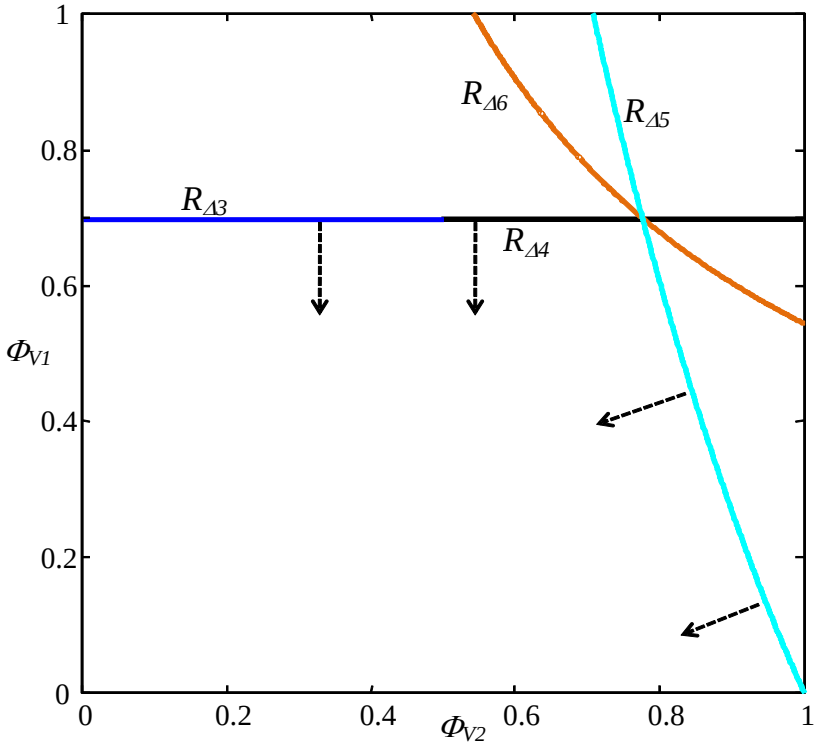
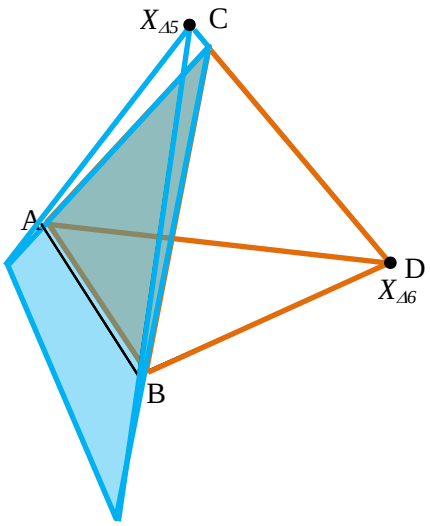
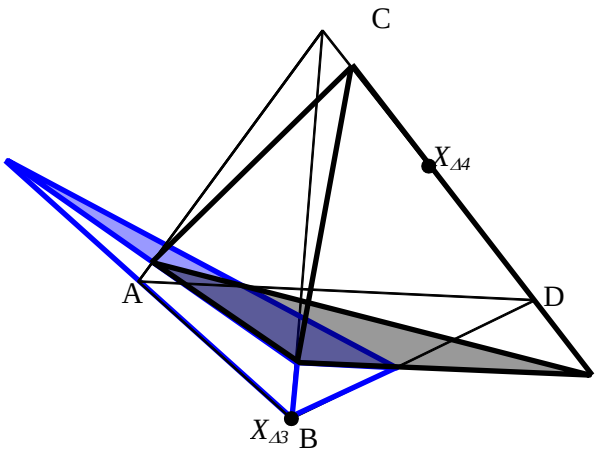


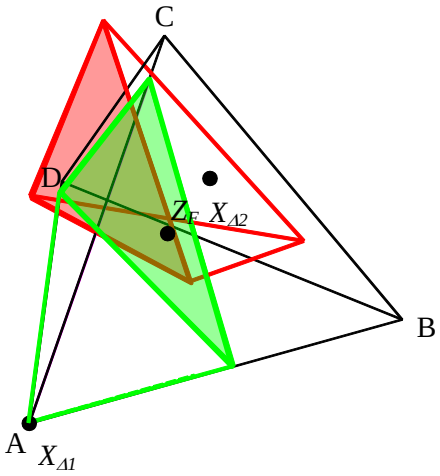
Figure 4.14: An iso-reflux plot for the DSR at minimum reflux.


$X_{\Delta 5}$
C
A
D
$X_{\Delta 6}$
B

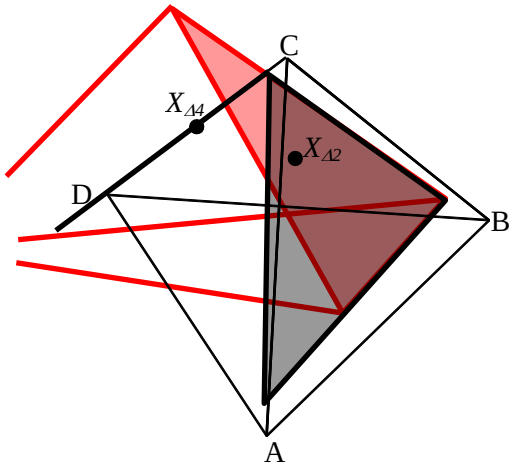
(a)


C
$X_{\Delta 4}$
A
D
$X_{\Delta 3}$
B

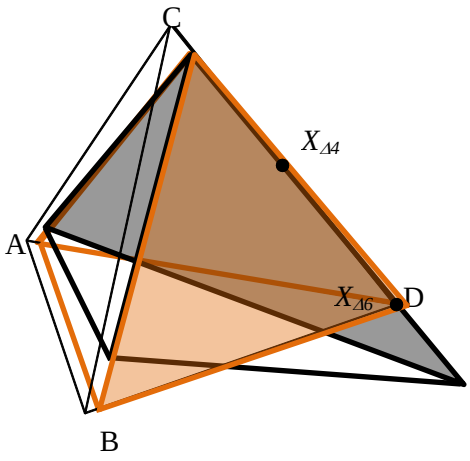
(b)


C
D
Z_E
$X_{\Delta 2}$
B
A
$X_{\Delta 1}$

(c)


C
$X_{\Delta 4}$
$X_{\Delta 2}$
D
B
A

(d)



(e)

Figure 4.15: Transformed tetrahedrons at minimum reflux for the DSR. (a) Column sections 5 and 6. (b) Column sections 3 and 4. (c) Column sections 1 and 2. (d) Column sections 2 and 4. (e) Column sections 4 and 6.

The DSR operating at minimum reflux may be interpreted in a similar way to DSS structure, but it should be noted that the split ratios are now vapour splits (Φ_V). The mass balance has been performed from the feed stage downwards, and thus the bottom column sections (4 and 6) are dependent on both split ratios. Again, there is an Attainable region indicated by the direction of the arrows, where over-refluxed feasible designs may be found when the column section 4 and 6 are at minimum reflux. Again, the shaded regions indicate where the planes touch each other.

In order to construct iso-reflux plots for the HSSR, it is important to point that the mass balance and minimum reflux calculation have to be initiated across the feed stage. The iso-reflux plots for the HSSR are thus unique because the feed is situated between the two split ratios. Thus, these split ratios are independent of one another at minimum reflux conditions. This is depicted in Figure 4.16, along with the corresponding shifted tetrahedrons in Figure 4.17.

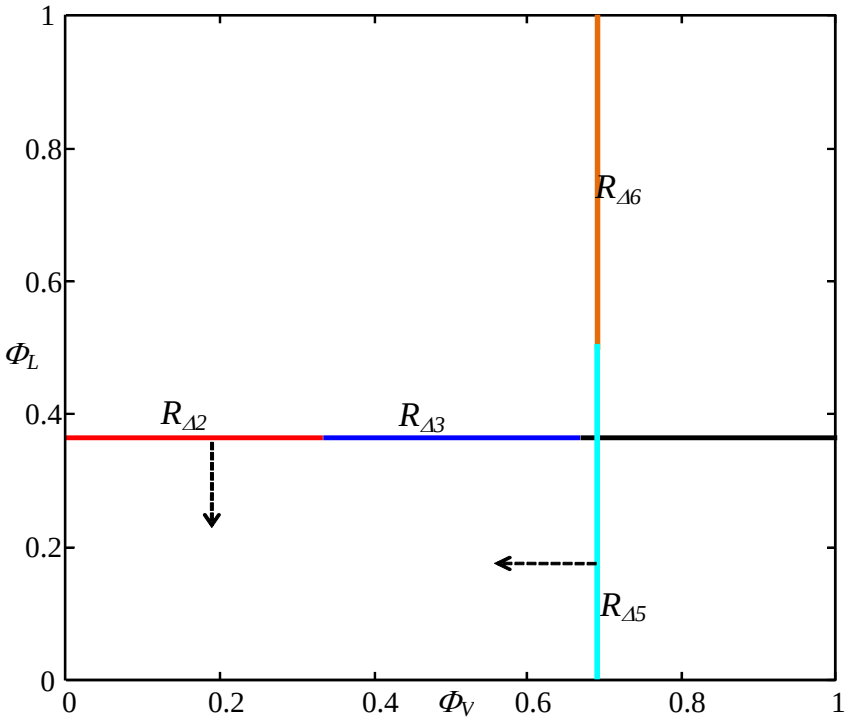
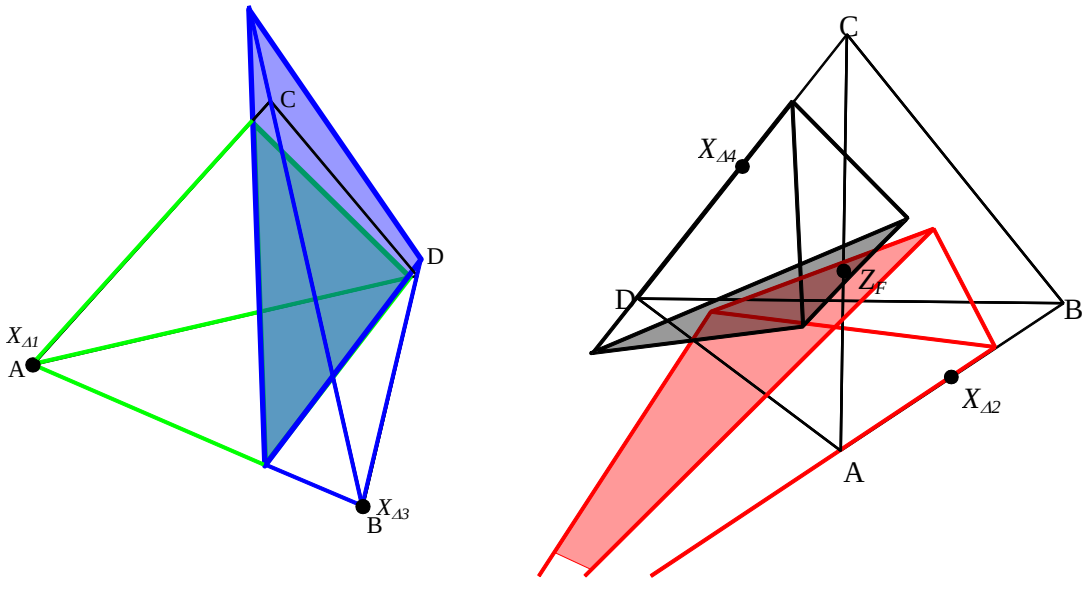


Figure 4.16: An iso-reflux plot for the HSSR and Kaibel column at minimum reflux.



(a) **(b)**

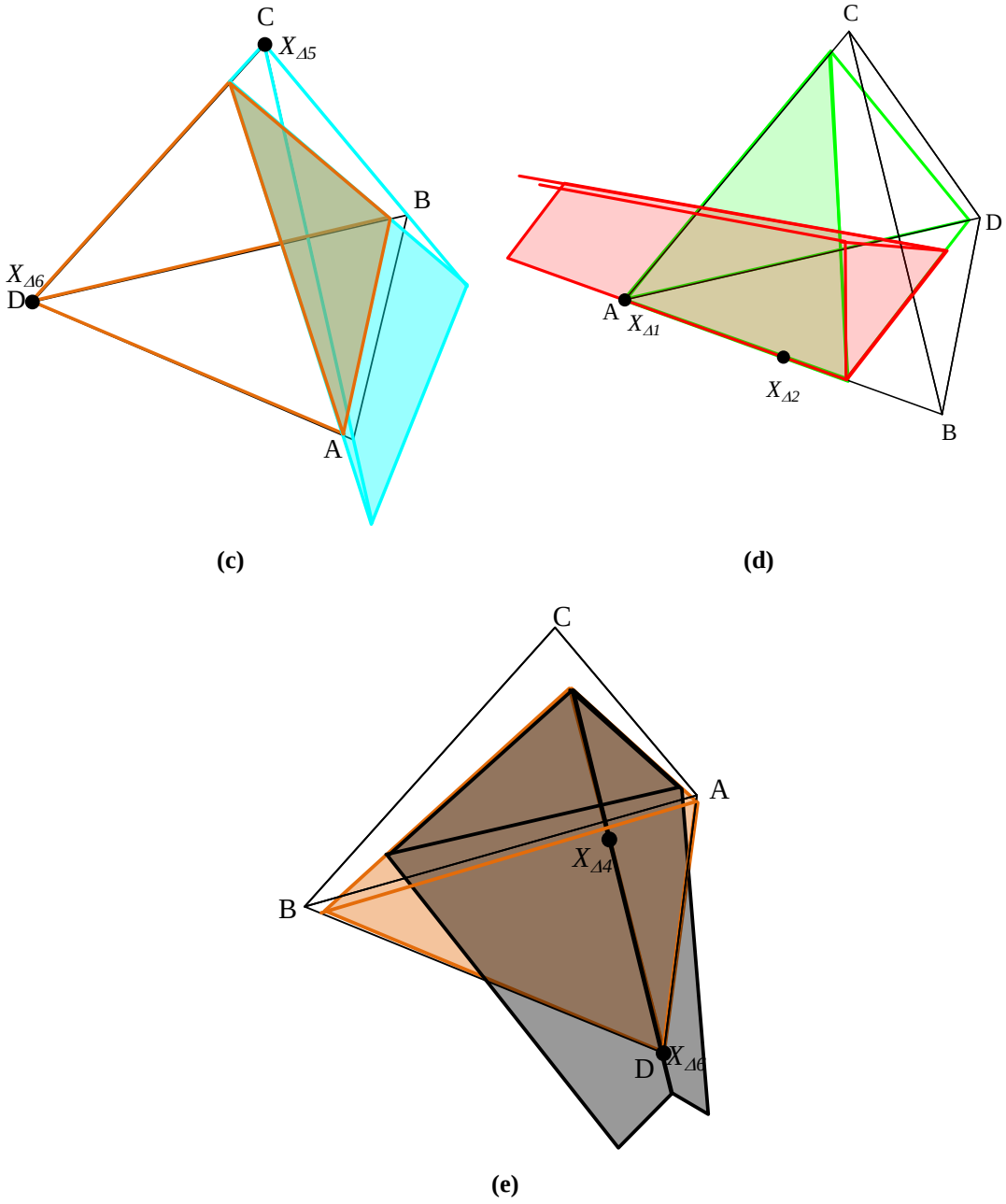


Figure 4.17: Transformed tetrahedrons at minimum reflux for the HSSR and Kaibel columns. (a) Column sections 1 and 3. (b) Column sections 2 and 4. (c) Column sections 5 and 6. (d) Column sections 1 and 2. (e) Column sections 4 and 6.

Figure 4.16 shows that the column sections associated to the vapour split, 5 and 6, are only dependent on the vapour split ratio, and conversely, column 1 and 3 are only

dependent on the liquid split ratio. Vapour and liquid shifted tetrahedrons have been constructed in Figure 4.17 that represents the appropriate feed condition.

Table 4.3: Reflux ratios at minimum reflux for all respective minimum structures

CS	DSS	DSR	HSSR	Kaibel
1	8.77	4.42	6.72	6.72
2	2.44	-2.81	1.22	1.22
3	-3.89	1.33	-4.27	-4.27
4	0.718	-4.88	-3.22	-3.22
5	-2.72	1.22	1.35	1.35
6	-6.16	-10.98	-7.79	-7.79
7	-	-	-	∞

4.4.2 IDENTIFYING OPTIMAL DESIGNS

We shall discriminate between good and bad designs based on the minimum energy requirement of a particular structure. As the reboiling column sections are typically the most expensive to operate in terms of utility cost, we will evaluate the vapour flow rates required in each of these column sections. In structures that contain multiple reboiling units, the overall vapour flowrate is merely the sum of all the vapour flows in respective column sections. We shall evaluate all designs based on minimum reflux operation, as this is a fair basis of comparison of the minimum achievable energy expenditure for each structure.

Furthermore, a unique property of multiple side rectifiers and strippers is the fact that they operate at multiple temperature levels. Thus, thermodynamic efficiencies (or second law efficiencies) also have an important role to play when deciding on an optimal structure since one structure may reject heat at a temperature where it is added to another. Once vapour flows have been obtained with our methods we can easily calculate the thermodynamic efficiency of the respective structures using a

modified version of the Clausius-Clayperon equation coupled with an energy and exergy balance across the structure (see Appendix D: Thermodynamic Efficiencies for a detailed derivation). Agrawal and Fidkowski (1998) used this same principle for calculating thermodynamic efficiencies of ternary structures. It is easy recognisable that the feed composition of the mixture may influence which structure is superior. In Table 4.4 we consider the effect of the feed composition on which structure is optimal by analysing the minimum vapour flows and the thermodynamic efficiency (η) for a mixture.

Table 4.4: Minimum vapour flows and thermodynamic efficiencies for all respective thermally coupled structures for volatilities of 6, 4, 2 and 1.

#	Feed Type	z_f	DSS		DSR		HSSR		Kaibel	
-	-	-	V_{TOT}/F	η	V_{TOT}/F	η	V_{TOT}/F	η	V_{TOT}/F	η
1	Equimolar	[0.25, 0.25, 0.25]	2.441	0.451	2.495	0.503	2.516	0.508	1.698	0.120
2	A rich	[0.85, 0.05, 0.05]	2.769	0.196	2.856	0.272	2.857	0.1875	1.506	0.035
3	B rich	[0.05, 0.85, 0.05]	3.700	0.157	3.709	0.130	3.702	0.145	1.927	0.027
4	C rich	[0.05, 0.05, 0.85]	2.864	0.134	2.828	0.160	2.830	0.196	2.713	0.089
5	D rich	[0.05, 0.05, 0.05]	1.142	0.318	1.065	0.461	1.159	0.474	1.023	0.172
6	AB rich	[0.45, 0.45, 0.05]	3.258	0.301	3.286	0.304	3.283	0.283	1.718	0.053
7	AC rich	[0.45, 0.05, 0.45]	2.295	0.298	2.547	0.399	2.553	0.370	1.968	0.104
8	AD rich	[0.45, 0.05, 0.05]	1.617	0.517	1.705	0.732	1.743	0.535	1.007	0.108
9	BC rich	[0.05, 0.45, 0.45]	3.291	0.250	3.297	0.246	3.301	0.285	2.340	0.071
10	BD rich	[0.05, 0.45, 0.05]	2.178	0.426	2.209	0.386	2.183	0.426	1.210	0.083
11	CD rich	[0.05, 0.05, 0.45]	2.030	0.323	1.998	0.399	2.015	0.475	1.892	0.203
12	ABC rich	[0.32, 0.32, 0.32]	3.003	0.333	3.088	0.360	3.091	0.364	2.035	0.083
13	ABD rich	[0.32, 0.32, 0.04]	2.353	0.483	2.392	0.501	2.378	0.469	1.269	0.089
14	ACD rich	[0.32, 0.04, 0.32]	1.833	0.436	1.966	0.605	2.000	0.569	1.600	0.169
15	BCD rich	[0.04, 0.04, 0.04]	2.526	0.377	2.509	0.390	2.535	0.446	1.847	0.115

Fifteen different feed compositions have been characterised and evaluated for each structure in Table 4.4. These compositions correspond to various combinations of purity for single components, binary, and ternary mixtures. The structure requiring the minimum vapour flowrate, excluding the Kaibel column, has been shaded grey while the structure with the highest thermodynamic efficiency has been shaded in red. Not considering the Kaibel column for the moment, the results indicate that the DSS

is by far the most prevalent structure in terms of minimum vapour flowrates, highlighted by grey shading. Out of the fifteen different feed compositions considered there are only four cases where the DSS does not have the minimum vapour flow rate. These four scenarios correspond to a feed rich in C and D, or a combination thereof, where the DSR has the minimum vapour flowrate. This can be attributed to the fact that, since the highest boiling components are plentiful, only a small amount of the lighter components have to be vaporised and sent through the column. Thus, the largest savings with the DSS can be achieved when the feed is rich in component A, and conversely the largest DSR savings when the feed is rich in components B, C and D, since these are the "condensing components".

This is a significant result, because it shows that the optimal configuration is dependent on the feed composition and that this has to be considered when deciding on refinery options. For the special case of synthetically produced crude via the Fisher-Tropsch synthesis reactions, there is however always more low-boiling component than high boiling component present as predicted through Anderson-Schulz-Floury product distribution model:

$$\alpha = \frac{C_n}{C_{n-1}} \tag{4.6}$$

Where C_n is carbon chain containing n-carbon atoms and α is the chain growth probability such that 1> α >0. Thus, crude generated synthetically through Fisher-Tropsch chemistry would be well suited to a side stripping arrangement, if the minimum heat duty were the only concern and it were assumed that the temperature at which the heat is added to the column is of no concern.

Apart from the quantity of the heat added the column however, the other factor to consider however is the second law efficiency of the columns, which gives an

indication of the quality heat added to the column, or in other words, the useful work added to the column and may be related trough the efficiency by:

$$W_{real} = W_{ideal} / \eta \qquad (4.7)$$

In essence, a high thermodynamic efficiency means heat is being added and rejected at intermediate temperature levels, and not at temperature extremes like the Kaibel which leads to low efficiencies. Despite requiring the least amount of heat, the DSS rarely has the best thermodynamic efficiency, meaning that the work being added to the distillation column is not being used as effectively as other structures are. In other words, some the work being added to the structure is being used only to vaporise liquid, and not to perform actual separation work and thus the column has a higher work requirement. Thus, in a perfect world, one would like to have a feed where the optimal structure has both the lowest heat duty as well as the highest efficiency, as in scenarios 3 and 10. This may imply that one may like to design upstream processes to obtain certain feed conditions to obtain this unique condition.

Interestingly, there is not one case where the HSSR is the optimal structure in terms of minimum vapour flowrate, but is extremely prevalent in terms of thermodynamic efficiencies. This can be attributed to the fact that heat is being both added and rejected at intermediate temperatures. At feed conditions like 11 and 15, for instance, there is a significant advantage to choosing the HSSR in terms of efficiency when compared to the other structures, and the vapour duties in both instances are very comparable with that of the DSS or DSR. Thus, in cases like these, the HSSR would in fact be the better option since it provides a higher efficiency (lower work requirement) without sacrificing too much on the heat duty. Furthermore, closer inspection reveals that the HSSR achieves minimum vapour flowrates where the feed mixture contains large fractions of B and C. The highest relative vapour flowrates of all structures seem to occur where component A is plentiful, since in all of the

structures, all of the A has to vaporised meaning that a large reboil load is required. Thus, if the amount of heat added at high temperature to the column is limited, one may consider the HSSR since it utilises the heat at temperature much better, in general.

Notably the thermodynamic efficiencies of the Kaibel are very low relative to all other structures, essentially because all the heat is added and rejected at the highest and lowest temperatures, respectively. However, Agrawal and Fidkowski showed that there are potential feed compositions in ternary separations where the fully thermally coupled columns have an advantage in terms of efficiency, but these were found to be very limited (Agrawal and Fidkowski, 1998). The Kaibel column does however offer vast savings in terms of the overall energy requirement, with as much as a 92% improvement in overall vapour flow over the best thermally coupled structure where the feed is rich in B. Although this may seem like an incredibly high number, it does make sense since the Kaibel column is structurally similar to the HSSR but it essentially does the reboiling of component B for free. Again, if the quality of the heat wasn't a factor, the Kaibel column would certainly be the best choice, assuming of course that its complex control issues can be dealt with. However, if the quality of the heating and or cooling agents to the column were of concern, this column would be the worst by far.

Finally, the reader should be aware of some of the underlying assumptions made in this comparison of structures. Firstly, comparing structures at minimum reflux conditions implies that an infinitely large column and therefore an infinitely large capital investment. This is obviously an unwanted operating condition. However, in modern times, energy has become increasingly important (and expensive), and thus the minimum energy requirements of a column is a key factor in discriminating between potential designs. One can simply design for minimum reflux and operate slightly above this value to obtain finite sized, realistic column. This in turn assumes that all structures reduce to finite sized columns equivalently, i.e. if an over-refluxed

factor of say 1.3 above minimum reflux is specified in all columns, then all columns are assumed to require the same capital investment. This may not necessarily be true, but our strategy allows one to, if nothing else, eliminate bad column designs from the decision making process. Also, our lost work calculations assume that the process receives reversible work when converting the feed into pure products. This assumption is generally not true and hence the thermodynamic efficiencies are just approximate. Nevertheless, these efficiencies serve as good guides for identifying more efficient columns.

4.5 DISCUSSION AND CONCLUSIONS

In this work, a method has been presented to design multiple thermally coupled distillation columns through the use of CPMs and eigenvector theory. This method allows one to quickly assess the minimum reflux for a simple column for the special case of sharp splits and constant relative volatilities. The key parameters used in the CPM technique are easily extendable to the design and analysis of complex structures, including multiple thermally coupled units.

Furthermore, iso-reflux plots are presented as a quick way of determining the minimum reflux conditions in a multiple thermally coupled column in a constrained split ratio space. The plots not only show the intersection of minimum reflux curves, but also indicate an Attainable Region of all possible operating parameters that result in a feasible design.

Using the aforementioned techniques we have considered four thermally coupled structures, each having one large main column. Of the these structures, the fully thermally coupled Kaibel column is for the fifteen different feeds considered by far the most prevalent in terms of minimum heat demand, but also has thermodynamic efficiencies which are comparatively very low. Of the “conventional” multiple

thermally coupled columns, it is in fact the side stripping column that appears to require the minimum amount of heat for the majority of feeds. This stripping type column is similar to one used in crude refineries and therefore can aid in explain why these type of columns are so widely used. However, there are certain feed scenarios when a multiple side rectifying column may be best in terms of heat demand, and using the techniques described in this work, it is a simple task to identify these feeds and design the process accordingly.

Importantly however, total heat demand may not be the only objective and/or constraints when deciding on a potential structure. In some cases, for instance, it may be advisable to choose a hybrid structure because this structure provides good thermodynamic efficiencies for a wide range of feeds, and in some instances still provides a comparatively good heat demand. This is because the HSSR uses the heat addition and removal to and from the column much more efficiently for the widest range of feeds because the heat is both being added and rejected at intermediate temperature levels. Thus, when deciding on a design it should be clear what the objective for the design is, as the columns with the lowest heat demand may not necessarily us this heat in the most efficient manner. Using the tools presented in this chapter, it is relatively easy to identify superior designs, especially in the early stages of the design process.

Chapter 5 : A PHENOMENA BASED COLUMN PROFILE MAP APPROACH TO UNDERSTANDING COUPLED REACTOR-COLUMN SECTIONS

This work has been prepared in the form of a paper for future publication. It has been presented at the AIChE annual meeting in Salt Lake City, USA in 2010. It is exclusively my own approach.

ABSTRACT

In this chapter, we address the reactive distillation design problem by designing a CSTR with simultaneous equilibrium separation and mixing, and feeding the product from this process to a non-reactive rectifying or stripping distillation column section depending on what component has to be removed. Three hypothetical cases are presented as well as an industrially relevant MTBE case study. Using a phenomena-based Column Profile Map approach, a novel, geometric understanding may be achieved which allows for quick feasibility screening. A unique understanding of the relation between phase equilibrium, mixing and chemical reaction is presented that provides insight into what set of process chemistry may be attractive for this reactive distillation arrangement. An attainable region is shown which depicts all possible process parameters that would result in a realizable design. This method also aids in the understanding of the unique, reverse interaction between pieces of process equipment and operating conditions.

5.1 INTRODUCTION

The concept of combining a chemical reaction and separation of the products in a single unit is by no means a new one, the idea being mentioned as early as 1948 (Berman et al., 1948). This combined process, reactive distillation, may be implemented to replace conventional reaction-separation networks, and has the potential to greatly reduce expenditures. Taylor and Krishna compiled a comprehensive review on reactive distillation and have identified several advantages, including significant savings on capital cost due to the simplification or elimination of the separation network; improved heat integration, especially if the reaction is exothermic, and an improvement in both selectivity and reactant conversion (Taylor and Krishna, 2000).

Due to the fact that reaction and separation (and mixing) occur in a single vessel, modelling of reactive distillation processes are considerably more complex than conventional systems. Models that have been proposed may be classified as either equilibrium or non-equilibrium stage based, almost all of which are computer orientated (Taylor and Krishna, 2000). Equilibrium based methods assume that vapour and liquid streams leaving each stage are in equilibrium with each other, while non-equilibrium models are rate based and consider mass and heat transfer effects. Non-equilibrium models are fundamentally more rigorous and complex than equilibrium models and often require large computer based optimization routines or specialised software packages. An example of a rigorous computer aided model used for the design of reactive distillation is determining the optimum number of equilibrium stages, feed tray location and reflux by combining tray-by-tray balances, kinetic rate based expressions and cost estimates using mixed integer non linear programming (Ciric and Gu, 1994). Although undoubtedly these all encompassing computer models are extremely effective and precise, due to the large amount of

equations and parameters required they do not always allow the user to obtain insights into the final solution.

In contrast to this, Hauan and co-workers have developed a phenomena-based approach for analyzing and synthesizing reactive separation processes, by considering the effects of the three phenomena present: chemical reaction, equilibrium separation and mixing (Hauan and Lien, 1996, Hauan and Lien, 1998, Hauan et al., 2000). Using this relatively simple technique, they showed how different phenomena influence the reactive distillation process, without using rigorous simulations. The advantages of this technique are that only physical and chemical data are required to estimate the phenomena, which are independent of the structural design of the unit; and furthermore, by only considering the key phenomena allows the designer to assess the process independently of equipment structure (Almeida-Rivera et al., 2004).

One particular version of a reactive distillation unit employs a continuously stirred-tank reactor (CSTR) with a rectifying or stripping column mounted above/below it. Both batch processes and continuous processes based on this technology are found in industry, but both the steady state design and the dynamics of these coupled units are poorly understood (Yi and Luyben, 1996a). In this chapter, we shall be concerned with designing a steady state CSTR with simultaneous equilibrium separation and mixing, and feeding the product from this process to a non-reactive rectifying or stripping distillation column section, depending on what component has to be removed. The column section will be designed using the Column Profile Map (CPM) technique proposed by Tapp, Holland and co-workers (Tapp et al., 2004, Holland et al., 2004a). CPMs were derived from an adaptation of differential equations proposed by Van Dongen and Doherty (Van Dongen and Doherty, 1985a). These maps take into account the net molar flows and reflux ratios in a column section and conveniently show all possible separations in a generalised column section.

Although this coupled reactor/column section problem has been tackled by other the researchers (Yi and Luyben, 1996a, Yi and Luyben, 1996c, Yi and Luyben, 1996b), the techniques proposed for use in this paper allows the designer to graphically assess the performance of the process and aims to bring forth a greater understanding into interaction of process equipment and design a process accordingly. The techniques and interpretations shown in this chapter aims to be a quick means of feasibility screening, especially in the conceptual design stage of a process, before resorting to expensive and time consuming rigorous simulations. Furthermore, by combining the phenomena based approach of Hauan and co-workers with the CPM technique allows for a quick assessment of the process and greatly aids in the understanding of why certain sets of process chemistry may be more attractive than others for reactive distillation.

5.2 DERIVATION OF MODEL

5.2.1 REACTIVE DISTILLATION

Consider a CSTR as in Figure 5.1, with a feed stream of flowrate F containing nc components, and the composition of the feed stream is $\mathbf{x_F}$. A single chemical reaction takes place in the liquid phase within the reactor with a certain reaction rate $\mathbf{r}=(r_1,r_2, r_i, ...r_{nc})= (\nu_1, \nu_2, \nu_i, ..\nu_{nc})\mathbf{r}$, where ν_i is the stoichiometric coefficient of component i. Volatile products are boiled off simultaneously with a flowrate of V and a composition of $\mathbf{y}$, where $\mathbf{y}$ is the vapour composition in phase equilibrium with the composition inside the reactor, $\mathbf{x}$. The molar holdup in the reactor is H and the reaction rate constant is k_f.

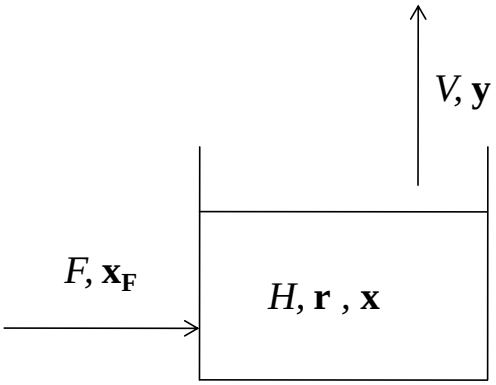


Figure 5.1: A CSTR with a continuous feed and simultaneous vapour liquid equilibrium separation

Following the phenomena based approach of Hauan & Lien (1998), an unsteady state component balance over the process described above yields:

$$\frac{dx}{dt} = (V/H)(x-y) + (F/H)(x_F - x) + k_f\left(r - x\sum_{i=1}^{nc} r_i\right) \qquad (5.1)$$

This phenomena based approach allows a simple means of assessing phenomena interaction from a topological perspective. There are essentially three phenomena present in this process: separation, mixing, and reaction. The three terms on the right hand side of Equation 5.1 represent these three processes respectively. Each term can be seen as a vector field, scaled by various process parameters. For example, the mixing vector field is given by:

$$\frac{dx}{dt} = \beta(x_F - x) \qquad (5.2)$$

where β is a scalar coefficient, defined here as F/H. Individual vector fields can be represented graphically in concentration space, as shown in Figure 5.2.

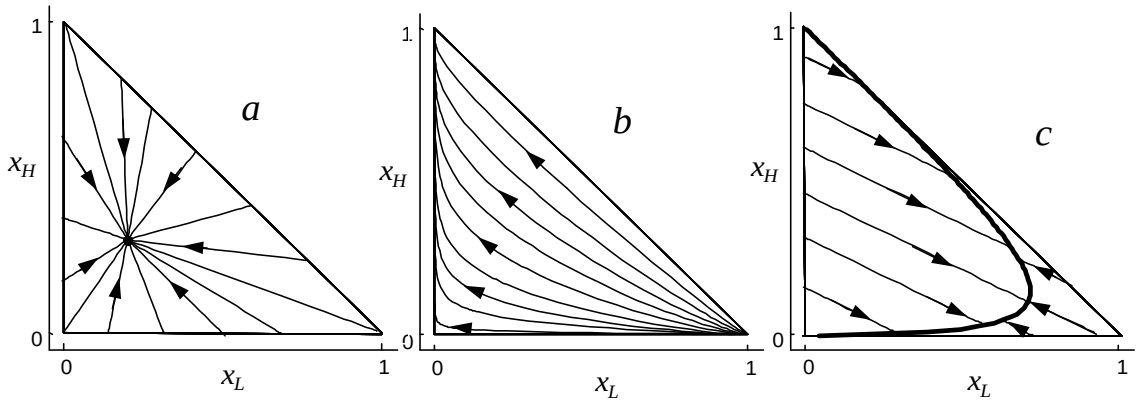


Figure 5.2: Phenomena vector fields for (a) Mixing with x_F= [0.2, 0.3]; (b) Separation for a constant relative volatility system with α= [5, 1, 2]; and (c) Reaction for 1I+1H↔2L with elementary reaction rate and K_{eq}=25

It can thus be said that the overall process is merely a linear combination of different phenomena, scaled by the appropriate process parameters. As apparent from Figure 5.2, and in general, mixing vectors point towards the mixing composition, the separation vectors point towards the highest boiling component and the reaction vectors towards the reaction equilibrium curve. For the overall process described by the individual phenomena in Figure 5.2 with a feed of 1 mol/s, a reaction coefficient k_f = 10, and a holdup of 5 mol, the overall process vector field can be constructed in concentration space, as shown in Figure 5.3.

The profiles in Figure 5.3. track the liquid composition in the reactor with changing time and are essentially a linear combination of all vector fields shown in Figure 5.2. Notice that all the profiles run towards a single point, *a stable node*. At this point the composition inside the reactor is no longer changing, and the process has reached a compositional steady state ($\frac{dx}{dt} = 0$). If one were for instance to increase the effect of the mixing vector field by increasing the feed flowrate, the profiles would be more attracted to the feed composition. The stable node would consequently be shifted nearer to the feed composition. When the feed flowrate is infinitely large, the overall

process field reduces exactly to that of the mixing vector field. The other process phenomena on the overall process may be interpreted in a similar way. Thus, by understanding the effect individual phenomena has on the entire process, we can, qualitatively at least, very quickly and easily determine whether a certain product specification can be achieved or not, and furthermore, design the process to achieve that specification.

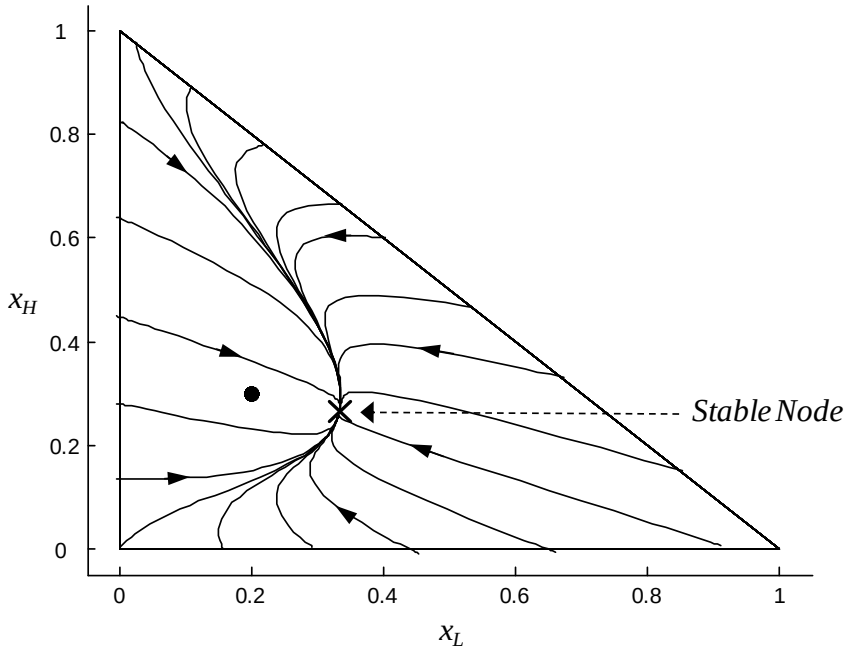


Figure 5.3: Overall reactive distillation process vector field with a feed composition of x_F= [0.2, 0.3] indicated by a black dot.

Perhaps more importantly, understanding the phenomena interaction allows one to gauge what can or cannot be achieved in a batch reactive distillation setup. For instance, for the conditions depicted in Figure 5.3 one can only achieve, at best, a final composition equal to the stable node composition. It is impossible to transform the composition in the still from one end of the composition space to the other. In fact, the upper limit is governed by the reaction equilibrium curve. The absolute best one can do with an initial reactor composition lying on either side of the reaction equilibrium curve and a feed entirely depleted of component low boiling component,

is achieving a final reactor composition that lies on the reaction equilibrium curve, and even this would require an infinitely large reactor.

5.2.2 COLUMN PROFILE MAPS

A Column Profile Map describes the behaviour of a multicomponent system in a column section by setting parameters such as the net molar flow and the reflux ratio. The first step in constructing a Column Profile Map is to define a column section, which per definition of is "a length of column between points of addition or removal of material and/or energy" (Tapp et al., 2004), as in Figure 5.4.

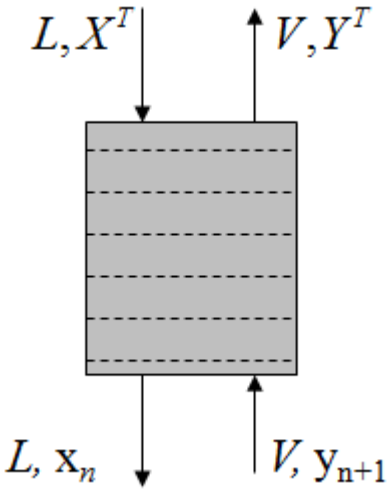


Figure 5.4 A generalised column section.

A steady state material balance over a column section, assuming constant molar overflow accompanied with a Taylor expansion around *n* yields:

$$\frac{dx}{dn} = \left(\frac{1}{R_\Delta} + 1\right)\left(x - y(x)\right) + \left(\frac{1}{R_\Delta}\right)\left(X_\Delta - x\right) \qquad (5.3)$$

where $X_{\Delta} = \left(\frac{VY^T - LX^T}{V - L} \right)$ and $R_{\Delta} = \frac{L}{V - L} = L / \Delta$

and V≠L. Equation 5.3 is known as the Difference Point Equation (DPE). R_{Δ} is the reflux ratio in the column section, *n* the number of stages, and X_{Δ} can be thought of as a pseudo composition vector, valid anywhere in the composition space and only needs to be a real composition in column sections that are terminated by a total condenser or reboiler. X_{Δ} basically indicates the net compositional flow of each individual component, a negative element entry just implies that that particular component is moving downward in the column section. X_{Δ} is also subject to the constraint that the sum of its components be 1. From an initial composition, integration may be performed from n=0 to values of n>0. Integration can be performed in the negative direction as well, equivalent to determining the composition profile in the column section from bottom to top. A complete derivation of the Difference Point Equation is given in Appendix G.

Notice that the DPE is, from a mathematical point of view, very similar to unsteady state balance on the CSTR. The DPE has two terms on the right hand side which are essentially equivalent to the vapour liquid separation and mixing vector fields in the unsteady state reactor, both scaled by respective scalar coefficients. Thus, even though both pieces of equipment differ greatly, they are in a mathematical sense very similar and can thus be interpreted in an analogous fashion.

Furthermore, notice that the DPE is not mathematically bound by positive compositions, thus Equation 5.3 may be integrated into the negative composition space too. Due to the fact that topological properties of positive compositions extend smoothly to the negative composition space, analyzing negative compositions does offer considerable insight in how to affect a separation. To illustrate this, consider the CPM in Figure 5.5 for an arbitrary choice of X_{Δ} and R_{Δ}.

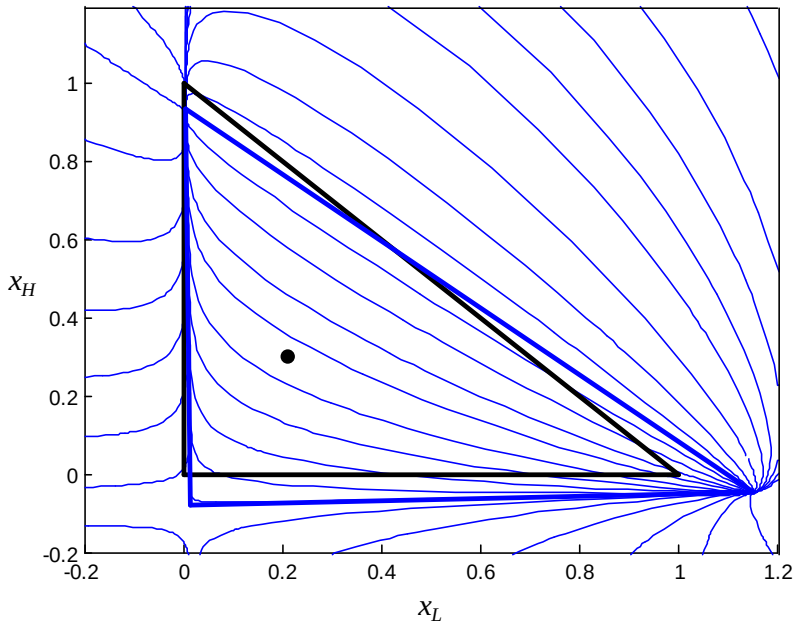


Figure 5.5 : A CPM for X_Δ= [0.2, 0.3] (black dot) and R_Δ=8. The blue lines represent the Column Profiles inside and outside the black Mass Balance Triangle (MBT).

Figure 5.5 shows that profiles are shifted from those in Figure 5.2 (b), and do not terminate at the pure component vertices. At infinite reflux, the DPE reduces to exactly the separation vector field, effectively the residue curve equation. The shifted stationary points have been connected by bold lines, resulting in a so called shifted triangle. By operating a column section with a certain combination of X_Δ and R_Δ, profiles may be manipulated in such a way to suit the exact specifications of the separation required. In fact, as shown in Figure 5.5, profiles and their nodes may be shifted outside the physically realizable composition space. Although this fact is not of immediate use in this paper, it is important to realise that liquid composition profiles may be manipulated in almost any desirable manner, depending on the selection of X_Δ and R_Δ. The reader is referred to Tapp et al. (2004) for an in depth analysis and design possibilities of this global topological view.

5.3 PROCESS INTEGRATION

In this section, we shall look at the implications of integrating a reactor with a non-reactive column section, in order to achieve a certain predefined product purity. Three hypothetical cases are studied using a conventional rectifying or striping column section terminated by a reboiler or condenser, where the equilibrium limited reactions form a low boiling, high boiling and an intermediate boiling product respectively. The reaction products are assumed to be the desired product for the process as well. In the same manner, the industrially relevant MTBE process is also studied using a stripping column section.

5.3.1 LOW BOILING PRODUCT

Suppose a stream of 1 mol/s containing a certain mole fraction of High (*H*) and Intermediate (*I*) boiling components, is fed to a reactor where the following liquid phase reaction takes place:

$$1H + 1I \Leftrightarrow 2L$$

Where *L* is a valuable low boiling component. The reaction may be described by an elementary rate law, given by:

$$\mathrm{r} = k_f \left(x_H x_I - \frac{x_L{}^2}{K_{eq}}\right) \quad \text{with } K_{eq} = 25$$

The Vapour Liquid Equilibrium may be determined by a constant relative volatility model, with volatilities of 5 and 2 for *L* and *I* relative to *H* respectively. The final product specification is set such that $x_L = 0.950$ with impurities $x_H = x_I = 0.025$. Since

we know that these high purities cannot be obtained using a simple batch distillation setup, this leads to the question: what else can be done to achieve the final product specification? By feeding the vapour product of the CSTR to a rectifying column section, we can cross the reaction equilibrium curve, and achieve an overhead product meeting the specified product specification, as in Figure 5.6. This process can effectively be described as a reactive reboiler. The concept of a reactive reboiler has been investigated by other authors, but the focus was largely on control (Svandova et al., 2006) and singularity analysis based design (Qi et al., 2004), and not on design and the interaction of phenomena as presented here.

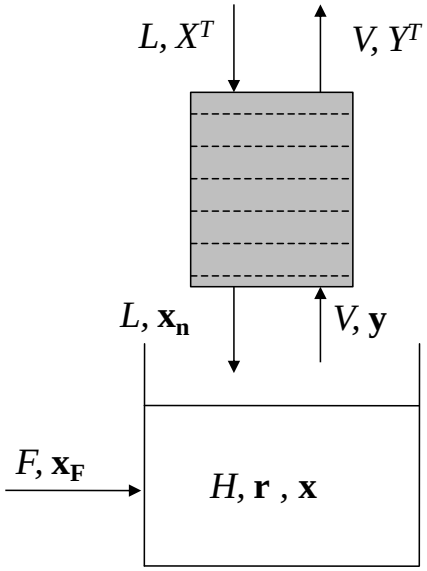


Figure 5.6: A CSTR coupled with a rectifying column section, a reactive reboiler.

Notice that the only difference between the reactor in Figure 5.6 and Figure 5.1 is an additional mixing stream (L) of composition $\mathbf{x_n}$, which is a strong function of the number of stages in the column section. Using the definition of X_Δ combined with a material balance over the column section yields:

$$X_{\Delta} = \left(\frac{VY^{T} - LX^{T}}{V - L} \right) = \left(\frac{V\mathrm{y} - L\mathrm{x}_{\mathrm{n}}}{V - L} \right) \qquad (5.4)$$

Assuming that the column section is terminated by a total condenser (effectively a rectifying column section), X_{Δ} is simply equal to the vapour and liquid compositions at the top of the column section, i.e. $X_{\Delta} = X^{T} = Y^{T}$, hence X_{Δ} = [0.950, 0.025], where X_{Δ} is in the form [L,H]. Since the sum of the individual entries of X_{Δ} are unity, component *I's* Difference Point composition may be easily inferred from this notation. By specifying a reflux value, the amount of stages in the column section, and using X^{T} as the initial integration condition, we are able to calculate the composition of material being recycled back into the reactor ($\mathbf{x_n}$) by integrating the DPE. Once this composition is known, the vapour composition, **y**, being fed to the reactor may be calculated from Equation 5.4 and hence the composition within the reactor, **x**, is known through the phase equilibrium relationship. Liquid composition profiles in the column section for different values of the reflux ratio and theoretical stages are shown in Figure 5.7.

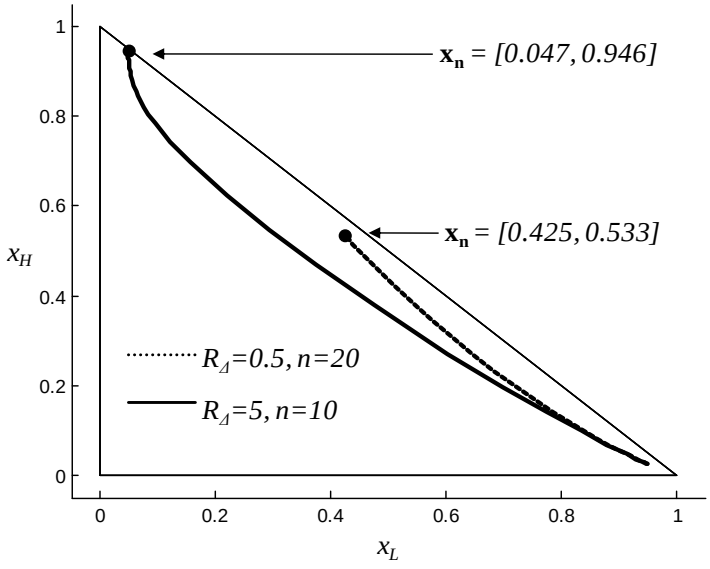


Figure 5.7: The effect of reflux and amount of stages on bottom liquid composition profiles for X_{Δ} = [0.950, 0.025]

From a topological point of view, notice that the specific combination of reflux and the amount of stages has a significant influence on the composition being recycled to the reactor. In order to link the two pieces of equipment with each other, a steady state component balance over the reactor along with the definition of R_{Δ} is performed, resulting in Equation 5.5:

$$F\mathrm{x}_{\mathrm{F}} + \varphi\mathrm{r} + FR_{\Delta}\mathrm{x}_{n} - F(1+R_{\Delta})\mathrm{y} = 0 \qquad (5.5)$$

$\boldsymbol{\varphi}$ is a variable defined by $k_f.H$ and is proportional to the size of the reactor, assuming as a first approximation that the reaction rate constant (k_f) is independent of temperature. Once R_{Δ}, X_{Δ} and the amount of stages are specified for the column section and $\mathbf{x_n}$ and $\mathbf{y}$ have been calculated by integrating the DPE, the problem described in Equation 5.5 above is completely specified. Hence, the reactor size and the remaining two feed compositions may be calculated. By specifying that the feed contains no product (x_{FL}=0**)** and arbitrarily chosen values of R_{Δ} =3 and n=5, the feed to the process and the reaction coefficient is determined to be $\mathbf{x_F}$ = [0, 0.5] and 8.243, respectively. However, without immediately imposing the constraint that the feed must not contain any of the final desired product (L), and specifying a range of possible values for x_{FL}, the entire process may be summarized graphically for different feed compositions, as shown in Figure 5.8.

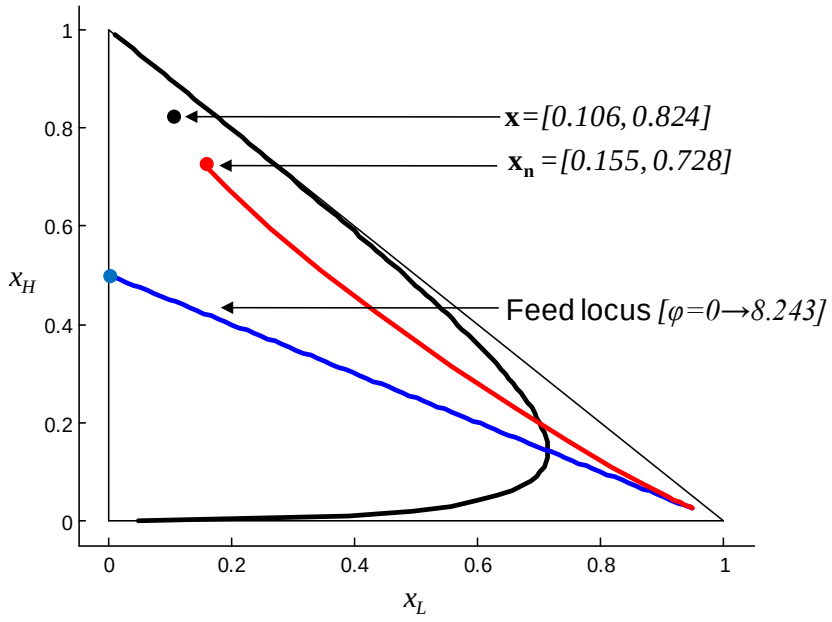


Figure 5.8: A CSTR coupled with a rectifying column section for R_A =3, n=5 and X_A = [0.950, 0.025]. The red and blue line represent the Column Profile and the Feed locus line, respectively, while the red, black and blue dots represent the bottom liquid composition of the column section, the reactor composition and the feed composition that contains no product, respectively. The black curve represents the reaction equilibrium curve.

The red line in Figure 5.8 represents the liquid composition profile in the column section for the given parameters and product specification. The blue line shows the locus of all possible feed compositions that would achieve the composition in the reactor to meet the product specification. The values of φ change along this feed locus, from 0 where the feed composition is exactly that of product specification, to 8.243 where there the feed is entirely depleted of component *L*. The fact that the reactor size reduces to zero may also be inferred by rearranging the definition of equation such that:

$$X_{\Delta} = \left(\frac{V\mathrm{y} - L\mathrm{x}_{\mathrm{n}}}{V - L} \right) = \left(\frac{F\mathrm{x}_{\mathrm{F}} + \varphi \mathrm{r}}{F + \varphi \sum r_i} \right) \qquad (5.6)$$

Furthermore, notice that feed locus line spans across almost the entire composition space. Although the range of φ across the feed locus line may differ for other choices of reflux and the number of stages, the feed line remains fixed. This implies, somewhat counter intuitively, that any feed composition that does not lie on the feed line will result in the product specification not being met, regardless of the choice other process parameters. The black dot Figure 5.8 represents the reactor composition and closely follows the profile termination point.

From Figure 5.7 and Figure 5.8 it is simple to deduce that there is a relationship between the size of the reactor or amount of catalyst (φ), the number of stages (n) and the reflux ratio (R_{Δ}). For example, a choice of n and R_{Δ} that forces the composition in the reactor to be near or on the reaction equilibrium curve, will cause the reactor size will grow sharply. On the other hand, if the column profile can be manipulated in such a way that the reactor composition lies close to the feed composition, the reactor will be comparatively small. The design engineer is thus faced with a trade off between the energy usage of the process (R_{Δ}), and the capital cost thereof (φ and n). Although the feed line in Figure 5.8 is useful when analyzing what the process is capable of, a feed which does not contain any valuable product ($x_{FL}=0$) is probably the most realistic scenario. Thus, using this condition and discrete values of n, we can represent all the design parameters of the process on one graph, as shown in Figure 5.9.

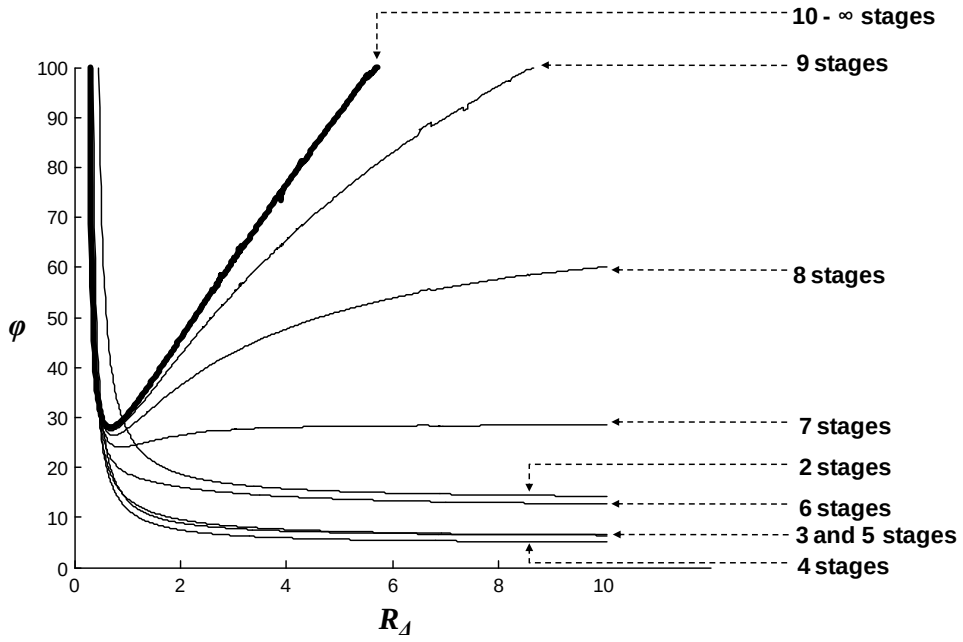


Figure 5.9: The effect of the number of stages and reflux ratio on reactor size for X_Δ = [0.950, 0.025] and x_{FL} = 0 for a CSTR coupled to a rectifying, non-reactive column section.

Figure 5.9 illustrates a very interesting result, as increasing the number of stages from 2 to 5 corresponds to a reduction in the size of the reactor for a specific reflux value. Up to approximately 5 stages the two pieces of equipment are interacting with each other in an inverse manner, as increasing the size of one piece of equipment associates with it a decrease in the other. For example, by operating with 3 separation stages almost halves the reactor size requirement as when operating with 2 stages, because the additional stage has pushed the reactor composition further from the reaction equilibrium curve. However, as the stage number starts to increase greater than 5, the interaction is such that an increase in one piece of equipment leads to an increase in the other too. This is because the stripping composition profile, and thus the reactor composition too, is pushed back towards the reaction equilibrium curve as the number of stages and reflux is increased.

This interaction between pieces of equipment poses an interesting design problem, as there exists a unique optimum where reflux, stage number, and reactor size are

minimised. Notice however that operating near the minimum feasibility bound for reflux (near R_Δ=2) causes the reactor size to change rapidly. Once again, this is caused by the reactor composition being forced near the reaction equilibrium curve. Even though minimum reflux corresponds to minimum energy usage, operating in the region where R_Δ<2 may not a desirable operating condition, as parameters are very sensitive to change in this range of reflux. From an operating point of view, a safe operating region is probably where the reactor size start to asymptote with changes in R_Δ and where both reactor size and stage number are minimized.

Figure 5.9 is also very useful in terms of showing the spectrum of feasibility, or in other words, where certain combinations of parameters simply would not result in a viable process. In effect, this is an Attainable Region, as it shows all possible process alternatives that will result in a feasible design (Hildebrandt and Glasser, 1990). For example, there is a minimum bound on the size of the reactor where no combination of reflux or stages that will compensate for such a small reactor. Analogously, there also exists an upper bound on the process. Beyond approximately 10 equilibrium stages an increase in reactor size merely associates with it an equivalent higher operating reflux ratio to ensure feasibility. This is almost equivalent to a pinch point in traditional distillation, where an infinite amount of stages can be used with no influence on process performance. Furthermore, the minimum number of stages for a feasible process is two, as one separation stage does not provide enough length to the column composition profile to force the composition at the top of the column section, and the reactor composition, past the reaction equilibrium curve. For the same reason there exists a minimum bound on the reflux too. Interestingly, only the extreme combination of infinitely many stages and infinite reflux will lead to an infeasible process at the upper bound, because these conditions correspond to residue curves. The final compositions on residue curves correspond to the pure component vertices in ideal systems, which also corresponds to a composition on the reaction equilibrium curve, causing an infinitely large reactor. Thus, apart from showing the interaction

between phenomena in a coupled reaction-separation process, it also shows an envelope of realizable designs.

5.3.2 HIGH BOILING PRODUCT

Analogously to the process described in the previous section, a process may be devised whereby a high purity of the high boiling component is achieved. Achieving this requires a slightly different process to the one described in the previous section, as the high boiling component cannot be effectively removed with a rectifying section. Instead, a stripping column section is proposed, fed with a stream that has the same composition as that in the CSTR, as depicted in Figure 5.10. Although this process is slightly different, the equations describing it are very similar.

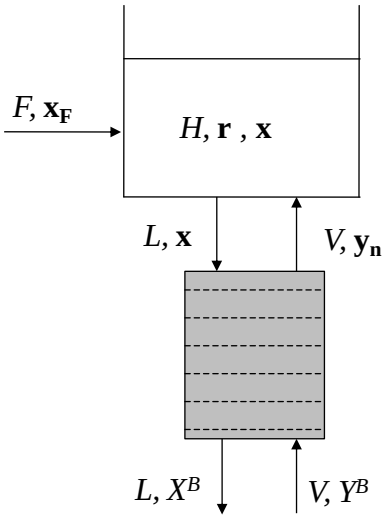


Figure 5.10: A CSTR coupled with a stripping column section, a reactive condenser.

Assuming that the column section is terminated by a reboiler (effectively a stripping column section), X_{Δ} is simply equal to the liquid product specification at the bottom of the column section, i.e. $X_{\Delta} = X^B$. Analogously to the previous example, specifying a reflux value, the amount of stages in the column section and using X^B as the initial

condition for integration, we are able to calculate what the composition at the top of the column section is, and therefore the composition in the reactor (**x**) since these two compositions are equivalent, through the DPE. Once this is known, the composition of the vapour being recycled back to the reactor (y) may be calculated from Equation 4 using the definition of X_{Δ}. Again using the parameters in the DPE along with a steady state component balance across the reactor then yields:

$$F\mathrm{x}_{\mathrm{F}} + \varphi\mathrm{r} + (F/R_{\Delta})\mathrm{x} + F(1-1/R_{\Delta})\mathrm{y}_{\mathrm{n}} = 0 \qquad (5.7)$$

It should be noted that for stripping columns, i.e. where net material flow is downward, values for R_{Δ} are negative since $L>V$. For this example, we shall study the reaction:

$$1L + 1I \Leftrightarrow 2H$$

where component H is a valuable high boiling component. In order to make a fair comparison between the light boiling process, assume that the reaction rate can be described by a similar expression to the previous example, with the exception that the product is now the high boiling component. The reaction equilibrium constant and the VLE behaviour are equivalent to the previous example, and the final product specification is set to x_H = 0.950 with impurities $x_L = x_I = 0.025$. The product specification automatically sets X_{Δ}, and by choosing an arbitrary reflux ratio and amount of stages, the process is then completely specified. The overall process for a range of feeds may then be represented as depicted in Figure 5.11 for R_{Δ}=-7 and n=5.

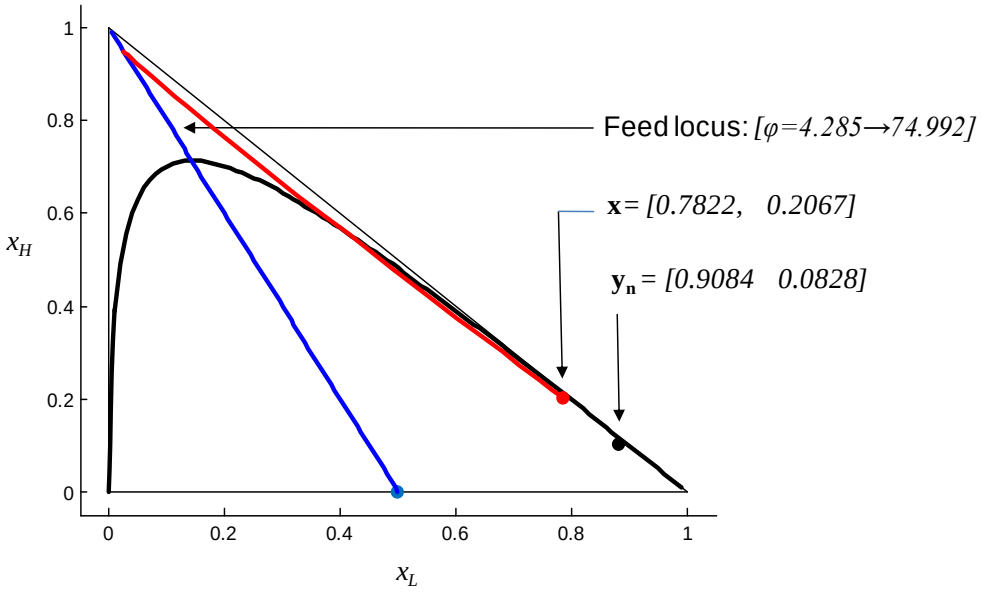


Figure 5.11: A CSTR coupled with a stripping column section for R_A=-7, n=5 and X_A=[0.025, 0.950]. The red and blue line represent the column profile and the feed locus line, respectively, while the red, black and blue dots represent the bottom liquid composition of the column section, the reactor composition and the feed composition that contains no product, respectively. The black curve represents the reaction equilibrium curve.

The blue feed locus line in Figure 5.11 is somewhat different to that presented in the previous example, because the reactor coefficient never drops to zero, even when the feed composition is exactly that of the product specification. Furthermore, the reactor composition is exactly the profile termination point. This may be inferred by arranging the mass balance in the form:

$$X_{\Delta} = \left(\frac{V\mathrm{y} - L\mathrm{x}}{V - L}\right) = -\left(\frac{F\mathrm{x}_{\mathrm{F}} + \varphi \mathrm{r}}{F + \varphi \sum r_i}\right) \qquad (5.8)$$

The interaction between process variables for the special case when x_{FA}=0 for this hypothetical problem may also be represented on a single graph, as in Figure 5.12. Note that reflux values presented here are negative, but the interpretation thereof

remains the same: a high negative reflux value corresponds to a high energy requirement since a large amount of vapour has to be produced through boiling.

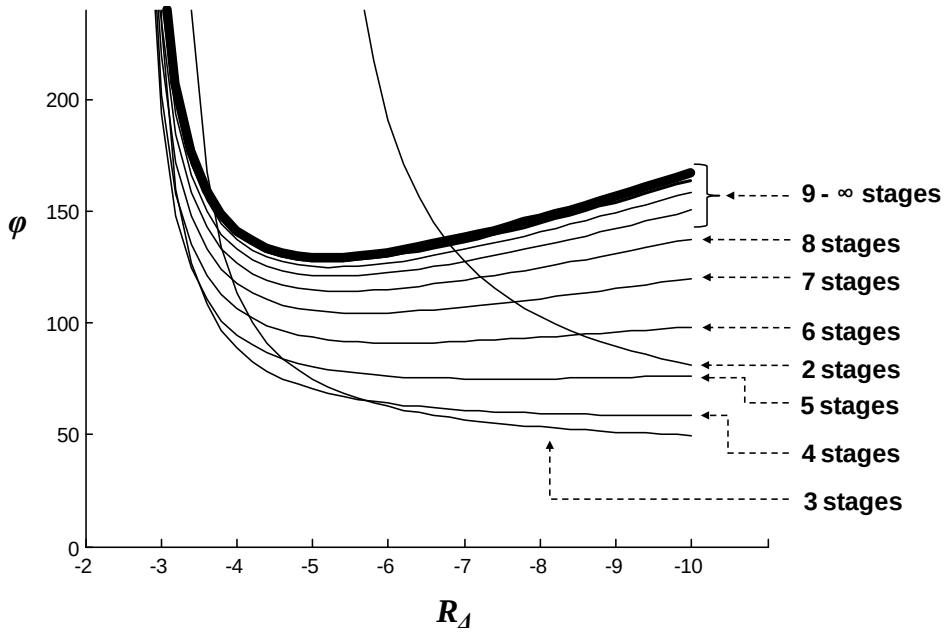


Figure 5.12: The effect of the number of stages and reflux ratio on reactor size for X_{Δ}=[0.025, 0.950] and x_{FH} = 0 for a CSTR coupled to a stripping, non-reactive column section.

Figure 5.12 shows a qualitatively similar result to that of the light-boiling product process in Figure 5.9, as in both cases there exists an optimum selection of process variables and there is a "reversal behaviour" in the equipment sizes. In this case, there is an inverse interaction between equipment up until 3 separation stages, but increasing the amount of stages past this point simply leads to an increase of reactor size. Again, operating near the minimum reflux bound makes the process very sensitive to changes in reflux and causes sharp rises in the reactor size. Furthermore, once more than 3 equilibrium stages is used, an increase in reflux causes an increase in the reactor size, meaning that overall the process requires high operating costs as well as high capital costs.

The operation envelope in this specific case is qualitatively similar to the light boiling case. There is again a lower bound on the number of stages, and reflux, where the top column section composition cannot cross the reaction equilibrium curve. Also notice that operating at minimum reflux is extremely sensitive to changes in reflux. Stages begin to asymptote to pinched conditions at around n=9, where no further increase on the number of stages will influence other process variables. However, noticeably different from light boiling process is the big leap between process conditions from stage two to three.

5.3.3 INTERMEDIATE BOILING PRODUCT

For the same general problem described in the previous section, we can extend our analysis method to achieving a high purity of the intermediate boiling component. This case is a relatively common problem in reactive distillation, as isomerisation reactions typically produce intermediate boiling components. The reaction to be analysed here is:

$$1H + 1L \Leftrightarrow 2I$$

Removing the intermediate boiler is possible via either one of the processes described above (reactive reboiler or condenser). Consider then firstly the reactive reboiler arrangement. In order to compare all the scenarios on the same basis, we assume that the reaction can be described with a similar expression for the reaction rate as in previous sections, with the exception that the product is now the intermediate boiling component. Furthermore, the reaction equilibrium constant is assumed to be the same as well as the VLE. The product specification is set to $x_I = 0.950$ with impurities $x_H = x_L = 0.025$. Once again, by specifying the amount of stages and the reflux ratio, the system is completely specified as the product specification is equivalent to X_Δ for a total condenser.

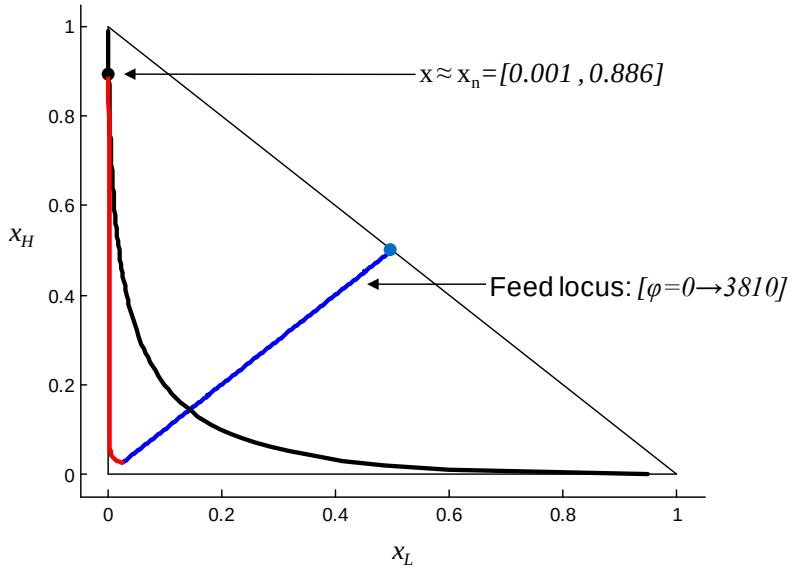


Figure 5.13: A CSTR coupled with a rectifying column section for R_A=10, n=12 and X_A = [0.025, 0.025]. The red and blue line represent the column profile and the feed locus line, respectively, while the red, black and blue dots represent the bottom liquid composition of the column section, the reactor composition and the feed composition that contains no product, respectively. The black curve represents the reaction equilibrium curve.

Figure 5.13 is useful for qualitatively understanding the difficulty of achieving a product with a high purity of the intermediate boiling component. The liquid profile in the column section (red line) simply does not provide enough curvature to move the reactor composition away from the reaction equilibrium curve, which leads to very large reactor volumes. Notice that the range of values for the reaction coefficient on the feed locus line is significantly higher than the case where the light or heavy boiling components were the desired product. Again there is a relationship between all process parameters, illustrated in Figure 5.14 for this process.

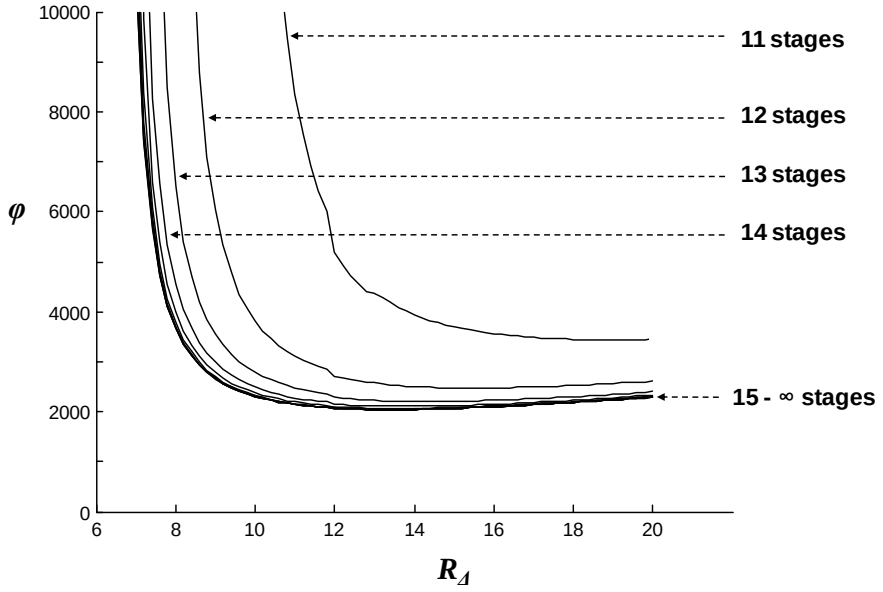


Figure 5.14: The effect of the number of stages and reflux ratio on reactor size for X_A = [0.025, 0.025] and x_{FI} = 0 for a CSTR coupled to a rectifying, non-reactive column section.

Conversely to the results shown in both the light and heavy boiling cases, for this specific process there are in fact potential gains in the process by increasing the amount of stages in the separation, as there is no reverse interaction between equipment. However, as seen from Figure 5.14, a continual increase of the amount of stages eventually does not offer any advantages, as the stages start to converge to pinched conditions after 15 stages.

There are a few interesting points that may be inferred about the operation envelope from this graph. Firstly, notice the incredibly large values for the reaction coefficient φ as well as the relatively high reflux ratios that are required for this process. Secondly, because the reactor composition has to lie on "the feed side" of the reaction equilibrium curve, the minimum amount of stages for the process to be feasible also increases. When compared to the analogous process for the low boiling component, the minimum amount of stages is extremely high, only starting at n=11. All of these factors indicate that it is extremely expensive to operate such a process, and it is certainly worth considering whether a conventional reactor-separation sequence is

more viable. For example, operating a system as described above requires a relatively high reflux ratio (and therefore a high energy demand due to the amount of boiling), but removing the intermediate boiling component in 2 columns may require less boiling overall and thus be more efficient.

As stated previously, the intermediate boiling component may also be removed by a reactive condensing process. However, due to the symmetrical nature of the problem we may expect similar results to those presented in Figure 5.14 for the reactive reboiler arrangement. The reactive condenser where the intermediate boiling component is assumed to be the valuable product is summarised in Figure 5.15.

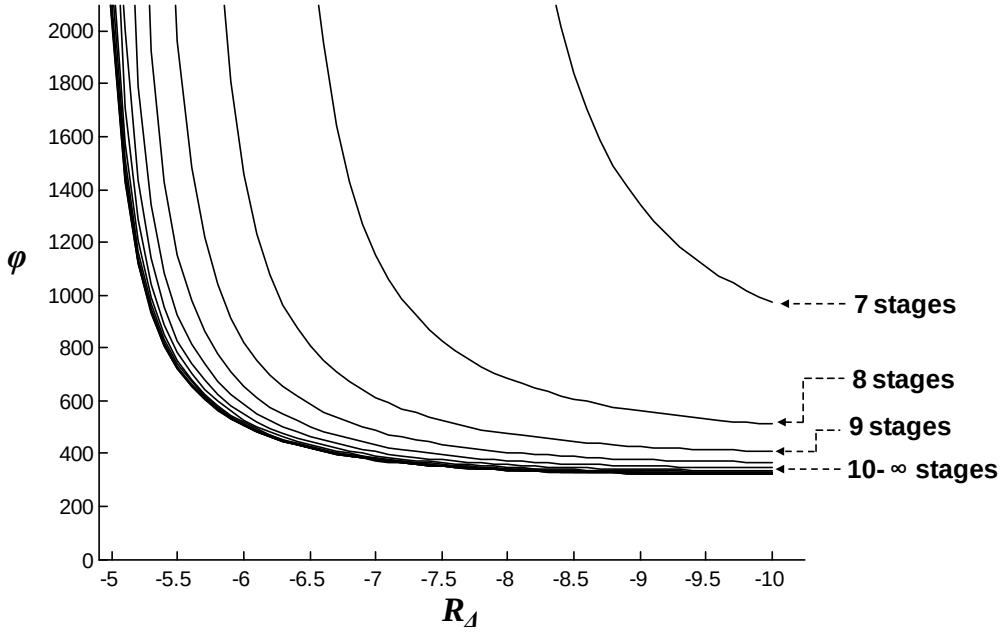


Figure 5.15: The effect of the number of stages and reflux ratio on reactor size for X_{Δ} = [0.025, 0.025] and x_{FI} = 0 for a CSTR coupled to a stripping, non-reactive column section.

The interaction between process equipment is similar to that shown in Figure 5.14, i.e. an increase in stage number leads to a decrease in reactor size and there is no reversal behaviour. However, this process appears to be advantageous, as in general reactor volumes smaller by a factor of approximately 5 may be attained. Furthermore,

the minimum number of stages for the process to be feasible is much lower, 7 for the reactive condenser versus 11 for the reboiler arrangement. The reflux ranges appear to be similar and no significant gain can be achieved from an energy expenditure point of view. Although this process does seem to offer some advantages, the reactor volumes are still extremely large relative to removing the high boiling component in a similar arrangement. Once again, this is due to the compositional profiles in the rectifying column section that do not provide enough curvature to push the reactor composition beyond the reaction equilibrium curve.

It might be inferred, rather paradoxically, that it is the ideal nature of this process that makes it an unattractive process alternative. Studying Figure 5.13 more closely shows that if there were a binary minimum or maximum boiling azeotrope between the light and heavy components, the liquid composition profile would terminate or pinch at this point, and thus be drawn further away from the reaction equilibrium curve. This would make reactor volumes significantly smaller as well decreasing the reflux needed to render the process feasible. This is highlighted by the highly non-ideal MTBE case study, shown in the following section.

5.3.4 THE MTBE PROCESS

Methyl Tert-Butyl Ether (MTBE) is widely used as a fuel additive and is one of the most well known applications of reactive distillation. As a final example, the well known reaction between methanol (MEOH) and iso-butene (IBUT) to form MTBE is studied. In the industrial version of the process, the IBUT stream is made up of inert hydrocarbons, but we will neglect these in this analysis. The reaction is given by:

$$1IBUT + 1MEOH \Leftrightarrow 1MTBE$$

and the rate law may be described by:

$$\mathrm{r} = k_f \left(\gamma_{IBUT} x_{IBUT} \gamma_{MEOH} x_{MEOH} - \frac{\gamma_{MTBE} x_{MTBE}}{K_{eq}} \right)$$

Where γ_i is the liquid phase activity coefficient, calculated here using the Non Random Two Liquid (NRTL) thermodynamic model with binary interaction parameters obtained from the ASPEN PLUS Databank. The reaction rate constant (k_f) and equilibrium constant (K_{eq}) are taken from the works of Venimadhavan et al. (1994) to be:

$$k_f = 1.240 \exp(3187.0/T) \quad [\mathrm{s}^{-1}]$$

$$K_{eq} = 8.33 \times 10^{-8} \exp(6820.0/T)$$

where T is in degrees Kelvin. The VLE behaviour of the system is highly non-ideal with two minimum-boiling binary azeotropes between MEOH and MTBE, and MEOH and IBUT, respectively, described by the modified Raoult's law:

$$y_i = \frac{\gamma_i x_i P_i^{SAT}}{P_{TOT}}$$

The liquid phase activity coefficients are calculated by the NRTL equation shown below, for Isobutene (1), Methanol (2) and MTBE (3):

$$\gamma_i = \exp\left[\frac{\sum_j x_j \tau_{ji} G_{ji}}{\sum_k x_k G_{ki}} + \sum_j \frac{x_j G_{ij}}{\sum_k x_k G_{kj}} \left(\tau_{ij} - \frac{\sum_m x_m \tau_{mj} G_{mj}}{\sum_k x_k G_{kj}} \right) \right]$$

where $\tau_{ij} = a_{ij} + b_{ij} / T(^oK)$, $G_{ij} = \exp(-c_{ij} \tau_{ij})$, and:

$$a=\begin{bmatrix}0 & 0 & 0\\ 0 & 0 & 0\\ 0 & 0 & 0\end{bmatrix}, b=\begin{bmatrix}0 & 840.5508 & -285.8313\\ 412.2995 & 0 & 205.7954\\ 417.2121 & 213.6208 & 0\end{bmatrix}, c=\begin{bmatrix}0 & 0.47 & 0.3\\ 0.47 & 0 & 0.3\\ 0.3 & 0.3 & 0\end{bmatrix}$$

The notation above is such that F_{ij} implies the i'th row and j'th column entry of matrix F. The vapour pressures, P_i^{SAT} are determined by using the Antoine Equation:

$$\log_{10} P_i^{SAT}(\text{Pa}) = A + \frac{B}{T(\text{K}) + C}$$

The Antoine Vapour Pressure coefficients are given in Table 5.1:

Table 5.1: Antoine constants for Isobutene, Methanol and MTBE

	Isobutene	Methanol	MTBE
A	20.6455	23.4999	20.7162
B	-2125.7489	-3643.3136	-2571.5846
C	-33.160	-33.434	-48.406

A residue curve map and reaction equilibrium curves at different temperatures are shown in Figure 5.16 a and b, respectively.

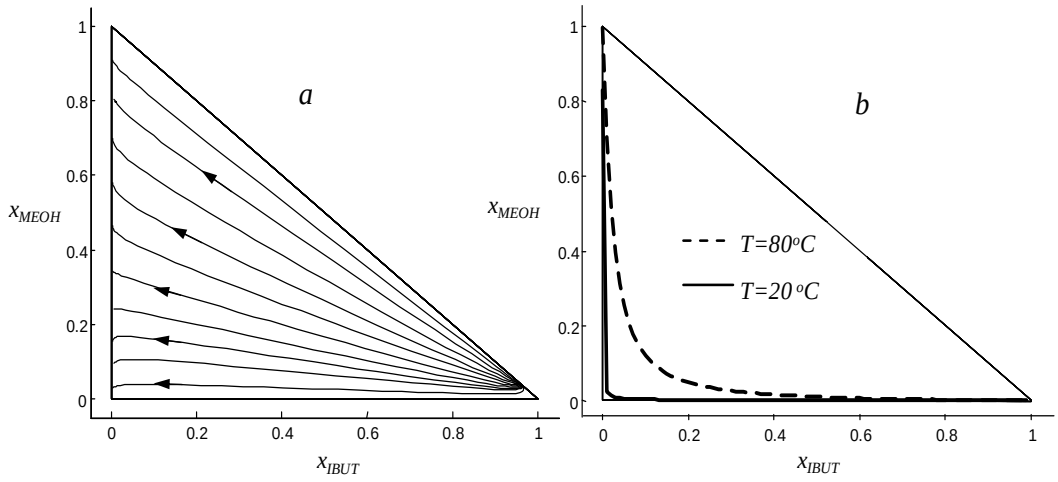


Figure 5.16: The IBUT-MEOH-MTBE system at 1atm: (a) a Residue Curve Map and (b), reaction equilibrium curves.

The residue curve map in Figure 5.16 indicates that the stationary point on the MTBE pure component vertex is a stable node, and can be seen as the high-boiling component within its distillation region. Hence we will use a CSTR coupled with a stripping section as in Figure 5.10 in our analysis. Although this system is considerably more complex than those discussed in the previous examples, the general method remains unchanged. We also shall assume that the streams leaving and entering the reactor are at their boiling points, and thus the reactor has to be at this temperature too. Thus, the reaction equilibrium curve will be different for a different combination of reflux and amount of equilibrium changes. For arbitrarily chosen process conditions of 1 atm system pressure, 5 equilibrium stages, a reflux of -8 and a product specification of x_{MTBE}=0.950 and x_{MEOH}=x_{IBUT}=0.025, the process may be represented as in Figure 5.17.

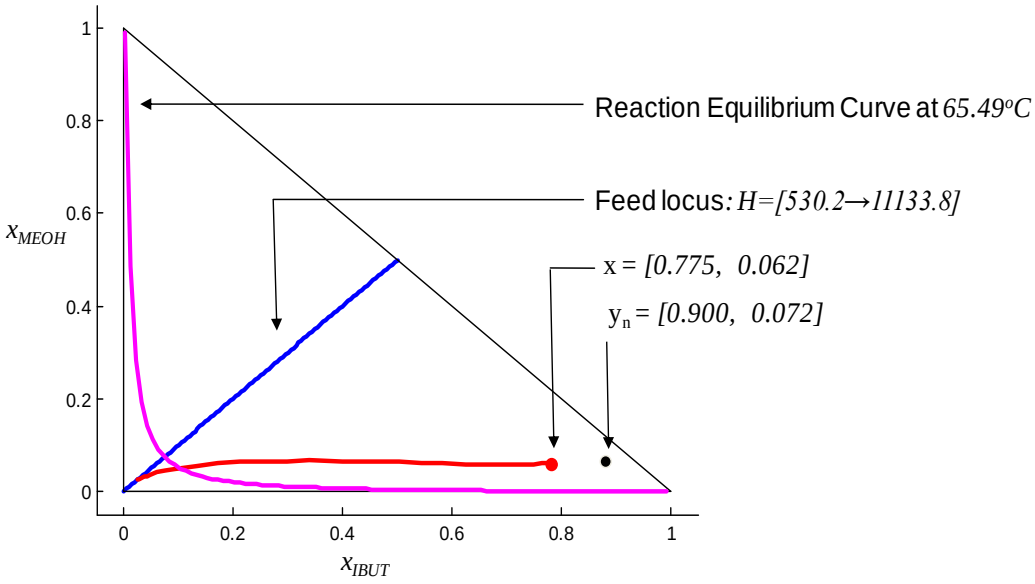


Figure 5.17: CSTR coupled with a stripping column section for the MTBE system at 1 atm, with R_Δ= -8, n=5 and X_Δ=[0.950, 0.025]. The red and blue line represent the column profile and the feed locus line, respectively, while the red, black and blue dots represent the bottom liquid composition of the column section, the reactor composition and the feed composition that contains no product, respectively. The purple line is the reaction equilibrium curve at 65.49°C

For the process parameters mentioned above, the reactor temperature has to be operated at $65.49^{o}C$. Also, as we have kinetic data available, we are able to calculate the actual molar holdup in the reactor. It is now apparent that there is not only an interaction between the size of the reactor and the stripping column section, but also, the operating conditions of the reactor are influenced by the choice of stages and reflux. A summary of the entire process for a feed containing no MTBE may be seen in Figure 5.18 and Figure 5.19 illustrating the molar holdup and operating temperature in the reactor, respectively. Importantly, notice from Figure 5.17 that even though the MTBE is the intermediate boiling component, the final composition on the stripping column section's liquid composition profile (**x**) is relatively far away from the reaction equilibrium curve. This is due to the MEOH-IBUT binary azeotrope attracting the profile, and not the stationary point situated on the pure component vertex, as in the previous intermediate boiling ideal example. Thus, this non-ideal VLE behaviour does make this a more attractive alternative from a topological perspective.

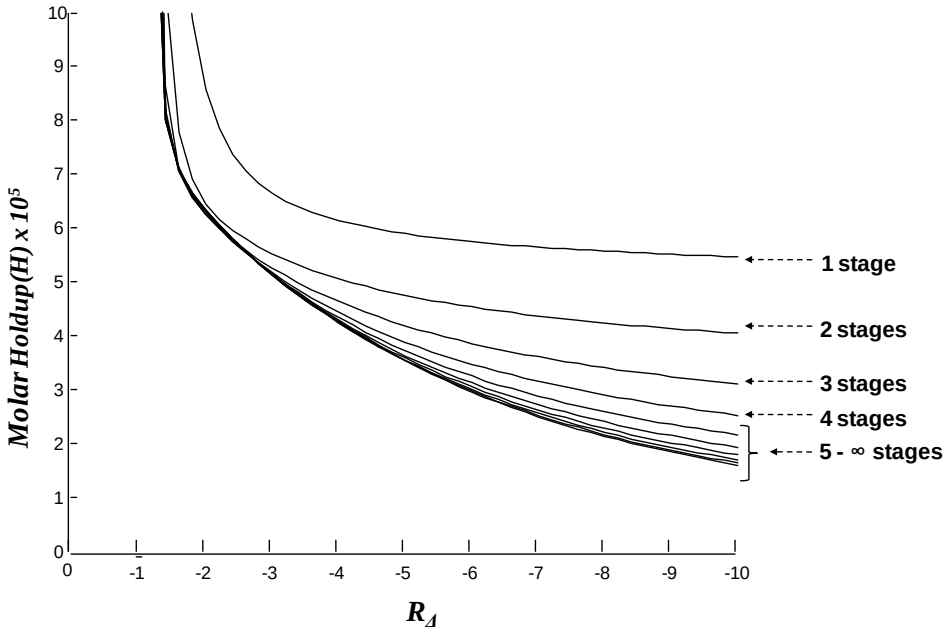


Figure 5.18: The effect of the number of stages and reflux ratio on molar holdup for the MTBE process at 1 atm, with X_A=[0.950, 0.025] and x_{MTBE}=0 for a CSTR coupled to a stripping, non-reactive column section.

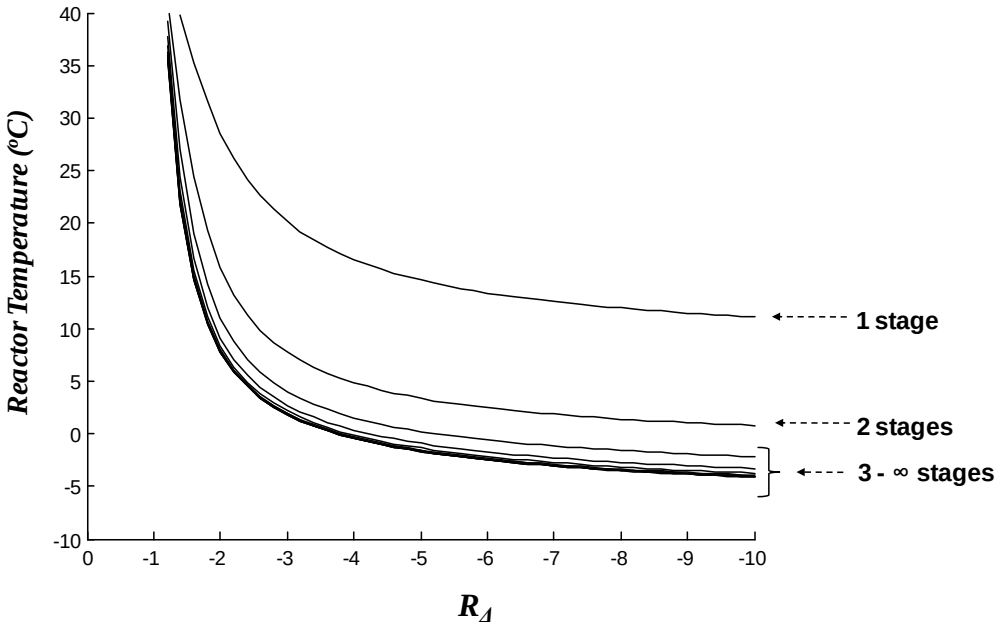


Figure 5.19 The effect of the number of stages and reflux ratio on reactor temperature for the MTBE process at 1 atm, with X_A=[0.950, 0.025] and x_{MTBE}=0 for a CSTR coupled to a stripping, non-reactive column section..

Figure 5.18 may offer some insight as to why the production of MTBE by a reactive distillation process has become so popular, as there is no reversing behaviour in the process design, i.e. although over-designing the process will result in higher equipment or operational costs, there are no additional penalties for it, as shown in Figure 5.9 and Figure 5.12. Reactor size decreases sharply with increasing reflux, but potential gains in increasing the amount of stages begin to asymptote after 5 stages. The relationship between Figure 5.18 and Figure 5.19 is also very interesting as it implies that, in general, smaller reactors result in lower operating temperatures in the reactor. However, for an operating pressure of 1 atm, the small reactors result in very low temperatures of approximately -5 ^{o}C, which is generally an unwanted process condition. This explains why the MTBE process is generally operated at relatively high pressures (~8 atm), (Venimadhavan et al., 1994) as increasing the operating pressure of the process will also increase both the boiling points of the mixtures and the operating temperature of the reactor. Thus, for a system pressure of 8 atm, we

may again analyse the interaction of process parameters as in Figure 5.20 and Figure 5.21.

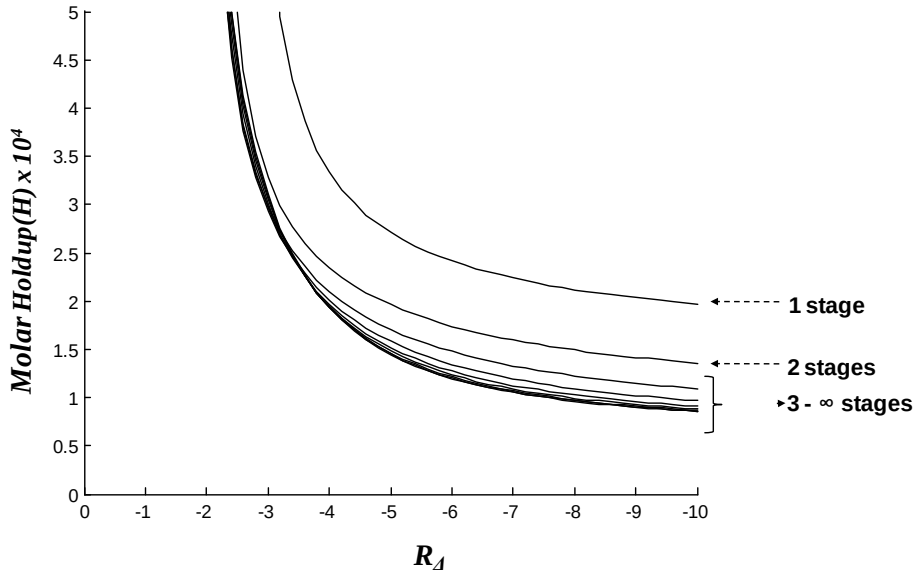


Figure 5.20: The effect of the number of stages and reflux ratio on reactor size for the MTBE process at 8 atm, X_{Δ}=[0.950, 0.025] and x_{MTBE}=0 for a CSTR coupled to a stripping, non-reactive column section.

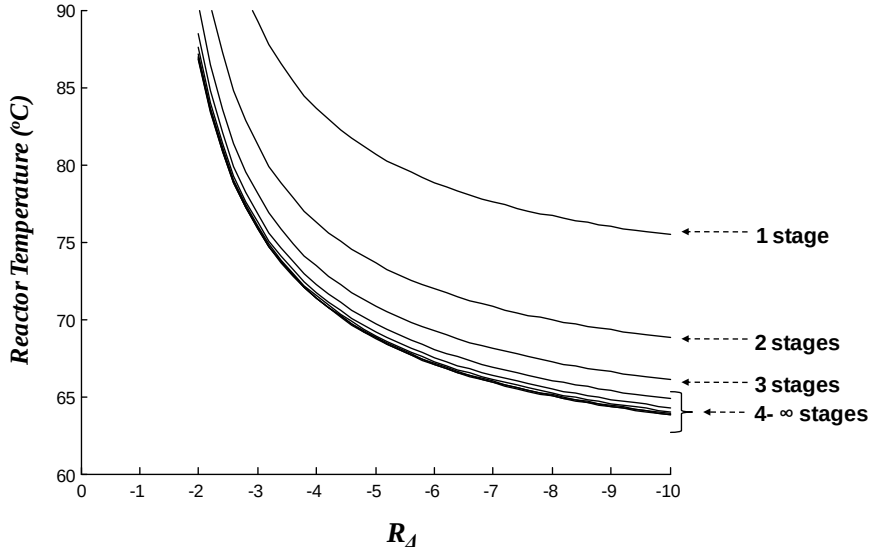


Figure 5.21: The effect of the number of stages and reflux ratio on reactor temperature for the MTBE process at 8 atm, X_{Δ}=[0.950, 0.025] and x_{MTBE}=0 for a CSTR coupled to a stripping, non-reactive column section.

Figure 5.20 shows that the trend in process interactions is similar at the elevated pressure of 8 atm, although the molar holdup in the reactor is approximately ten times smaller than that at 1 atm. Also, the stages begin to asymptote to pinched conditions much quicker at around 3 stages, implying that there is a greater risk of over-designing the system at pressure. From Figure 5.21 it can also be seen that operating at a higher pressure also allows for more reasonable reactor temperatures (± 70^{o}C). If one considers the feasible regions for the two scenarios depicted above, it may be said that the high pressure process has a smaller region, but the gains in reactor size are considerable. These figures now give the designer freedom of choice when deciding on the feasibility of a process. It is up to the designer to decide on operating conditions and to weigh up the cases for low energy costs (high reflux) against high capital cost (mainly reactor size and stages), and vice versa. In modern chemical industries the drive is towards low energy usage, but here, it comes with a price as a large reactor is required to offset this. However, by understanding the interactions between the processes involved, one might be able to save on the amount of stages required, and hence lower the capital cost.

5.4 CONCLUSIONS

In this contribution, a method is presented to better understand the effects of phenomena interaction in a so called coupled reactor-separation process. This is achieved by utilising the graphical CPM method for modelling the rectifying or stripping column section, coupled with a steady state, CSTR with simultaneous mixing, reaction and equilibrium separation. A novel, graphical understanding of the overall process is presented which could be particularly useful in the early stages of conceptual design. It has been shown why some vapour liquid equilibrium and reaction behaviour do not allow for a desirable process in the whole. In some cases, it may be desirable to have non-ideal phase equilibrium behaviour as this could present topological advantages that can benefit a reactive distillation process. A specific

example of this is the industrially relevant MTBE system, where the azeotropic behaviour reduces reactor size as well as reflux requirements.

Three different hypothetical cases have been studied, where the forward chemical reaction produces a low, intermediate and high boiling component respectively. A region of feasible operation for each process has been determined, which indicates the minimum (and maximum) values for process parameters to achieve a certain product specification. A graphical summary of each process has been presented and it has been shown that the interaction between separation and reaction parameters (reactor size, reflux ratio and amount of stages) has to be understood, as over designing the problem could lead to an overall worse process in some scenarios. Producing an intermediate boiler as final product is by far the worst overall process because the liquid composition profiles do not provide sufficient curvature away from the reaction equilibrium curve for an ideal system.

.

Chapter 6 : PINCH POINT CALCULATIONS AND ITS APPLICATION TO ROBUST DISTILLATION DESIGN

This work for this chapter was completed during my stay at the University of Illinois at Chicago. Parts of this chapter was included in a peer-reviewed conference paper for ESCAPE 20 in Naples, Italy. Both Seon Kim and Prof. Andreas Linninger made valuable contributions to this chapter, but it is largely my own work. It has been accepted in the Chinese Journal of Chemical Engineering under the same title as above.

Rising energy costs and growing environmental awareness motivates a critical revision of the design of distillation units. Systematic design techniques, such as the Rectification Body, Column Profile Map, and Temperature Collocation methods, require exact knowledge of all Pinch Points in a particular system, because these stationary points delineate the possible composition trajectories realizable in separation columns. This paper demonstrates novel methods for rigorously determining all Pinch Points for the constant relative volatility, ideal and non-ideal systems. Constant relative volatility and ideal solution systems are transformed into one-dimensional polynomial and nonlinear functions, regardless of the number of the components. A deflation method is proposed to locate all roots in ideal and non-ideal zeotropic problems. For more challenging non-ideal problems, a novel hybrid sequential niche algorithm is used to solve hard azeotropic problems successfully. Finally, the design implications of these Pinch Point locations are investigated to show how new separation configurations can be devised. Methodically the paper points out the use of rigorous Pinch Point computations in conjunction with continuous composition profiles for robust distillation design.

6.1 INTRODUCTION

Distillation is by far the most utilized large scale industrial method of liquid mixture separation. It is an energy intensive process and accounts for a significant percentage of plant utility costs. A survey conducted in the mid 1990's estimates that energy inputs to distillation columns in the United States accounts for approximately 3% of the country's total energy consumption.(Ognisty, 1995) Due to the significant costs associated with operating distillation units and the rising cost of energy and environmental concerns, new methods are required to improve the understanding of these systems so that more energy efficient processes can be designed.

A rigorous means of determining whether a distillation unit, simple or complex, is feasible requires solving multiple tray-by-tray mass, equilibrium, summation and heat (MESH) equations. However, solving separation problems with MESH equations become difficult as the number of components increase and exceeds current optimization techniques. Numerous simplified techniques, such as the Rectification Body Method (Bausa et al., 1998) and the Underwood Method (Underwood, 1945, Underwood, 1946b), have been proposed to facilitate the design of distillation systems. Specifically, the Rectification Body Method proposes the estimation of column feasibility by investigating a design space delineated by Pinch Points. This method has been applied to azeotropic separations, complex column arrangements as well as reactive distillation problems. The Underwood equation applies only to solutions that can be approximated with a constant relative volatility model. Recently, Hildebrandt and Glasser's group introduced Column Profile Maps, a graphical technique that approximates stage-by-stage liquid composition profiles through a first order ordinary differential equation (Holland et al., 2004a, Holland et al., 2004b). Their generalized difference point equation is an adaptation of rectifying and stripping profile equations first proposed by Van Dongen and Doherty.(Van Dongen and Doherty, 1985b) The general nature of these equations allows the designer to

assess both simple and complex columns as well as thermally coupled column such as Petlyuk columns (Petlyuk et al., 1965). Furthermore, they suggested the advantage of extending the study of profiles, and Pinch Points, seen outside the physically realizable space. They demonstrate that this global topological view renders critical novel insights into the design, before being bound by a predefined structures.

Linninger's group devised a Temperature Collocation technique for systematically ascertaining feasible column configurations searching for liquid composition profile intersections using a bubble point distance objective function (Zhang and Linninger, 2004). This technique was successfully used to synthesize simple column networks (Zhang and Linninger, 2006b). Recently, they extended the Temperature Collocation method to systems of columns, both simple and complex, using elements of the generalised Column Profile Map technique and were able to show that their designs matched; a rigorous, MESH solving, process simulation package (Ruiz et al., 2009, Ruiz et al., 2010, Kim et al., 2010b). A central part of this automated design procedure is finding *all* Pinch Points.

A recurring theme in the aforementioned design methods (Rectification Body Method, Column Profile Maps, and Temperature Collocation) is that determining the Pinch Points is a prerequisite for finding interesting distillation configurations. Lucia has presented an extensive review of other separation synthesis techniques that also make use of the knowledge of the Pinch Points in distillation, such as the Zero Volume method (Julka and Doherty, 1990), Eigenvalue methods (Poellmann et al., 1994) and minimum vapour diagrams (Halvorsen and Skogestad, 2003a). However, previous works focused on simple column configurations. In this paper we shall address Pinch Point locations for generalised Column Profile Maps needed for the design of complex and heat integrated columns. Several novel techniques that guarantee convergence at speed are presented. The aim of these works is thus to present an in-depth understanding and highlight underlying properties of Pinch Point

calculations for all solutions, both zeotropic and azeotropic, and to explore the design implications.

The chapter is structured as follows: Section 6.2 gives a theoretical background of the Column Profile Map, Temperature Collocation and Rectification Body Methods. It also discusses general properties of the difference point equation, such as the significance of the vapour liquid equilibrium model and the validity of negative compositions for analysis. Section 6.3 describes novel mathematical techniques for solving each respective phase equilibrium model. The applicability of the considered design methods and the significance of Pinch Points are then discussed in section 6.4, followed by several conclusions that may be drawn from this work in section 6.5.

6.2 THEORETICAL BACKGROUND

6.2.1 THE DIFFERENCE POINT EQUATION

The Difference Point Equation was developed by Glasser and Hildebrandt (Tapp et al., 2004) for a generalized column section from which a Column Profile Map may be constructed by setting parameters such as the reflux ratio and net compositional flows. The definition of generalised column section is given as a length of column between points of material addition or removal, as shown in Figure 6.1 (a). The equation describing the liquid compositional change, **x(n)**, along the column section may then be derived through a steady state material balance over a column section, assuming equilibrium of liquid-vapour phases on each stage and constant molar overflow, accompanied by a Taylor expansion, which yields in a vectorised form:

$$\frac{d\mathrm{x}}{dn} = \left(\frac{1}{R_\Delta} + 1\right)\left[\mathrm{x} - \mathrm{y(x)}\right] + \left(\frac{1}{R_\Delta}\right)(X_\Delta - \mathrm{x}) \qquad (6.1)$$

where $X_\Delta = \left(\frac{VY^T - LX^T}{\Delta}\right)$, $R_\Delta = \frac{L}{\Delta}$, and $\Delta = V - L$.

In this equation, R_Δ is a generalized reflux ratio in the column section, n the number of stages, and X_Δ is known as the mixing or Difference Point, can be thought of as a pseudo composition vector, valid anywhere in the composition space. X_Δ need only be a real composition in column sections that are terminated by a condenser or reboiler, and like real compositions it is also subject to the constraint that the sum of its components be unity. A negative element entry for vector X_Δ is entirely possible in practical design situations, and merely implies that the corresponding component is flowing downward in the column section. Also, a column section with a positive value of R_Δ corresponds to an equivalent rectifying section, with net upwards flow., while a column section operating with a negative R_Δ corresponds to an equivalent stripping section. The vapour composition **y(x)** can be related to the liquid composition using an appropriate Vapour-Liquid Equilibrium model. For a given operating condition like the generalized reflux R_Δ and Difference Point, X_Δ, composition profiles may be drawn by integrating Equation 6.1. We term a principal profile one which terminates in a real product like the distillate in Figure 6.1 (a). In this case, the product composition is equal to the Difference Point composition.

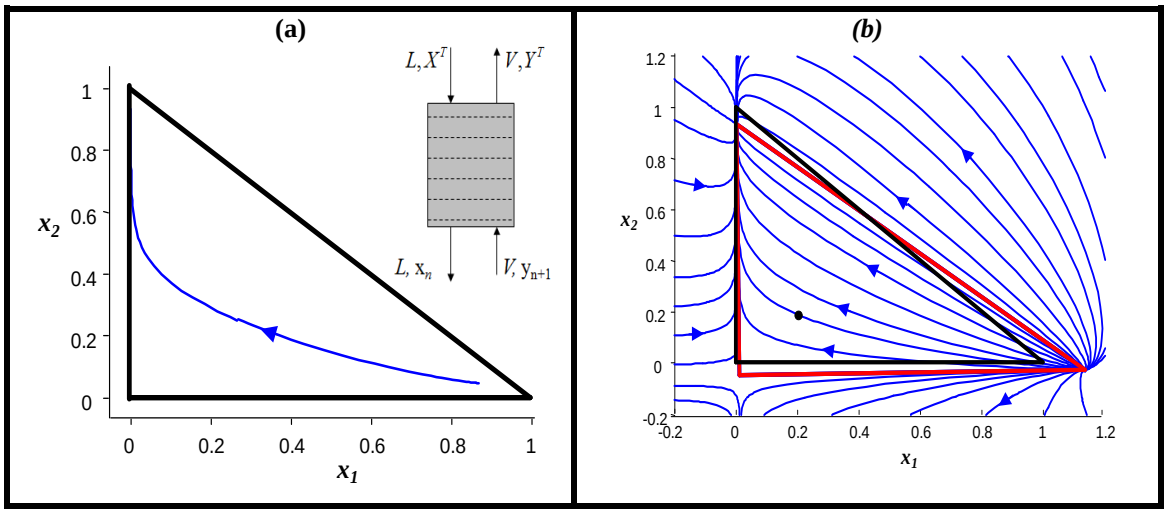


Figure 6.1: (a) A single liquid composition profile with R_Δ=9 and X_Δ= [0.2, 0.2], with the definition of a generalized Column Section, and (b) a Column Profile Map with R_Δ=9 and X_Δ=[0.2, 0.2]where the blue lines represent the column profiles, inside and outside the positive composition space, and the red triangle indicates the shifted Pinch Points.

There are also other profiles corresponding to internal column sections, found in complex distillation structures, satisfying the same mass balance constraints, but that produce a liquid and a vapour stream whose mixing composition is equal to the Difference Point composition. Hence, secondary profiles do not produce a product, but two streams whose combination would give the Difference Point. These secondary profiles give unique design opportunities for complex column configurations and have previously not been investigated systematically. A family of such secondary composition profiles with different initial compositions are depicted in the Column Profile Map of Figure 6.1 (b). Note that when our view is confined to a single profile only existing within the mass balance as in Figure 6.1 (a), one gains a very limited perspective into how to realize a desired separation task. Furthermore, the topological features in Figure 6.1 (b) extend smoothly from the mass balance triangle (in black) to regions in which some species compositions are negative. The Pinch Points are stationary points of all composition profiles shown in Figure 6.1 (a) and (b), which means that the liquid and vapour compositions no longer change with respect to stage numbers and may be determined by solving dx/dn=0 The Pinch Points' location is cardinal for understanding the topology of a specific separation

task, because they delineate all composition profile trajectories attainable in a certain column section. Also, notice in Figure 6.1 (b) that the Pinch Points influence the paths of all profiles. Valuable insights may be gleaned by viewing profiles, and their Pinch Points, outside the physically realizable space as they have a marked effect on topology of real column profiles inside the mass balance triangle.

Previous work on Column Profile Maps have investigated the topological effects of varying the two relevant design parameters in the Difference Point Equation, R_Δ and X_Δ and moreover, the design implications using the CPM method (Tapp et al., 2004). They showed that placement of the X_Δ parameter has a significant effect on the locus of Pinch Points and identified discrete regions of X_Δ placement that have similar topological features. Furthermore, at the extreme case of infinite reflux ($R_\Delta=\infty$), the Difference Point Equation simply reduces to the residue curve equation and the Pinch Points are located on the pure component vertices of the mass balance triangle. A network of column sections, which constitute a complete column, may be rendered feasible if two liquid composition profiles of neighbouring column sections intersect one another. A design technique based on Column Profile Maps for multi-component separation, entitled Temperature Collocation, has been developed to rigorously search for feasible designs (Zhang and Linninger, 2004).

6.2.2 RECTIFICATION BODY METHOD

The Rectification Body Method was developed by Marquardt's group (Bausa et al., 1998) as a rapid means of determining minimum energy requirements for a proposed split involving non-ideal and azeotropic n-component mixtures. This method requires that the saddle and stable/unstable nodes be known for each column section. A rectification body can then be constructed by connecting these two points with each other as well as the product specification's coordinate with a straight line. The reflux ratio can then altered until the rectification bodies of adjacent Column Sections intersect which constitutes a feasible design, as shown in Figure 6.2. However, it will

be shown in section 6.5 that in general the Rectification Body method is neither a necessary nor a sufficient feasibility criterion, because there are cases where pinch point compositions are complex or where the convex rectification bodies do not contain all realizable column section profiles.

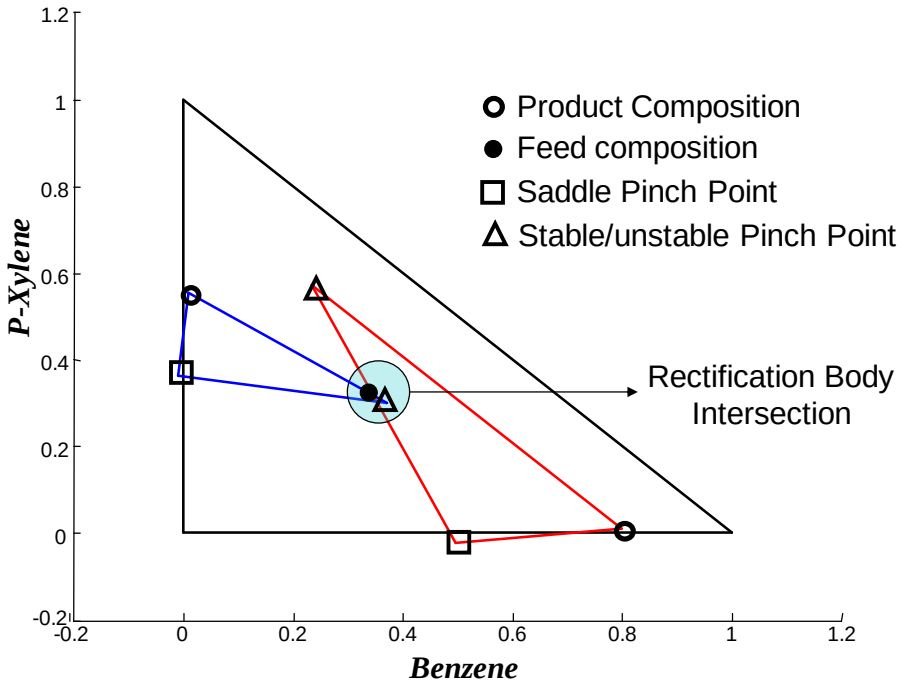


Figure 6.2: Intersecting Rectification Bodies for the Benzene / Xylene / Toluene system

6.2.3 VAPOUR – LIQUID EQUILIBRIUM MODELS

At first glance, calculating the Pinch Points of the Difference Point Equation seems to be easy. However, non-linear phase equilibrium models may introduce several complexities. Phase equilibrium models can be divided in to three main categories, namely constant relative volatilities, ideal solutions obeying Raoult's law, and non-ideal solutions (both zeotropic and azeotropic) which may be modelled with a modified Raoult's law. These respective models are shortly discussed in the following sections.

Constant relative volatilities

The simplest means of relating vapour and liquid compositions is by assuming that the relative volatilities between respective components do not change with temperature, i.e.

$$y_i = \frac{\alpha_i x_i}{\sum \alpha_i x_i} \qquad (6.2)$$

Interestingly, the number of roots obtained from this equation is always equivalent to the number of components in the system (see Figure 6.1 b and the "Shifted Triangle for a ternary system).

Ideal solutions

The first degree of complexity for solving the stationary points in the Difference Point Equation is modelling saturated vapour pressures by the Antoine equation and relating vapour and liquid compositions through Raoult's law which is given by:

$$y_i = \frac{P_{i,sat} x_i}{P} \qquad (6.3)$$

where $\log(P_{i,sat}) = A_i - \frac{B_i}{T(^oC) + C_i}$, and A_i, B_i, C_i are the Antoine coefficients for component *i*. Similarly to the constant relative volatility model, this model also produces the same amount of solutions as components in the system and is topologically similar to the constant relative volatility system described above and shown in Figure 6.1 b.

Non-Ideal solutions

Numerous models relating vapour and liquid compositions for non ideal mixtures exist in the literature, such as the Non Random Two Liquid (NRTL), Wilson, UNIQUAC, etc. These models allow one to determine an activity coefficient (γ_i), whereby the vapour composition may be determined using a modified Raoult's law:

$$y_i = \frac{\gamma_i P_{i,sat} x_i}{\phi_i P}, \qquad \text{where } \gamma_i = f(x,T), \quad \phi_i = (y,T) \qquad (6.4)$$

The activity coefficient allows for the presence of azeotropes and other non-ideal phase equilibrium behaviour. The non-ideality of the gas phase is usually neglected in separations design by setting the fugacity (Φ) to unity.

6.2.4 THERMODYNAMIC CONSISTENCY OF NEGATIVE COMPOSITIONS

From Figure 6.1 one may see that stationary points may be shifted outside positive composition space at finite reflux. The location of the Pinch Point outside the mass balance triangle is relevant, because all trajectories are connected through the constellation of the Pinch Points. To achieve desired separations, the designer may purposefully position certain Pinch Points inside or outside the positive composition space. However, it is fair to ask whether these negative compositions are thermodynamically consistent and if Pinch Points outside the composition space permit drawing meaningful conclusions for separations. Models such as UNIQUAC and Wilson can immediately be excluded because both contain logarithms which are undefined for negative compositions. However, other models such as van Laar and Margules, as well as the NRTL model can safely be extrapolated to negative compositions, as shown in the residue curve map in Figure 6.3 for the azeotropic Acetone / Benzene / Chloroform system. Notice that there are multiple stationary points, both inside and outside the composition space. In a similar way to which

stationary points were shifted from their original positions in the Residue Curve Map for a constant relative volatility system in Figure 6.1, so to may stationary points be shifted in Figure 6.3 for finite choices of R_{Δ}.

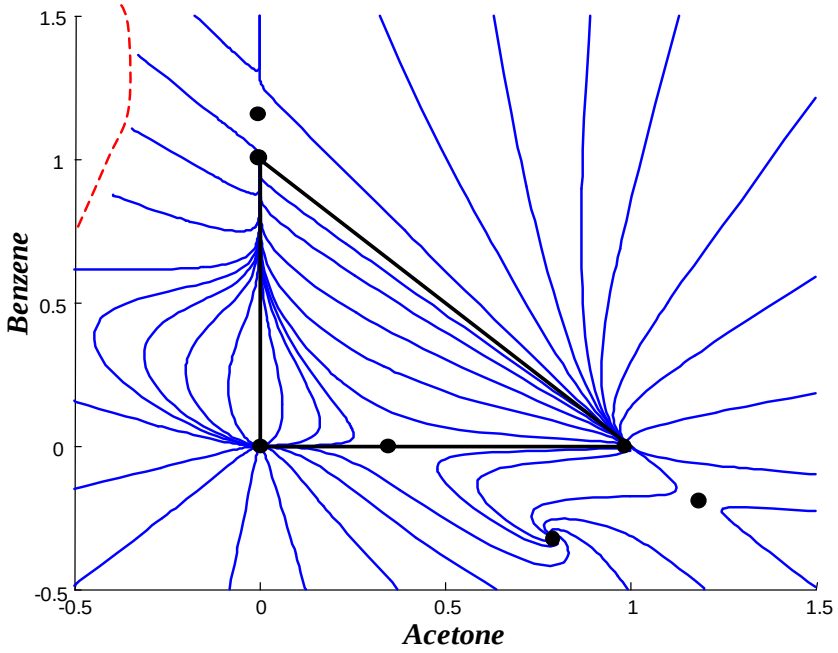


Figure 6.3: Residue curve map for the Acetone/Benzene/Chloroform using the NRTL activity coefficient model in positive and negative composition space showing multiple stationary points.

Interestingly, there is a locus of indeterminate behaviour shown as a dashed red line in Figure 6.3, caused by a denominator in the NRTL function which tends to zero for some values of composition. Even for simple constant volatility models, it is possible for the denominator to tend to zero, which leads to a line of discontinuity. Indeterminacies in the ideal solution model occur only where temperatures tend to negative value of Antoine coefficient C_i. However, C_i is usually in the range of 150–250, and even if a temperature outside the composition space is found that satisfies the indeterminacy condition, it is extreme enough not to have a visible influence within the space of realizable compositions. However, in all equilibrium models, discontinuities never occur in real composition space.

For any equilibrium model to be valid, they have to adhere to the *Gibbs-Duhem* relationship shown in Equation 6.5:

$$\sum_{i=1}^{nc} x_i \frac{d\ln(\gamma_i)}{dx_j} = 0 , \qquad \text{for } j = 1,2,...,nc \tag{6.5}$$

Intuitively, all vapour-liquid equilibrium models obey this relationship in positive composition space, but in order to be sure that is useful, and valid, to analyze negative compositions, the *Gibbs-Duhem* relationship should be maintained for negative composition too. Since γ_i=1 for the ideal and constant relative volatility cases, this condition is always valid for the entire composition spectrum. For the NRTL model, we have found that the residual errors of Equation 6.5 is in the order of 10^{-15} for all compositions, confirming that the non-ideal equilibrium model is also valid for analysis throughout the composition spectrum. The only region where these models fail to abide by the *Gibbs-Duhem* relationship is at the discontinuity locus, as indicated in Figure 6.3. We therefore conclude that extrapolation of column profile maps does not cause inconsistencies in most thermodynamic vapour-liquid equilibrium models, and that the topology of profiles should not be limited to the mass balance triangle to obtain a global computation about a specific separation problem.

6.3 ROBUST AND EFFICIENT PINCH POINT LOCATION

It has been demonstrated that design techniques such as the Rectification Body Method, Column Profile Map, and the Temperature Collocation method all require the exact location of all Pinch Points. Even points that lay outside physically realizable space have to be considered as they determine the path of liquid composition profiles and delineate areas of reachable compositions for the final

design. Next, strategies are discussed for the efficient and rigorous location of all Pinch Points, for the three VLE models discussed in the previous section.

6.3.1 PINCH POINT LOCATION FOR CONSTANT RELATIVE VOLATILITIES

We demonstrate here that Pinch Points for this model which is the simplest of the three phase equilibrium models may be solved with polynomial arithmetic. The derivation will also introduce a unique new parameter providing a thermodynamically insightful basis for the bubble point temperature approach (Zhang and Linninger, 2004). It will be shown that the Bubble Point temperature allows one to solve for the Pinch compositions using a simple polynomial transformation. The derivation of polynomial starts from Equation 6.1 subject to a pinched condition, $d\mathrm{x}/dn = 0$, as shown in Equation 6.6.

$$R_{\Delta,i}x_i - \left(R_{\Delta,i}+1\right)y_i + X_{\Delta.i} = 0 \tag{6.6}$$

Substituting y_i defined in Equation 6.3 for a constant relative volatility system into Equation 6.6 we have

$$R_{\Delta,i}x_i - \left(R_{\Delta,i}+1\right)\frac{\alpha_i x_i}{\sum_{j=1}^{c}\alpha_j x_j} + X_{\Delta,i} = 0 \tag{6.7}$$

Equation 6.7 may be rewritten in terms of x_i such that

$$x_i = \frac{X_{\Delta,i}\sum_{j=1}^{c}\alpha_j x_j}{\left(R_{\Delta,i}+1\right)\alpha_i - R_{\Delta,i}\sum_{j=1}^{c}\alpha_j x_j} \tag{6.8}$$

We now define a new parameter, $\Psi = \sum_{j=1}^{c}\alpha_j x_j$, which can be interpreted as the mixture's vapour pressure, and is thus inversely related to the Bubble Point

temperature (Zhang and Linninger, 2004). This parameter is also related to the classical Underwood Roots, although Underwood never used this method for pinch point location. Replacing Ψ in Equation 6.8 results in an expression for the Pinch Points as shown in Equation 6.9.

$$x_i = \frac{X_{\Delta,i}\Psi}{\left(R_{\Delta,i}+1\right)\alpha_i - R_{\Delta,i}\Psi} \tag{6.9}$$

Using the fact the compositions sum to unity:

$$\sum_{i=1}^{nc} \frac{X_{\Delta,i}\Psi}{\left(R_{\Delta,i}+1\right)\alpha_i - R_{\Delta,i}\Psi} = 1 \tag{6.10}$$

By multiplying the denominator throughout in Equation 6.10, the equation may be transformed into a polynomial function in terms of Ψ, as in Equation 6.11

$$a_{nc}\Psi^{nc} + a_{nc-1}\Psi^{nc-1} + a_{nc-2}\Psi^{nc-2} \ldots + a_2\Psi^2 + a_1\Psi + a_0 = 0 \tag{6.11}$$

The polynomial coefficients a_0 to a_{nc} are completely determined by specifying the generalized reflux ratio R_Δ and X_Δ. The order of this transformed polynomial is equal to the number of components in the system. This scalar equation is a simple, one-dimensional polynomial, regardless of the amount components that are being considered. Once the polynomial roots have been determined, the pinch compositions, x_i, can be calculated from Equation 6.9. Note that Equation 6.10 and 6.11 is a function of Ψ only, and no implicit or iterative procedure is required to solve the roots of Equation 6.11.

The fact that the Difference Point Equation reduces to a polynomial for a constant relative volatility system, makes it entirely possible for the solutions to have imaginary parts. Thus, although for a three component system there are always three

solutions, only one of these may be real as the other two are conjugate complex pairs. Even though two pinch points are complex, the column profile with X^T and Y^T as the entering composition has no odd or unrealistic behaviour. However, complex solutions are only found in systems where the Difference Point lies outside the composition triangle (Tapp et al., 2004). A ternary Column Profile Map with only one real root is shown in Figure 6.4 for constant relative volatilities (α_A=5, α_B=2, α_C=1). The design implications of this result will be discussed in greater detail in the section 6.4.1.

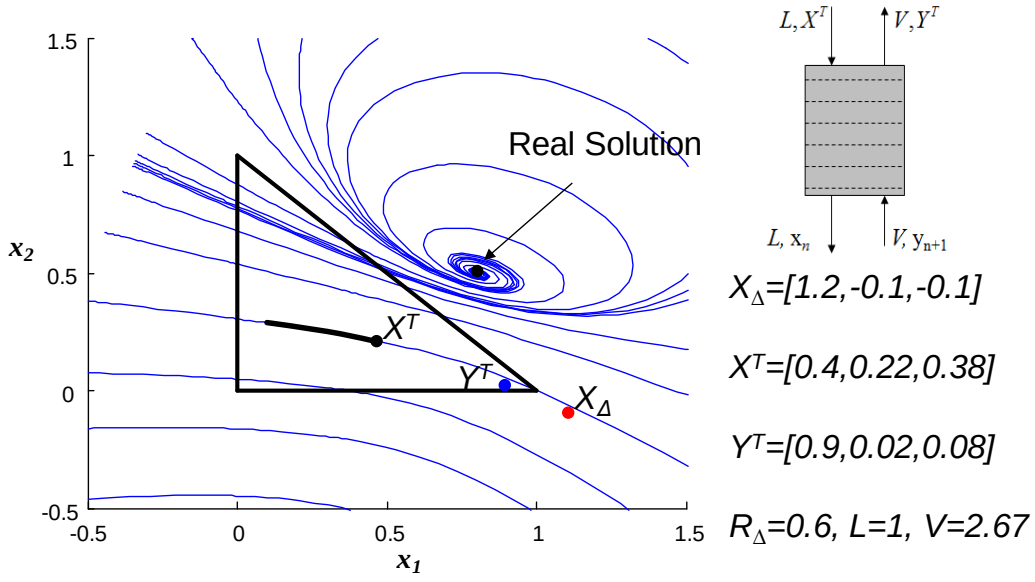


Figure 6.4: A Column Profile Map for a mixture with constant relative volatilities of (α_1=5, α_2=2) showing with only one real solution at a reflux of 0.6 and X_Δ= [1.2, -0.1]. The thick black trajectory indicates a realizable liquid composition profile of a typical Column Section.

It is important to reiterate that the pinch solutions found using the aforementioned parameter transformation are exactly equivalent to those found via the Underwood method (Underwood, 1946a) (the derivation in fact initiates from the same point – Equation 6.6). However, the method shown here may have advantages over Underwood's procedure because:

- The polynomial form of the equation allows for very rapid solution. In fact, software packages like Matlab have tailor-made solution methods for finding polynomial root-finding problems and convergence is obtained very quickly and reliably, even when the order of the polynomial is high.
- Once the polynomial equation has been obtained (Equation 6.11), it is very easy to see when and why roots are complex or equal; as both scenarios may have interesting and counter-intuitive behaviour on topology.

Furthermore, quick and reliable solution of the classic Underwood equation may be difficult at times, as demonstrated by Billingsley (Billingsley, 2002). Billingsley showed an alternate technique that also ensures rapid convergence to a desired root of the pinch equation, much more complex than the one showed here. Although not presented in this thesis, it is thought that these aforementioned polynomial type equations, and the Underwood method, can be used for non-ideal systems. This, however, is likely to be extremely complex since the volatility is a function of both composition and temperature, and thus potentially simpler techniques have been sought.

6.3.2 PINCH POINT LOCATION FOR IDEAL SOLUTIONS

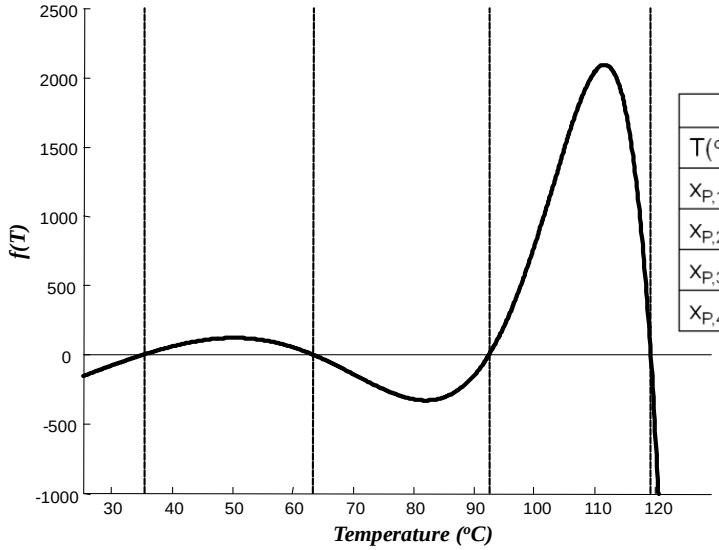
Ideal solutions that adhere to Raoult's law already elevate the complexity for solving the pinch point equations due to the presence of an exponential term in the Antoine equation. Although a single solution may be found with a basic numerical technique such as the Newton method, this firstly requires a good initial guess of both composition and temperature and secondly, even a good initial guess does not guarantee convergence to the specific root that one wishes to find. Again using the Bubble Point temperature will allow reducing the search for all Pinch Points to a single non-linear equation. The Difference Point Equation, for pinched conditions, may be rewritten in terms of the liquid composition, such that:

$$x_i = \frac{X_{\Delta,i}}{(R_\Delta + 1)K_i(T) - R_\Delta} \tag{6.12}$$

where K_i is the equilibrium constant defined as $K_i(T) = \frac{P_{i,sat}}{P}$, and T is the Bubble Point temperature. Again exploiting the fact that compositions sum to unity, the Pinched Difference Point Equation may then be rewritten in the following form for an *nc*-component mixture:

$$f(T) = \sum_{i=1}^{nc} \frac{X_{\Delta,i}}{(R_\Delta + 1)K_i(T) - R_\Delta} - 1 \tag{6.13}$$

Even though this function does not reduce to a polynomial function like in the case of constant volatility system, this single non-linear equation, $f(T)$, is significantly simpler to solve than the original pinched Difference Point Equation system in Equation 6.6 because it only depends on temperature and not composition (since the equilibrium constant K_i is a function of temperature only). Once all roots are obtained in terms of the Bubble Point temperature, the Pinch Point compositions can be found by using Equation 6.13. To better elucidate this scheme, in Figure 6.5 plots Equation 6.13 for a particular case of a quaternary mixture of Pentane/Hexane/Heptane/Octane, for a specific reflux of 5 and a difference point (X_Δ) of [0.9, 0.05, 0.03].



	Pinch 1	Pinch 2	Pinch 3	Pinch 4
T(°C)	35.75	63.38	92.55	119.00
$x_{P,1}$	0.972	0.011	0.007	1.017
$x_{P,2}$	0.005	0.943	-0.010	-0.160
$x_{P,3}$	0.002	0.007	0.897	-0.007
$x_{P,4}$	0.020	0.039	0.106	1.017

Figure 6.5: A one dimensional Pinch Point temperature search showing all pinch temperatures where f(T)=0 for X_{Δ}=[0.9, 0.05, 0.03] and R_{Δ}=5, accompanied by a table showing all pinch temperatures and compositions. The Pinch temperatures indicated on the graph (T1-T4) are the bubble point temperatures of the four pinch points.

Again, the transformation has the distinct advantage that the problem reduces to a simple one-dimensional problem that is only a function of single variable, temperature, regardless of the number of components. However, although the dimensionality of the problem has been reduced, it is still not a trivial matter to locate all the respective roots. The following section aims to address this.

6.3.3 ONE DIMENSIONAL DEFLATION METHOD

Although the one-dimensional equation transformation described in the preceding discussion significantly reduces the numerical complexity of the problem, a numerical technique such as the Newton Method may still not find all desired roots, especially if two roots are located nearby one another. To this end, a novel deflation method is proposed. By starting with an initial guess for temperature greater than the maximum pinched temperature, convergence to the highest pinch temperature is guaranteed. In order to locate all subsequent roots quickly and efficiently without

convergence problems, we modify the original pinched Difference Point Equation, $f(T)$ in Equation 6.13 to create a surrogate function, $g(T)$, preventing the algorithm from converging to a previous root. The surrogate function, $g(T)$, features previously found roots in the denominator, forcing it to near infinity near a previously found root and thus preventing repeated convergence to this specific solution. The sequence of surrogate equations, $g_{nr}(T)$, is given in Equation 6.14.

$$g_{nr}(T) = \frac{f(T)}{\prod_{j=1}^{nr}(T - T_{P,j})} \tag{6.14}$$

Where nr is the number of roots previously found and $T_{P,j}$ is a previously found pinch temperature. This equation may then be solved in a relatively straightforward manner with a simple numerical technique such as the Newton-Method. Moreover, this method guarantees convergence to all roots as Equation 6.14 nears infinity near previously found solutions. An illustration of the systematic elimination of previously found roots is shown in Figure 6.6 (a), (b), and (c).

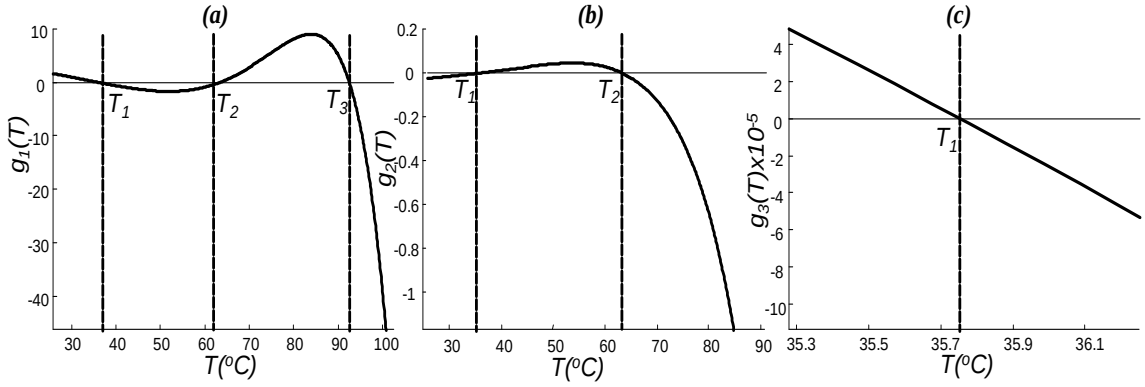


Figure 6.6: (a) Surrogate function $g_1(T)$ vs. Bubble Point temperature where the highest Pinch Point has been eliminated, (b) surrogate function $g_2(T)$ vs. Bubble Point temperature where the two highest Pinch Points have been eliminated, and (c) surrogate function $g_2(T)$ vs. Bubble Point temperature where the three highest Pinch Points have been eliminated

Figure 6.6 (a) shows the surrogate function, $g_1(T)$, versus bubble Point temperature after the highest Bubble Point temperature has been eliminated. All subsequent solutions may then also be obtained by systematically dividing by the product of all previous roots as shown in Figure 6.6 (b) and (c).

6.3.4 PINCH POINT LOCATION FOR NON-IDEAL SOLUTIONS

Preceding sections have shown that, even for simple phase equilibrium models, the Difference Point Equation requires some modification in order to efficiently find all solutions. Due to the fact that temperature and composition are implicitly linked to one another by the activity coefficients, $\gamma_i(x,T)$ a one dimensional equation transformation is not possible. This implicit relationship between temperature and composition may be seen in the NRTL activity coefficient model given in Equations 6.15-17

$$\gamma_i(x,T) = \exp\left[\frac{\sum_j x_j \tau_{ji} G_{ji}}{\sum_k x_k G_{ki}} + \sum_j \frac{x_j G_{ij}}{\sum_k x_k G_{kj}}\left(\tau_{ij} - \frac{\sum_m x_m \tau_{mj} G_{mj}}{\sum_k x_k G_{kj}}\right)\right] \qquad (6.15)$$

$$\tau_{ij} = a_{ij} + b_{ij} / T(^{o}K) \qquad (6.16)$$

$$G_{ij} = \exp(-c_{ij}\tau_{ij}) \qquad (6.17)$$

Other numerical techniques such as Interval and Continuation methods have been applied in an attempt to solve these non-linear equations. The interval method was shown to be a quick and reliable tool for finding all azeotropes in both reactive (Maier et al., 2000) and non-reactive systems (Maier et al., 1998). However, in these earlier works the search for azeotropic points was confined to the mass balance triangle and global pinch point location was not pursued. Although a Newton interval

method may have potential to solve the Pinch Point problem, our trials with an interval toolbox in MATLAB, INTlab (Rump, 2009), were not successful. This is mainly due to the fact that Newton interval method requires the entire interval to be smooth and differentiable, and the multidimensional, highly non-linear nature of the NRTL equation is particularly difficult for current interval computation techniques. Furthermore, even when confining the search interval to differentiable regions, this method may not succeed in finding solutions that are located near one another. Continuation methods, on the other hand, have the drawback that it requires pre-existing knowledge of number and location of stationary points in the entire composition space and can also be time consuming as an entire reflux locus has to be generated for a specified X_{Δ}.

With these limitations in mind, we have tested two new techniques: (i) a multidimensional deflation method, and (ii) a novel hybrid sequential niche algorithm. Both these methods are discussed in the following sections:

6.3.5 MULTI-DIMENSIONAL DEFLATION METHOD

Extending the one-dimensional deflation method discussed in the previous section is a robust and easily implemented method for finding all roots in non-ideal zeotropic mixture. The general equation/procedure for the extension of the deflation method from one dimension to multi-dimension is given in Equation 6.18

$$h_{nr}(x,T)=\frac{\left(\frac{1}{R_{\Delta}}+1\right)\left[\text{x-y(x)}\right]+\left(\frac{1}{R_{\Delta}}\right)(X_{\Delta}-\text{x})}{\sqrt{\sum_{j=1}^{nr}(x-x_{P,j})^2+\sum_{j=1}^{nr}(T-T_{P,j})^2}} \tag{6.18}$$

where *nr* is the number of roots previously found and $T_{P,j}$ and $x_{P,j}$ is a previously found pinch temperature and composition, respectively. Similarly to the one

dimensional version, the surrogate function, $h_i(T)$ will tend to infinity near any previously found root. Notice however that denominator in this case is the residual error of all previous roots. However, without good initial guesses, convergence to specific roots is still not guaranteed. To ensure that all roots can be found reliably, the multivariable deflation method has to be employed in conjunction with good initial guesses obtained from the ideal solution model discussed in the previous section. This approach is very effective in locating all fixed points, even for highly non-ideal zeotropic mixtures, as depicted in Figure 6.7 for the Acetone / Ethanol / Acetic Acid system.

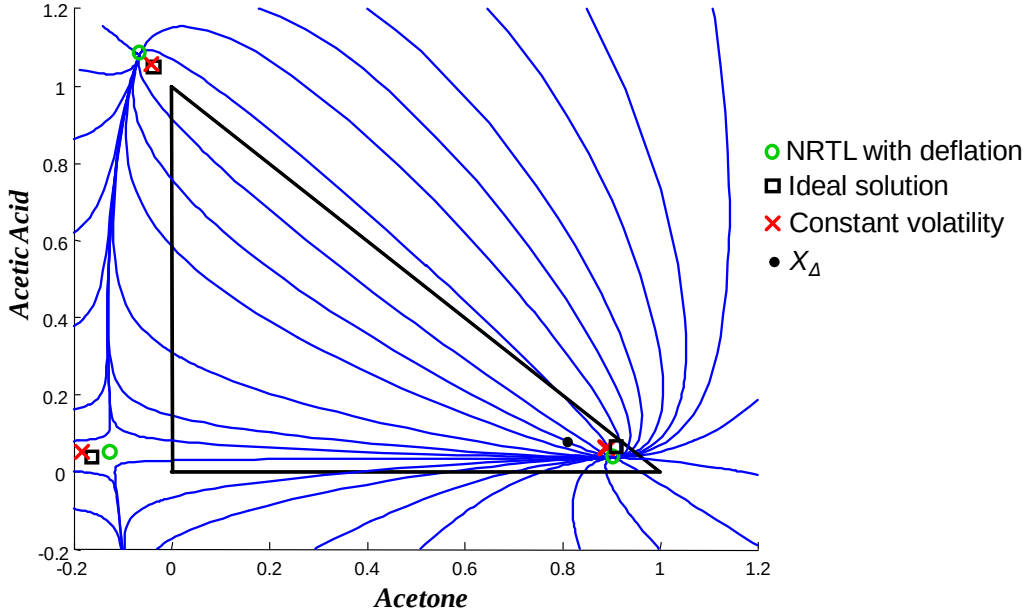


Figure 6.7: Comparison of stationary points using the NRTL model for the Acetone / Ethanol / Acetic Acid system (green circle) with the multivariable deflation method, the ideal solution model (black square), and the constant relative volatility model (red cross), for choices of X_Δ= [0.8, 0.1] and R_Δ=-3

Notice in Figure 6.7 that there is a marked difference in the pinch compositions calculated by different thermodynamic models. This difference is caused by the non-ideal nature of the components, and it is imperative to use a method that robustly solves the pinched solution using the NRTL model for systems that display some non-ideality as this one (notice the curvature between Pinch Points). The only instance where this multivariate deflation method fails to find all Pinch Points is

when the search space is discontinuous, or when the initial guesses for each root are bad. The method's major advantage is that one is assured that convergence won't occur to the same root. Thus, although this method is useful in locating all Pinch Points for zeotropic problems, it is not sufficient for more complex azeotropic problems, as the method requires reasonably good initial guesses to converge to a solution using numerical methods. The next section discusses a method for overcoming these limitations.

6.3.6 HYBRID SEQUENTIAL NICHE ALGORITHM

The use of hybrid algorithms can overcome many of the shortcomings associated with conventional numerical techniques for locating all roots. Specifically, a hybrid sequential niche algorithm developed by Linninger's group has been proposed to solve problems with multiple local minima (Moon and Linninger, 2009). They have demonstrated that this method can locate all minima in difficult global optimization problems found in the open literature, even when they are in close approximation of one another. Because the algorithm does not need derivative information when searching for clusters around a minimum, it can handle non-differentiable spaces.

A brief description of the algorithm follows, a more detailed explanation can be found elsewhere (Moon and Linninger, 2009). The algorithm initiates by performing a global, stochastic search, that converges to regional clusters around extrema points. When derivative information of the cost function is available, *Newton*, *Quasi–Newton* or *simplex* algorithms are deployed, but if the search space is undifferentiable or ill-conditioned, as in areas of discontinuity, the *Nelder–Mead* downhill simplex method is employed. Once a cluster around an area of attraction has been identified, the algorithm switches to a traditional, deterministic local optimizer such as Newton to precisely locate the extreme points in the second stage. The algorithm then returns to a new genetic search stage, where a new population sample is generated randomly. If the precise solution is new, a novel cluster is registered. If the precise solution has

already been identified, the radius of its cluster is enlarged to block an expanding area of attraction. Thus, cluster radii are dynamically adjusted, which ensures locating all solutions even when their distribution is not uniform. This technique requires neither pre-existing knowledge about the search space nor informed initial guesses regarding the number and distribution of solutions. The algorithm terminates after a preset generation or solution count has been reached.

In order to demonstrate the algorithm's applicability and efficiency, two challenging problems are presented here: The Acetone / Methanol / Chloroform system shown in Figure 6.8 and the Isobutene / MTBE / Methanol system shown in Figure 6.9. The exact Pinch coordinates and temperatures are given in Table 6.1 for the Acetone / Methanol / Chloroform and the Isobutene / MTBE / Methanol systems, respectively. Notice that for Acetone / Methanol / Chloroform system that all Pinch temperatures are located within $\pm 10^{o}$C of one another.

Table 6.1: All Pinch compositions and temperatures for both the Acetone / Methanol / Chloroform and the Isobutene / MTBE / Methanol systems.

Residue Curve Map					**Column Profile Map at R_Δ=8 and X_Δ=[0.8, 0.1]**				
	Acetone	Chloroform	Methanol	T (°C)		Acetone	Chloroform	Methanol	T (°C)
P1a	-0.0002	0.6504	0.3498	54.0733	P1b	-0.1424	0.3157	0.8267	52.3508
P2a	0.7756	-0.0012	0.2256	55.3295	P2b	0.7735	0.2602	-0.0336	54.9455
P3a	0.9997	-0.0009	0.0012	56.2607	P3b	0.9908	0.034	-0.0248	55.6163
P4a	0.3277	0.2358	0.4365	57.2933	P4b	0.3845	0.496	0.1195	57.1328
P5a	-0.0002	1.0001	0.0001	61.7216	P5b	-0.1583	0.002	1.1563	59.399
P6a	0.0001	0.0003	0.9997	64.4888	P6b	0.0809	0.9097	0.0093	61.7423
P7a	0.3333	0.6666	0.0001	64.6017	P7b	0.4587	0.0047	0.5366	63.8488
Residue Curve Map					**Column Profile Map at R_Δ=-5 and X_Δ=[0.8, 0.1]**				
	I-butene	MTBE	Methanol	T (°C)		I-butene	MTBE	Methanol	T (°C)
P1a	0.9909	0.0091	0.0000	-6.2870	P1b	0.9442	0.0346	0.0211	-5.7269
P2a	1.0001	-0.0001	0.0000	-6.2585	P2b	1.0019	-0.0237	0.0218	-5.0952
P3a	0.0000	0.3121	0.6880	51.2931	P3b	-0.0179	0.3457	0.6722	56.8094
P4a	0.0000	0.0000	1.0000	55.1463	P4b	-0.0252	-0.0152	1.0404	62.2397
P5a	0.0000	1.0000	0.0000	64.7553	P5b	-0.0029	1.0101	-0.0072	70.0436

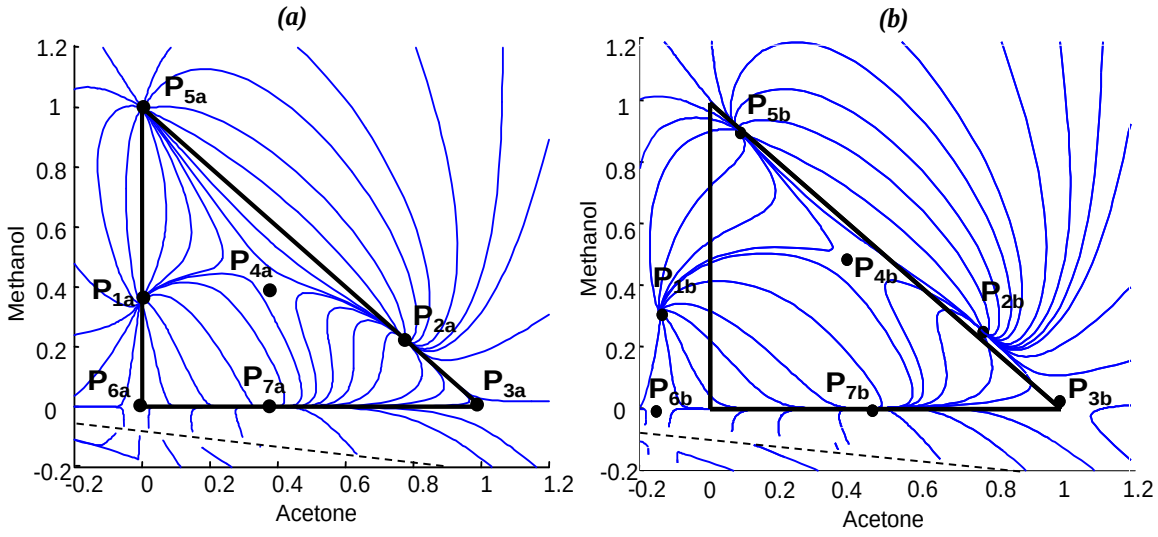


Figure 6.8: Column Profile Maps showing all stationary points for the Acetone/ Methanol/ Chloroform system at (a) infinite reflux and (b) at a finite reflux of R_{Δ}=8 and X_{Δ}=[0.8, 0.1]. Composition profiles are indicated by blue lines, while pinched compositions are given by black dots. Discontinuous regions are represented by a dashed black line.

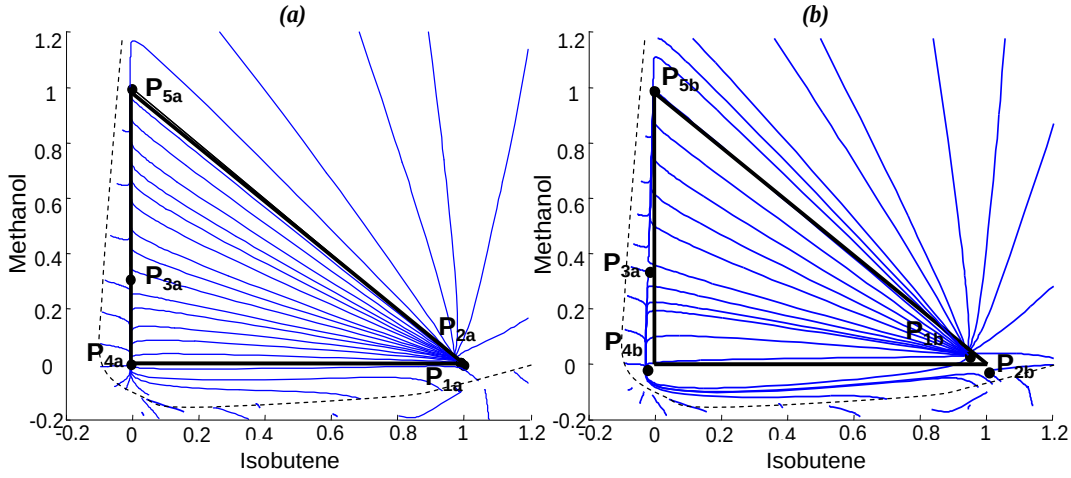


Figure 6.9: Column Profile Maps showing all stationary points for the Isobutene / MTBE / Methanol system at (a) infinite reflux and (b) at a finite reflux of R_{Δ}=-5 and X_{Δ}=[0.8, 0.1]. Composition profiles are indicated by blue lines, while pinched compositions are given by black dots. Discontinuous regions are represented by a dashed black line.

A range of 0.2 was chosen either side of the pure component vertices to search for potential solutions. Notice that the respective Pinch Points correspond very well to composition profiles in both systems. Moreover, there are two Pinch Points in the

Isobutene / MTBE / Methanol system that are extremely close to one another, within 0.03°C. The algorithm successfully identified all pinched compositions in all cases, irrespective of their proximity to one another as well as near un-differentiable regions. These solutions are typically found within a few milliseconds. This efficacy is hard to achieve with traditional numerical techniques, especially for challenging pinch point location in highly non-ideal mixtures as displayed here. The method is especially attractive for searching the entire composition space since it does not fail to find solutions even when the space has discontinuous regions. Various case studies for all the proposed methods are summarized in Table 6.2 at infinite reflux conditions.

Table 6.2: A comparison of various algorithms tested for Pinch Point location

System	Method	Roots identified	CPU time (ms)
Pentane / Hexane / Heptane / Octane (Ideal)	One dimensional Deflation	4/4	177
Benzene/ Xylene /Toluene (Ideal)	Interval method using INTlab	0/3	-
Acetone / Ethanol / Acetic Acid (NRTL)*	Multidimensional Deflation	3/3	1084
Acetone / Ethanol / Acetic Acid (NRTL)	Sequential niche	3/3	35
Acetone / Ethanol / Acetic Acid (NRTL)	Interval method using INTlab	0/3	-
Isobutene / MTBE / Methanol (NRTL)*	Multidimensional Deflation	2/5	11560
Isobutene / MTBE / Methanol (NRTL)	Sequential niche	5/5	78
Acetone/ Methanol/ Chloroform (NRTL)	Sequential niche	7/7	121

*Random initial guesses

Table 6.2 shows that the sequential niche algorithm finds all roots, even for hard azeotropic problems. The computing time is generally very fast when compared to other methods. The computing time shown here is the average of twenty different trials. Although significantly slower than the sequential niche algorithm, the multidimensional deflation method still manages to find all roots for zeotropic problems (Acetone / Ethanol / Acetic Acid). However, the multidimensional

deflation method does not perform as well with azeotropic systems, since one has no knowledge of the approximate location of the roots as in ideal systems. The interval method, using the Matlab toolbox INTlab, fails even for simple problems. The one dimensional deflation works very well for ideal systems, because it is firstly easily implementable and secondly relatively fast.

6.4 DESIGN OBSERVATIONS

The preceding discussions highlight several techniques for solving the Difference Point Equation at pinched conditions. This section discusses design implications that can be derived from knowing Pinch Compositions.

6.4.1 LIMITATIONS OF THE RECTIFICATION BODY METHOD

The Rectification Body Method relies explicitly on the fact that all Pinch Points are known in order to estimate minimum refluxes. However, as may be seen even for the constant relative volatility system, that complex solutions may exist. The immediate consequence of this result is that it is impossible to construct a convex Rectification Body for Column Sections that display these properties, since there is only one real root. Although such Column Sections do not occur in simple distillation configurations (as the Difference Point always lies within the Composition Triangle), several other important column configurations may display this property, such as complex, thermally coupled and reactive columns. It should be noted that even though some pinch points are complex, the composition profiles are still completely valid. Thus, for rigorous and robust design it is imperative to know not only the Pinch compositions, but also the respective composition profiles. A simple example with constant relative volatilities highlighting this fact is shown in Figure 6.10, where a feed is distributed in the column, thus creating an internal Column Section which has

have complex roots. In this specific example, the operating conditions (shown in Figure 6.10) in the internal column section cause its three Pinch Points to be:

$$\text{Pinch Point } 1 = [0.3666 + 0.0375i, 0.2678 - 0.0057i, 0.3655 - 0.0318i]$$
$$\text{Pinch Point } 2 = [0.3666 - 0.0375i, 0.2678 + 0.0057i, 0.3655 + 0.0318i]$$
$$\text{Pinch Point } 3 = [0.0800, 1.0965, -0.1765]$$

Clearly, it is impossible to form a convex rectification body in real composition space with complex Pinch Points. As evidence that this design is in fact realistic, even with complex Pinch Points, an AspenPlus validation of the design in Figure 6.10 is shown in Figure 6.11.

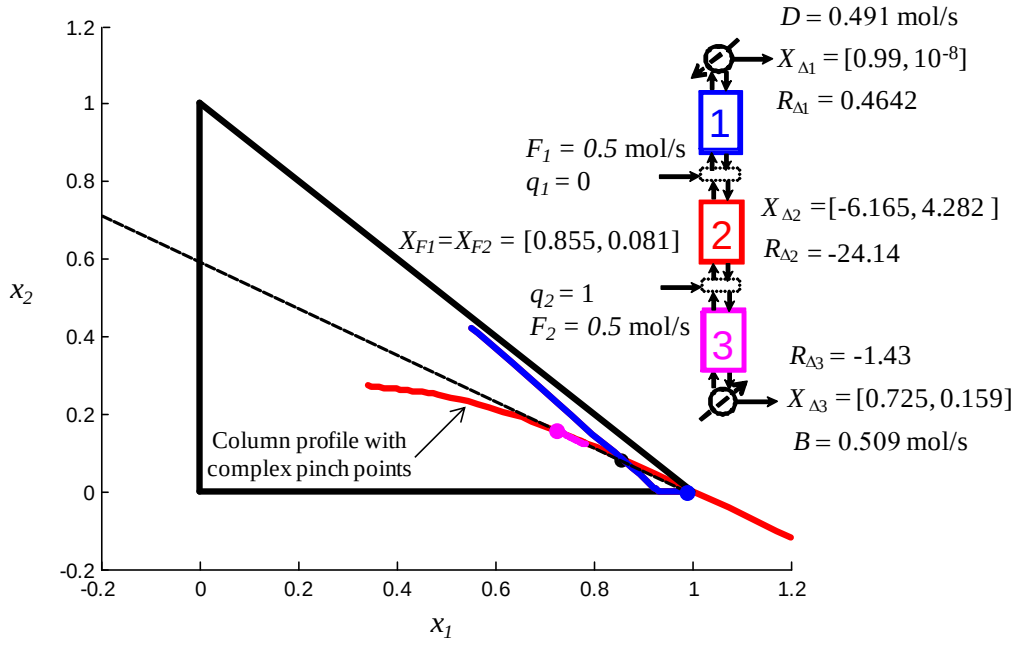


Figure 6.10: An example of a feasible distributed feed column where the internal Column Section has complex Pinch Points. Constant relative volatilities of 5 and 2 have been assumed. All composition profiles intersect one another, indicating a feasible design.

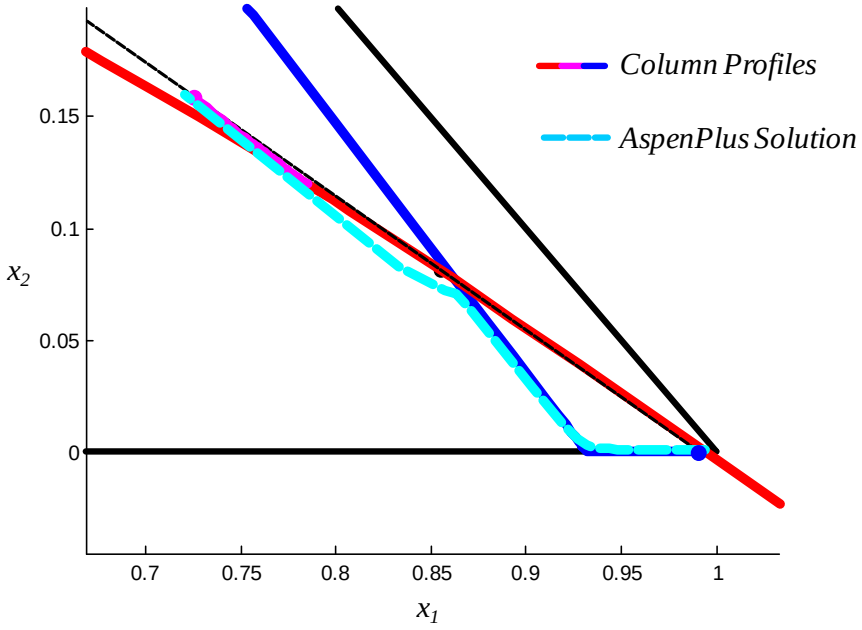


Figure 6.11: A comparison of the design with complex Pinch Points shown in Figure 6.10 and an AspenPlus design

The design in Figure 6.11 was obtained using a column with 20 stages in total and the feed streams located on stage 16 and 17. Furthermore, Benzene, p-Xylene and Toluene were chosen as the three components since their relative volatility behaviour is very close that specified in Figure 6.10. It is clear from Figure 6.11 that the design is in fact realizable. Further motivation for not relying explicitly on pinch compositions, but on the composition profiles too, may be seen in Figure 6.12 (a) and (b) below. These figures show two different, arbitrarily chosen feed and product specifications for the Acetone/ Benzene/ Chloroform system. Figure 6.12 (a) indicates that there is an intersection of composition profiles but not rectification bodies, while Figure 6.12 (b) shows the inverse result, rectification body intersection but not composition profile intersection. The assumption that the faces of the rectification bodies are linear has the consequence that the method fails both as a necessary as well as sufficient condition for design, especially in systems that have significant non-ideal behaviour. Thus, the Rectification Body Method is a useful tool for fast reflux approximations, but the method is neither a necessary nor sufficient

condition for determining column feasibility. It is not rigorous for feasibility screening, especially when the non-ideal behaviour of the system is considerable.

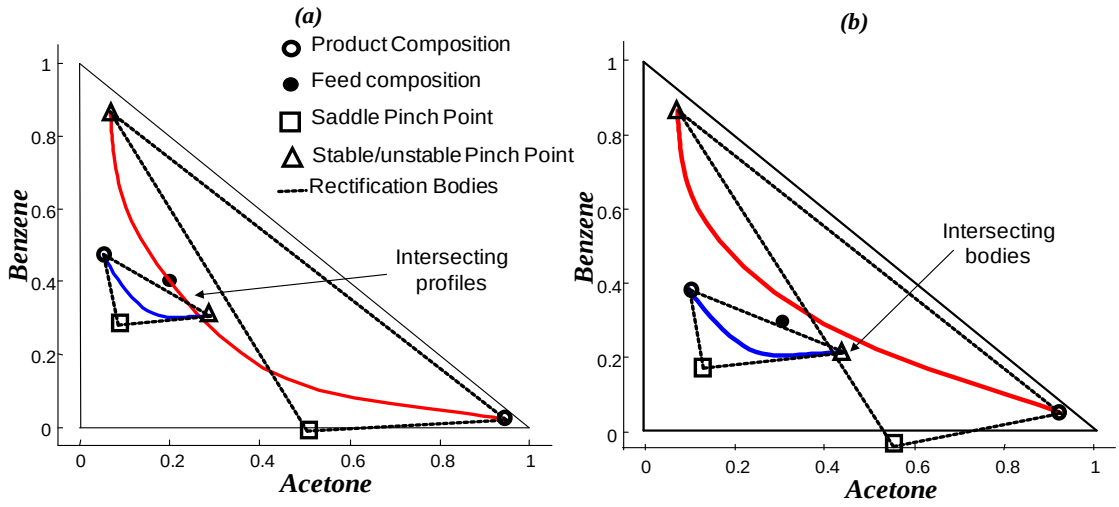


Figure 6.12: Failure of the Rectification Body Method as a rigorous feasibility test: (a) Composition profiles intersect indicating a feasible design, but Rectification Bodies do not touch, (b) Rectification Bodies intersect but composition profiles do not intersect. The design is infeasible despite the positive Rectification Body method indication.

6.4.2 COLUMN SECTION DESIGN THROUGH COLUMN PROFILE MAPS

Although the Column Profile Map method does not explicitly rely on Pinch Point location, finding them are still useful from a design point of view as the designer can quickly scan the Pinch Points which can aid in the understanding of the Maps. Furthermore, Holland et al. showed that Pinch Points be placed at will to affect a certain separation and from this design the process accordingly (Holland et al., 2004b). For instance, one may decide to devise a separation where azeotropic compositions are completely shifted outside the composition space. By specifying the desired Pinch Composition and a reflux value, one may algebraically determine X_{Δ} and construct a Column Profile Map. A particular case of this "inverse" design is shown in Figure 6.13 (a) and (b) for the extremely non-ideal Acetone / Methanol / Chloroform system.

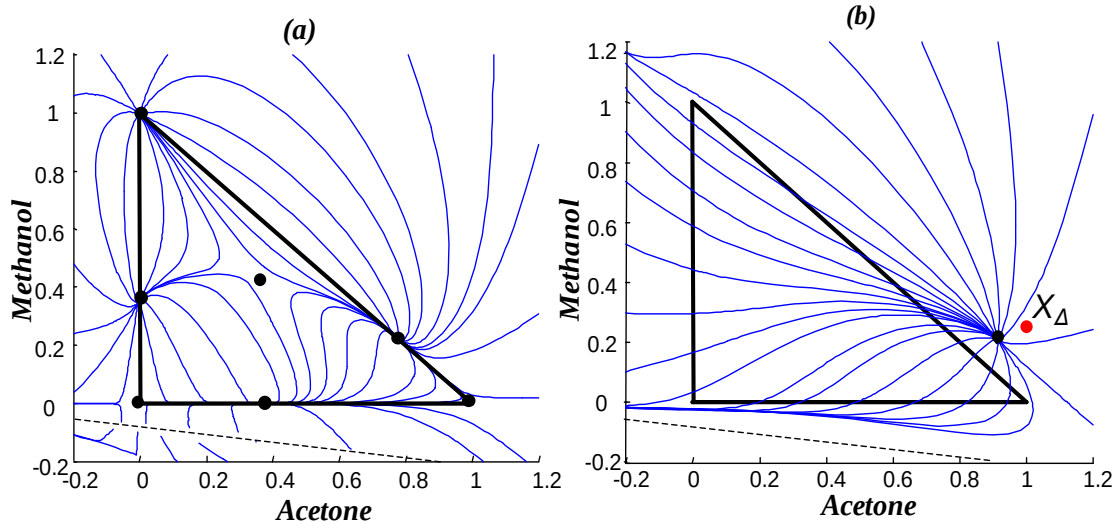


Figure 6.13: The Acetone / Methanol / Chloroform showing (a) a Residue Curve Map with seven Pinch Points inside mass balance triangle, and (b) no Pinch Points inside the mass balance triangle at X_Δ= [1.0, 0.25] and R_Δ=-3

Notice in Figure 6.13 (b) that there are no pinched compositions within the real composition space, even though the Residue Curve Map contains seven. Any desirable separation may be devised to suit the needs of the separation by creatively placing parameters X_Δ and R_Δ. This result is quite noteworthy from a practical point of view, especially if one considers that these large topological transformations are only a result of a combination of mixing through reflux and liquid-vapour phase separation.

6.4.3 RIGOROUS SEPARATION DESIGN USING TEMPERATURE COLLOCATION

The Temperature Collocation approach, originally proposed by Zhang and Linninger (Zhang and Linninger, 2004) for conventional rectifying and stripping sections, is a novel thermodynamic transform whereby the independent integration variable in the Difference Point Equation is changed from the stage number (n) to temperature (T). Recently, they expanded the technique to a generalized form which allowed them to

design entire networks of simple and complex columns (Ruiz, 2009). This variable transformation has the advantage that designs may be rigorously and quickly assessed in an algorithm using a *bubble point distance* (BPD) function. The thermodynamic transform is given by:

$$\frac{dx}{dT} = \frac{-\left\{\left(1+ {}^{1}\!/\!_{R_\Delta}\right)(x-y)+\left({}^{1}\!/\!_{R_\Delta}\right)(X_\Delta - x)\right\}}{\sum_{i=1}^{nc}\left[\left(1+ {}^{1}\!/\!_{R_\Delta}\right)(x-y)+\left({}^{1}\!/\!_{R_\Delta}\right)(X_\Delta - x)\right]K_i}\sum_{i=1}^{nc}\frac{dK_i}{dT}x_i \qquad (6.19)$$

where K_i is the equilibrium constant relating vapour and liquid compositions with each other, defined by $K_i = \frac{\gamma_i P_{i,SAT}}{P}$. Although the Column Profile Map technique is useful in devising new separations, it is not well suited for rigorous feasibility testing in an algorithmic fashion. The Temperature Collocation technique, on the other hand, allows one to determine whether a network of Column Sections will result in a feasible design through searching for profile intersection. Pinch Points are needed in these calculations for three main reasons:

Search space reduction. By merely using the Pinch Point temperatures, designs may be quickly excluded if there does not exist an overlapping temperature window between two Column Sections. If a Temperature overlap is found, one may then proceed to construct profiles.

Rigorous profile computation. To assess whether profiles of two adjacent column sections intersect each other, a polynomial is fitted to the composition profile. However, in order to ensure that the fit is accurate, the profile is divided in to finite elements. In areas of high curvature close to the saddle points, the element division has to be more dense to ensure an accurate polynomial fit.

Profile validation. By exactly knowing the coordinates where profiles initiate, terminate and are attracted to, the composition profiles may be easily validated and affirmed. Furthermore, by precisely specifying the integration boundaries through the Pinch Points, one is assured that profiles will terminate at the exact Pinch Point, and thereby limiting the numerical errors or approximation.

By rigorously computing composition profiles, one does not need to assume that convex rectification bodies intersect in order for a design to be feasible. An example of the application of finding all Pinch Points for the Temperature Collocation method is shown in Figure 6.14 for a simple quaternary column for the Benzene / Toluene / Octane / Nonane system.

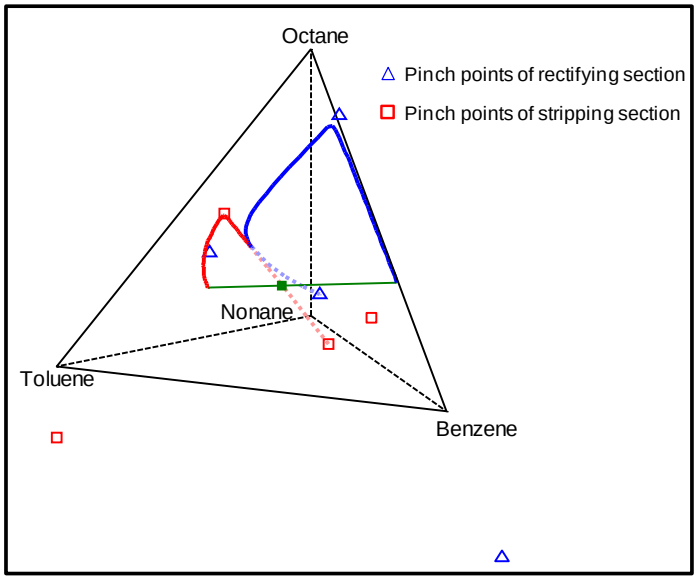


Figure 6.14: Intersecting liquid profiles by fitting a polynomial and finding all Pinch Points. Pinch points are marked for both rectifying (blue triangle), and stripping (red square) column sections. Profiles of rectifying (blue) and stripping (red) intersect, indicating a feasible design.

Figure 6.14 shows profiles generated through the Temperature Collocation method fitted with a piecewise orthogonal polynomial. All Pinch Points are indicated for both rectifying and stripping column sections. Profiles in red and blue indicate rectifying and stripping sections, respectively, while the lighter, dashed profiles show the

continuation of the respective profiles toward Pinch Points. Notice the high profile curvature near the saddle points which require dense element division. The quaternary solution was obtained readily with the help of the Temperature Collocation and pinch point location and may be validated with AspenPlus.

6.5 CONCLUSIONS

This paper presents the significance of Pinch Point location in separation synthesis problem and highlights novel, robust, fast and reliable techniques for calculating Pinch Point compositions for constant relative volatility, ideal and non-ideal systems, as well as illustrating the importance of finding all pinched solutions, even when they are located outside the mass balance triangle. The Bubble Point temperature transformation reduces the Pinch Point location to a simple one-dimensional search in both the constant relative volatility and ideal solution models. In both instances, this allows for a rapid, convenient way of assessing Pinch Points.

Furthermore, a deflation method is presented to systematically and robustly find *all* roots of these one dimensional transformations. It has been described how the deflation method may be extended to a multivariate non-ideal zeotropic problem, where temperature and composition are implicitly linked with one another. For more difficult, azeotropic problems, a hybrid niche algorithm (Moon and Linninger, 2009) is applied which successfully locates all pinch solutions, even for challenging problems with narrow temperature ranges and ill-conditioned search spaces.

Finally, the design applications of finding all pinched compositions are discussed. Three, state of the art design methods requiring Pinch Point calculations, the Rectification Body, Column Profile Map and Temperature Collocation methods have been evaluated. Specifically, the Rectification Body Method relies exclusively on pinched compositions and assumes that these compositions are connected by linear

faces. It was demonstrated that Pinch Points may be complex so that rectification bodies cannot be constructed. Furthermore, when considering non-ideal systems the assumption of linear rectification faces appears to be particularly limited. These assumptions cause the method to be neither a necessary nor sufficient condition to distinguish whether a separation task is realizable or not.

It has been shown how new separations may be devised by wilfully placing Pinch Points in composition space to suit the needs of the separation. Specifically, the Acetone / Chloroform / Methanol that contains seven Pinch Points at infinite reflux may be transformed to not contain any Pinch Points in the positive composition space. Furthermore, it has been shown how knowledge of the Pinch Points may be applied to the Temperature Collocation method to rigorously assess column feasibility. Therefore, the authors advocate the use of continuous composition profile computations in conjunction with rigorous Pinch Point calculations for reliable distillation design.

Chapter 7 : DISCUSSION

7.1 OVERALL THESIS CONCLUSIONS

This thesis has aimed to bring forth mathematical techniques, mostly graphically based, for the synthesis of separation systems. The methods that have been presented are mainly to aid the design engineer to make informed decisions about process feasibility, operability and profitability. Since these techniques have a graphical basis, through the use of Column Profile Maps (CPMs), they lend themselves to be easily interpreted and in gaining and understanding of the fundamental process involved in a separation system.

Furthermore, the thesis has attempted to illustrate that, unlike many other existing design techniques, the CPM design and analysis methodology is not configuration specific. Although the design parameters and selection (and number of degrees of freedom may differ from structure to structure, the design procedure is in essence the same because the generalized definition of the column section fits in with any counter-current vapour-liquid separation device. Many other short-cut design techniques are produced specifically for a particular configuration, which limits their applicability to a great extent. As such, we have demonstrated that it is possible to synthesize counter-intuitive column sections by merely imposing a sharp split constraint on the system, resulting in unique and potentially useful profile behavior. Significant results that stem from this includes:

- It is possible to place any stationary point, i.e. saddle, stable or unstable node, on any pure component vertex causing the direction of profiles to be manipulated at will.

- There exists unique reflux ranges for which these stationary may be placed, and this is conveniently depicted in a novel *Zone-graph*.
- It is thought that these distinctive sharp split profiles have the greatest potential in complex columns which contain internal column sections.

Thermally coupled columns have received increasing attention in the separations community due to the large energy and capital savings they have promised. As with reactive distillation systems, thermally coupled are notoriously hard to design without making constricting assumptions. A key feature of the CPM method is that it is generalized, allowing it to be applied to any conceivable distillation structure. In this thesis, two chapters are presented on the design of thermally coupled columns. The first chapter deals with the generic design of single side rectifiers and side strippers, without making assumptions with regard to the vapour liquid equilibrium or sharp product splits, as is currently the practice with design using the traditional Underwood equations. Perhaps the biggest contribution from this chapter is the fact that side rectifier and stripper column design was performed automatically in an algorithmic fashion using elements of the CPM method as well as the closely related Temperature Collocation method. Significant outcomes from this chapter include, among others:

- A stepwise design algorithm for designing single side rectifying or stripping columns, regardless of the phase equilibrium properties or the product distribution. Additionally, an inverse design methodology is given, which allows the designer to set product targets, and from this determine feasibility as well as rationally determine values for operating variables that generally require significant insight or design experience, such as the overall stage requirement, the feed tray, the side draw tray location, etc. This is in contrast to rigorous simulation packages, which requires the designer to set the aforementioned parameters and “fiddle” until the desired product specifications have been met.

- For a specific choice of feed and product compositions, a spectrum may be obtained that contains all feasible designs.
- Systematic methods are presented to hone in on good design and eliminate bad design decisions based on the overall heat demand, the overall number of stages required and the energy efficiency.
- Feasible designs obtained using the Column Profile Map agree very well with rigorous simulation package such as AspenPlus and generally leads to rapid convergence, thereby saving on valuable engineering time.

The design of thermally coupled columns using the CPM method has been expanded in Chapter 4, which handles multiple side rectifying and stripping units for the special case of constant volatility and sharp product specifications. This study is extremely relevant to the crude refining industry since separation is achieved via a multiple side stripping unit with one main column. The special simplifying case, although idealistic, does present an opportunity for rapid first approximation design using eigenvector theory.

For all possible thermally coupled designs using a main column and thermally coupled sidestream units in a quaternary system, a novel iso-reflux plot shows the exact conditions for the entire column to operate at minimum reflux. This is not a trivial matter using conventional methods, as *all* column sections are linked to one another in such columns. The iso- reflux plot also shows part of an Attainable Region, and interestingly, that a design may still be infeasible even if some column sections operate under residue curve conditions. Furthermore, it has been shown how such complex columns may be systematically analyzed using the CPM method by merely breaking down the column into a series of simple columns using the CPM parameters.

To further demonstrate the versatility of the CPM method, it has also been applied to reactive distillation problems, specifically problems where a rectifying/stripping

section is mounted above/below a reactor unit. Reactive distillation has traditionally been considered a difficult design problem, mainly thanks to the non-linear interaction of reaction, mixing and separation phenomena. However, we have shown that CPM method aids significantly in the interpretation of this phenomena interaction and therefore the design of such integrated units. Furthermore, we have shown with the CPM method that:

- The design of reactive distillation system with a particular set of process chemistry differs greatly from another set.
- There are certain sets of reactions that result in a "reverse" interaction between the number of stages, the reactor size and the reflux ratio, meaning that increasing, for example, the reactor size, may actually lead to the entire process performing much worse. Thus, there exists a unique optimum variable selection for each for each process.
- There exists an Attainable Region for each design problem that conveniently shows the trade-offs between process variables.
- Unlike conventional distillation, non-ideal phase equilibrium behavior is not only useful, it may even be necessary for overall process feasibility.

The final working chapter offers insight into an often neglected part of CPM theory, finding all stationary points in a given system quickly and efficiently. The stationary points are very important because the indicate the extreme operating bounds of columns at stable or unstable nodes, i.e. pinched conditions, as well as areas of high profile curvature at saddle points. It has been shown that for constant volatility systems, the pinched Difference Point Equation simply reduces to a polynomial with the same order as the number of components. This can be done for any number of components, and since polynomials are expressions that are easy to compute, the roots may be easily identified. Similar techniques are given for ideal systems, although some manipulation is required for fast and reliable computation.

Furthermore, a hybrid sequential niche algorithm was tested and proved very efficient for difficult azeotropic problems.

The design implications of robust pinch point calculation was also given. With knowledge of CPM topology and pinch point behavior, we transformed a complex azeotropic system, Acetone Methanol / Chloroform, containing seven stationary points in the mass balance space at residue curve conditions, to not containing any stationary points at finite reflux conditions. This is a powerful demonstration to what CPMs are capable of: *that the designer is able to manipulate column profiles (and pinch points) before being constrained by pre-conceived structures and thereby devise a separation strategy.*

In this thesis, we have thus covered a large body of separation synthesis problems with a single, versatile technique. The problems range from reactive distillation to thermally coupled columns to new column section synthesis.

7.2 FUTURE WORK

In this work, special attention was given mostly to ternary and quaternary systems to exploit the graphical characteristics of the technique. However, a systematic procedure for designing higher order systems is yet to be explored. Although the Temperature Collocation method address this matter mathematically, it is difficult to synthesize new columns without having some graphical insight into the system's phase equilibrium behavior. The use of eigenvector theory as shown in Chapter 4 may prove invaluable in this endeavor. Thus, a certain area of future research is applying Column Profile Maps to higher order systems.

The family of CPM related techniques is rapidly expanding. Reactive Distillation has received considerable attention in this thesis as well as from other members of the

COMPS research group (Mulopo et al., 2008). Other members of the family include Membrane separation processes (Peters et al., 2006, Peters et al., 2008) and the experimental validation of column profiles (Modise et al., 2005, Modise et al., 2007). It is foreseeable that CPM technique may be adapted to encompass other staged equilibrium based separation processes in a similar manner. These may include, but are not limited to: solvent extraction or liquid-liquid equilibrium based separations, leaching processes for solid liquid equilibrium separations, or batch distillation for small-scale separation.

REFERENCES

ABBAS, R. 2010. *Complex distillation design.* Ph.D (Chemical Engineering), University of the Witwatersrand.

ABBAS, R., HOLLAND, S. & HALVORSEN, I. 2010. Novel minimum reflux calculation using eigenvector maps. *In:* HAAN, A. B. D., KOOIJMAN, H. & GÓRA, A. (eds.) *Distillation and Absorption 2010.* Eindhoven, The Netherlands.

AGRAWAL, R. 1996. Synthesis of distillation column configurations for a multicomponent separation. *Industrial & Engineering Chemistry Research,* 35**,** 1059-1071.

AGRAWAL, R. 2000a. A Method to Draw Fully Thermally Coupled Distillation Column Configurations for Multicomponent Distillation. *Chemical Engineering Research and Design,* 78**,** 454-464.

AGRAWAL, R. 2000b. Multieffect distillation for thermally coupled configurations. *AIChE Journal,* 46**,** 2211-2224.

AGRAWAL, R. 2000c. Thermally coupled distillation with reduced number of intercolumn vapor transfers. *AIChE Journal,* 46**,** 2198-2210.

AGRAWAL, R. 2001. Multicomponent distillation columns with partitions and multiple reboilers and condensers. *Industrial & Engineering Chemistry Research,* 40**,** 4258-4266.

AGRAWAL, R. & FIDKOWSKI, Z. T. 1998. Are thermally coupled distillation columns always thermodynamically more efficient for ternary distillations? *Industrial & Engineering Chemistry Research,* 37**,** 3444-3454.

AGRAWAL, R. & FIDKOWSKI, Z. T. 1999. New thermally coupled schemes for ternary distillation. *AIChE Journal,* 45**,** 485-496.

AL-ARFAJ, M. & LUYBEN, W. L. 2000. Comparison of Alternative Control Structures for an Ideal Two-Product Reactive Distillation Column. *Industrial & Engineering Chemistry Research,* 39**,** 3298-3307.

ALBERTO PORRAS-RODRÍGUEZ, J., HERNÁNDEZ-ESCOTO, H., GABRIEL SEGOVIA-HERNÁNDEZ, J. & HERNÁNDEZ, S. 2007. Design and control of thermally coupled and heat integrated distillation sequences for quaternary separations. *In:* VALENTIN, P. & PAUL SERBAN, A. (eds.) *Computer Aided Chemical Engineering.* Elsevier.

ALMEIDA-RIVERA, C. P., J., S. P. L. & GRIEVINK, J. 2004. Designing reactive distillation processes: present and future. *Comp. and Chem. Eng.,* 28**,** 1997–2020.

ALSTAD, V., HALVORSEN, I. J. & SKOGESTAD, S. 2004. Optimal operation of a petlyuk distillation column: Energy savings by over-fractionating. *In:* BARBOSA-PÓVOA, A. & MATOS, H. (eds.) *Computer Aided Chemical Engineering.* Elsevier.

ARISTOVICH, V. Y. S., A. Y.; ARISTOVICH, Y. V.; FULMER, J. W.; KRISHNAN, C.; RAMANI, M. V.; TATAKE, P. 2004. Novel energy saving method of rectification. *Chemical Engineering Communications,* 191**,** 844-859.

BAGAJEWICZ, M. & JI, S. 2000. Rigorous Procedure for the Design of Conventional Atmospheric Crude Fractionation Units. Part I: Targeting. *Industrial & Engineering Chemistry Research,* 40**,** 617-626.

BAGAJEWICZ, M. & SOTO, J. 2000. Rigorous Procedure for the Design of Conventional Atmospheric Crude Fractionation Units. Part II: Heat Exchanger Network. *Industrial & Engineering Chemistry Research,* 40**,** 627-634.

BAGAJEWICZ, M. & SOTO, J. 2003. Rigorous Procedure for the Design of Conventional Atmospheric Crude Fractionation Units. Part III: Trade-off between Complexity and Energy Savings†. *Industrial & Engineering Chemistry Research,* 42**,** 1196-1203.

BAGAJEWICZ, M. J. 1998. ON THE DESIGN FLEXIBILITY OF ATMOSPHERIC CRUDE FRACTIONATION UNITS. *Chemical Engineering Communications,* 166**,** 111 - 136.

BAUSA, J., WATZDORF, R. V. & MARQUARDT, W. 1998. Shortcut methods for nonideal multicomponent distillation: I. Simple columns. *AIChE Journal,* 44**,** 2181-2198.

BERMAN, S., ISBENJIAN, H., SEDOFF, A. & OTHMER, D. F. 1948. Esterification. Continuous production of Dibutyl phthalate in a distillation column. *Industrial and Engineering Chemistry,* 40**,** 2139-2148.

BILLINGSLEY, D. S. 2002. Iterative solution for equations. *Computers & Chemical Engineering,* 26**,** 457-460.

BRÜGGEMANN, S. & MARQUARDT, W. 2004. Rapid screening of design alternatives for nonideal multiproduct distillation processes. *Computers & Chemical Engineering,* 29**,** 165-179.

CARLBERG, N. A. & WESTERBERG, A. W. 1989. Temperature-heat diagrams for complex columns; Underwood's method for side strippers and enrichers. *Ind. Eng. Chem. Res.,* 28**,** 1379-1385.

CHENG, Y.-C. & YU, C.-C. 2005. Effects of feed tray locations to the design of reactive distillation and its implication to control. *Chemical Engineering Science,* 60**,** 4661-4677.

CIRIC, A. R. & GU, D. 1994. Synthesis of non equilibrium reactive distillation processes by MINLP optimization. *AICHE Journa,* 40**,** 1479-1487.

DOE. 2005. *Technical Topic Description* [Online]. Available: www.doe.gov [Accessed].

DOHERTY, M. F. & CALDAROLA, G. A. 1985. Design and Synthesis of Homogeneous Azeotropic Distillations. 3. The Sequencing of Columns for Azeotropic And Extractive Distillations. *Industrial & Engineering Chemistry, Fundamentals,* 24**,** 474-485.

DOHERTY, M. F. & PERKINS, J. D. 1979. On the dynamics of distillation processes--III : The topological structure of ternary residue curve maps. *Chemical Engineering Science,* 34**,** 1401-1414.

EMMRICH, G., GEHRKE, H. & RANKE, U. 2001. The Progressive Extractive Distillation Arrangement for the Morphylane Extractive Distillation Process. *Chemie Ingenieur Technik,* 73**,** 715.

ENGELIEN, H. K. & SKOGESTAD, S. 2005a. Minimum Energy Diagrams for Multieffect Distillation Arrangements. *AIChE Journal,* 51**,** 1714-1725.

ENGELIEN, H. K. & SKOGESTAD, S. 2005b. Multi-effect distillation applied to an industrial case study. *Chemical Engineering and Processing,* 44**,** 819-826.

FIDKOWSKI, Z. & KROLIKOWSKI, L. W. 1987. Minimum energy requirements of thermally coupled distillation systems. *Aiche Journal,* 33**,** 643-653.

FIDKOWSKI, Z. T. & AGRAWAL, R. 2001. Multicomponent thermally coupled systems of distillation columns at minimum reflux. *AIChE Journal,* 47**,** 2713-2724.

FREY, R. M., DOHERTY, M. F., DOUGLAS, J. M. & MALONE, M. F. 1984. Controlling thermally linked distillation columns. *Industrial & Engineering Chemistry Process Design and Development,* 23**,** 483-490.

GIRIDHAR, A., VENKATASUBRAMANIAN, V. & AGRAWAL, R. Year. Formulation of search spaces for separation networks. *In*, 2005 New York, NY 10016-5991, United States. American Institute of Chemical Engineers, 6880.

GLINOS, K. & MALONE, M. F. 1985a. Minimum vapor flows in a distillation column with a sidestream stripper. *Ind. Eng. Chem. Res. Proc. Des,* 24**,** 1087-1090.

GLINOS, K. N. & MALONE, M. F. 1985b. Design of sidestream distillation columns. *Industrial & Engineering Chemistry Process Design and Development,* 24**,** 822-828.

HALVORSEN, I. J. & SKOGESTAD, S. 1997. Optimizing control of Petlyuk distillation: Understanding the steady-state behavior. *Computers & Chemical Engineering,* 21**,** S249-S254.

HALVORSEN, I. J. & SKOGESTAD, S. 2003a. Minimum Energy Consumption in Multicomponent Distillation. 1. Vmin Diagram for a Two-Product Column. *Industrial & Engineering Chemistry Research,* 42**,** 596-604.

HALVORSEN, I. J. & SKOGESTAD, S. 2003b. Minimum Energy Consumption in Multicomponent Distillation. 2. Three-Product Petlyuk Arrangements. *Industrial & Engineering Chemistry Research,* 42**,** 605-615.

HAUAN, S. & LIEN, K. M. 1996. Geometric visualization of reactive fixed points. *Comp. and Chem.Eng.,* 20**,** S133-S138.

HAUAN, S. & LIEN, K. M. 1998. Phenomena based design approach to reactive distillation. *Chemical Engineering Research & Design, Transactions of the Institute of Chemical Engineers, Part A,* 76**,** 396-407.

HAUAN, S., WESTERBERG, A. W. & LIEN, K. M. 2000. Phenomena-based analysis of fixed points in reactive separation systems. *Chem. Eng. Science,* 55**,** 1053-1075.

HERNANDEZ, S. & JIMENEZ, A. 1999. Controllability Analysis of Thermally Coupled Distillation Systems. *Industrial & Engineering Chemistry Research,* 38**,** 3957-3963.

HILDEBRANDT, D. & GLASSER, D. 1990. The attainable region and optimal reactor structures. *Chemical Engineering Science,* 45**,** 2161-2168.

HOLLAND, S. T. 2005. *Column Profile Maps: A tool for the design and analysis of complex distillation columns.* PhD, Univeristy of the Witwatersrand.

HOLLAND, S. T., ABBAS, R., HILDEBRANDT, D. & GLASSER, D. 2010. Complex Column Design by Application of Column Profile Map Techniques: Sharp-Split Petlyuk Column Design. *Industrial & Engineering Chemistry Research,* 49**,** 327-349.

HOLLAND, S. T., TAPP, M., HILDEBRANDT, D. & GLASSER, D. 2004a. Column profile maps. 2. Singular points and phase diagram behaviour in ideal and nonideal systems. *Industrial & Engineering Chemistry Research,* 43**,** 3590-3603.

HOLLAND, S. T., TAPP, M., HILDEBRANDT, D., GLASSER, D. & HAUSBERGER, B. 2004b. Novel separation system design using "moving triangles". *Computers & Chemical Engineering,* 29**,** 181-189.

HUSS, R. S. & WESTERBERG, A. W. 1996. Collocation Methods for Distillation Design. 2. Applications for Distillation. *Industrial & Engineering Chemistry Research,* 35**,** 1611-1623.

JOBSON, M., HILDEBRANDT, D. & GLASSER, D. 1995. Attainable products for the vapour-liquid separation of homogeneous ternary mixtures. *The Chemical Engineering Journal and the Biochemical Engineering Journal,* 59**,** 51-70.

JULKA, V. & DOHERTY, M. F. 1990. Geometric behavior and minimum flows for nonideal multicomponent distillation. *Chemical Engineering Science,* 45**,** 1801-1822.

KAIBEL, G. & SCHOENMAKERS, H. 2002. Process synthesis and design in industrial practice. *In:* JOHAN, G. & JAN VAN, S. (eds.) *Computer Aided Chemical Engineering.* Elsevier.

KAUCHALI, S., MCGREGOR, C. & HILDEBRANDT, D. 2000. Binary distillation re-visited using the attainable region theory. *Computers & Chemical Engineering,* 24**,** 231-237.

KIM, S. B., RUIZ, G. J. & LINNINGER, A. A. 2010a. Rigorous Separation Design. 1. Multicomponent Mixtures, Nonideal Mixtures, and Prefractionating Column Networks. *Industrial & Engineering Chemistry Research*.

KIM, S. B., RUIZ, G. J. & LINNINGER, A. A. 2010b. Rigorous Separation Design. 1. Multicomponent Mixtures, Nonideal Mixtures, and Prefractionating Column Networks. *Industrial & Engineering Chemistry Research,* 49**,** 6499-6513.

KISTER, H. Z. 1992. *Distillation design,* New York, McGraw-Hill.

LEVY, S. G. & DOHERTY, M. F. 1986. Design and Synthesis of Homogeneous Azeotropic Distillations. 4. Minimum Reflux Calculations for Multiple-Feed Columns. *Industrial & Engineering Chemistry, Fundamentals,* 25**,** 269-279.

LEVY, S. G., VAN DONGEN, D. B. & DOHERTY, M. F. 1985. Design and Synthesis of Homogeneous Azeotropic Distillations. 2. Minimum Reflux Calculations for Nonideal and Azeotropic Columns. *Industrial & Engineering Chemistry, Fundamentals,* 24**,** 463-474.

LIEBMANN, K. & DHOLE, V. R. 1995. Integrated crude distillation design. *Computers & Chemical Engineering,* 19**,** 119-124.

LUCIA, A., AMALE, A. & TAYLOR, R. 2006. Energy efficient hybrid separation processes. *Industrial & Engineering Chemistry Research,* 45**,** 8319-8328.

LUCIA, A. & MCCALLUM, B. R. 2009. Energy targeting and minimum energy distillation column sequences. *Computers & Chemical Engineering,* doi:10.1016/j.compchemeng.2009.10.006.

LUCIA, A. & MCCALLUM, B. R. 2010. Energy targeting and minimum energy distillation column sequences. *Computers & Chemical Engineering,* 34**,** 931-942.

MAIER, R. W., BRENNECKE, J. F. & STADTHERR, M. A. 1998. Reliable computation of homogeneous azeotropes. *AIChE Journal,* 44**,** 1745-1755.

MAIER, R. W., BRENNECKE, J. F. & STADTHERR, M. A. 2000. Reliable computation of reactive azeotropes. *Computers & Chemical Engineering,* 24**,** 1851-1858.

MCCABE, W. L. & THIELE, E. W. 1925a. Graphical Design of Fractionating Columns. *Industrial and Engineering Chemistry,* 17**,** 606-611.

MCCABE, W. L. & THIELE, E. W. 1925b. Graphical Design of Fractionating Columns. *Ind. & Eng. Chem.,* 17**,** 606-611.

MIX, T. W. D., J.S.; WEINBERG, M.; ARMSTRONG, R.C. 1981. Energy conservation in distillation.

MODISE, T., HAUSBERGER, B., KAUCHALI, S., GLASSER, D. & HILDEBRANDT, D. 2005. Experimental Simulation of Distillation Column Section Profiles Using a Batch Apparatus. *Ind. Eng. Chem. Res.*, 44**,** 7511-7519.

MODISE, T., KAUCHALI, S., HILDEBRANDT, D. & GLASSER, D. 2007. Experimental Measurement of the Saddle Node Region in a Distillation Column Profile Map by Using a Batch Apparatus. *Chem. Eng. Res. Des.,* 85**,** 24-30.

MOON, J. & LINNINGER, A. A. 2009. A hybrid sequential niche algorithm for optimal engineering design with solution multiplicity. *Computers & Chemical Engineering,* 33**,** 1261-1271.

MULOPO, J. L., HILDEBRANDT, D. & GLASSER, D. 2008. Reactive column profile map topology: continuous distillation column with non-reversible kinetics. *Computers & Chemical Engineering,* 32**,** 622-9.

OGNISTY, T. P. 1995. Analyze distillation columns with thermodynamics. *Chemical Engineering Progress,* 91**,** 40-46.

PETERS, M., KAUCHALI, S., HILDEBRANDT, D. & GLASSER, D. 2006. Derivation and Properties of Membrane Residue Curve Maps. *Industrial & Engineering Chemistry Research,* 45**,** 9080-9087.

PETERS, M., KAUCHALI, S., HILDEBRANDT, D. & GLASSER, D. 2008. Application of Membrane Residue Curve Maps to Batch and Continuous Processes. *Ind. Eng. Chem. Res.,* 47**,** 2361-2376.

PETLYUK, F., B. 2004. *Distillation theory and its application to optimal design of separation unit,* Cambridge, Cambridge University Press.

PETLYUK, F. B., PLATONOV, V. M. & SLAVINSKII, D. M. 1965. Thermodynamically optimal method of separating multicomponent mixtures. *International Chemical Engineering,* 5**,** 555-561.

POELLMANN, P., GLANZ, S. & BLASS, E. 1994. Calculating minimum reflux of nonideal multicomponent distillation using eigenvalue theory. *Computers & Chemical Engineering,* 18**,** S49-S53.

QI, Z., KIENLE, A., STEIN, E., MOHL, K. D., TUCHLENSKI, A. & SUNDMACHER, K. 2004. MTBE decomposition in a reactive distillation column. *Chemical Engineering Research and Design,* 82**,** 185-191.

RUIZ, G., KIM, S., MOON, J., ZHANG, L. & LINNINGER, A. A. 2009. Design and Optimization of Energy Efficient Complex Separation Networks. *Manuscript sumbitted for publication*.

RUIZ, G. J., KIM, S. B., BENEKE, D. A. & LINNINGER, A. A. 2010. Robust Thermodynamically-guided Algorithms for Synthesis of Energy Efficient Separation Networks. *In:* PIERUCCI, S. & FERRARIS, G. B. (eds.) *Computer Aided Chemical Engineering.* Elsevier.

RUIZ, G. J., KIM, S., MOON, J., ZHANG, L., AND LINNINGER, A.A. 2009. Design and Optimization of Energy Efficient Complex Separation Networks. *In:* LINNINGER, A. A., AND EL-HALWAGI, M. (ed.) *7th International Conference on Foundations of Computer-Aided Process Design.* Breckenridge, CO: CRC Press, Taylor and Francis.

RUMP, S. M. 2009. INTLAB. *Institute of Reliable Computing,* http://www.ti3.tu-harburg.de/.

SCHREINEMAKERS, F. A. H. 1902. Einige Bemerkungen ueber Dampfdruecke Ternaerer Gemische. *Z. Phys. Chem,* 43**,** 671-685.

SEADER, J. D. & HENLEY, E. J. 2006a. *Separation process principles,* Hoboken, N.J., Wiley.

SEADER, J. D. & HENLEY, E. J. 2006b. *Separation process principles,* Hoboken, N.J., Wiley.

SEGOVIA-HERNÁNDEZ, J. G., HERNÁNDEZ, S. & JIMÉNEZ, A. 2005. Analysis of dynamic properties of alternative sequences to the Petlyuk column. *Computers & Chemical Engineering,* 29**,** 1389-1399.

SHIRAS, R. N., HANSON, D. N. & GIBSON, C. H. 1950. Calculation of Minimum Reflux in Distillation Columns. *Industrial & Engineering Chemistry,* 42**,** 871-876.

SMITH, J. M., VAN NESS, H. C. & ABBOTT, M. M. 2005. *Introduction to Chemical Engineering Thermodynamics,* Boston, McGraw-Hill.

SOAVE, G. & FELIU, J. A. 2002. Saving energy in distillation towers by feed splitting. *Applied Thermal Engineering,* 22**,** 889-896.

SOREL, E. 1893. La Rectification de L'alcool. *Gauthiers - Villais et fils*.

STICHLMAIR, J. G. & HERGUIJUELA, J.-R. 1992. Separation regions and processes of zeotropic and azeotropic ternary distillation. *AIChE Journal,* 38**,** 1523-1535.

SVANDOVA, Z., KOTORA, M., MARKOS, J. & JELEMENSKY, L. 2006. Dynamic behaviour of a CSTR with reactive distillation. *Chemical Engineering Journal* 119**,** 113-120.

SWARTZ, C. L. E. & STEWART, W. E. 1987. Finite-element steady state simulation of multiphase distillation. *AIChE Journal,* 33**,** 1977-1985.

TAPP, M., HOLLAND, S. T., HILDEBRANDT, D. & GLASSER, D. 2004. Column Profile Maps. 1. Derivation and Interpretation. *Industrial & Engineering Chemistry Research,* 43**,** 364-374.

TAYLOR, R. & KRISHNA, R. 1993. *Multicomponent Mass Transfer,* New York, NY, John Wiley and Sons.

TAYLOR, R. & KRISHNA, R. 2000. Modelling reactive distillation. *Chemical Engineering Science,* 55**,** 5183-5229.

UNDERWOOD, A. J. V. 1945. Fractional distillation of ternary mixtures -- Pt I. *Institute of Petroleum -- Journal,* 31**,** 111-118.

UNDERWOOD, A. J. V. 1946a. Fractional distillation of multi-component mixtures -- Calculation of minimum reflux ratio. *Institute of Petroleum -- Journal,* 32**,** 614-626.

UNDERWOOD, A. J. V. 1946b. Fractional distillation of ternary mixtures -- Pt II. *Institute of Petroleum -- Journal,* 32**,** 598-613.

VAN DONGEN, D. B. & DOHERTY, M. F. 1985a. Design and synthesis of homogeneous azeotropic distillations. 1. Problem formulation for a single column. *Industrial & Engineering Chemistry, Fundamentals,* 24**,** 454-463.

VAN DONGEN, D. B. & DOHERTY, M. F. 1985b. Design and synthesis of homogeneous azeotropic distillations. 1. Problem formulation for a single column. *Industrial & Engineering Chemistry Fundamentals,* 24**,** 454-463.

VENIMADHAVAN, G., BUZAD, G., DOHERTY, M. F. & MALONE, M. F. 1994. Effect of kinetics on residue curve maps for reactive distillation. *AIChE Journal,* 40**,** 1814.

WATKINS, R., N. 1979. *Petroleum Refinery Distillation,* Houston, Gulf Pub. Co.

WOLFF, E. A. & SKOGESTAD, S. 1995. Operation of Integrated Three-Product (Petlyuk) Distillation Columns. *Industrial & Engineering Chemistry Research,* 34**,** 2094-2103.

YI, C. K. & LUYBEN, W. L. 1996a. Design and control of coupled reactor/column systems--Part 1. A binary coupled reactor/rectifier system. *Computers & Chemical Engineering,* 21**,** 25-46.

YI, C. K. & LUYBEN, W. L. 1996b. Design and control of coupled reactor/column systems--Part 2. More complex coupled reactor/column systems. *Computers & Chemical Engineering,* 21**,** 47-67.

YI, C. K. & LUYBEN, W. L. 1996c. Design and control of coupled reactor/column systems--Part 3. A reactor/stripper with two columns and recycle. *Computers & Chemical Engineering,* 21**,** 69-86.

ZHANG, L. & LINNINGER, A. A. 2004. Temperature collocation algorithm for fast and robust distillation design. *Industrial & Engineering Chemistry Research,* 43**,** 3163-3182.

ZHANG, L. & LINNINGER, A. A. 2006a. Towards computer-aided separation synthesis. *AIChE Journal,* 52**,** 1392-1409.

ZHANG, L. & LINNINGER, A. A. 2006b. Towards computer-aided separation synthesis. *AIChE Journal,* 52**,** 1392-1409.

PUBLICATIONS AND PRESENTATIONS

Posters and Presentations:

1. *New Insights In Distillation Design Via Column Profile Maps: Sharp Splits*. Daniel A. Beneke, Diane Hildebrandt and David Glasser. Presented at the AIChE Annual Meeting, 2008, Philadelphia, PA, USA.
2. *Sharp split distillation synthesis via Column Profile Maps.* Daniel A. Beneke, Diane Hildebrandt and David Glasser. Poster presented at the SAIChE Post-graduate conference, 2008, Pretoria, South Africa.
3. *Computer-Aided graphical tools for synthesizing complex columns.* Daniel A. Beneke, Ronald Abbas, Michaela Vrey, Simon Holland, Brendon Hausberger, Diane Hildebrandt and David Glasser. Presented at the Foundations of Computer Aided Process Design (FOCAPD) conference, 2009, Breckenridge, CO, USA.
4. *Robust Thermodynamically-guided Algorithms for Synthesis of Energy Efficient Separation Networks.* Gerardo J. Ruiz, Seon B. Kim, Daniel A. Beneke and Andreas A. Linninger, presented at the European Symposium for Computer Aided Process Engineering (ESCAPE) 20, 2010, Naples, Italy.
5. *A Phenomena-Based Column Profile Map Approach to Designing Coupled Reactors and Column Sections.* Daniel A. Beneke, Diane Hildebrandt and David Glasser. Presented at the AIChE Annual Meeting, 2010, Salt Lake City, UT, USA.

Publications and peer reviewed conference proceedings:

1. *Computer-Aided graphical tools for synthesizing complex columns.* Daniel A. Beneke, Ronald Abbas, Michaela Vrey, Simon Holland, Brendon Hausberger, Diane Hildebrandt and David Glasser. FOCAPD 2009 conference journal: *Design for Energy and the Environment*, 2009.

2. *Robust Thermodynamically-guided Algorithms for Synthesis of Energy Efficient Separation Networks.* Gerardo J. Ruiz, Seon B. Kim, Daniel A. Beneke and Andreas A. Linninger. ESCAPE 20 conference journal, 2009.
3. *Column profile maps as a tool for synthesizing complex column configurations.* Diane Hildebrandt, Daniel A. Beneke, Ronald Abbas, Michaela Vrey, Simon Holland, and David Glasser. Computers and Chemical Engineering Journal, 2009.
4. *Design and analysis of thermally coupled sidestream columns using Column Profile Maps and Temperature Collocation.* Daniel A. Beneke and Andreas A. Linninger. AIChE Journal, 2010
5. *Column Profile Maps: Application to sharp splits in ideal systems.* Daniel A. Beneke, Diane Hildebrandt and David Glasser. Industrial and Engineering Chemistry Research, 2011.
6. *Pinch Point Calculation and its application to robust distillation design.* Daniel A. Beneke, Seon B. Kim and Andreas A. Linninger. Article in press, Chinese Journal of Chemical Engineering, 2011.

APPENDIX A: NODE DERIVATION AND CLASSIFICATION

For the ternary system with components x_1, x_2 and x_3, the following DPE matrix may be written describing the change in liquid composition of each of the tree components as the stage number (n) progresses in a column section:

$$\mathrm{DPE} = \begin{bmatrix} (1/R_\Delta + 1)(x_1 - y_1) + (1/R_\Delta)(X_{\Delta 1} - x_1) \\ (1/R_\Delta + 1)(x_2 - y_2) + (1/R_\Delta)(X_{\Delta 2} - x_2) \\ (1/R_\Delta + 1)(x_3 - y_3) + (1/R_\Delta)(X_{\Delta 3} - x_3) \end{bmatrix} = \begin{bmatrix} dx_1/dn \\ dx_2/dn \\ dx_3/dn \end{bmatrix} = \begin{bmatrix} DPE_1 \\ DPE_2 \\ DPE_3 \end{bmatrix} \quad \text{(A-1)}$$

Note that DPE_3 need not be computed since it may be inferred through the unity summation properties of compositions, i.e. $DPE_3=1-DPE_2-DPE_1$. The system is therefore completely described by DPE_1 and DPE_2. Now, according to Lyapunov's theory for dynamic stability it is required to determine the Jacobian matrix (J) of the DPE matrix above. Thus:

$$J = \begin{bmatrix} \dfrac{\partial DPE_1}{\partial x_1} & \dfrac{\partial DPE_1}{\partial x_2} \\ \dfrac{\partial DPE_2}{\partial x_1} & \dfrac{\partial DPE_2}{\partial x_2} \end{bmatrix} = \begin{bmatrix} J_1 & J_2 \\ J_3 & J_4 \end{bmatrix} \quad \text{(A-2)}$$

It can be shown that J is only a function of R_Δ, x, and the thermodynamics of the system. Assuming the thermodynamic relationship and R_Δ has been specified, and the stationary points (X_S) of the system is known, it is possible to determine the characteristic eigenvalues (λ) of the stationary point X_S by solving for $\det(J-\lambda I)=0$:

$$\det(J - \lambda I) = 0 = (J_1 - \lambda_1)(J_4 - \lambda_2) - J_2 J_3 \quad \text{(A-3)}$$

Where I is the identity matrix. For a ternary system, Equation A-3 is a quadratic polynomial in terms of λ and can be solved for λ_1 and λ_2. The following cases are then possible which characterize the nature of the singularity:

(1) The roots λ_1 and λ_2 are distinct and real:
(a) $\lambda_1 < 0$ and $\lambda 2 < 0$. The singular point is asymptotically stable (stable node).
(b) $\lambda_1 > 0$ and $\lambda_2 > 0$. The singular point is asymptotically unstable (unstable node).
(c) $\lambda_1 < 0$ and $\lambda_2 > 0$. The singular point is asymptotically unstable (saddle point).

(2) The roots of the characteristic equation are complex and in the form:
$\lambda_1 = p + iq$ and $\lambda_2 = p - iq$

(a) $p < 0$ and $q = 0$. The singular point is asymptotically stable (stable focus).
(b) $p > 0$ and $q = 0$. The singular point is asymptotically unstable (unstable focus).
(c) $p = 0$ and $q \neq 0$. The singular point is asymptotically stable (midpoint).

(3) The roots of the characteristic equation are not distinct:
(a) $\lambda_1 = \lambda_2 < 0$. The singular point is an asymptotically stable node.
(b) $\lambda_1 = \lambda_2 > 0$. The singular point is an asymptotically unstable node.

(4) The roots of the characteristic equation have at most one zero eigenvalue:
(a) $\lambda_1 = 0$ and $\lambda_2 < 0$. The singular point is an asymptotically stable half-node/saddle (Doherty).
(b) $\lambda_1 = 0$ and $\lambda_2 > 0$. The singular point is an asymptotically unstable half-node/saddle.

APPENDIX B: THE BUMPING POINTS

From the knowledge that pinch point curves for sharp splits are linear, we could calculate the bumping point by simply knowing what the general equation of the pinch point is.To determine the general equation of a straight line at least 2 points in the x_1-x_1 space are required. The points required here are 2 points of 2 shifted triangles. Note, for sharp splits, 2 corners of the shifted triangle always lie on an axis. The coordinates of these 2 corners are useless for determining the bumping point. The coordinates that are of interest here are the ones that cause the pinch point curve to have a skewed slope.

The procedure for calculating the bumping point is thus to solve for x_1 and x_2 when the DPE=0, for 2 different values for R_Δ which would give the 2 points that are required. Generally, there are 3 solutions for x_1 and x_2 respectively (The 3 coordinates for the shifted triangle's corners), although there are exceptions. However, as mentioned, 2 of these solutions are useless. By identifying the x_1 and x_2 solutions that would give a skewed slope and defining them as point 1: $(x_{2,1}; x_{1,1})$ and point 2: $(x_{2,2}; x_{1,2})$ respectively it follows fairly quickly that the slope of the pinch point curve (m) will be

$$m = \frac{x_{2,1} - x_{2,2}}{x_{1,1} - x_{1,2}} \qquad \text{(B-1)}$$

and the y-intercept *(c)*,can be written as:

$$c = x_{2,1} - x_{1,1}.m \qquad \text{(B-2)}$$

From this knowledge, the general equation for a pinch point curve for sharp splits can be written as:

$$x_2 = \left(\frac{x_{2,1} - x_{2,2}}{x_{1,1} - x_{1,2}} \right) x_1 + \left(x_{2,1} - x_{1,1} . \left(\frac{x_{2,1} - x_{2,2}}{x_{1,1} - x_{1,2}} \right) \right) \qquad \text{(B-3)}$$

Now that the equation has been derived, it can easily be calculated at what points the pinch point curve will intersect the axes. It is important to note that depending on which pure component axis X_Δ is chosen, the bumping point will differ. When X_Δ lies on the x_1 axis, the bumping point occurs on the x_1 axis ($x2$=0); when X_Δ lies on the x_2 axis, the bumping point occurs on the x_2 axis ($x1$=0); and when X_Δ lies on the x_3 axis, the bumping point will occur on the x_3 axis, i.e. where x_2=x$_1$-1. Furthermore one of the axis intersections has to be at 1 or 0, seeing as the pinch point curve always has to pass through the pure component vertices.

Consider now an example where X_Δ is chosen as X_Δ= [0.5, 0]. By solving the DPE=0 for x_1 and x_2 at say R_Δ=5 and R_Δ=3, one would get 2 shifted triangles. By identifying the coordinates that do not lie on an axis, the equation of the skewed pinch point curve can be calculated. In this case, the 2 points are: Point 1: [0.0833 , 0.5833] and Point 2: [0.0500, 0.7500]. It follows directly then that that the equation for this selection of X_Δ is given by:

$$x_2 = -5x_1 + 1 \qquad \text{(B-4)}$$

The example given above is illustrated in Figure B-1. From the derived equation for this system it can easily be calculated where the bumping point will occur. For this case, it occurs at x_1 = 0.2. From Figure B-1 it can also be seen that the pinch point curve does indeed intersect a pure component vertex. By following the algorithm described above, one could determine the bumping points of any sharp split.

Now that the bumping points have been identified, the questions still remain: at what R_Δ value the bumping will occur? and what is happening to the nodes at this point? It would be helpful now to define this unique R_Δ where node bumping occurs as *the*

critical R_Δ. The section that follows will discuss the critical R_Δ value as well as the nature of the nodes at the bumping point.

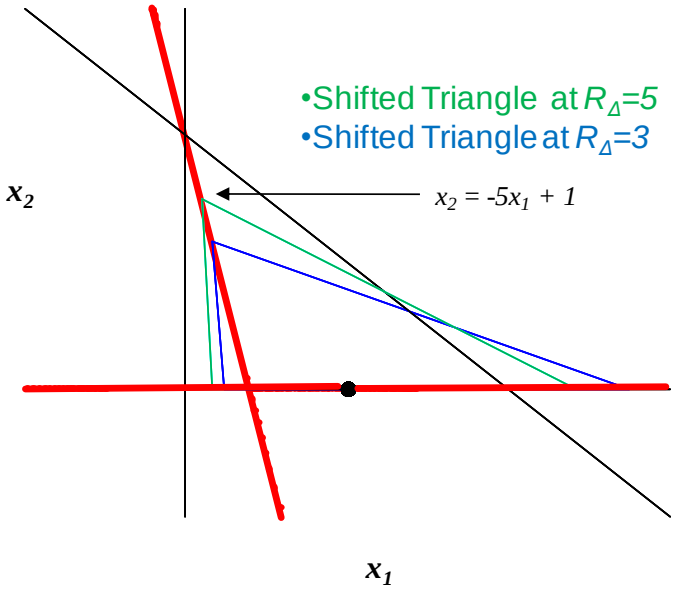


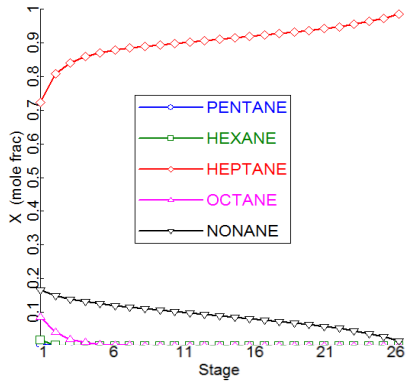
Figure B-1: Pinch point curve calculation with = X_Δ = [0.5, 0]

APPENDIX C: MULTICOMPONENT EXAMPLE

Table C-1: Multicomponent hydrocarbon example with sharp split specifications XΔ=[0,0,1,0,0] where the reflux is such that an intermediate boiling component (Hexane) is removed from as a high boiling component in a single column section (Case A); and where the high boiling component (Nonane) is removed as an high boiling component (Case B)

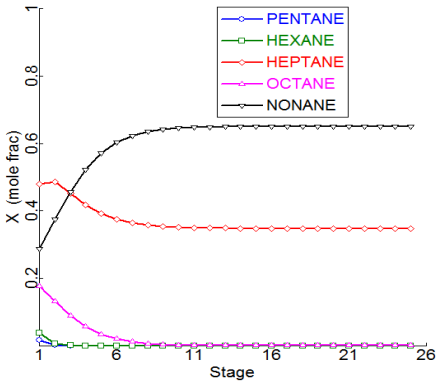
Case A: R_Δ=0.25, X_Δ=[0,0,1,0,0]

	Molar flows	Pentane	Hexane	Heptane	Octane	Nonane
LB	0.990	0.000	0.000	1.000	0.000	0.000
LT	1.000	0.200	0.200	0.200	0.200	0.200
VB	5.000	0.000	0.000	1.000	0.000	0.000
VT	5.010	0.040	0.040	0.840	0.040	0.040
X_Δ	-	0.000	0.000	1.000	0.000	0.000



Case B: R_Δ=1, X_Δ=[0,0,1,0,0]

	Molar flows	Pentane	Hexane	Heptane	Octane	Nonane
LB	0.990	0.000	0.000	0.348	0.001	0.650
LT	1.000	0.200	0.200	0.200	0.200	0.200
VB	2.000	0.001	0.002	0.696	0.001	0.300
VT	2.010	0.100	0.100	0.621	0.100	0.078
X_Δ	-	0.001	0.001	1.038	0.001	-0.043



APPENDIX D: THERMODYNAMIC EFFICIENCIES

Given an arbitrary column with a set of reboilers (*R*) and condensers (*C*) with heat (*Q*) being added and rejected respectively, an energy balance across the column yields equation D-1. For the energy balance we have assumed that heating and mixing effects are negligible (i.e feed and products enter and leave at ambient conditions), and that the latent heats of vaporisation are equal. These assumptions are essentially the constant molar overflow assumptions and hold quite well for ideal mixtures. These assumptions also allows one to relate the heat duties to the vapour flowrates in the respective column sections:

$$\sum Q_R = \sum Q_C, \quad \Rightarrow H_{Vap} \sum V_R = H_{Vap} \sum V_C \tag{D-1}$$

Assuming heat is added to the reboiler at temperature T_R (boiling point of component(s) in the reboiler) and rejected at T_C (boiling point of component(s) in the condenser), we can write an expression for the lost work (*LW*) in the column through the following relationship (again assuming negligible heat effects) (Seader and Henley, 2006a):

$$LW = T_o \Delta S_{irr} = T_o (F \Delta S_{MIX,F} - \Sigma P \Delta S_{MIX,P} + \sum Q_R / T_R - \sum Q_C / T_C)$$

(D-2)

Where *P* denotes a product stream. The entropy of mixing of a particular stream *K* may be calculated through:

$$\Delta S_{MIX,K} = -R \sum x_{Ki} \ln(x_{Ki}) \tag{D-3}$$

Note that for the special case of pure product streams (sharp splits) that ΔS_{MIX}=0. By replacing the heat duty terms with vapour flowrates (D-1) in equation D-2, and assuming sharp splits, equation D-2 becomes:

$$LW = T_o \left(F \Delta S_{MIX,F} + H_{Vap} \left[\sum V_R / T_R - \sum V_C / T_C \right] \right), \tag{D-4}$$

The *LW* function in D-4 is only a function of the vapour flowrates in the respective column sections, the feed composition, and the boiling temperatures. Agrawal showed that, using the Clausius Clayperon relationship (Smith et al., 2005), it is possible to write the boiling temperatures temperatures in terms of the relative volatilities of the mixture (assuming they are constant) (Agrawal and Fidkowski, 1998)

$$\ln(\alpha_{CR}) = \frac{-H_{Vap}}{R}\left(1/T_C - 1/T_R \right) \tag{D-3}$$

Now, the definition of thermodynamic efficiency is as follows (Smith et al., 2005):

$$\eta = \frac{W_{IDEAL}}{W_{IDEAL} + LW} \tag{D-4}$$

Where W_{IDEAL} is the ideal theoretical work required by a process. In terms of sharp split distillation, the ideal work required by a process is merely the Gibbs free energy of mixing in the feed. Thus:

$$W_{IDEAL} = \Delta G_{MIX} = \Delta H_{MIX} - T_0 \Delta S_{MIX} = -T_0 F \Delta S_{MIX,F} \tag{D-5}$$

The thermodynamic efficiency the reduces to:

$$\eta = \frac{T_0 F \Delta S_{MIX,F}}{T_0 F \Delta S_{MIX,F} + LW} \tag{D-6}$$

For each of the structures defined in chapter 4, we can identify the appropriate V_R and V_C streams, and substitute α for the boiling temperatures in each stream using D-3:

Double Side Stripper:
$$\eta = \frac{-F \sum x_{Fi} \ln(x_{Fi})}{(V_3 + V_5 + V_6)\ln(\alpha_1) - V_3 \ln(\alpha_2) + V_5 \ln(\alpha_3)} \tag{D-6}$$

Double Side Rectifier:
$$\eta = \frac{-F \sum x_{Fi} \ln(x_{Fi})}{V_1 \ln(\alpha_3) + V_3 \ln(\alpha_1) + V_5 \ln(\alpha_2)} \tag{D-7}$$

Hybrid Rectifier/Stripper: $$\eta = \frac{-F\sum x_{Fi}\ln(x_{Fi})}{V_1\ln(\alpha_1)+V_5\ln(\alpha_3)-(V_1+V_5-V_6)\ln(\alpha_2)} \qquad \text{(D-8)}$$

Kaibel: $$\eta = \frac{-F\sum x_{Fi}\ln(x_{Fi})}{V_1\ln(\alpha_1)} \qquad \text{(D-9)}$$

Notice that in each of these equations, the R and ΔH_{Vap} have disappeared. Equations D-6 to D-9 give the thermodynamic efficiencies of all structures and are only a function of the relative volatilities, feed composition and vapour flowrates in the relevant column sections. The vapour flowrates may be calculated through the eigenvector criterion elucidated in chapter 4. Chapter 4 elucidates some of the underlying assumption made with these calculations.

APPENDIX E: REFLUX RATIO EQUATIONS

Reflux Ratio equations in terms of defining Column Section for the various configurations

Double Side Stripper

$$R_{\Delta 1} = -\frac{R_{\Delta 6}B + Fq}{\Phi_{L2}\Phi_{L1}D} \Rightarrow \Phi_{L2} = -\frac{R_{\Delta 6}B + Fq}{\Phi_{L1}R_{\Delta 1}D} \quad \textbf{(E-1)}$$

$$R_{\Delta 2} = \frac{R_{\Delta 6}B + Fq}{\Phi_{L2}(F - B - S_2)} \Rightarrow \Phi_{L2} = \frac{R_{\Delta 6}B + Fq}{R_{\Delta 2}(F - B - S_2)} \quad \textbf{(E-2)}$$

$$R_{\Delta 3} = \frac{(1-\Phi_{L1})(R_{\Delta 6}B + Fq)}{\Phi_{L2}\Phi_{L1}S_1} \Rightarrow \Phi_{L2} = \frac{(1-\Phi_{L1})(R_{\Delta 6}B + Fq)}{R_{\Delta 3}\Phi_{L1}S_1} \quad \textbf{(E-3)}$$

$$R_{\Delta 4} = \frac{R_{\Delta 6}B + Fq}{B - F} \Rightarrow \text{Not a funtion of the split ratio} \quad \textbf{(E-4)}$$

$$R_{\Delta 5} = \frac{(1-\Phi_{L2})(R_{\Delta 6}B + Fq)}{\Phi_{L2}S_2} \Rightarrow \Phi_{L2} = \frac{R_{\Delta 6}B + Fq}{R_{\Delta 6}B + Fq + R_{\Delta 5}S_2} \quad \textbf{(E-5)}$$

Double Side Rectifier

$$R_{\Delta 2} = \frac{R_{\Delta 1}D + Fq}{D - F} \Rightarrow \text{Not a funtion of the split ratio} \quad \textbf{(E-6)}$$

$$R_{\Delta 3} = \frac{\dfrac{(1-\Phi_{V1})(D(1+R_{\Delta 1}) - F(1-q))}{\Phi_{V1}} - S_1}{S_1}$$

$$\Rightarrow \Phi_{V1} = \frac{D(1+R_{\Delta 1}) - F(1-q)}{D(1+R_{\Delta 1}) - F(1-q) + S_1(1+R_{\Delta 3})} \quad \textbf{(E-7)}$$

$$R_{\Delta 5} = \frac{\frac{(1-\Phi_{V2})(D(1+R_{\Delta 1})-F(1-q))}{\Phi_{V1}\Phi_{V2}} - S_2}{S_2}$$

$$\Rightarrow \Phi_{V1} = \frac{(1-\Phi_{V2})D(1+R_{\Delta 1}) + (1+\Phi_{V2})F(1-q)}{\Phi_{V2}(1+R_{\Delta 5})S_2} \quad \textbf{(E-8)}$$

$$R_{\Delta 6} = \frac{\frac{D(1+R_{\Delta 1})-F(1-q)}{\Phi_{V1}\Phi_{V2}} + B}{B} \Rightarrow \Phi_{V1} = -\frac{D(1+R_{\Delta 1})-F(1-q)}{\Phi_{V2}(1+R_{\Delta 1})B} \quad \textbf{(E-9)}$$

Hybrid Side Stripper and Rectifier

$$R_{\Delta 2} = \frac{\Phi_L R_{\Delta 1} D}{D(1+R_{\Delta 1}) - (1-\Phi_L)R_{\Delta 1}D + S_1 - \Phi_L R_{\Delta 1} D} \Rightarrow \Phi_L = \frac{R_{\Delta 2}(D+S_1)}{R_{\Delta 1}D} \quad \textbf{(E-10)}$$

$$R_{\Delta 3} = \frac{(\Phi_L - 1)R_{\Delta 1}D}{S_1} \Rightarrow \Phi_L = \frac{R_{\Delta 1}D + R_{\Delta 3}S_1}{R_{\Delta 1}D} \quad \textbf{(E-11)}$$

$$R_{\Delta 4} = \frac{\Phi_L R_{\Delta 1} D + Fq}{D + S_1 - F} \Rightarrow \Phi_L = \frac{(D+S_1-F)R_{\Delta 4} - Fq}{R_{\Delta 1}D} \quad \textbf{(E12)}$$

-

$$R_{\Delta 5} = \frac{\frac{(1-\Phi_L)(D+S_1-\Phi_L R_{\Delta 1}A - F(1-q))}{\Phi_V} - S_2}{S_2}$$

$$\Rightarrow \Phi_L = \frac{-(D+S_1-F(1-q))(1+\Phi_V) + \Phi_V S_2(1+R_{\Delta 5})}{(1-\Phi_V)R_{\Delta 5}D} \quad \textbf{(E-13)}$$

$$R_{\Delta 6} = \frac{\frac{D+S_1-F(1-q)+\Phi_L R_{\Delta 1}D}{\Phi_V} + B}{B}$$

$$\Rightarrow \Phi_L = -\frac{D+S_1-F(1-q)+\Phi_V(1+R_{\Delta 6})B}{R_{\Delta 1}D} \quad \textbf{(E-14)}$$

APPENDIX F: FOCAPD 2009 SUMMARY PAPER

COMPUTER-AIDED GRAPHICAL TOOLS FOR SYNTHESIZING COMPLEX COLUMNS

Daniel A. Beneke, Ronald Abbas, Michaela Vrey, Simon Holland, Brendon Hausberger, Diane Hildebrandt and David Glasser

Centre of Material and Process Synthesis (COMPS), University of the Witwatersrand, Johannesburg, South Africa

Abstract

There has recently been a renewed interest in the design of distillation processes due to the development of Column Profile Maps (CPMs). Using CPMs one is able to change topology within the composition space and hence many separations that have been thought of as difficult or unviable, can now be achieved. The CPM technique has also been proven to be extremely useful as a design tool as any column configuration, irrespective of complexity, can be modelled and graphically understood. This paper aims to summarize the most important and interesting results and applications obtained using the CPM technique. It shows how CPMs may be used to synthesize complex columns like a Petlyuk or Kaibel column, as well as showing how new sharp split separations can be devised.

Keywords

Column Profile Maps, Distillation design, Sharp splits

INTRODUCTION

In modern chemical industries, the task of separation is a very energy consuming process, where distillation is used for about 95% of liquid separations. The energy usage from this process accounts for around 3% of the world energy consumption, as estimated by Hewitt et al. (1999).

Graphical methods for designing distillation schemes have been popular over the years. Residue Curve Maps (RCMs) are often used as a graphical method for designing multi component distillation systems. RCMs are basically a range of trajectories that track the liquid compositions of the chemical species over time in a simple distillation operation. RCMs can tell one much about the feasibility of separation and the nature of singular points, such as azeotropes and pure component vertices.

However, the RCM technique has its limitations in that it only gives information at infinite reflux, quite an impractical condition for the design engineer. Recently, in a series of papers by Tapp et al. (2004) and Holland et al. (2004 a, b) a new theory was explored in distillation: Column Profile Maps (CPMs). CPMs were derived from an adaption of ODEs proposed by Van Dongen and Doherty (1985), which take into account the net molar flows and reflux ratios in a column section. CPMs were shown to display the same topological behaviour as RCMs, as well as being an extremely useful tool in distillation design by allowing the designer to set reflux ratios and net molar flows to suit the specifications of the separation.

* Corresponding author email: diane.hildebrandt@wits.ac.za

COLUMN PROFILE MAPS

A CPM describes the behaviour of a multicomponent system by setting appropriate parameters such as the net molar flow and the reflux ratio. The first step in constructing a CPM is to define a Column Section, which according to the definition of Tapp et al. (2004) is "a length of column between points of addition or removal of material and/or energy". A steady state material balance over a Column Section accompanied with a Taylor expansion yields:

$$\frac{dX}{dn} = \left(\frac{1}{R_\Delta} + 1\right)\left(X - Y(X)\right) + \left(\frac{1}{R_\Delta}\right)\left(X_\Delta - X\right) \quad (1)$$

Where $X_\Delta = \left(\frac{VY^T - LX^T}{V - L}\right)$ and $R_\Delta = \frac{L}{V - L} = L/\Delta$

Equation (1) is known as the Difference Point Equation (DPE). X_Δ can be thought of as a pseudo composition vector and is valid anywhere in the composition space, even in the space outside the Mass Balance Triangle (MBT). It is however subject to the constraint that the sum of the components of X_Δ be 1. X_Δ need only be a real composition in columns sections that are terminated by a condenser or reboiler. Notice that the DPE is not bound by physically relevant initial conditions, thus one is able to perform the integration outside of the composition space. Furthermore, notice that the DPE reduces to the Residue Curve Equation at infinite reflux. Thus, for an arbitrary choice of X_Δ and R_Δ one can now begin to construct a CPM for an ideal system*, as in Figure 1.

* *In this paper, an ideal system refers to the assumption of constant relative volatilities. Unless it is otherwise stated,* $\alpha_1 = 3$, $\alpha_2 = 1$, *and* $\alpha_3 = 1.5$, *which means that* x_1 *is the low boiler,* x_3 *is the intermediate boiler and* x_2 *is the high boiler.*

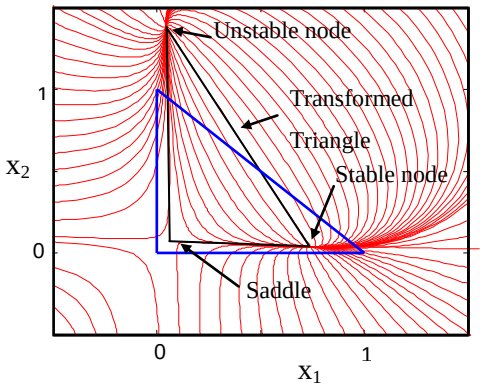


Figure 1: CPM for X_Δ = [0.3, -0.2] and R_Δ = 9

Notice in Figure 1 how stationary points (nodes) have been shifted in the composition space, resulting in completely different profiles within the blue Mass Balance Triangle (MBT). These stationary points can be determined by algebraically solving the DPE=0. If we connect these shifted nodes with straight lines we can see a Transformed Triangle (TT) being formed. In theory, one can now move these nodes in composition space by simply fixing the aforementioned parameters. This could lead to many new and exciting designs that have been previously thought to be unviable.

APPLICATIONS

Petlyuk design

Using the CPM design methodology, one is able to break down any column configuration into simpler Column Sections, and from there design the entire column according to the separation specifications. The famed Petlyuk Column, which offers significant savings in energy, can also be broken down into Column Sections (CS) as shown in Figure 2. For simplicity, we shall look at

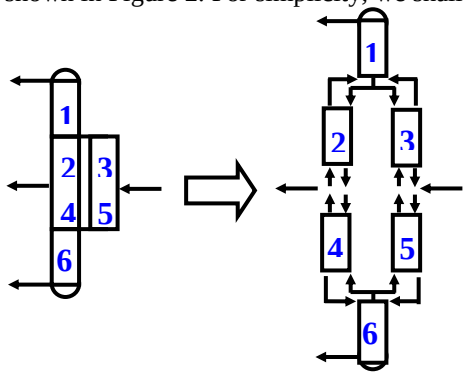


Figure 2: Column section breakdown for the Petlyuk column

a the case where the Petlyuk operates at overall infinite reflux, but with CS 2-5 operating at a finite reflux, i.e. a column that draws infinitesimal product flows, but does not necessarily operate with L=V in sections 2, 3, 4 and 5. For this example, we shall set an intermediate product specification of 90% and achieving this specification will be the primary concern when deciding on a X_Δ. CS 1-6 will simply operate on Residue Curves.

It can be shown mathematically that the constraints placed on this system leads to:

- CS 2 and 4 have identical TTs
- CS 3 and 5 have identical TTs
- CS 2 and 4 and CS 3 and 5 operate on the same Difference Point, with equal magnitude but opposite signs for R_Δ.

The criteria for feasible column profiles is that the liquid profiles intersect twice. If one then superimposes the 2 CPMS for the coupled sections, for an appropriate selection of X_Δ and R_Δ, it can be seen that the feasible region intersects with the product specification. Hence a feasible design has been found, as shown in Figure 3.

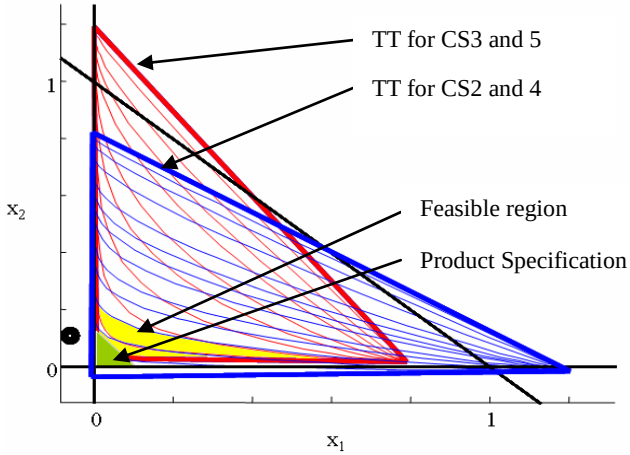


Figure 3: Superimposed transformed triangles for coupled column system

Modelling Sharp Splits with CPMs

Invariably, the aim of any separation process is to achieve essentially pure products. Thus the sharp split constraint presents an interesting and relevant case study.

Tapp et al (2004) have shown that there are 7 regions of X_Δ placement which result in unique Pinch Point curves (see Figure 4). The boundaries of these regions correspond to the extended axes of the MBT. In terms of CPMs, a sharp split effectively means that X_Δ is placed on the boundary of these regions. A sharp split thus displays Pinch Point Curve behaviour of 2 regions.

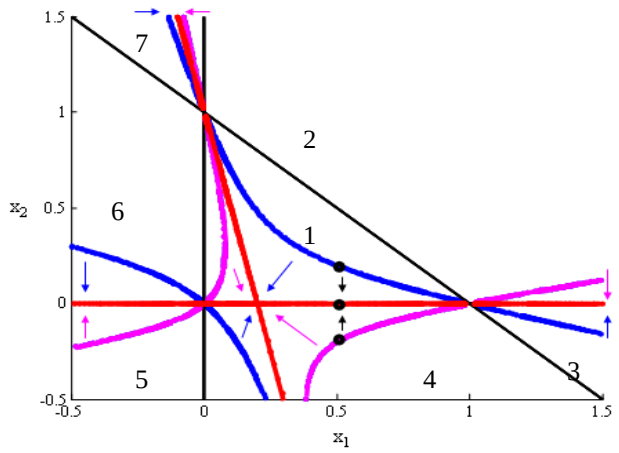


Figure 4: Pinch Point Curve Behaviour for different placement of X_Δ.

It is interesting to note that the nodes for sharp splits are shifted in composition space in a different manner to non-sharp splits. Pinch point curves for sharp splits are linear, and appear to intersect at a point. In fact, the curves don't intersect, but merely meet at a point. The point at which this occurs is termed the "bumping point", because at this point nodes "bump" each other from their positions. For example, a saddle could be bumped from its position and be replaced by a stable node and thereby altering the topology within the MBT drastically. This result is very useful, as one could now theoretically place a node almost anywhere in composition space to suit the separation by simply choosing R_Δ and X_Δ appropriately.

An immediate application of this is fixing X_Δ to the intermediate boiler vertex. By making use of the "node bumping" phenomenon, it is now possible to fix a stable node or an unstable node to the intermediate boiling vertex, as shown in Figure 5. This result suggests that the intermediate boiler can be completely removed in a single stripping section, and hence making the removal of the intermediate boiler significantly easier. Similarly, there are certain choices for R_Δ and X_Δ which can fix a saddle to the high or low boiler vertex, and hence making separation much more difficult for these components.

It is of special interest to determine when and how a certain node can be fixed in composition space. For the special case where X_Δ is placed on one of the 3 pure component vertices, a node is also fixed to the same vertex. So, by knowing the position of a stationary point and X_Δ, we can trace the nature of the node by varying R_Δ. For example, Figure 6 shows which values of R_Δ correspond to a specific node on the intermediate boiler vertex. The nature of the nodes are defined by the eigenvalues of the Jacobian when the DPE=0.

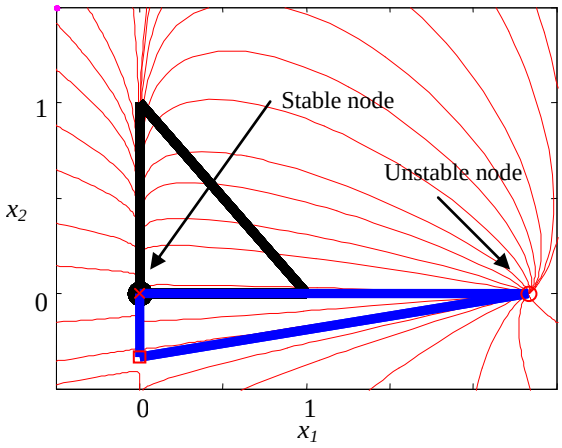


Figure 5 : A stable node fixed on the intermediate boiler

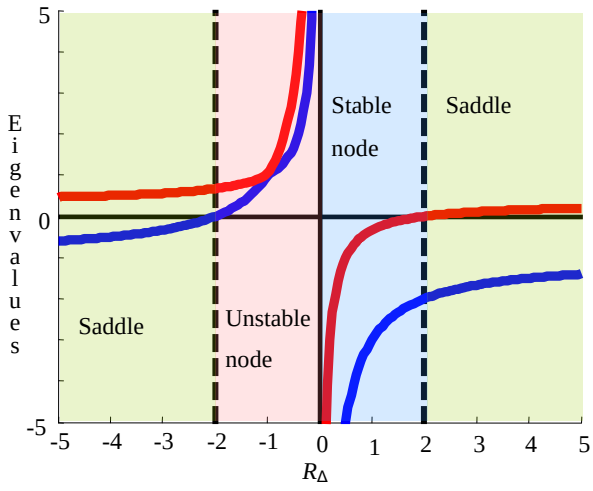


Figure 6: Operating regions for X_Δ=[0;0;1] Sharp split Kaibel column design

This work considers the implementation of a Kaibel column, (i.e. a fully-thermally coupled column with an adiabatic wall dividing the column into two equal halves for the production of four product streams). The Kaibel Column allows for a feed mixture of four or more components from which it produces a distillate, bottoms and two product side streams. Compared to the conventional 3 column direct split sequence, the Kaibel column can be built in a single shell, making it an

attractive alternative in terms of capital cost savings along with its counterpart; the Petlyuk Column. Further, the reduction in the number of reboilers and condensers' required leads to improved operating costs.

In this section of work we demonstrate the use of CPMs for the comprehensive analysis and design of Kaibel columns by applying the CPM technique for a system at sharp-split conditions. From the results of the topological analysis, it is shown that, for set product composition specifications, when using an ideal system (constant relative volatilities), there is only one set of feasible operating parameters.

The Kaibel Column Section breakdown is similar to the Petlyuk in Figure 2 but with an additional CS between CS 2 and 4, as two products are removed between these CSs. It can be shown that for the Kaibel column, CS 2 and 4's X_{Δ}'s are placed on the intermediates pure components. A mass balance shows that the net flow through the connecting CS of the side draws is zero. As a result, this mass balance can only be satisfied completely if the difference point for component 2 (B) in this same CS ($X_{\Delta 7,2}$) is infinitely big. Due to the fact that this CS has a net zero flow, does not mean that the profile produced will be a residue curve, but by substituting zero net flow into the DPE the differential becomes an infinite reflux expression. Figure is the only correct CS mass balance layout in the quaternary system mass balance space. As can be seen from Figure 7 only one solution is possible as this is the only feasible mass balance that exists.

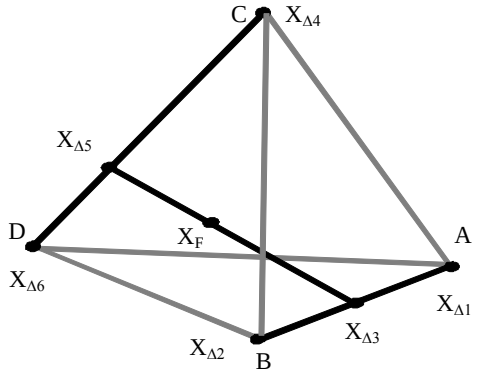


Figure 7: Mass balance lines between intersecting CSs

We can represent the results on a phi space diagram as shown by Figure 8. The single zero net flow line for CS 7 of the Kaibel arrangement is the only operating line that will produce feasible results for a double shell-single reboiler system (Red line). If we shift over to a Kaibel Dividing Wall Column (DWC) we operate at a single point (black dot in Figure 8), as one cannot throttle the vapour split at the bottom of the column. This shows that there is no movement allowed to change the system by changing the liquid and vapour splits. As can be seen from Figure 8, the Petlyuk feasible region in the Phi space is much larger and thus much more operable than the single operating line for the Kaibel.

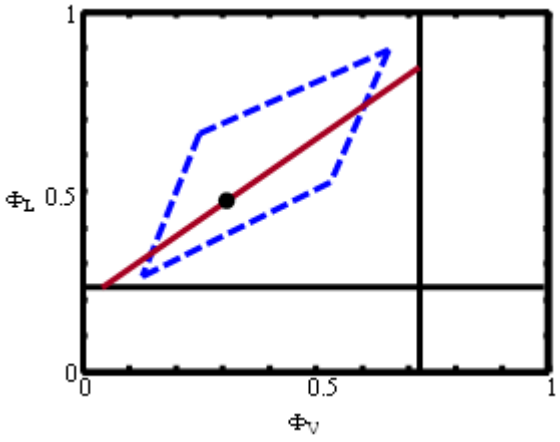


Figure 8: Phi space diagram for the Petlyuk and Kaibel

CONCLUSION

In this paper it has been shown that CPMs have tremendous potential in designing and understanding simple and complex distillation systems. Nodes can almost be placed at will in composition space to suit the requirements of the separation, so much so that it is possible to place stable or unstable nodes on the intermediate boiler's vertex. The CPM technique offers a better understanding of the interaction between parameters due to its graphical nature. Furthermore, it has been shown that CPMs are extremely useful in designing complex distillation systems such as the Petlyuk or Kaibel column, and hence more efficient and creative designs can be thought of.

REFERENCES

Hewitt G, Quarini J, Morell M. More efficient distillation. *Chem Eng*. 1999;Oct. 21

Holland, S.T., Tapp, M.; Hildebrandt, D. and Glasser, D, Column Profile Maps. 2. Singular Points and Phase Diagram Behavior in Ideal and Nonideal Systems, *Ind. Eng. Chem. Res.*,43(14), p3590-3603, (2004 a).

Holland, S.T., Tapp, M.; Hildebrandt, D. and Glasser, D. and Hausberger, B., Novel Separation System Design Using "Moving Triangles", *Comp. and Chem. Eng.*,29, p181-189, (2004 b).

Tapp, M., Holland, S.T.; Hildebrandt, D., and Glasser, D., Column Profile Maps. 1. Derivation and Interpretation, *Ind. Eng. Chem. Res.*,43(2), p364-374, (2004).

Van Dongen, D. B.; Doherty, M. F. Design and Synthesis of Homogeneous Azeotropic Distillations. 1. Problem Formulation for a Single Column. *Ind. Eng. Chem. Fundam.*, *24*, p.454, 1985.

APPENDIX G: DERIVATION OF DPE

In order to derive the DPE, it is necessary to firstly define a column a length of where no material or energy is being added or removed, as shown in Figure G-1, with stream definitions.

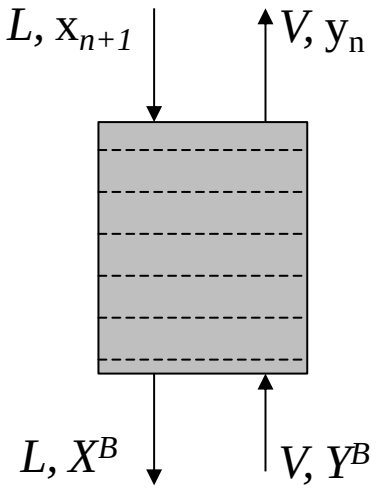


Figure G-1:Definition of a Column Section (CS)

Notice that in this column section, constant molar overflow is assumed, meaning that the liquid (L) and vapour (V) streams remain constant throughout the section. With this in mind, it is possible to write a component balance for the column section:

$$L\mathrm{x}_{\mathrm{n+1}} + VY^{B} - LX^{B} + V\mathrm{y}_{\mathrm{n+1}} = 0 \qquad \text{(G-1)}$$

It is now convenient to define a parameter known as the Difference Point as (Tapp et al., 2004)

$$X_{\Delta} = \frac{VY^{B} - LX^{B}}{\Delta} \qquad \text{(G-2)}$$

$$\text{Where: } \Delta = V - L, \quad \text{and} \quad V \neq L \qquad \text{(G-3)}$$

Replacing the definition of the X_Δ into Equation G-1:

$$x_{n+1} = \frac{V}{L} y_n - \frac{\Delta}{L} X_\Delta \qquad \text{(G-4)}$$

Furthermore, defining a generalised reflux ratio as $R_\Delta = \frac{L}{\Delta}$, Equation G-4 can be written as:

$$x_{n+1} = \left(1 + \frac{1}{R_\Delta}\right) y_n - \frac{1}{R_\Delta} X_\Delta \qquad \text{(G-5)}$$

Now, expanding $\mathbf{x_{n+1}}$ around stage *n* in Equation G-5 using a Taylor Series gives:

$$\mathrm{x}_{n+1} = \mathrm{x}_n + \frac{d\mathrm{x}}{dn}\Delta n + \frac{d^2\mathrm{x}}{dn^2}\Delta n^2 + \ldots \qquad \text{(G-6)}$$

Assuming that only the first order derivative is significant in G-6 and noting that $\Delta n=(n+1)-n=1$, we obtain:

$$\frac{d\mathrm{x}}{dn} = \mathrm{x}_{n+1} - \mathrm{x}_n \qquad \text{(G-7)}$$

Finally, replacing x_{n+1} in Equation G-5 by the definition in Equation G-7 and rearranging, results in a first order differential equation describing the change in composition across column section, known as the Difference Point Equation (DPE):

$$\frac{d\mathrm{x}}{dn} = \left(1 + \frac{1}{R_\Delta}\right)(\mathrm{x} - \mathrm{y}) + \left(\frac{1}{R_\Delta}\right)(X_\Delta - \mathrm{x}) \qquad \text{(G-8)}$$

It is important to note that X_Δ at the bottom of the column section ($X_{\Delta B}$) and X_Δ at the top of the column section ($X_{\Delta T}$) are equivalent, and this derivation could initiated with either definition of X_Δ. Integration in a positive direction of *n* indicates tracing composition upwards in the CS, while integration in a negative direction of *n* indicates change in composition from the top-down.

APPENDIX H: TEMPERATURE COLLOCATION

The transformation of the DPE (derived in Appendix G) from a stage dependent integration coordinate to a Temperature dependant integration coordinate initiates by first stating the classical DPE (in vector form):

$$\frac{d\mathrm{x}}{dn} = \left(1 + \frac{1}{R_\Delta}\right)(\mathrm{x} - \mathrm{y}) + \left(\frac{1}{R_\Delta}\right)(X_\Delta - \mathrm{x}) \qquad \text{(H-1)}$$

Where y is the vapour composition in equilibrium with its liquid composition x, and may be modelled as follows:

$$\mathrm{y} = K\mathrm{x}\,, \qquad \text{where} \qquad K = f(P, T, \mathrm{x}(T)) \qquad \text{(H-2)}$$

Where T is the bubble point temperature at which x and y are at equilibrium, and P is the total system temperature. Now, it is known that the sum of liquid and vapour composition each have to be unity. Thus, it is possible to write:

$$\frac{d\sum_{j=1}^{nc}[K_j(P,T,x(T))x_j]}{dx_1} = 0 \qquad \text{(H-3)}$$

Using the product rule for differential calculus, it is possible to expand H-3 further:

$$\sum_{j=1}^{nc}\left[\frac{dK_j}{dx_1}x_j + K_j\frac{dx_j}{dx_1}\right] = 0 \qquad \text{(H-4)}$$

H-4 can also be rewritten as:

$$\sum_{j=1}^{nc}\left[\frac{dK_j}{dT}\frac{dT}{dx_1}x_j + K_j\frac{dx_j}{dx_1}\right] = 0 \qquad \text{(H-5)}$$

The terms in H-5 van be rearranged and collected and rewritten to yield equations H-6 and H-7:

$$\sum_{j=1}^{nc}\left[\frac{dK_j}{dT}\frac{dT}{dx_1}x_j\right] = -\sum_{j=1}^{nc}K_j\frac{dx_j}{dx_1} \qquad \text{(H-6)}$$

$$\frac{dx_1}{dT} = -\frac{\sum_{j=1}^{nc} \frac{dK_j}{dT} x_j}{\sum_{j=1}^{nc} K_j \frac{dx_j}{dx_1}} \qquad \text{(H-7)}$$

The derivates dx_j/dx_1 can be eliminated in H-7 in terms of the stage number (n):

$$\frac{dx_1}{dT} = -\frac{\sum_{j=1}^{nc} \frac{dK_j}{dT} x_j}{\sum_{j=1}^{nc} K_j \frac{dx_j}{dn}\frac{dn}{dx_1}} = -\frac{dx_1}{dn}\frac{\sum_{j=1}^{nc} \frac{dK_j}{dT} x_j}{\sum_{j=1}^{nc} K_j \frac{dx_j}{dn}} \qquad \text{(H-8)}$$

Finally, inserting H-1 into equation H-8, yields:

$$\frac{dx_1}{dT} = -\frac{\left[\left(1+\frac{1}{R_\Delta}\right)(x_1 - y_1) + \left(\frac{1}{R_\Delta}\right)(X_{\Delta 1} - x_1)\right]\sum_{j=1}^{nc} \frac{dK_j}{dT} x_j}{\sum_{j=1}^{nc} K_j \left[\left(1+\frac{1}{R_\Delta}\right)(x_j - y_j) + \left(\frac{1}{R_\Delta}\right)(X_{\Delta j} - x_j)\right]} \qquad \text{(H-9)}$$

H-9 describes the change in bubble point temperature in a column section with change in composition of component x_1. H-9 may be derived analogously for all other components x_j. The derivative $\frac{dK_j}{dT}$ may be computed as follows. First, the exact definition for K_j is:

$$K_j = \frac{\gamma_j P_j^{VAP}}{P}, \qquad \text{for} \quad j = 1, 2...nc \qquad \text{(H-10)}$$

γ is known as the activity coefficient, which accounts for non-ideal behaviour and is a function of both temperature and composition. P^{VAP} is the vapour pressure and is only a function of temperature through the familiar Antoine equation. Now, the derivative of H-10 with respect to temperature is:

$$\frac{dK_j}{dT} = \frac{1}{P}\left[P_j^{VAP}\frac{d\gamma_j}{dT} + \gamma_j \frac{dP_j^{VAP}}{dT}\right], \qquad \text{for} \quad j = 1, 2...nc \qquad \text{(H-11)}$$

The differential of the activity coefficient with respect to tempertature may obtained through the chain rule as:

$$\frac{d\gamma_j}{dT} = \sum_{k=1}^{nc} \frac{\partial \gamma_j}{\partial x_k} \frac{d\gamma_k}{dT} + \frac{\partial \gamma_j}{\partial T} \qquad \text{(H-12)}$$

Finally, replacing H-12 into H-11, we obtain the full expression for dK_j/dT:

$$\frac{dK_j}{dT} = \frac{1}{P}\left[P_j^{VAP} \sum_{k=1}^{nc} \frac{\partial \gamma_j}{\partial x_k} \frac{d\gamma_k}{dT} + \frac{\partial \gamma_j}{\partial T} + \gamma_j \frac{dP_j^{VAP}}{dT} \right], \qquad \text{for} \quad j = 1, 2 \ldots nc \qquad \text{(H-13)}$$